Thesis

Consistency relations in cosmology

PERRIER, Hideki

Abstract

We study the large-scale structure of the Universe using the analytical technique of the consistency relations which enable to compute the squeezed bispectrum of correlation functions using symmetries of the system at hand. We study their consequences for bias models, non-perturbative models of structure formation and modified gravity. We compute the squeezed limit of the bispectrum of galaxy number counts, the quantity that galaxy surveys measure. We also compute the contamination to the non-Gaussian parameter fNL that relativistic effects produce. These are crucial if the goal of reaching a constraint on fNLloc of order unity is to be attained. Finally, we compute the squeezed bispectrum of the cross-correlation between cosmic microwave background temperature and two po- larization modes. The measurement of such correlation might be useful for distinguishing between a primordial gravitational waves background and polarization from galactic dust.

Reference

PERRIER, Hideki. *Consistency relations in cosmology*. Thèse de doctorat : Univ. Genève, 2016, no. Sc. 4971

URN : urn:nbn:ch:unige-903222
DOI : 10.13097/archive-ouverte/unige:90322

UNIVERSITÉ DE GENÈVE
Section de physique
Département de physique théorique

FACULTÉ DES SCIENCES
Professeur Antonio RIOTTO

Consistency Relations in Cosmology

THÈSE

présentée à la Faculté des sciences de l'Université de Genève
pour obtenir le grade de
Docteur ès sciences, mention physique

par

Jean-François Hideki Perrier

de

Sainte-Croix (VD) et Orges (VD)

Thèse N° 4971

GENÈVE
Atelier de reproduction UNI-Mail
2016

UNIVERSITÉ
DE GENÈVE

FACULTÉ DES SCIENCES

Doctorat ès sciences
Mention physique

Thèse de *Monsieur Jean-François Hideki PERRIER*

intitulée :

"Consistency Relations in Cosmology"

La Faculté des sciences, sur le préavis de Monsieur A. RIOTTO, professeur ordinaire et directeur de thèse (Département de physique théorique), Madame R. DURRER, professeure ordinaire (Département de physique théorique) et Monsieur F. VERNIZZI, professeur (Institut de physique théorique, Université Paris Saclay, Commissariat à l'énergie atomique et aux énergies alternatives, Gif-sur-Yvette, France), autorise l'impression de la présente thèse, sans exprimer d'opinion sur les propositions qui y sont énoncées.

Genève, le 31 août 2016

Thèse - 4971 -

Le Doyen

N.B. - La thèse doit porter la déclaration précédente et remplir les conditions énumérées dans les "Informations relatives aux thèses de doctorat à l'Université de Genève".

Abstract

We study the large-scale structure of the Universe using the analytical technique of the *consistency relations* which enable to compute the squeezed bispectrum of correlation functions using symmetries of the system at hand. We apply it to the matter overdensity correlations of matter and galaxies and study their consequences for bias models, non-perturbative models of structure formation and modified gravity. As a step towards more practical theoretical predictions, we compute the squeezed limit of the bispectrum of galaxy number counts, the quantity that galaxy surveys measure. We also compute the contamination to the non-Gaussian parameter $f_{\rm NL}$ that relativistic effects produce. These are crucial if the goal of reaching a constraint on $f_{\rm NL}^{\rm loc}$ of order unity is to be attained. This goal is of particular importance as any detection of local primordial non-Gaussianity would eliminate all single-field models of inflation. Finally, we compute the squeezed bispectrum of the cross-correlation between cosmic microwave background temperature and two polarization modes. The measurement of such correlation might be useful for distinguishing between a primordial gravitational waves background and polarization from galactic dust.

Reviewing commitee

- Prof. Antonio Riotto, Département de physique théorique, University of Geneva
- Dr. Filippo Vernizzi, IPhT, CEA, Saclay
- Prof. Ruth Durrer, Département de physique théorique, University of Geneva

Acknowledgements

First of all, I would like to thank the reviewing committee who took time to review my thesis and for useful remarks. I would like to thank my supervisor, Toni Riotto, who has advised me during the last four years through a wide variety of projects. I also thank Ruth Durrer who has been a great supervisor during my master thesis and who has inspired me and lead me to do reasearch. She has always had a very positive and motivating attitude.

I thank Lenardo Senatore who has invited me to work in Stanford for one year during the third year of my Ph.D. It has been very instructing to work with him. I am also very grateful to all the people I have met in Stanford: Matteo Cataneo and Marco who were very fun office mates for the first months there, Matteo Fasiello, Zvonimir, Ashley, Matt and of course Simon with whom it has been a pleasure to work with: "that was fun". I also thank all the co-authors of my papers in Geneva and abroad, in particular Jorge, Enea, Vincent, Azadeh, Matteo, Enrico and Alex. It is has been a pleasure to have had Enea as a roommate during the first two years of my thesis, a time during which we had interesting discussions. He is also a great friend to me. I would also like to thank other people here in Geneva, Wilmar, Marco, Cécile and Francine.

Du coté personnel, je remercie ma grand-maman, Ginette qui m'a toujours inconditionnellement soutenu dans mes projets. Elle a toujours cru en moi, m'a encouragé depuis petit, et soutenu dans mes études. Sa délicieuse cuisine a sans doute joué un grand rôle dans ma croissance :) Je pense également à ma mère qui aurait été fière de me voir terminer mon doctorat. Je pense également à Alba avec qui il a été un plaisir d'étudier. Je remercie aussi Sébastien que j'ai rencontré à l'EPFL et avec qui je ne me suis jamais ennuyé durant les travaux pratique, Renata et leur fille Solène qui est également ma filleule. Je dois également remercier Frédéric Ferrero, qui m'a enseigné les maths au gymnase. Il a été un excellent enseignant qui a su me motiver et me montrer la beauté des mathématiques. Finalement je remercie aussi mes amis avec qui j'ai passé de belles sorties et barbecues: Aline, les deux David, Pradeep, Jospip, Yannick, Médéric, Julie, Héloïse et Salomé, mes meilleures amies d'enfance.

Finalement, je remercie aussi Marcel et Clément qui ont partagé une partie de ma vie durant ce temps et qui on été d'un grand soutien.

Résumé en français

La cosmologie cherche à décrire les lois physique qui gouvernent l'évolution de l'Univers. Le modèle dominant, appelé ΛCDM, est basé sur les solutions symétriques des équations d'Einstein [1]. Celles-ci relient la géométrie de l'Univers à son contenu. En particulier, l'expansion de l'Univers dépend de la matière qui s'y trouve. Grâce aux observations, on conclut qu'il faut de la matière ordinaire comme les étoiles mais aussi de la matière noire (CDM), non lumineuse, mais qui possède une masse, et de l'énergie sombre, appelée aussi constante cosmologique (Λ). Un dernier ingrédient est probablement nécessaire pour des raisons théoriques telles que le problème de *l'horizon* ou pour expliquer la très faible courbure de l'Univers [2, 3, 4, 5]: une période d'expansion exponentielle extrêmement rapide et brève juste après le Big Bang (le début de l'Univers) appelée *inflation*. Dans les modèles les plus simples d'inflation, l'énergie qui la provoque est celle d'un champ scalaire, l'inflaton. Des perturbations dans la densité de d'énergie du champ sont transmises à la métrique qui décrit la géométrie de l'Univers. Ces perturbations vont ensuite être transmises à la matière présente dans l'Univers primordial qui est constitué principalement d'un plasma d'hydrogène et de photons. Avec l'expansion de l'Univers, la matière refroidit et l'attraction gravitationnelle va agréger la matière autour des sur-densités. La pression va ensuite former des étoiles, puis des galaxies et constituer ce que l'on appelle la *grande structure de l'Univers* (LSS). C'est la distribution des galaxies que les télescopes mesurent et l'on pense que ce sera la principale source d'information cosmologiques dans la décennie à venir.

La plupart des informations que l'ont est capable d'obtenir de l'Univers proviennent d'objets lumineux telles que les galaxies et le fond diffus cosmologique (CMB), une lumière émise environ 400'000 ans après le Big Bang. Ces deux observables constituent les principales sources d'informations disponibles pour les cosmologistes. Le processus de création de l'Univers ne s'étant produit qu'une seule fois, on ne peut espérer décrire la distribution exacte des galaxies ou des perturbations dans l'énergie des photons du CMB, mais uniquement leur propriétés statistiques. Celles-ci sont décrites par leurs *fonctions de corrélations* telles que le spectre et le bispectre (transformées de Fourier de la fonction de corrélation à deux et trois points respectivement). Ce dernier est particulièrement important pour distinguer et décrire les possibles mécanismes d'inflation. En effet, une propriété appelée non-gaussianité, le fait que les perturbations ne suivent pas une distribution gaussienne, permet de séparer les nombreux modèles d'inflation. Toute détection de non-gaussianité éliminerait la possibilité que l'inflation soit provoquée par un seul champ scalaire standard [6, 7]. Si les perturbations sont gaussiennes, alors le bispectre est nul. Dans cette thèse qui est basée sur cinq articles, dont quatre ont déjà été publiés [8, 9, 10, 11], je m'intéresse à une limite particulière du bispectre, appelée *limite serrée*, où l'un des trois vecteurs d'onde est très court ($k_1 \ll k_2, k_3$). Cette limite a l'avantage qu'elle peut être calculée relativement simplement grâce à un changement de coordonnées appliqué au spectre de l'observable en question. On obtient alors une relation entre la limite serrée du bispectre et le spectre appelée *relation de cohérence*. Celle-ci a le grand avantage que les modes courts k_2, k_3 peuvent être non-linéaires, c'est-à-dire dans le régime où les conditions initiales ne sont plus simplement reliées à l'observable par une relation linéaire. Du point de vue théorique, faire des prédictions dans ce régime est très difficile et l'on a rarement d'autre choix de s'en remettre à des simulations numériques qui sont très lentes. L'autre possibilité est d'utiliser la théorie des perturbations au deuxième ordre, mais cela n'étant que peut le domaine de validité et peut dans certains cas amener à des expression extrêmement compliquées. Les relations de cohérence on déjà été appliquées avec succès aux fonctions

de corrélation des perturbation de l'inflation [7, 12] et du CMB [6, 12, 13, 14, 15, 16, 17]. Dans cette thèse, je présente de nouvelles relations ainsi qu'une étude de leur conséquences sur certains modèles perturbatifs et non-perturbatifs décrivant la structure à grande échelle.

Dans le chapitre 2, je présente une généralisation des relations de cohérence existantes pour la surdensité de matière noire où j'inclus l'effet d'un champ gravitationnel jusqu'à une deuxième dérivée sur les modes courts. Le bispectre est alors non-nul à temps égaux. Comme exemple, j'ai vérifié que le *modèle du halo* décrivant la distribution de matière dans le régime non-linéaire reproduisait bien la relation jusqu'à des échelles d'environ $k \simeq \mathcal{O}(1)$ h/Mpc.

Dans le chapitre 3, j'explore les conséquences de la dérivation par les équations du fluide des relations de cohérence. Je montre que l'expansion eulérienne locale du biais (la relation entre la distribution des galaxies et de la matière noire) satisfait les relations de cohérence mais que les symétries des équations impliquent que la relation doit être non-locale. Comme première étape vers une prédiction théorique qui puisse être comparée directement aux observations, je dérive aussi une relation de cohérence en incluant les distorsions du décalage vers le rouge. Finalement, je montre comment les relations de cohérence peuvent être violées dans le cas d'un exemple de *gravité modifiée* où la cinquième force est présente ou non selon l'environnement de la galaxie.

Ensuite, je calcule la limitée serrée du bispectre des quantités directement mesurées par les études de galaxies: les comptes du nombre de galaxies, c'est-à-dire la densité de galaxies par angle solide et décalage vers le rouge. Prédire des relations pour les quantités mesurées est très important pour exploiter au mieux les données à venir car l'on entre dans une ère de précision pour la cosmologie. La relation entre les quantités pratiques du point de vue théoriques définies dans l'espace de Fourier et les quantités observées devient importante. En particulier, je montre que si l'on analyse naïvement les données, on pourrait faussement conclure à la mesure d'une non-gaussianité locale $f_{\rm NL}^{\rm loc}$ d'ordre unité.

Le chapitre 5 est dédié à l'étude plus profonde des non-gaussianités dans les mesures des comptes de nombre de galaxies. Je calcule différent types de non-gaussianités en terme du bispectre des nombres de galaxies et projette différents termes issu de la relation de cohérence ainsi que de calculs au deuxième ordre [18, 19] afin d'obtenir une estimation de la non-gaussianité effective. Je trouve que pour atteindre une précision d'ordre unité sur les non-gaussianités primordiales, il est nécessaire de prendre ces effets en compte et de les soustraire. Ultimement, il apparaît qu'il faudra évaluer tous les termes de l'expression au deuxième ordre et de la soustraire aux mesures du bispectre car des annulations peuvent se produire.

Finalement, dans le chapitre 6, je dérive une relation de cohérence pour le bispectre entre un mode de la température du CMB et deux modes de polarization. Bien qu'il est probablement difficile de mesurer une telle corrélation, elle permet en principe de distinguer la polarisation primordiale de la polarisation émise par la poussière interstellaire.

Pour conclure, j'ai développé des méthodes analytiques permettant de mieux comprendre et exploiter les futures mesures de polarisation du CMB ainsi que de la structure à grande échelle de l'Univers. La pertinence de ces résultats dépendra cependant très probablement de la compréhension des processus astrophysiques qui viendront contaminer les mesures. Du côté théorique, encore beaucoup de problèmes sont présent comme par exemple comment intégrer la théorie du biais dans la description des comptes de nombre de galaxies. Il faudra probablement s'en remettre à des simulations si l'on désire exploiter les données dans le régime totalement non-linéaire. Bien que certaines simula-

tions relativistes existent, il reste encore du chemin à parcourir. D'autre types d'observables comme les ondes gravitationnelles ou le fond diffus infrarouge (CIB) fourniront également plus d'information sur l'Univers. La question sera ensuite : *L'Univers nous donnera-t-il assez d'information pour que l'on puisse le comprendre?*

Publications related to this thesis

- **"A Consistency Relation for the Observed Galaxy Bispectrum and the Local non-Gaussianity from Relativistic Corrections"**, A. Kehagias, A. M. Dizgah, J. Noreña, H. Perrier and A. Riotto, arXiv:1503.04467 [astro-ph.CO], DOI: 10.1088/1475-7516/2015/08/018, JCAP **1508**, no. 08, 018 (2015)
- **"A Consistency Relation for the CMB B-mode Polarization in the Squeezed Limit"**, A. Kehagias, A. Moradinezhad-Dizgah, J. Noreña, H. Perrier and A. Riotto, arXiv:1407.6223 [astro-ph.CO], DOI: 10.1088/1475-7516 /2014/10/011, JCAP **1410**, no. 10, 011 (2014)
- **"Equal-time Consistency Relations in the Large-Scale Structure of the Universe"**, A. Kehagias, H. Perrier and A. Riotto, arXiv:1311.5524 [astro-ph.CO], DOI: 10.1142/S02177323 14501521, Mod. Phys. Lett. A **29**, 1450152 (2014)
- **"Consequences of Symmetries and Consistency Relations in the Large-Scale Structure of the Universe for Non-local bias and Modified Gravity"**, A. Kehagias, J. Noreña, H. Perrier and A. Riotto, arXiv: 1311.0786 [astro-ph.CO], DOI: 10.1016/j.nuclphysb.2014.03.020, Nucl. Phys. B **883**, 83 (2014)
- **"Non-Gaussianities due to Relativistic Corrections to the Observed Galaxy Bispectrum"**, Di Dio, E. and Perrier, H. and Durrer, R. and Marozzi, G. and Moradinezhad Dizgah, A. and Noreña, J. and Riotto, A., in preparation for submission to JCAP (2016)

Other publications

- **"Precision Comparison of the Power Spectrum in the EFTofLSS with Simulations"**, S. Foreman, H. Perrier and L. Senatore, arXiv:1507.05326 [astro-ph.CO], DOI: 10.1088/1475-7516/2016/05/027, JCAP **1605**, no. 05, 027 (2016)
- **"Symmetries of Vector Perturbations during the de Sitter Epoch"**, M. Biagetti, A. Kehagias, E. Morgante, H. Perrier and A. Riotto, arXiv: 1304.7785 [astro-ph.CO], DOI: 10.1088/1475-7516/2013/07/030, JCAP **1307**, 030 (2013)
- **"Testing the running of non-Gaussianity through the CMB μ-distor-tion and the halo bias"**, M. Biagetti, H. Perrier, A. Riotto and V. Desjacques, arXiv:1301.2771 [astro-ph.CO], DOI: 10.1103/PhysRevD.87.063521, Phys. Rev. D **87**, 063521 (2013)
- **"Non-Gaussianities from the Standard Model Higgs"**, A. De Simone, H. Perrier and A. Riotto, arXiv:1210.6618 [hep-ph], DOI: 10.1088/1475-7516 /2013/01/037, JCAP **1301**, 037 (2013)
- **"Explosive particle production in non-commutative inflation"**, H. Perrier, R. Durrer and M. Rinaldi, arXiv:1210.5373 [gr-qc], DOI: 10.1007/JHEP01 (2013)067, JHEP **1301**, 067 (2013)

Units, Symbols and Conventions

Unless state otherwise, we work in "natural" in units such that $c = \hbar = k_B = 1$. We use the following notation:

- t cosmic time
- a scale factor
- $\vec{x}$ comoving coordinates
- $\tau = \int 1/a(\tau)$ conformal time
- $' = d/d\tau$
- $\dot{} = d/dt$
- $H = \dot{a}/a$ Hubble parameter
- $\mathcal{H} = a'/a = aH$ comoving Hubble parameter
- $\vec{k}$ conformal wavenumber
- z redshift
- $\hat{n}$ unit vector, direction in the sky
- r comoving distance
- r_T tensor-to-scalar ratio
- G Newton's constant
- ϕ inflaton field
- ζ primordial curvature perturbation
- P_ζ primordial curvature power spectrum
- Φ gravitational potential
- $\Omega_\mathrm{m} = \frac{8\pi G\bar{\rho}}{3H^2}$ matter density parameter
- ρ matter density
- $\bar{\rho}$ mean matter density
- $\vec{v}$ peculiar velocity
- v velocity potential
- D linear growth factor

- $\delta_k, \delta(k)$ matter overdensity contrast in Fourier space
- $\delta_{\mathrm{g},k}, \delta_{\mathrm{g}}(k)$ galaxy overdensity contrast in Fourier space
- $\vec{s} = \vec{x} + \frac{1}{\mathcal{H}}(\vec{v}\cdot\hat{x})\hat{x}$ redshift space coordinate
- δ_s matter overdensity contrast in redshift space
- b_1, b_2 Eulerian bias coefficients
- $\Delta_g(\hat{n}, z)$ galaxy number counts per solid angle per redshift
- δ_L, $\delta^{(1)}$ linear matter overdensity constrast
- $P_L(k)$ linear matter power spectrum
- $\mathcal{P}$ dimensionless power spectrum
- B bispectrum in Fourier space
- $\Delta_\ell(k,\tau)$ CLASSgal transfer function
- $a_{\ell m}$ the angular modes
- $C_\ell^X Y$ the angular cross power spectrum of the quantities X and Y.
- $B^{m_1 m_2 m_3}_{\ell_1 \ell_2 \ell_3}$ angular bispectrum
- $b_{\ell_1 \ell_2 \ell_3}$ reduced angular bispectrum
- Θ the temperature anisotropy

We use the perturbed FLRW metric in the Poisson gauge which takes the form

$$\mathrm{d}s^2 = a^2(\tau)\Big[-(1+2\Phi)\mathrm{d}\tau^2 + (1-2\Psi)\mathrm{d}\vec{x}^2\Big], \tag{0.0.1}$$

for scalar perturbations. Note that Ψ and Φ are switched with respect the convention of [20, 21] and the CLASSgal code [22]. We choose our Fourier transform as

$$f(\vec{x}) = \frac{1}{(2\pi)^3}\int d^3k f(\vec{k}) e^{-i\vec{k}\cdot\vec{x}}. \tag{0.0.2}$$

The inverse is therefore

$$f(\vec{k}) = f_{\vec{k}} = \int d^3r f(\vec{r}) e^{i\vec{k}\cdot\vec{x}}. \tag{0.0.3}$$

We define the velocity potential v by

$$\vec{v} = \nabla v, \tag{0.0.4}$$

such that

$$\vec{v}(\tau,\vec{k}) = -i\vec{k}v(\tau,\vec{k}). \tag{0.0.5}$$

In our Fourier convention, the power spectrum of a quantity X is

$$\langle X(\tau_1,\vec{k}_1)X(\tau_2,\vec{k}_2)\rangle = (2\pi)^3\delta_D^{(3)}(\vec{k}_1+\vec{k}_2)P_X(k_1,\tau_1,\tau_2), \tag{0.0.6}$$

where we assumed the field to be statistically isotropic and homogeneous. The dimensionless (possibly unequal times) power spectrum is

$$\mathcal{P}_X(k,\tau_1,\tau_2) \equiv \frac{(2\pi)^3}{4\pi}k^3P_X(k,\tau_1,\tau_2). \tag{0.0.7}$$

The initial conditions are described by the power spectrum of curvature perturbation after inflation which is parametrized as

$$P_\zeta(k) = \frac{A}{k^3}\left(\frac{k}{k_p}\right)^{n_s-1}, \tag{0.0.8}$$

where k_p is a pivot scale. This is the choice of [20] and what is used in the NG shape templates (see appendix B). The dimensionless curvature power spectrum is parametrized as

$$\mathcal{P}_\zeta(k) = A_s\left(\frac{k}{k_p}\right)^{n_s-1}, \tag{0.0.9}$$

where A_s and n_s are the usual values quoted e.g. in the Planck papers and we have $A = 2\pi^2A_s \simeq 4\times10^{-8}$. This is the "_primordial_Pk.dat" output from the CLASSgal code. The bispectrum is defined in terms of Fourier modes by

$$\langle X(\tau_1,\vec{k}_1)X(\tau_2,\vec{k}_2)X(\tau_3,\vec{k}_3)\rangle \equiv (2\pi)^3\delta_D^{(3)}(\vec{k}_1+\vec{k}_2+\vec{k}_3)B_X(k_1,k_2,k_3,\tau_1,\tau_2,\tau_3) \tag{0.0.10}$$

for a statistically isotropic and homogeneous field.

Contents

Chapter 1

Introduction

Cosmology is the science of the Universe as a whole. It studies the origins and the evolution of the Universe. In this introduction, we review the ΛCDM which is the main cosmological model which is compatible with observations. In this model, the Universe is believed to start in an extremely dense and hot state followed by a period of exponential expansion called *inflation*. During this period, perturbations are generated in the fabric of space-time which are then imprinted in the matter content of the Universe. These are seen as temperature anisotropy in the cosmic microwave background (CMB) and as variations in the distribution of galaxies throughout the Universe which is called the large-scale strucuture (LSS). We review how these perturbations are generated in the prevailing model of *single-field slow-roll* inflation and introduce the notion of *non-Gaussianity*. We explain why it is a crucial notion which can help understand the physics of inflation. A huge amount of data about the LSS is expected from upcoming surveys. This drives the need for a better understanding of the large-scale structure in the non-linear regime. It is in this optic that we introduce the notion of *consistency relations* (CR), a technique which relates correlation functions of cosmological observables. The subject of this thesis is the application of this technique to the LSS and the study of its consequences.

1.1 The ΛCDM model

One can trace the origins of modern cosmology to Einstein's Theory of General Relavity (GR). General Relativity describes gravity through the geometry of the Universe (represented by the metric $g_{\mu\nu}$) and the influence of the distribution of matter and energy in it. This is described at the fundamental level by the Einstein's equations [1]

$$G_{\mu\nu} = 8\pi G T_{\mu\nu} - \Lambda g_{\mu\nu} \tag{1.1.1}$$

where $G_{\mu\nu}$ is the Einstein tensor made of second derivatives of the metric and Λ is the so-called cosmological constant present as it is allowed by the symmetries. The content of the Universe is described by the energy momentum tensor $T_{\mu\nu}$. In general, these equations are very difficult to solve. However, Friedman [23], Lemaître [24], Robertson [25] and Walker [26] studied simple solutions of these. In particular, one was interested in isotropic and homogenous solutions which could describe the Universe on large scales. Indeed, one believes that the Universe should be self-similar under

translations (homogeneity) and rotations around each point (isotropy) as there is no reason that there should be any preferred location or direction. The ansatz of such a solution is the basis of modern cosmology, known as the FLRW metric, and takes the simple form

$$g_{\mu\nu}dx^\mu dx^\nu = -dt^2 + a(t)^2\gamma_{ij}dx^i dx^j. \tag{1.1.2}$$

The coordinate t is called *cosmic time* and $\vec{x}$ is the *comoving position*. The spatial metric is γ_{ij} and accounts for possible curvature K. The energy-momentum tensor has to take the form

$$T_{\mu\nu} = \begin{pmatrix} -\rho g_{00} & \vec{0} \\ \vec{0} & P g_{ij} \end{pmatrix} \tag{1.1.3}$$

where ρ describes the density and P to the pressure of matter. This leads to the Friedman equations [23]

$$\frac{\ddot{a}}{a} = -\frac{4\pi G}{3}(\rho + 3P) + \frac{\Lambda}{3} \tag{1.1.4}$$

$$\left(\frac{\dot{a}}{a}\right)^2 + \frac{K}{a^2} = \frac{8\pi G}{3}\rho + \frac{\Lambda}{3}. \tag{1.1.5}$$

where the curvature of the Universe is given by K. These equations govern the evolution of the scale factor a which describes the expansion of the Universe as a function of its content. Since Hubble's discovery of the expansion of the Universe in 1929 [27] multiple observations, in particular of the cosmic microwave background have allowed to determine the left-hand side of these equations. Four main constituents are found to be necessary: baryonic matter, cold dark matter (CDM), radiation, a cosmological constant Λ while the curvature K is found to be negligible. This model is called the "ΛCDM" or "concordance" model of cosmology.

While being extremely successful, this standard model of cosmology comes with three main puzzles which are the focus of modern cosmology:

- *dark matter*
- *dark energy*
- *inflation*

Observations of supernovae of type Ia made in 1998 [28] led to the conclusion that the Universe is undergoing an *accelerated* expansion which is compatible with a cosmological constant Λ also called *dark energy*. Measurement of galaxy rotation curves [29] did not match the ones expected from the visible mass. The most widely accepted explanation is that there exist a halo of matter which interacts only gravitationally, called *dark matter*. A topic which we shall briefly consider in this thesis is called Modified Gravity (MG). It consists in explaining the behaviour of matter in the Universe by a modification of gravity at large distances instead of the presence of dark matter and / or dark

energy. While gravity is very well tested on solar system scales, there is a possibility that it behaves differently on galactic scales. The modification of gravity can generally be recast as a "fifth force" which modifies the trajectories of objects. We shall apply the *consistency relations* to a toy model of MG where the fifth force is either present or not.

The third puzzle with the ΛCDM model stems basically from two conceptual problems. The *horizon problem*: regions which were causally disconnected in the past have extremely similar properties; and the *flatness problem*: it can be shown that a curved universe is unstable under evolution. The observed level of curvature today would require an extreme fine tuning of the initial conditions. The most elegant solution to these problems emerged in the 1980s and consists in a period of exponential expansion of the Universe right after the Big Bang called *inflation*. It provides a unified way of solving the issues mentioned above [2, 3, 4, 5] along with others, like monopoles [30] or domain walls [31, 32]. However, the exact mechanism through which this happens is yet unknown and dozens of models of inflation have been proposed (for a review, see e.g. [33]).

Such a period of accelerated expansion $\ddot{a} > 0$ of the Universe can be achieved if the constituents of the Universe satisfies $P > \rho/3$ as seen from the Friedman equation (1.1.4) (we exclude the cosmological constant for now). This can be achieved by a scalar field ϕ, called the *inflaton*, evolving in a potential $V(\phi)$. The equations of motion are then

$$\ddot{\phi} + 3H\dot{\phi} - \frac{\nabla^2\phi}{a^2} + V'(\phi) = 0, \tag{1.1.6}$$

where $V'(\phi) = \mathrm{d}V/\mathrm{d}\phi$ and a dot represents a derivative with respect to cosmic time t and gradients are with respect to comoving coordinates. The energy momentum tensor has components

$$T_{00} = \rho_\phi = \frac{\dot{\phi}^2}{2} + V(\phi) + \frac{(\nabla\phi)^2}{2a^2} \tag{1.1.7}$$

$$T_{ii} = P_\phi = \frac{\dot{\phi}^2}{2} - V(\phi) - \frac{(\nabla\phi)^2}{6a^2} \tag{1.1.8}$$

$$\tag{1.1.9}$$

If the gradients are dominant, then $P_\phi = -\rho_\phi/3$ which cannot drive inflation. One then splits the field in a homogenous part and a perturbation,

$$\phi(t) = \phi_0(t) + \delta\phi(\vec{x}, t), \tag{1.1.10}$$

where $\phi_0(t)$ is the classical part, the value of the field on the background and $\delta\phi(\vec{x}, t)$ the (Gaussian) quantum fluctuations around it. As we neglect the space-dependent part, we see that if time derivatives are small, $V(\phi_0) \gg \dot{\phi_0}^2$, we obtain an accelerated expansion $P_\phi \simeq -\rho_\phi$. This means that the field is *slowly rolling* down the potential, hence the name *single-field slow-roll* inflation. During the slow roll,

the Hubble parameter is almost constant $H^2 \simeq \frac{8\pi G}{3} V(\phi_0)$ and the scale factor grows exponentially

$$a(t) = a_I e^{H(t-t_I)}, \tag{1.1.11}$$

where the subscript I denotes the beginning of inflation. The level of constancy of the Hubble parameter, or equivalently the smallness of the kinetic terms of the scalar field are characterised by the *slow-roll parameters*:

$$\epsilon = -\frac{\dot{H}}{H} = \frac{1}{16\pi G}\left(\frac{V'}{V}\right)^2, \qquad \eta = \frac{1}{8\pi G}\frac{V''}{V} = \frac{1}{3}\frac{V''}{H^2}, \tag{1.1.12}$$

which need to be much smaller than unity. Different types of potentials which satisfy these conditions give rise to different types of single-field slow-roll inflation.

1.2 Non-Gaussianities

Of course, the Universe is not homogenous and isotropic on small scales. Structures that we see today are believed to be formed from perturbations in the early universe, ultimately generated during inflation. In this section, we briefly review how these perturbations are generated and characterized. In particular, we introduce the concept of *non-Gaussianity* (NG), which will be the focus of this work. It is a crucial property of perturbations which allows to distinguish between different inflation models in cosmological observables.

In addition to solving the problems mentionned in the previous section, the principal role of inflation is to provide the "seeds" for the perturbations in the initial plasma constituting the Universe at early times. By Einstein's equations, perturbations in the inflaton field generated during inflation also induce metric perturbations. At the end of inflation, the inflaton has rolled down its potential and oscillates where it decays into radiation. The metric perturbations are then transmitted to this early universe plasma. Once the Universe has cooled down, and photons travel freely, these perturbations are seen as anisotropies in the CMB temperature. The over- and under-densities in the plasma eventually collapse to form stars and galaxies seen in the large-scale structure.

The perturbations have to be defined with respect to a homogeneous and isotropic reference universe. However, general relativity has an internal redundancy in the form of coordinates transformations from one frame to another. The mapping between the real, perturbed universe and the reference one is therefore not unique. Quantities whose value is independent from choice of gauge are called *gauge-invariant variables*. The variable of choice to describe initial perturbations is *curvature perturbation on slices of uniform energy density* which takes the following form in a generic gauge

$$\zeta \equiv \Psi + \mathcal{H}\frac{\delta\rho}{\rho'}, \tag{1.2.1}$$

where $\mathcal{H}$ is the comoving Hubble parameter and a prime denotes a derivative with respect to conformal time. Throughout this work, where we shall deal only with scalar perturbations and use the perturbed

FLRW metric in the Poisson gauge which takes the form

$$\mathrm{d}s^2 = a^2(\tau)\Big[-(1+2\Phi)\mathrm{d}\tau^2 + (1-2\Psi)\mathrm{d}\vec{x}^2\Big], \tag{1.2.2}$$

where Φ and Ψ have the advantage to be equal to the gauge invariant Bardeen's potentials.

Using the perturbed Einstein and Klein-Gordon equations describing the dynamics of the inflaton and its interactions with the metric, one can compute the resulting curvature perturbation. One finds that on sub-Hubble scales, perturbations oscillates whereas they become time-independent on super-Hubble scales. At the end of inflation, all perturbations, which have a physical wavelength a/k, are super-Hubble ($a/k \gg 1/H$) because H is roughly constant while the scale factor increases exponentially.

As we only have one realisation of the physical processes which have created the Universe, we can only hope to describe the statistical properties of fluctuations. This is done through their correlation functions in Fourier space. In the case of single-field slow-roll inflation, non-linearities are small and the resulting curvature perturbation is Gaussian distributed. All higher order correlation functions are then determined by the two-point function, the *power spectrum* $P_\zeta(k)$:

$$\langle \zeta_{\vec{k}}\zeta_{\vec{k}'}\rangle = (2\pi)^3\delta_D^{(3)}(\vec{k}+\vec{k}')P_\zeta(k) = (2\pi)^3\delta_D^{(3)}(\vec{k}+\vec{k}')\frac{k^3}{2\pi^2}\mathcal{P}_\zeta(k), \tag{1.2.3}$$

where we have also defined the *dimensionless power spectrum*[1] $\mathcal{P}_\zeta(k)$.

Solving the equations of motion on super-Hubble scales, one finds that the power spectrum of the curvature perturbation is given by

$$\mathcal{P}_\zeta(k) = \frac{1}{2M_{\mathrm{P}}^2\epsilon}\left(\frac{H}{2\pi}\right)^2\left(\frac{k}{aH}\right)^{n_s-1} \equiv \frac{A}{2\pi^2}\left(\frac{k}{k_p}\right)^{n_s-1}. \tag{1.2.4}$$

where we have introduced the *spectral index*

$$n_s - 1 = \frac{\mathrm{d}\ln\mathcal{P}_\zeta}{\mathrm{d}\ln k} = 2\eta - 6\epsilon, \tag{1.2.5}$$

the amplitude of the power spectrum A and k_p is a pivot scale. Because the k-dependence is weak, proportional to the slow-roll parameters, this is referred to as a *scale invariant* power spectrum. Observations [34] have confirmed this predictions found $n_s \simeq 0.96$.

The scale-invariance of the perturbations can be understood in terms of the symmetries present during the inflationary phase [14]. Inflation corresponds to *quasi de Sitter* phase. A de Sitter universe has symmetries among which dilation symmetry $\vec{x} \to \lambda\vec{x}$ which impose the two-point correlation function to be scale invariant $P_\zeta(k) = \frac{A}{k^3}$, see also section 1.4. Inflation is however only a *quasi* de Sitter phase as e.g. H has a time dependence proportional to the slow-roll parameters. Because this symmetry is only approximate, the two-point function can have a slight scale-dependence also

[1] Conventions are summarized in appendix A.

proportional to the slow-roll parameters as it is the case in (1.2.4).

Along with scalar perturbations, inflation is also notably believed to produce tensor perturbations or (primordial) gravitational waves (GW). While these have yet to be detected, direct observation of GW generated by astrophysical sources has been made in September 2015 [35] which leaves hope for future detection. One expects to observe them in the form of a stochastic background in the CMB polarization through patterns called *B-modes*. The amount of GW is usually defined by the *tensor-to-scalar ratio*

$$r_T \equiv \frac{\frac{1}{100}A_T}{\frac{4}{25}A_s}, \tag{1.2.6}$$

where the tensor power spectrum is parametrized as $\mathcal{P}_T(k) = A_T \left(\frac{k}{k_p}\right)^{n_T}$. Current bounds from the CMB are $r_T \lesssim 0.12$ at 95% CL from the Planck collaboration [34]. In this work, we shall derive a *consistency relation* for the squeezed bispectrum of the cross-correlation of a long mode of the temperature perturbation and two polarization modes.

In single field inflation, the perturbations are referred to as *adiabatic* as any perturbation is equally shared among all quantities $H\delta t = H\delta X/\dot{X}$ for all quantities X. This is the case for the pressure and density $\frac{\delta\rho}{\dot{\rho}} = \frac{\delta P}{\dot{P}}$ which implies that $P = P(\rho)$, hence the name *adiabatic*. Instead, if more than one field is involved, perturbations are called *isocurvature* perturbations. This is the case in the *curvaton* scenario [36, 37, 38]. One assumes the existence of a second field σ (the curvaton) which has negligible contribution to the energy density during inflation. In addition, one assumes that its interactions with the inflaton are small and that it evolves in a potential $V(\sigma)$. Well after the end of inflation, the field oscillates in the potential and decays into radiation. The pressure of the mix of the curvaton and the radiation is *not* adiabatic. At that moment, the curvature perturbation on large scales is generated as it obeys the equation of motion

$$\zeta' = -\frac{\mathcal{H}}{\rho + P}\delta P_{\rm nad} \tag{1.2.7}$$

where $P_{\rm nad}$ is the non-adiabatic pressure. This will have consequences in terms of the properties of the non-Gaussianities of the perturbations as it will be made clear in section 1.4.

Detecting a possible primordial source of NG in the cosmological perturbations is one of the main targets of current and future experiments measuring the properties of the CMB anisotropies and of the large-scale structure. Indeed, measuring a certain level of NG in the three-point (bispectrum) and four-point (trispectrum) correlator of the perturbations opens up a unique window into the physics of inflation. This is because the different mechanisms giving rise to the inflationary perturbations correspond to specific shapes of bispectra. These include models with higher-derivative interactions, multi-field models such as the curvaton mechanism explained above (see section 1.4), and models with non-standard vacuum produce large NG. Any detection of NG would eliminate a whole class of inflation models, namely all standard slow-roll single-field models [6, 7].

The bispectra they produce have a specific dependence F on the momenta k_1, k_2, k_3, called the

shape, which depends on the model.

$$\langle \zeta_{\vec{k}_1} \zeta_{\vec{k}_2} \zeta_{\vec{k}_3} \rangle = (2\pi)^3 \delta_D(\vec{k}_1 + \vec{k}_2 + \vec{k}_3) f_{\rm NL} F(k_1, k_2, k_3). \tag{1.2.8}$$

One usually considers three basic *shapes* which cover most models, possibly through combinations, called *local*, *equilateral* and *orthogonal* defined in appendix B.

The simplest model of NG is called *local*. In this model, one expresses the curvature perturbation ζ in terms of a Gaussian field ζ_g with a quadratic term[2]

$$\zeta(\vec{x}) = \zeta_g(\vec{x}) + \frac{3}{5} f_{\rm NL}^{loc} \left(\zeta_g(\vec{x})^2 - \langle \zeta_g(\vec{x}) \rangle \right). \tag{1.2.9}$$

The resulting field is non-Gaussian and leads in particular to a non-vanishing *bispectrum*, the Fourier transform of the three-point function

$$\begin{aligned} \langle \zeta_{\vec{k}_1} \zeta_{\vec{k}_2} \zeta_{\vec{k}_3} \rangle = (2\pi)^3 \delta_D(\vec{k}_1 + \vec{k}_2 + \vec{k}_3) \frac{5}{6} f_{\rm NL}^{local} \\ \times \left(P_{\zeta_g}(k_1) P_{\zeta_g}(k_2) + P_{\zeta_g}(k_2) P_{\zeta_g}(k_3) + P_{\zeta_g}(k_1) P_{\zeta_g}(k_3) \right). \end{aligned} \tag{1.2.10}$$

The final set of data gathered by the Planck satellite collaboration, released in 2015 [39], provides, so far, the most stringent constraint on the level of non-Gaussianities. They are

$$f_{\rm NL}^{loc} = 0.8 \pm 5.0, \tag{1.2.11}$$

$$f_{\rm NL}^{eq} = -4 \pm 43, \tag{1.2.12}$$

$$f_{\rm NL}^{orth} = -26 \pm 21, \tag{1.2.13}$$

when combining both temperature anisotropy and polarization data. These constraints are believed to be the best ones physically obtainable from CMB.

Improvement is instead expected to come from large-scale structure data through the statistical properties of the clustering of galaxies. This has been identified to be a powerful probe of NG in the local case thanks to the fact that NG introduces a *scale-dependent bias* between the power spectra of halos and dark matter [40, 41]. Indeed, in the local model, the gravitational potential is sourced by a quadratic term $\Phi \propto f_{\rm NL}^{\rm loc} \Phi_G^2$. Expressing the matter power spectrum in perturbation theory valid on large scales, this gives rise to the following scaling $P \propto (\Phi \delta^{(1)})(\delta^{(1)} \delta^{(1)}) \propto (1/k^2)(\delta^{(1)} \delta^{(1)})(\delta^{(1)} \delta^{(1)})$. This is an extra factor of $1/k^2$ compared to the Gaussian contribution to the power spectrum. It is

[2] the $\frac{3}{5}$ factor comes from historical reasons as this model was first written in terms of the gravitational potential during matter domination related to ζ by $\Phi_{\rm P} = \frac{3}{5}\zeta$ which corresponds to the gravitational potential super-horizon scales in matter domination.

also believed that measurement of the bispectrum of galaxies will improve constraints on all types of NG.

Other observables like the 21 cm emission of hydrogen will potentially allow to probe higher redshifts than LSS [42, 43] and possibly put better contraints on NG, but foreground emission from galactic and extragalactic sources are still very challenging. Let me also mention that CMB *spectral distortions*, which will be probed by the PIXIE experiment [44] for example, can also constraint primordial NG [45, 46].

We shall however concentrate on the LSS in this work, for which the hope is to reach sensitivity of order $f_{\rm NL} \sim \mathcal{O}(1)$. The modelling of LSS poses however many challenges before the excepted constraints on primordial NG can be reached. These are presented in the next section.

1.3 The large-scale structure of the Universe

Since the discovery of the cosmic microwave background in 1964 [47], most of cosmology was dedicated to its study. The energy and the polarization of these photons provide us with information about the physics of the early universe. Because perturbations in the temperature of the photons are extremely small, of the order of 10^{-5}, they are very suitable for a description by perturbation theory. In particular, the perturbations in the CMB can be related *linearly* to the initial power spectrum generated by inflation. As the CMB is defined on a sphere of constant redshift, one describes its anisotropies through their angular power spectrum

$$C_\ell = \frac{2}{\pi} \int k^2 \mathrm{d}k P_\zeta(k) T(k)^2 j_l(kr)^2 \tag{1.3.1}$$

where the transfer function T depends on the physics taking place in the photon-baryon plasma, r is the comoving distance to the CMB. The relative simplicity of the theoretical treatment of the CMB together with the fact that it is a very "clean" probe (in the sense that photons travel almost unperturbed since their emission) explains why much of the early work has been focused on exploiting the CMB to test predictions of the ΛCDM model.

However, observation of the large-scale structure is thought to be the next big source of cosmological data. Indeed, the CMB gives us information mostly[3] about a fixed time in the past: the time of emission of the last scattering surface, a two dimensional observable. In contrast, the large-scale structure consists in the galaxies all around us *and* at different redshifts, up to $z \simeq 3$ depending on the performance of the instruments. The LSS potentially contains more information as the number of modes at our disposal increases like the cube of the maximum k that we are able to exploit. Many LSS surveys are on-going or planned in the coming decade such as BOSS [48], DES [49], LSST [50, 51], Dark Energy Spectroscopic Instrument (DESI) [52], the Wide-Field InfraRed Survey Telescope (WFIRST) [53], and Euclid [54, 55]. The trend to cover progressively a larger fraction of the sky and deeper redshift range will continue in the future, providing an unprecedented amount of data. This explains the need for a better understanding and description of the LSS. We believe that tools

[3] One also obtains some information about the matter density distribution between the last scattering through the ISW-lensing effect and lensing.

such as the *consistency relations* and studies presented in this thesis contributes to this objective.

Contrarily to the CMB, the LSS poses several challenges when one wants to connect the observables to the underlying fundamental physics. This complicates, limits or even prevents an analytical description of the LSS. The main obstacles are the following:

- The gravitational interactions governing the matter distribution are non-linear and the matter distribution is non-linear at late time and /or on small scales.
- One does not observe the matter distribution directly but only light-emitting objects such as galaxies.
- The observed quantities are the redshift and the angular position of each galaxy, while the models describing the matter distribution or inflation are best solved in Fourier-space.

A good approximation to structure formation is to treat matter one large-scales as a self-gravitating fluid characterized by its overdensity contrast $\delta = (\rho(\vec{x},\tau)/\overline{\rho} - 1)$ over the mean matter density $\overline{\rho}$ and its velocity perturbations $\vec{v}$ evolving under gravity [56]. On scales small compared to the horizon $k \gg \mathcal{H}$, this can be accomplished by a Newtonian treatment. The fluid equations are the continuity, Euler and Poisson equations, which read in conformal time τ:

$$\frac{\partial\delta(\vec{x},\tau)}{\partial\tau} + \vec{\nabla}\cdot[(1+\delta(\vec{x},\tau))\vec{v}(\vec{x},\tau)] = 0, \tag{1.3.2}$$

$$\frac{\partial\vec{v}(\vec{x},\tau)}{\partial\tau} + \mathcal{H}(\tau)\vec{v}(\vec{x},\tau) + [\vec{v}(\vec{x},\tau)\cdot\vec{\nabla}]\vec{v}(\vec{x},\tau) = -\vec{\nabla}\Phi(\vec{x},\tau), \tag{1.3.3}$$

$$\nabla^2\Phi(\vec{x},\tau) = \frac{3}{2}\Omega_{\rm m}\mathcal{H}^2(\tau)\delta(\vec{x},\tau), \tag{1.3.4}$$

where $\mathcal{H}$ the comoving Hubble radius, and Φ the Newtonian gravitational potential. Finally $\Omega_{\rm m} = 8\pi G\bar{\rho}a^2/3\mathcal{H}^2$ is the density parameter. Note that these equations assume the stress tensor of the dark matter fluid to be negligible. This approximation corresponds to single coherent flow of the particles. It breaks down on very small scales because of the presence of multiple streams, called *shell-crossing*, which generate velocity dispersion.

These equations contain non-linear interactions which make them difficult to solve. There are two general methods in making predictions from these equations: numerical and analytical methods. Among the analytical approaches which we shall use in this thesis is the standard perturbation theory (SPT) [56]. It consists on an expansion of the non linear solution δ_{NL} in powers of the linear one $\delta^{(1)}$. By increasing the number of terms in the expansion one hopes to increase the reach of the theory to midly non-linear scales $k \sim 0.1\ h/Mpc$. This approach poses however some problems for different types of universes as divergences can arise. Other perturbative approaches such as RPT [57], EFT [58] or iPT [59] try to answer these problems with relative success. In any case, however, one cannot hope to describe the fully non-linear regime with a perturbative treatment. Non-perturbative approaches such as the *halo model* [60] may provide a good description of matter clustering on small scales but have the disadvantage of not being derived from first principles.

For accurate predictions, one usually resorts to numerical simulations. They are however extremely computationally demanding, in particular when one desires to make parameter estimations for upcoming surveys. This indeed requires to have hundreds of power spectra with various values of the cosmological parameter, in which we include the non-Gaussian parameters which will mainly interest us.

The bias problem stems from the fact that one does not observe the dark matter distribution directly but only light-emitting objects like galaxies. The relation between the galaxy distribution δ_g and the dark matter distribution δ is called the *bias*. On very large scales $k/\mathcal{H} \sim 1$, linear bias $\delta_g = b_1\delta_m$ provides a good description. A simple bias model is the local Eulerian bias. It reads up to second order

$$\delta_g(\tau, \vec{x}) = b_1\delta(\tau, \vec{x}) + b_2\delta^2(\tau, \vec{x}). \tag{1.3.5}$$

The particularity is that the galaxy distribution depends only on the matter density at the same location. Because of the non-linear gravitational evolution, one expects that all the terms allowed by the symmetries of the system are generated. One generally considers the *non-local* bias expansion [61, 62], written symbolically as

$$\delta_g(\tau, \vec{x}) = f\left(\delta(\tau, \vec{x}), \partial_i v_j(\tau, \vec{x}), \partial_i\partial_j\Phi, ...\right). \tag{1.3.6}$$

where any rotational invariant term which is at least two derivatives in the gravitational potential is allowed. We shall show how theses terms can be understood in terms of the symmetries of equations (1.3.2)-(1.3.4). The idea is very simple: the terms appearing in the bias expansion need to transform in the same way as δ_g under the symmetries.

Although some bias models provide a good description of the galaxy distribution, none can achieve the level of agreement on all relevant scales as what has been achieved with the CMB.

There is a final complication when one wants to compare the predictions of theories with observations. One does not observe a time slice of the whole Universe but instead our (perturbed) past light-cone. More precisely, galaxy surveys measure the directions $\hat{n}$ of galaxies and their redshifts z. This is in contrast with Fourier space where inflation models, structure formation, and bias models are developed. Both the redshift and the angle are affected by the presence of matter perturbations at the location of the galaxy and between the observer and the galaxy.

The first correction to include is the *redshift space distortions* (RSD). This implements the fact that the peculiar velocity of the galaxy affects the perceived redshift. This was first derived by Kaiser [63] in the linear regime and one obtains at linear order

$$\delta_s(\vec{k}) = \left[1 + f(\hat{n}\cdot\hat{k})^2\right]\delta(\vec{k}), \tag{1.3.7}$$

where $f = \frac{a}{D}\frac{\mathrm{d}D}{\mathrm{d}a}$ is the derivative of the linear growth factor D and $\hat{n}$ is the radial unit vector pointing to the center of the galaxy of interest.

A more complete treatment consists in using directly the quantity that galaxy surveys measure:

the number of galaxies in a direction $\hat{n}$ at redshift z within solid angle $\mathrm{d}\Omega$ and redshift interval $\mathrm{d}z$: $N(\hat{n}, z)\mathrm{d}\Omega$. The perturbations are then the *galaxy number counts overdensity*

$$\Delta_g(\hat{n}, z) \equiv \frac{N(\hat{n}, z) - \langle N \rangle(z)}{\langle N \rangle(z)} \tag{1.3.8}$$

where $\langle\rangle$ is the average over the angle at fixed redshift. Decomposing the angle $\hat{n}$ in spherical harmonics leads to a gauge invariant prediction for the linear (angular) power spectrum of galaxies which has been computed in [20, 64, 65, 66]. This decomposition is also referred to as $z\ell m$-space. These corrections are particularly important on the largest scales, where k starts to become of the same order as $\mathcal{H}$. This is of particular relevance as the increasing size of the LSS surveys gives us access to scales ever closer to the horizon scale where $k \sim \mathcal{H}$.

Computing the bispectrum of galaxy number counts in perturbation theory is a much harder task as it requires the handling of second-order expressions for the number counts which are very cumbersome. Three groups [67, 68, 19] have been working on the subject in recent years and comparing the expressions obtained from the different formalisms is already a colossal task.

This explains the need for better analytical descriptions of the large-scale structure. The next section is dedicated to the introduction of the concept of *consistency relations*. They can be of great use as they are analytical relations involving the *non-linear* power spectra thereby greatly extending the amount of exploitable data. We shall present how this idea can be applied to the galaxy number counts. This enables the computation of the so-called *squeezed limit* of the bispectrum using linear expressions *without* having to involve the full second-order computation.

1.4 Consistency relations

The idea of consistency relation, that we shall apply to CMB polarization and the LSS, has three main advantages:

- It potentially allows to exploit data in the non-linear regime, thereby extending the range of usual perturbative approaches
- It can be used as a consistency check for perturbative computations or bias or structure models such as the halo model, non-local bias and perturbative approaches
- If tested against observations, a violation could be a sign of modified gravity

Let me explain the idea in the case of the bispectrum of curvature perturbation. The bispectrum consists in the expectation value for the correlation of three modes $\zeta_{k_1}, \zeta_{k_2}, \zeta_{k_3}$. This can be written symbolically as

$$\begin{aligned}\langle \zeta_{k_1}\zeta_{k_2}\zeta_{k_3}\rangle &= \int P[\zeta_{k_1}, \zeta_{k_2}, \zeta_{k_3}]\zeta_{k_1}\zeta_{k_2}\zeta_{k_3} \\ &= \int P[\zeta_{k_1}]P[\zeta_{k_1}, \zeta_{k_2} \mid \zeta_{k_1}]\zeta_{k_1}\zeta_{k_2}\zeta_{k_3}\end{aligned}$$

$$= \langle \zeta_{k_1} \langle \zeta_{k_2} \zeta_{k_3} \rangle_{\zeta_{k_1}} \rangle \tag{1.4.1}$$

where the expectation value is written as the integral of all the values that the ζ's can take times their probability P. The second line expresses it as a conditional probability. The three-point function is therefore a modulation of the two point function *in presence of the third mode*[4] $\langle \zeta_{k_2} \zeta_{k_3} \rangle_{\zeta_{k_1}}$. In general, one it is very complicated to compute the effect of the mode ζ_{k_1} on the two-point function. However, in the squeezed limit where $k_1 \ll k_2 \simeq k_3$, it is simple. During inflation, the long mode $\zeta_L \equiv \zeta_{k_1}$ exits the horizon first and becomes constant in time. The fluctuations with short wavelength $k_S \equiv k_2 = k_3$ therefore see a metric

$$ds^2 = -dt^2 + a(t)^2 e^{-2\zeta_L} d\vec{x}^2. \tag{1.4.2}$$

Because $k_1 \to 0$, ζ_L can be approximated to be constant in space and its presence is therefore equivalent to a rescaling of the coordinates

$$\vec{x} \to e^{-\zeta_L} \vec{x}. \tag{1.4.3}$$

Writing the real space transformation $\zeta(\vec{x}) \to \zeta(e^{-\zeta_L}\vec{x})$ in terms of the Fourier transform tells how the Fourier modes transform :

$$\zeta_{k_S} \to e^{3\zeta_L} \zeta_{e^{\zeta_L} k_S}. \tag{1.4.4}$$

Applying this transformation on the two-point function (1.2.3), (1.2.4) at linear order in ζ_L leads to

$$\begin{aligned} \langle \zeta_{\vec{k}_2'} \zeta_{\vec{k}_3'} \rangle &= e^{6\zeta_L} (2\pi)^3 \delta_D^{(3)}(e^{\zeta_L}\vec{k}_2 + e^{\zeta_L}\vec{k}_3) \frac{A}{(e^{\zeta_L}k)^3} \left(\frac{e^{\zeta_L}k}{k_*} \right)^{n_s - 1} \\ &\simeq \langle \zeta_{\vec{k}_2} \zeta_{\vec{k}_3} \rangle \left(1 + (n_s - 1)\zeta_L\right) \end{aligned} \tag{1.4.5}$$

Finally, correlating this two point function with another ζ_L and taking the expectation value leads to the squeezed bispectrum

$$\begin{aligned} \lim_{k_1 \to 0} \langle \zeta_{k_1} \zeta_{k_2} \zeta_{k_3} \rangle &= \langle \zeta_{k_1} \langle \zeta_{\vec{k}_2'} \zeta_{\vec{k}_3'} \rangle_{\zeta_{k_1}} \rangle \\ &\simeq (2\pi)^3 \delta^{(3)}(\vec{k}_1 + \vec{k}_2 + \vec{k}_3)(n_s - 1) P_\zeta(k_1) P_\zeta(k_2). \end{aligned} \tag{1.4.6}$$

This relation was first introduced in [7] and shown to be more general in [12]. It implies that all single-field slow-roll models of inflation generate a negligible amount of local NG.

[4] I thank Jorge Noreña for helping me understand this point in this way.

One now understands why in the curvaton mechanism, large NG can be produced: the perturbations are generated long after Hubble crossing and the curvature perturbation is not constant on large-scales in presence of non-adiabatic pressure. A long mode perturbation no longer acts as a rescaling on the short modes as it is not frozen while the short modes of perturbations are being generated.

The smallness of the 3-pt function can be understood as a consequence of the (approximate) symmetries of the inflationary phase. A perfect de Sitter universe is invariant under spatial dilations $\vec{x} \to \lambda\vec{x}$. The derivation above corresponds to $\lambda = e^{-\zeta_L}$. This imposes the 2-point function to be scale invariant [69], $n_s - 1 = 0$ and therefore the 3-pt function to be zero. In the real universe, inflation ends and it is not a perfect de Sitter phase. The 2-pt function is slightly scale dependent parametrised by $n_s - 1$ which leads to the *almost* zero squeezed 3-pt function (1.4.6).

This method can also be applied to any higher order correlation functions, linking the squeezed limit of an $(N+1)$-point function to an N-point one. Consistency relations for primordial perturbations have been extensively studied and generalized to include the long mode up to constant gradient [7, 6, 12, 13, 14, 15, 16, 17] . This method can be applied for any observables for which we have a way of computing the effect of a long mode on the two-point function. It has been succefully applied to correlation functions involving actual observables like the CMB temperature anisotropy [70, 71, 72, 73, 74]. Computing the actual observed level of NG from standard inflation is important in order not to confuse it with other sources of NG. Indeed, other effects such as the ISW-lensing effect is a major contamination and produce a large level of local NG in the observed bispectrum [75, 76]. This has to be subtracted from the measured level in order to reveal the amount of *primordial* NG. It this work, we shall present a similar calculation for the CMB polarization and for the observed galaxy numbers count bispectrum. As with the CMB, these contributions must be subtracted from any observation to estimate the level of primordial NG. We shall also generalize the consistency relation for the matter perturbations to include the long mode up to a second derivative in a special case.

Consistency relations in the context of the LSS have been pioneered by [77, 78] using the symmetries of the Newtonian equaions of motion and generalised to the relativistic limit in [79]. Extensive work has since been made [80, 9, 81, 82, 83, 84, 85, 86]. We present the idea of the approach presented in [77] which is particularly simple. It's based on the fact that the fluid equations (1.3.2)-(1.3.4) possess some symmetries under which the velocity perturbation transforms non-linearly. For a ΛCDM cosmology, one shows that the change of coordinates

$$\tau' = \tau, \quad \vec{x}' = \vec{x} + \vec{n}(\tau), \tag{1.4.7}$$

for a generic vector $\vec{n}(\tau)$ is a symmetry of the equations (1.3.2)-(1.3.4) provided that the fields transform as

$$\delta'(\vec{x}, \tau) = \delta(\vec{x}', \tau'), \tag{1.4.8}$$

$$\vec{v}'(\vec{x}, \tau) = \vec{v}(\vec{x}', \tau') - \dot{\vec{n}}(\tau), \tag{1.4.9}$$

$$\Phi'(\vec{x},\tau) = \Phi(\vec{x}',\tau') - \left(\mathcal{H}\dot{\vec{n}}(\tau) + \ddot{\vec{n}}(\tau)\right)\cdot\vec{x}. \tag{1.4.10}$$

Using the relations

$$\frac{\partial}{\partial\tau} = \frac{\partial}{\partial\tau'} + \dot{\vec{n}}\cdot\nabla', \qquad \nabla = \nabla', \tag{1.4.11}$$

which implies that the operator

$$D_\tau \equiv \frac{\partial}{\partial\tau} + \vec{v}(\vec{x},\tau)\cdot\nabla \tag{1.4.12}$$

is invariant, it is easy to see that equations (1.3.2)-(1.3.4) are indeed invariant under this transformation. Because this symmetry is exact at the level of the fluid equations it is valid for its true, fully non-linear solution[5]. This means that it is possible to generate a constant gradient of the gravitational potential $\Phi \supset \vec{x}\cdot(\nabla\Phi)(\vec{0})$, or equivalently a long mode of the velocity perturbation $\vec{v}_L(\tau,\vec{0})$, through a change of coordinates by choosing properly the vector $\vec{n}(\tau)$:

$$\vec{n}(\tau) = -\int^\tau \mathrm{d}\eta\, \vec{v}_L(\eta,\vec{0}) + \mathcal{O}(qRv_L^2), \tag{1.4.13}$$

where q is the momentum of the long wavelength mode and R is the size of the patch where the long mode is approximated by a gradient. Note that although we have shown that this symmetry is true at the level of the fluid equations, it can be shown that it is in fact also valid at the level of the Boltzmann equation, this is for the phase-space distribution function of the particles [87].

The correlator of the short wavelength density modes in the background of the long wavelength mode perturbation is therefore given by a change of coordinates [77] :

$$\Big\langle \delta(\tau_1,\vec{x}_1)\delta(\tau_2,\vec{x}_2)\cdots\delta(\tau_n,\vec{x}_n)\Big\rangle_{v_L} = \Big\langle \delta(\tau_1',\vec{x}_1')\delta(\tau_2',\vec{x}_2')\cdots\delta(\tau_n',\vec{x}_n')\Big\rangle. \tag{1.4.14}$$

Note that here the points are supposed to be contained in a sphere of radius R much smaller than the long wavelength mode of size $\sim 1/q$ and centred at the origin of the coordinates.

The variation of the n-point correlator under the infinitesimal transformation is given in momentum space by

$$\delta_n\Big\langle \delta(\tau_1,\vec{x}_1)\cdots\delta(\tau_n,\vec{x}_n)\Big\rangle = \int \frac{\mathrm{d}^3\vec{k}_1}{(2\pi)^3}\cdots\frac{\mathrm{d}^3\vec{k}_n}{(2\pi)^3}\Big\langle \delta(\vec{k}_1,\tau_1)\cdots\delta(\vec{k}_n,\tau_n)\Big\rangle$$
$$\times\sum_{a=1}^{n}\delta x_a^i(ik_a^i)e^{i(\vec{k}_1\cdot\vec{x}_1+\cdots\vec{k}_n\cdot\vec{x}_n)}$$

[5] By non-linear, we mean down to scales where the fluid description is valid, that is as long as there is no shell-crossing.

$$= \int \frac{\mathrm{d}^3\vec{k}_1}{(2\pi)^3}\cdots\frac{\mathrm{d}^3\vec{k}_n}{(2\pi)^3}\Big\langle \delta(\vec{k}_1,\tau_1)\cdots\delta(\vec{k}_n,\tau_n)\Big\rangle$$

$$\times\sum_{a=1}^{n} n^i(\tau_a)(ik_a^i)e^{i(\vec{k}_1\cdot\vec{x}_1+\cdots\vec{k}_n\cdot\vec{x}_n)}. \tag{1.4.15}$$

The squeezed n-pt function is then deduced by correlating with another long mode $\delta(\vec{q},\tau)$

$$\Big\langle \delta(\vec{q},\tau)\delta(\vec{k}_1,\tau_1)\cdots\delta(\vec{k}_n,\tau_n)\Big\rangle_{q\to 0}$$

$$= \Big\langle \delta(\vec{q},\tau)\Big\langle \delta(\vec{k}_1,\tau_1)\cdots\delta(\vec{k}_n,\tau_n)\Big\rangle_{v_L}\Big\rangle$$

$$= i\sum_{a=1}^{n}\Big\langle \delta(\vec{q},\tau)n^i(\tau_a)\Big\rangle k_a^i\Big\langle \delta(\vec{k}_1,\tau_1)\cdots\delta(\vec{k}_n,\tau_n)\Big\rangle. \tag{1.4.16}$$

Finally we use the linear relation between the velocity and density $\int^\tau \mathrm{d}\eta\,\vec{v}_L(\vec{q},\eta) = i\frac{\vec{q}}{q^2}\delta_L(\vec{q},\tau)$ to obtain [77, 78, 79]

$$\Big\langle \delta(\vec{q},\tau)\delta(\vec{k}_1,\tau_1)\cdots\delta(\vec{k}_n,\tau_n)\Big\rangle'_{q\to 0} = -P_L(q,\tau)$$

$$\times\sum_{a=1}^{n}\frac{D(\tau_a)}{D(\tau)}\frac{\vec{q}\cdot\vec{k}_a}{q^2}\Big\langle \delta(\vec{k}_1,\tau_1)\cdots\delta(\vec{k}_n,t_n)\Big\rangle', \tag{1.4.17}$$

where the primes indicate that one should remove the Dirac delta coming from the momentum conservation, P_L is the linear matter power spectrum and D is the linear growth factor. In particular, the squeezed bispectrum is found to be

$$\lim_{k_1\to 0}\langle\delta(\vec{k}_1,\tau_1)\delta(\vec{k}_2,\tau_2)\delta(\vec{k}_3,\tau_3)\rangle' =$$

$$P(k_1,\tau_1)\left(\frac{D_1(\tau_2)}{D_1(\tau_1)}-\frac{D_1(\tau_3)}{D_1(\tau_1)}\right)\frac{\vec{k}_1\cdot\vec{k}_2}{k_1^2}\langle\delta(\vec{k}_2,\tau_2)\delta(\vec{k}_3,\tau_3)\rangle' + \mathcal{O}\left(\frac{k_1}{k_2}\right)^2, \tag{1.4.18}$$

where the modes $\delta(k_2)$, $\delta(k_3)$ can be non-linear. The important feature of this relation is that, in Fourier space, the squeezed bispectrum of matter is zero at equal times up to terms of order $(k_{short}/k_{long})^2$. This is an expected consequence as a constant gradient of the gravitational potential should not have any physical consequence on the short modes. Moreover, galaxies can also be modelled by analogous fluid equations and therefore also possess a consistency relation, which we derive in

section 3.2. Using both consistency relations, we shall show that, at the perturbative level, the Eulerian local bias model satisfies the galaxy consistency relation for the bispectrum if the dark matter does.

We shall also show that a violation of this relation could be a sign of modified gravity. We consider the situation where the fifth force depends on the location : it can be either present or not depending on the density of the environment which is called *screening mechanism*. Correlating galaxies situated in the two types of environment, it is then no longer possible to make a unique change of coordinate that removes the fifth force everywhere, violating the consistency relation.

One does not expect the generation of a gravitational potential which contains two gradients $\Phi \supset \vec{x}^2(\nabla^2\Phi)(\vec{0})$ to be equivalent to a simple coordinate transformation. It was however shown that a constant isotropic mode quadratic in the potential is equivalent to adding curvature which can be used to compute the effect of such a mode on the two-point function. We shall use this to derive a consistency relation which does not vanish at equal times. This will be used to show that the halo model does satisfy this relation to which re-enforces the legitimacy of this model. These relations were also derived by [83].

Finally, we shall derive a fully relativistic version of the consistency condition making use of the linear relations for the galaxy number counts. For this derivation, we shall use the relativistic derivation of the consistency relation of [79] which makes use of the fact that a long wavelength mode solution of the equation of motions for the Bardeen potentials is equivalent to a residual gauge transformation. The presence of the long mode induces several effects on the galaxy number counts overdensity $\Delta_g(\hat{n}, z)$: It changes the redshfit and the angle under which one sees the galaxy as well as the observed volume $d\Omega dz$, the luminosity distance considering that surveys are flux limited and redefines the mean number counts density. We then decompose the result in spherical harmonics to obtain the bispectrum of galaxy number counts in zlm-space. The derivation above includes the effect of the long mode on the short ones up to a constant gradient. This produces terms which have the same ℓ dependence as the local template in the squeezed limit and could therefore be mistaken for a sign of local primordial NG. We first provide a naive estimate of the resulting $f_{\rm NL}^{\rm loc}$. We then proceed to a finer analysis where we estimate the contamination to the local and equilateral shape from different terms derived in from second order number counts [18, 19]. We also confirm the level of contamination to the local shape resulting from the terms derived using the consistency condition. We find that these give a contamination of $f_{\rm NL}^{\rm loc} \sim -2$ at $z = 0.55$ while terms with different scalings are sub-dominant with contamination of $f_{\rm NL}^{\rm loc} \sim 0.5$.

1.5 Structure of the dissertation

This dissertation is organized as follows:

The first two chapters are dedicated to the consistency relation for the matter and galaxy overdensity and their consequences. In chapter 2, we extend previous studies by considering the effect of a long mode up to a second gradient. Using an approximate symmetry we are able to derive an expression for the angular averaged squeezed bispectrum at equal times. Because a second derivative of the gravitational potential corresponds to a physical mode, this bispectrum does not vanish. As an example we check that the halo model satisfies this relation-

In chapter 3, we present how the symmetries of the fluid equations, which describe the matter distribution, can help understand the terms appearing in the non-local bias expansion. Secondly, we show that the local Eulerian bias model satisfies the consistency condition for galaxies in perturbation theory. Thirdly, we study a toy model of modified gravity and show how a violation of the consistency relations can be seen either as a violation of the equivalence principle or as a signature of modified gravity. As a step towards observed quantities, we derive the consistency relations in redshift space.

The following two chapters are dedicated to the application of consistency conditions to the observed galaxy number counts and their consequences for the non-Gaussianity induced from relativistic effects. In chapter 4, we apply the formalism of the consistency relations directly to the galaxy number counts per solid angle per redshift bin. We find that contrarily to Fourier space, the bispectrum in squeezed configurations does not vanish due to so-called 'projection effects'.

In chapter 5, we present an application of the observed consistency relations together with a study of non-Gaussianities in zlm-space. We show that relativistic corrections to the matter power spectrum have to be taken into account if one hopes to access to primordial non-Gaussianities in the large-scale structure. We find that a contamination of order $f_{\rm NL} \sim -3$ is given to the bispectrum in the squeezed limit through a simple estimate. Secondly, we have developed a way to compute the different non-Gaussian shapes, defined in Fourier space, in zlm space. This is particularly computationally demanding as techniques used for the CMB are not applicable. We show that these shapes are not well separated in zlm space and that higher order terms in the bispectrum can give a contribution to the value of $f_{\rm NL}$ relevant for the analysis of data from future surveys. In particular, in the local shape, the terms derived from the consistency relation are the dominant ones. For the equilateral shape, second-order terms of the type "Newtonian $\times$ lensing" and "three derivatives" give a large contribution.

Finally, in chapter 6, we present a derivation of the consistency relation for the polarization modes of the CMB. We consider the effect on a long temperature mode on two short polarization modes. This consistency relation is a tool which will help understand possible primordial gravitational waves signatures in the CMB. This can possibly help distinguishing them from galactic dust in the upcoming polarization data. We also estimate the detectability of such effect for three proposed experiments.

Chapter 2

Equal-time consistency relations for the dark matter

2.1 Dark matter consistency relations from a constant gradient

The consistency relations (1.4.17) have been derived considering the effect of a mode of the gravitational potential up to a constant gradient $\Phi \propto \vec{x} \cdot (\vec{\nabla}\Phi)(\vec{0})$. This corresponds to a change of frame for the matter (δ) or galaxy perturbations (δ_g) where one adds or remove a homogeneous gravitational force. It has therefore locally no physical effect on the short modes correlations functions. As a consequence, the squeezed bispectrum of dark matter or galaxies vanishes at equal time.

In this chapter, which builds up on previous works [88, 89], we discuss what happens if we include two spatial gradients in the game, that is a non-uniform gravitational force. Based on the previous arguments, we expect that the equal-time correlators will not vanish in the soft limit, as short-scale perturbations will now feel the non-homogeneity of the gravitational force. Indeed, we shall find a consistency relation for the soft limit of the dark matter correlators which is valid even for non-linear scales and that can be checked against analytical models modelling the clustering of dark matter on short scales.

The chapter is organized as follows. In section 2.2 we discuss the derivation of the equal-time consistency relation, while in section 2.3 we check it against the halo model. Finally, in section 2.4 we provide our conclusions.

2.2 The equal-time consistency relation for the dark matter bispectrum

It is well-known that the effect of a long wavelength mode of the gravitational potential of momentum q and including two spatial gradients on the short-scale dynamics is encodable in a local spatial curvature $K = (3/5)(\delta_L/a)$ (valid in a matter-dominated universe and after performing an angular average), where δ_L is the linear overdensity [88]. In other words, the physics in a sphere of radius $R \ll 1/q$ should not be distinguishable from the physics with the same curvature as the one induced by the linear mode. To account for the effects of the long wavelength mode there are three effects one

should take into account. First of all, the change in scales with respect to the case in which the local system is spatially flat. As the overdensity in the sphere is simply given by

$$1+\delta_L = \frac{a^3}{a_K^3}, \tag{2.2.1}$$

where we have indicated by a the scale factor in the region outside the sphere of radius R and by a_K the one in the inner region, one simply gets $a/a_K \simeq (1+\delta_L/3)$. This means that comoving momenta are shifted from $\vec{k}$ in the spatially flat outer region to $\vec{k}(1-\delta_L/3)$ in the inner region.

The second effect is that we have to define the short-mode overdensities with respect to the global average $\overline{\rho}$ and not with respect to the local overdensity $\overline{\rho}(1+\delta_L)$. This brings an extra factor $(1+\delta_L)$ for each density contrast on short scales. Finally, we have to account for the fact that one may trade the time variable of the correlators with the linear growth factor $D(a)$ if no other time dependencies are present in the problem. This is true if $\mathrm{d}\ln D(a)/\mathrm{d}\ln a = \Omega_{\mathrm{m}}^{1/2}$ (being Ω_{m} the abundance of dark matter with respect to the critical one) which is the condition leading to separability between the density contrast and the peculiar velocity at any order in standard perturbation theory [56]. While not exactly true, the mapping between time and the linear growth factor is good at the $\mathcal{O}(10\%)$ level for most redshifts [90]. It turns out that in a spatially local closed universe the linear growth factor is enhanced by a factor $(1+13/21\delta_L)$ with respect to the spatially flat case [88]. This is because in a spatially closed universe linear perturbations growth faster than their flat region counterparts if the curvature is positve.

All in all, the dark matter correlation functions on small scales depend on the long wavelength mode as

$$\begin{aligned}\xi_{\delta_L}(r,a) \simeq\ & \xi_0(r,a) \\ & + 2\delta_L \xi_0(r,a) \\ & + \frac{1}{3}\delta_L\, r\, \frac{\partial}{\partial r}\xi_0(r,a) \\ & + \frac{13}{21}\delta_L\, \frac{\partial}{\partial \ln D(a)}\xi_0(r,a) + \mathcal{O}(\delta_L^2).\end{aligned} \tag{2.2.2}$$

These arguments allow to calculate the soft limit of the three-point correlators of dark matter when the wavenumber q is much smaller than the other two: $k_1 \simeq k_2 \simeq 1/r \gg q$. Indeed, multiplying the result (2.2.2) by the long wavelength mode δ_L, averaging over many realizations and going to momentum space, we obtain

$$\boxed{\begin{aligned}\left\langle \delta_{\vec{q}}(\tau)\delta_{\vec{k}_1}(\tau)\delta_{\vec{k}_2}(\tau)\right\rangle'^{\,\mathrm{av}}_{q\to 0} &= P_L(q,\tau)\\ &\times\left[1-\frac{1}{3}\frac{\partial}{\partial\ln k_1}+\frac{13}{21}\frac{\partial}{\partial\ln D(a)}\right]P(k_1,\tau)\end{aligned}} \tag{2.2.3}$$

where we have used the fact that

$$\int \mathrm{d}^3x\, e^{i\vec{k}\cdot\vec{x}}\, r\,\frac{\partial}{\partial r}\xi_0(r,a)=\left(-3-\frac{\partial}{\partial\ln k}\right)P(k,\tau). \tag{2.2.4}$$

The label $'^{\,\mathrm{av}}$ in the bispectrum indicates we have removed the momentum conservation and that the angular average over the angle between the long and the short wavelength modes needs to be taken: in all our considerations we have assumed a spherical average to be able to define a constant spatial curvature to begin with. As expected, the bispectrum does not vanish in the equal-time correlator. The relation (2.2.3) extends that one found in Ref. [89] which is valid only in the mildly non-linear regime where $P(k_1,\tau)\sim D^2(a)$. Of course, the relation (2.2.3) does not hold in the presence of a primordial non-Gaussianity as the latter introduces an extra correlation among the long and the short wavelength modes.

The generalization of Eq. (2.2.3) to higher-order correlators is straightforward. Taking into account that there is a factor of $(1+\delta_L/3)$ for each position vector and a $(1+13/21\delta_L)$ enhancement of the growth factor with respect to the spatially flat case, we obtain for the equal-time correlator in the long wavelength mode

$$\begin{aligned}\left\langle \delta(\vec{x}_1,\tau)\cdots\delta(\vec{x}_n,\tau)\right\rangle_{\delta_L} &= \left\langle \delta(\vec{x}_1,\tau)\cdots\delta(\vec{x}_n,\tau)\right\rangle_0\\ &+ n\delta_L\left\langle \delta(\vec{x}_1,\tau)\cdots\delta(\vec{x}_n,\tau)\right\rangle_0\\ &+ \frac{1}{3}\delta_L\sum_{i=1}^{n}\vec{x}_i\cdot\nabla_{\vec{x}_i}\left\langle \delta(\vec{x}_1,\tau)\cdots\delta(\vec{x}_n,\tau)\right\rangle_0\\ &+ \frac{13}{21}\delta_L\frac{\partial}{\partial\ln D(a)}\left\langle \delta(\vec{x}_1,\tau)\cdots\delta(\vec{x}_n,\tau)\right\rangle_0.\end{aligned} \tag{2.2.5}$$

Multiplying the above relation by the long wavelength mode and averaging over angles, we obtain the relation

$$\left\langle \delta_{\vec{q}}(\tau)\delta(\vec{k}_1,\tau)\cdots\delta(\vec{k}_n,\tau)\right\rangle^{\rm av}_{q\to 0} = P_L(q,\tau) \times\left[n-\sum_{i=1}^{n}\left(\frac{1}{3}\frac{\partial}{\partial\ln k_i}+1\right)+\frac{13}{21}\frac{\partial}{\partial\ln D(a)}\right]\left\langle\delta(\vec{k}_1,\tau)\cdots\delta(\vec{k}_n,\tau)\right\rangle. \quad (2.2.6)$$

Using the fact that

$$\sum_{i=1}^{n}\frac{\partial}{\partial\ln k_i}\delta(\vec{k}_t) = \vec{k}_t\nabla_{\vec{k}_t}\delta(\vec{k}_t), \quad (2.2.7)$$

where $\vec{k}_t = (\vec{k}_1+\cdots\vec{k}_n)$ as well as the general property $f(x)\delta'(x) = -\delta(x)f'(x)$, we obtain

$$\left\langle \delta_{\vec{q}}(\tau)\delta(\vec{k}_1,\tau)\cdots\delta(\vec{k}_n,\tau)\right\rangle'^{\rm av}_{q\to 0} = P_L(q,\tau) \times\left[1-\sum_{i=1}^{n}\frac{1}{3}\frac{\partial}{\partial\ln k_i}+\frac{13}{21}\frac{\partial}{\partial\ln D(a)}\right]\left\langle\delta(\vec{k}_1,\tau)\cdots\delta(\vec{k}_n,\tau)\right\rangle'. \quad (2.2.8)$$

Notice that all the considerations made so far are valid for the dark matter overdensities, but not for the galaxies as the trade of the time with the linear growth factor is expected not to hold when including further time dependencies as galaxies form at a range of redshifts and merge. Nevertheless, the result (2.2.2) should be useful to test analytical models describing the correlation functions of dark matter, as the halo model [91, 92, 60]. This is what we proceed to do in the following section.

2.3 The equal-time dark matter consistency relation and the halo model

In its simplest formulation, the halo model assumes that all matter in the Universe belongs to dark matter halos, identified by their mass. Therefore, two distinct particles will either belong to the same halo or to two different ones. The power spectrum of density perturbations is the sum of two contributions: the 2-halo term, mainly accounting for the spatial correlations of the distribution of different halos, and the 1-halo term which depends instead on the spatial distribution of matter inside a single halo. Clearly, while the 2-halo term is expected to describe large-scale correlations, the 1-halo term provides predictions in the nonlinear regime. More concretely, the expression for the matter power spectrum is given by

$$P(k) = P_{2h}(k) + P_{1h}(k), \quad (2.3.1)$$

with the 2- and 1-halo contributions given by

$$P_{2h}(k,z) = \frac{1}{\bar{\rho}^2}\left[\prod_{i=1}^{2}\int \mathrm{d}m_i\, n(m_i,z)\,\hat{\rho}(k,m_i,z)\right] P_h(k,m_1,m_2), \tag{2.3.2}$$

$$P_{1h}(k,z) = \frac{1}{\bar{\rho}^2}\int \mathrm{d}m\, n(m,z)\,\hat{\rho}^2(k,m,z), \tag{2.3.3}$$

where $n(m)$ is the halo mass function with $n(m)\mathrm{d}m$ the number density of halos of mass between m and $(m+\mathrm{d}m)$, and $\hat{\rho}(k,m,z)$ is the Fourier transform of the spatial density profile $\rho(z,r,m)$ of a halo of mass m normalized so that $\hat{\rho}(0,m) = m$. The 2-halo term depends as well on the halo power spectrum, $P_h(k,m_1,m_2)$, describing the correlation between the centers of halos of mass m_1 and m_2. As we expect halos to be tracers of the underlying matter distribution, we can assume a linear bias relation between the halo and the matter density contrasts, so that $\delta_h \approx b_1\delta$. Thus, at large scales, the halo power spectrum can be approximated as

$$P_h(k,m_1,m_2) = b_1(m_1)\,b_1(m_2)P_L(k), \tag{2.3.4}$$

where $b_1(m)$ represents the linear bias function for halos of mass m. Note that for Gaussian initial conditions, b_1 only depends on the mass m, as implictly assumed in Eq. (2.3.4). The 2-halo term can be rewritten as

$$P_{2h}(k,z) = \frac{1}{\bar{\rho}^2}\left[\prod_{i=1}^{2}\int \mathrm{d}m_i\, n(m_i,z)\,\hat{\rho}(k,m_i,z)\,b_1(m_i,z)\right] P_L(k,z). \tag{2.3.5}$$

This description can be easily extended to the matter bispectrum. In the case of a three-point function, we should account for the possibility that the three points belong to just one, two or three dark matter halos. This means that there are now three distinct contributions to the halo model expression for the matter bispectrum, that is

$$\begin{aligned}\left\langle \delta_{\vec{k}_1}(\tau)\delta_{\vec{k}_2}(\tau)\delta_{\vec{k}_3}(\tau)\right\rangle &\equiv B(k_1,k_2,k_3)\\ &= B_{3h}(k_1,k_2,k_3) + B_{2h}(k_1,k_2,k_3) + B_{1h}(k_1,k_2,k_3),\end{aligned} \tag{2.3.6}$$

where

$$\begin{aligned}B_{3h}(k_1,k_2,k_3,z) = \frac{1}{\bar{\rho}^3}&\left[\prod_{i=1}^{3}\int \mathrm{d}m_i\, n(m_i,z)\,\hat{\rho}(m_i,z,k_i)\right]\\ &\times B_h(k_1,m_1;k_2,m_2;k_3,m_3;z),\end{aligned} \tag{2.3.7}$$

$$B_{2h}(k_1,k_2,k_3,z) = \frac{1}{\overline{\rho}^3}\int \mathrm{d}m\, n(m,z)\,\hat{\rho}(m,z,k_1)\int \mathrm{d}m'\, n(m',z) \times\ \hat{\rho}(m',z,k_2)\,\hat{\rho}(m',z,k_3)P_h(k_1,m,m',z) + \text{cyc.}, \tag{2.3.8}$$

$$B_{1h}(k_1,k_2,k_3,z) = \frac{1}{\overline{\rho}^3}\int \mathrm{d}m\, n(m,z)\,\hat{\rho}(k_1,m,z)\,\hat{\rho}(k_2,m,z)\,\hat{\rho}(k_3,m,z). \tag{2.3.9}$$

In this case, while the 2-halo term depends on the halo power spectrum as in the previous case, the 3-halo term involves the halo bispectrum, $B_h(k_1,m_1;k_2,m_2;k_3,m_3;z)$. Assuming again a local bias relation between halos and matter, $\delta_h(m) = f(\delta)$, expanded perturbatively as $\delta_h(m) = b_1(m)\delta + [b_2(m)/2]\delta^2 + \mathcal{O}(\delta^3)$, it is possible to derive the tree-level expression for the halo bispectrum, valid only in the large-scale limit, in terms of the matter power spectrum $P(k)$ and the bispectrum $B(k_1,k_2,k_3)$. This reads

$$B_h(k_1,m_1;k_2,m_2;k_3,m_3;z) = b_1(m_1)\,b_1(m_2)\,b_1(m_3)\,B(k_1,k_2,k_3) + \left[b_1(m_1)\,b_1(m_2)\,b_2(m_3)\,P(k_1)\,P(k_2) + \text{cyc.}\right], \tag{2.3.10}$$

where $b_2(m)$ is the quadratic bias function. For Gaussian initial conditions b_1 and b_2 are scale independent. Moreover, since this equation is valid on large scales, we can replace the matter power spectrum P by its linear prediction P_L and the matter bispectrum B by its gravitational contribution $B_{\rm G}$

$$B_{\rm G}(k_1,k_2,k_3) = 2\,F_2(\vec{k}_1,\vec{k}_2)\,P_L(k_1)P_L(k_2) + 2 \text{ perm.}, \tag{2.3.11}$$

F_2 being the kernel representing the second-order solution in standard perturbation theory and given by

$$F_2(\vec{k}_i,\vec{k}_j) = \frac{5}{7} + \frac{1}{2}\left(\frac{k_i}{k_j}+\frac{k_j}{k_i}\right)(\hat{k}_i\cdot\hat{k}_j) + \frac{2}{7}(\hat{k}_i\cdot\hat{k}_j)^2. \tag{2.3.12}$$

The spatial distribution of matter in a halo of mass m is specified by the halo density profile $\rho(r,m)$, interpreted as an average over all halos of the same mass. We consider the Navarro, Frenk and White form for the halo density profile [93] $\rho(r) = \rho_s/\left[(r/r_s)(1+r/r_s)^2\right]$, which assumes a universal profile as a function of r. The parameters r_s and ρ_s can be expressed in terms of the virial mass of the halo m and the concentration parameter c. In particular, the virial mass is given by $m \equiv (4\pi/3)\,R_v^3\,\Delta_v\,\overline{\rho}$, with R_v the virial radius, defined as the radius of a sphere within which the mean density of the halo is Δ_v times that of the Universe. We take $\Delta_v = 200$. The concentration parameter c is defined as $c = R_v/r_s$ and is typically a function of m. The halo mass function $n(m)$ [94] characterizes the number density of halos per unit mass. The fraction of the total mass of the Universe contained in

all the halos with mass in the range m and $(m, m + \mathrm{d}m)$ can be written as

$$\frac{1}{\overline{\rho}}\, n(m)\, m\, \mathrm{d}m = f(\nu)\, \mathrm{d}\nu. \tag{2.3.13}$$

The function $f(\nu)$ has an approximately universal form and depends on the variable

$$\nu \equiv \frac{\delta_{\mathrm{c}}}{\sigma(m, z)}, \tag{2.3.14}$$

with δ_{c} representing the critical density for spherical collapses (we assume the Einstein-de Sitter value $\delta_{\mathrm{c}} = 1.68$ at zero redshift) while $\sigma(m, z) = D(z)\sigma(m, z = 0)$ is the square root of the variance of matter fluctuations in spheres of radius $R = (3m/4\pi\overline{\rho})^{1/3}$ (associated to the Fourier transform $W_R(k)$ of the top-hat function in real space), $\sigma^2(m) \equiv 4\pi \int \mathrm{d}k\, k^2\, P_L(k)\, W_R(k)$. We shall adopt the Sheth and Tormen form of the halo mass function [95] expression

$$f(\nu) = A\sqrt{\frac{a\,\nu^2}{2\pi}}\left[1 + \frac{1}{(a\,\nu^2)^p}\right] e^{-a\nu^2/2}, \tag{2.3.15}$$

where $a = 0.707$ and $p = 0.3$ while $A = 0.322$ ensures a proper normalization. Finally, the bias functions can be derived from the unconditional halo mass function and, in the case of the Sheth-Tormen form, one obtains for the first two the expressions [95]

$$b_1(\nu) = 1 + \frac{a\,\nu^2 - 1}{\delta_{\mathrm{c}}} + \frac{2p}{\delta_{\mathrm{c}}(1 + (a\,\nu^2)^p)}, \tag{2.3.16}$$

$$\begin{aligned} b_2(\nu) = {} & \frac{8}{21}[b_1(\nu) - 1] + \frac{a\,\nu^2}{\delta_{\mathrm{c}}}\frac{a\,\nu^2 - 3}{\delta_{\mathrm{c}}} \\ & + \left(\frac{1 + 2p}{\delta_{\mathrm{c}}} + 2\frac{a\,\nu^2 - 1}{\delta_{\mathrm{c}}}\right)\frac{2p/\delta_{\mathrm{c}}}{1 + (a\,\nu^2)^p}. \end{aligned} \tag{2.3.17}$$

The requirement for the total matter density to be given by

$$\rho(\vec{x}) \equiv \overline{\rho}\,[1 + \delta(\vec{x})] = \int \mathrm{d}m\, m\, n(m)\left[1 + \sum_i \frac{b_i(m)}{i!}\delta^i(\vec{x})\right], \tag{2.3.18}$$

imposes the condition

$$\int \mathrm{d}m\, m\, n(m) = \overline{\rho}, \tag{2.3.19}$$

along with the constraints on the bias functions,

$$\frac{1}{\bar{\rho}}\int \mathrm{d}m\, m\, n(m)\, b_i(m) = \int \mathrm{d}\nu\, f(\nu)\, b_i(\nu) = \delta_{i1}. \tag{2.3.20}$$

Such relations assure that, on large scales ($k \to 0$, $\hat{\rho} \to m$), the 2-halo term of the power spectrum reduces to the linear power spectrum and the 3-halo term of the bispectrum reduces to the large-scale matter bispectrum.

We are now ready to study the squeezed limit of the bispectrum. It allows for a significant simplification of the halo model expressions. As physical intuition dictates, in this limit the largest contribution to the bispectrum comes from the position-space configuration where two points are close and belong to the same halo while the third one is at larger distance from the first two, and hence is likely to belong to another halo. In this case we expect the halo model prediction to be dominated by the 2-halo contribution, with the 1-halo and 3-halo terms being subdominant. This expectation is confirmed numerically [96]: taking the smallest wavenumber to be $q = 0.014h\,\mathrm{Mpc}^{-1}$, B_{2h} becomes dominant over the other two terms for $k_1 \sim k_2 \sim 0.3\,h\,\mathrm{Mpc}^{-1}$ and at $k_1 \sim k_2 \sim 1\,h\,\mathrm{Mpc}^{-1}$ the sum of B_{1h} and B_{3h} contribute less than 10%.

If q is still in the linear regime, then we can safely set the Fourier transform of the halo profile to be

$$\hat{\rho}(m, z, q) \simeq m, \tag{2.3.21}$$

in all bispectrum terms involving q in Eqs. (2.3.7), (2.3.8) and (2.3.9). By making this substitution, the expressions for the 1-, 2- and 3-halo terms greatly simplify. Moreover, by using the conditions in Eqs. (2.3.19) and (2.3.20), together with Eq. (2.3.21), the halo model bispectrum contributions become, at leading order in q [96]

$$B_{1h}(q, k_1, k_2) = \frac{1}{\bar{\rho}}\,\epsilon_2^{[m]}(k_1), \tag{2.3.22}$$

$$B_{2h}(q, k_1, k_2) = \epsilon_2^{[b_1]}(k_1)\, P_L(q), \tag{2.3.23}$$

$$B_{3h}(q, k_1, k_2) = 2\left[\frac{13}{14} + \left(\frac{4}{7} - \frac{1}{2}\frac{\partial \ln P_L}{\partial \ln k_1}\right)(\hat{q}\cdot\hat{k}_1)^2 + \frac{\epsilon_1^{[b_2]}(k_1)}{\epsilon_1^{[b_1]}(k_1)}\right] \times P_L(q)\, P_{2h}(k_1). \tag{2.3.24}$$

The functions $\epsilon_i^{[F]}$ in these expressions are defined as

$$\epsilon_i^{[F]}(k) \equiv \frac{1}{\bar{\rho}^i}\int \mathrm{d}m\, n(m, z)\, \hat{\rho}^i(m, z, k)\, F(m, z), \tag{2.3.25}$$

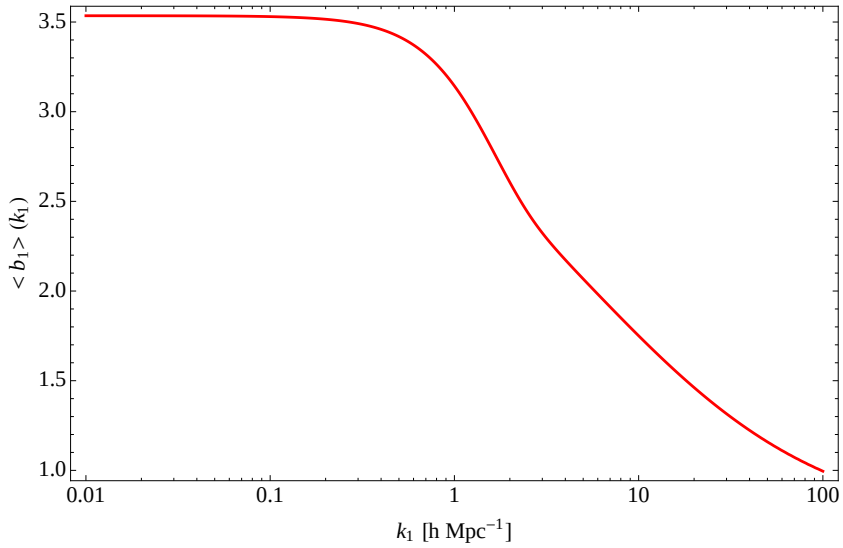

Figure 2.1: *The function* $\langle b_1(m,k_1)\rangle$ *as a function of* k_1.

where $F(m,z)$ represents a generic function of mass and redshift. Thus, these functions are like an "average" of the function F, weighted by the mass function and the i-th power of the Fourier transform of the density profile. The first two terms inside the bracket of Eq. (2.3.24) have been derived by taking the squeezed limit $q \ll k_1 \simeq k_2$ of $B_{\rm G}(k_1,k_2,k_3)$ in Eq. (2.3.11)

$$\begin{aligned} B_{\rm G}(q,k_1,k_2) &\simeq 2\left[F_2(\vec{q},\vec{k}_1)P_L(q)P_L(k_1)+F_2(\vec{q},\vec{k}_2)P_L(q)P_L(k_2)\right] \\ &= 2\left[\frac{13}{14}+\left(\frac{4}{7}-\frac{1}{2}\frac{\partial \ln P_L}{\partial \ln k_1}\right)(\hat{q}\cdot\hat{k}_1)^2+\mathcal{O}\left(\frac{q}{k_1}\right)^2\right] \\ &\quad \times P_L(q)P_L(k_1). \end{aligned} \tag{2.3.26}$$

Let us first consider the angular averaged of the squeezed limit of the bispectrum in the limited range of momenta where it is dominated by the 3-halo piece, that is in the limit in which all momenta are in the linear regime, and one can safely take $P(k_1) \simeq P_{2h}(k_1) \simeq P_L(k_1)$. In such a case

$$\begin{aligned} \left\langle \delta_{\vec{q}}(\tau)\delta_{\vec{k}_1}(\tau)\delta_{\vec{k}_2}(\tau)\right\rangle'^{\rm av}_{q\to 0} &\simeq 2\left[\frac{13}{14}+\frac{1}{3}\cdot\frac{4}{7}-\frac{1}{6}\frac{\partial \ln P_L}{\partial \ln k_1}+\frac{\epsilon_1^{[b_2]}(k_1)}{\epsilon_1^{[b_1]}(k_1)}\right]P_L(q)\,P_{2h}(k_1) \\ &\simeq \left[\frac{47}{21}-\frac{1}{3}\frac{\partial}{\partial \ln k_1}+2\frac{\epsilon_1^{[b_2]}(k_1)}{\epsilon_1^{[b_1]}(k_1)}\right]P_L(q)\,P(k_1). \end{aligned} \tag{2.3.27}$$

This has to be compared with the prediction of the consistency relation (2.2.3) which gives, taking

into account that in the present case $P(k_1) = P_L(k_1) \propto D^2(a)$,

$$\left\langle \delta_{\vec{q}}(\tau)\delta_{\vec{k}_1}(\tau)\delta_{\vec{k}_2}(\tau)\right\rangle'^{\rm av}_{q\to 0} \simeq \left[\frac{47}{21} - \frac{1}{3}\frac{\partial}{\partial \ln k_1}\right] P_L(q)\, P(k_1). \tag{2.3.28}$$

Since in the limit we are taking

$$\epsilon_1^{[b_2]}(k_1) = \frac{1}{\bar{\rho}}\int \mathrm{d}m\, m\, n(m)\, b_2(m,k_1) = 0,$$
$$\epsilon_1^{[b_1]}(k_1) = \frac{1}{\bar{\rho}}\int \mathrm{d}m\, m\, n(m)\, b_1(m,k_1) = 1, \tag{2.3.29}$$

we conclude that the halo model prediction (2.3.27) reproduces the consistency relation.

Let us now consider the most realistic case in which the momenta k_1 and k_2 are in the non-linear regime. In such a case, the bispectrum is dominated by the 2-halo piece and one gets

$$\left\langle \delta_{\vec{q}}(\tau)\delta_{\vec{k}_1}(\tau)\delta_{\vec{k}_2}(\tau)\right\rangle'^{\rm av}_{q\to 0} \simeq P_L(q)P_{1h}(k_1)\frac{\int \mathrm{d}m\, n(m,z)\,\hat{\rho}^2(m,z,k_1)\, b_1(m,k_1)}{\int \mathrm{d}m\, n(m,z)\,\hat{\rho}^2(m,z,k_1)}$$
$$= \langle b_1(k_1)\rangle P_L(q)P_{1h}(k_1), \tag{2.3.30}$$

where the ratio of the two integrals provides an average of the first bias parameter. We see from Fig. 2.1 that $\langle b_1(k_1)\rangle$ is constant up to $k_1 = \mathcal{O}(1)\, h\,\mathrm{Mpc}^{-1}$ and its value is approximately 3.5. At much larger values of k_1 the average $\langle b_1(k_1)\rangle$ acquires a strong momentum dependence. To check if the analytical prediction of the halo models satisfies the consistency relation we need to compute the 1-halo power spectrum. At large values of k_1 the power spectrum is dominated by contributions near the mass scale for which $k_1 r_s \simeq 1$ [92]. The mass function behaves as $\mathrm{d}n/\mathrm{d}m \sim m^{-2}\nu^{1-2p}\exp(-a\nu^2/2)$. Since the scale radius r_s depends on the mass as $r_s = R_v/c \sim m^{1/3}/m^{-(3+n)/6} = m^{(5+n)/6}$, where n is the spectral index of the linear power spectrum, we find that the power spectrum at high momenta goes as [92]

$$P_{1h}(k_1) \sim \int \mathrm{d}m\, \nu^{1-2p}\hat{\rho}^2(k_1 r_s). \tag{2.3.31}$$

We change variables to $x = k_1 r_s \sim k_1[m/m_*(z)]^{(5+n)/6}$, where we have defined $m_*(z)$ the mass scale for which $\sigma\,[(m_*(z)] = 1$. Accounting for the fact that $\sigma(m) \sim (m/m_*)^{-(3+n)/6}$, we obtain

$$P_{1h}(k_1) \sim [D(a)]^{\frac{6}{n+3}+1-2p}\, k_1^{\gamma-3}, \quad \gamma = \frac{9+3n}{5+n} - (1-2p)\left(\frac{3+n}{5+n}\right). \tag{2.3.32}$$

The consistency relation (2.2.3) therefore would give

$$\left\langle \delta_{\vec{q}}(\tau)\delta_{\vec{k}_1}(\tau)\delta_{\vec{k}_2}(\tau)\right\rangle'^{\rm av}_{q\to 0} \simeq \left[1-\frac{1}{3}(\gamma-3)+\frac{13}{21}\left(\frac{6}{n+3}+1-2p\right)\right] \times P_L(q)P_{1h}(k_1), \quad (2.3.33)$$

which seems reproduce the result (2.3.30) quite remarkably. For instance, for $n \simeq -1$, which fits well the non-linear power spectrum on mildly non linear scales, one gets a coefficient of order of 3.6 in Eq. (2.3.33) in front of $P_L(q)P_{1h}(k_1)$. On general grounds, as the spectral index of the short-mode power spectrum is negative and the dependence on the growth factor is such that the non-linear power spectrum is suppressed at high redshifts, implying a positive power of $D(a)$, this leads to the conclusion that the overall coefficient in front of $P_L(q)P_{1h}(k_1)$ in the bispectrum is predicted to be larger than unity by the consistency relation. This is in good agreement with the prediction of the halo model: the halo model reproduces the remarkable property predicted by the consistency relation that the bispectrum in the squeezed limit factorizes in terms of the product of the linear power spectrum times the non-linear one. This conclusion seems to be valid up to scales $\mathcal{O}(1)\,h\,\mathrm{Mpc}^{-1}$.

2.4 Summary

In this chapter we have derived a consistency relation which applies for dark matter over-densities and involves the soft limit of the $(n+1)$-point correlation functions. While this result can be hardly extended to the more interesting case of galaxy overdensities, we have used it to investigate the ability of the halo model to satisfy the consistent relations. We have concluded that the halo model satisfies rather well the features predicted by the consistency relation up to scales $\mathcal{O}(1)\,h\,\mathrm{Mpc}^{-1}$.

Chapter 3

Consequences of symmetries and consistency relations in the large-scale structure of the Universe for non-local bias and modified gravity

3.1 Matter and galaxy consistency relations

The large-scale consistency relations have the virtue of being true also for the galaxy overdensities, independently of the bias between galaxy and dark matter. As such, they may serve as a guidance in building up a bias theory. Indeed, we shall argue that the non-local Eulerian bias model can be seen as being built of quantities which are invariant under the symmetries enjoyed by the Newtonian fluid equations. Furthermore, they might be useful in testing theories of modified gravity where extra degrees of freedom appear mediating extra long-range forces (other than the gravitational one) and possibly leading to a violation of the Equivalence Principle (EP) in the late universe and therefore to a violation of the consistency relation. In fact, assuming adiabatic Gaussian initial conditions, an observed violation of the consistency relations would either indicate a breakdown of the non-local Eulerian bias model (and also the presence of terms in the effective fluid equations for galaxies that break the aforementioned symmetries), or a violation of the EP in the underlying theory of gravity.

It is in the spirit of exploring these topics that in this chapter we aim to investigate what the large-scale consistency relations may tell us about the galaxy bias and how they can be used to scrutinize modified gravity theories. In particular, we shall show that the symmetries leading to the consistency relations allow the presence of what is commonly dubbed non-local bias, that is a relation between the galaxy and the dark matter overdensities which is not a simple function of the local dark matter abundance. We shall identify a series of invariants (with respect to the symmetries) which should appear in the galaxy bias expansion, precisely because they are allowed by the symmetries of the problem. Furthermore, we shall investigate under which conditions the consistency relations are valid in the case in which a modification of gravity is attained far in the infrared on cosmological scales.

This chapter is organized as follows. In section 3.2 we discuss the symmetries of the non-relativistic

fluid equations for galaxies and we derive galaxy consistency relations for the n-point correlators of short wavelength modes in the background of a long wavelength mode perturbation. In section 3.3 we provide the invariants under the symmetries of the galaxy and dark matter fluids and we discuss their implications for the non-local bias. We also check that the galaxy consistency relation holds at tree- and one-loop level in the bias model. In section 3.4 we show how to extend the galaxy consistency relations to redshift space where actual experiments are made. In section 3.5 we discuss the consequences of the symmetries for the theories of modified gravity and how such modifications are imprinted in the $(n+1)$-point correlators in the squeezed limit. Finally, section 3.6 presents our conclusions.

3.2 Symmetries and consistency relation of galaxy correlation functions in Fourier space

Galaxies (or more precisely, some population thereof), once formed, obey analogous equations to the dark matter (1.3.2)- (1.3.4) on sub-Hubble scales :

$$\frac{\partial \delta_{\rm g}(\vec{x},\tau)}{\partial \tau} + \vec{\nabla}\cdot[(1+\delta_{\rm g}(\vec{x},\tau))\vec{v}_{\rm g}(\vec{x},\tau)] = 0, \tag{3.2.1}$$

$$\frac{\partial \vec{v}_{\rm g}(\vec{x},\tau)}{\partial \tau} + \mathcal{H}(\tau)\vec{v}_{\rm g}(\vec{x},\tau) + [\vec{v}_{\rm g}(\vec{x},\tau)\cdot\vec{\nabla}]\vec{v}_{\rm g}(\vec{x},\tau) = -\vec{\nabla}\Phi(\vec{x},\tau), \tag{3.2.2}$$

$$\nabla^2\Phi(\vec{x},\tau) = \frac{3}{2}\Omega_{\rm m}\mathcal{H}^2(\tau)\delta(\vec{x},\tau), \tag{3.2.3}$$

where again, we have denoted by $\vec{x}$ the comoving spatial coordinates, $\tau = \int {\rm d}t/a$ the conformal time. In addition, $\delta_{\rm g}(\vec{x},\tau)$ and $\vec{v}_{\rm g}(\vec{x},\tau)$ are the galaxy overdensity and peculiar velocity while $\delta(\vec{x},\tau)$ is the overdensity of dark matter. Eq. (3.2.1) assumes number conservation [97]. Eventually, one would like to go beyond the treatment presented here in order to account for phenomena like formation and merging, which could be done for example by adding a source term to the right hand side of Eq. (3.2.1).

Following Ref. [77], in ΛCDM cosmology, the set of equations (3.2.1-3.2.3) is invariant under the transformations (for a generic vector $\vec{n}(T)$)

$$\tau' = \tau, \quad \vec{x}' = \vec{x} + \vec{n}(T), \tag{3.2.4}$$

where

$$T(\tau) = \frac{1}{a(\tau)}\int^{\tau} {\rm d}\eta\, a(\eta), \tag{3.2.5}$$

provided that one transforms the fields describing the galaxies as

$$\delta'_{\rm g}(\vec{x},\tau) = \delta_{\rm g}(\vec{x}',\tau'), \tag{3.2.6}$$

$$\vec{v}'_{\rm g}(\vec{x},\tau) = \vec{v}_{\rm g}(\vec{x}',\tau') - \dot{\vec{n}}(T), \tag{3.2.7}$$

in addition to the transformations (1.4.8) and (1.4.10) for the dark matter and the gravitational potential. This is true even if we do not set $\vec{v}_{\rm g}(\vec{x},\tau) = \vec{v}(\vec{x},\tau)$, that is if we do not assume that the galaxy peculiar velocity is unbiased. Note that if one adds a source term to the right hand side of Eq. (3.2.1) to account for the change of the number density of galaxies in time, and such a source term depends only on quantities which transform as scalars, the equations of motion are still invariant under these transformations.

We now derive consistency conditions for the galaxy correlation analogously to the dark matter ones. We can generate a long wavelength mode for the dark matter velocity perturbation $\vec{v}_L(\tau,\vec{0})$ just by choosing properly the vector $\vec{n}(\tau)$

$$\vec{n}(\tau) = -\int^{\tau} {\rm d}\eta\, \vec{v}_L(\eta,\vec{0}) + \mathcal{O}(qRv_L^2). \tag{3.2.8}$$

The effect of a physical long wavelength velocity perturbation onto the short modes should be indistinguishable from the long wavelength mode velocity generated by the transformation with $\delta x^i = n^i(\tau)$. The correlator of the short wavelength modes therefore satisfies the relation [77]

$$\Big\langle \delta_{\rm g}(\tau_1,\vec{x}_1)\delta_{\rm g}(\tau_2,\vec{x}_2)\cdots\delta_{\rm g}(\tau_n,\vec{x}_n)\Big\rangle_{v_L} = \Big\langle \delta_{\rm g}(\tau'_1,\vec{x}'_1)\delta_{\rm g}(\tau'_2,\vec{x}'_2)\cdots\delta_{\rm g}(\tau'_n,\vec{x}'_n)\Big\rangle. \tag{3.2.9}$$

Proceeding as for the dark matter, we find that the squeezed bispectrum of galaxies is given by

$$\begin{aligned}
&\Big\langle \delta_{\rm g}(\vec{q},\tau)\delta_{\rm g}(\vec{k}_1,\tau_1)\cdots\delta_{\rm g}(\vec{k}_n,\tau_n)\Big\rangle_{q\to 0} \\
&\qquad = \Big\langle \delta_{\rm g}(\vec{q},\tau)\Big\langle \delta_{\rm g}(\vec{k}_1,\tau_1)\cdots\delta_{\rm g}(\vec{k}_n,\tau_n)\Big\rangle_{v_L}\Big\rangle \\
&\qquad = i\sum_{a=1}^{n}\Big\langle \delta_{\rm g}(\vec{q},\tau)n^i(\tau_a)\Big\rangle k_a^i\Big\langle \delta_{\rm g}(\vec{k}_1,\tau_1)\cdots\delta_{\rm g}(\vec{k}_n,\tau_n)\Big\rangle.
\end{aligned} \tag{3.2.10}$$

Using

$$\int^{\tau} {\rm d}\eta\, \vec{v}_L(\vec{q},\eta) = i\frac{\vec{q}}{q^2}\delta_L(\vec{q},\tau), \tag{3.2.11}$$

where $D(\tau)$ is the linear growth factor, we obtain the consistency relation

$$\boxed{\begin{aligned}&\Big\langle \delta_{\rm g}(\vec{q},\tau)\delta_{\rm g}(\vec{k}_1,\tau_1)\cdots\delta_{\rm g}(\vec{k}_n,\tau_n)\Big\rangle'_{q\to 0} = \\ &\quad -\Big\langle \delta^L_{\rm g}(\vec{q},\tau)\delta_L(\vec{q},\tau)\Big\rangle' \sum_{a=1}^{n} \frac{D(\tau_a)}{D(\tau)}\frac{\vec{q}\cdot\vec{k}_a}{q^2}\Big\langle \delta_{\rm g}(\vec{k}_1,\tau_1)\cdots\delta_{\rm g}(\vec{k}_n,\tau_n)\Big\rangle',\end{aligned}} \tag{3.2.12}$$

where the primes indicate that one should remove the Dirac delta's coming from the momentum conservation. Notice that, if the correlators are computed all at equal times, the right-hand side of Eq. (3.2.12) vanishes by momentum conservation and the $1/q^2$ infrared divergence will not appear when calculating invariant quantities.

As a special case, the three-point correlator of galaxies reads explicitely

$$\begin{aligned}\Big\langle \delta_{\rm g}(\vec{q},\tau)\delta_{\rm g}(\vec{k}_1,\tau_1)\delta_{\rm g}(\vec{k}_2,\tau_2)\Big\rangle'_{q\to 0} = -\Big\langle \delta^L_{\rm g}(\vec{q},\tau)\delta_L(\vec{q},\tau)\Big\rangle' \\ \times\left(\frac{D(\tau_1)}{D(\tau)}-\frac{D(\tau_2)}{D(\tau)}\right)\frac{\vec{q}\cdot\vec{k}_1}{q^2}\Big\langle \delta_{\rm g}(\vec{k}_1,\tau_1)\delta_{\rm g}(\vec{k}_2,\tau_2)\Big\rangle'.\end{aligned} \tag{3.2.13}$$

3.3 Consequences of the symmetries for the galaxy bias theory

3.3.1 The non-local bias expansion

As the galaxy and dark matter overdensities equations of motion (3.2.1-3.2.3) and (1.3.2-1.3.4) are invariant under the set of transformations (1.4.7-1.4.10), an immediate consequence is that one can construct scalar quantities, i.e. quantities $S(\vec{x},\tau)$ which upon the transformation (1.4.7) are such that

$$S'(\vec{x},\tau) - S(\vec{x},\tau) = \vec{n}\cdot\vec{\nabla}S(\vec{x},\tau). \tag{3.3.1}$$

As the spatial gradients remain invariant, $\vec{\nabla} = \vec{\nabla}'$, one can easily realize that there are the following scalar quantities in the dark matter sector at our disposal

$$\boxed{\begin{aligned} &\delta(\vec{x},\tau), \\ &s_{ij}(\vec{x},\tau) = \partial_i\partial_j\Phi(\vec{x},\tau) - \frac{\delta_{ij}}{2}\Omega_{\rm m}\mathcal{H}^2\delta(\vec{x},\tau), \\ &t_{ij}(\vec{x},\tau) = \partial_i v_j(\vec{x},\tau) - \frac{\delta_{ij}}{3}\theta(\vec{x},\tau) - \frac{2f}{3\Omega_{\rm m}\mathcal{H}}s_{ij}(\vec{x},\tau), \end{aligned}} \tag{3.3.2}$$

where $\theta(\vec{x},\tau) = \vec{\nabla}\cdot\vec{v}(\vec{x},\tau)$, $f = {\rm d}\ln D/{\rm d}\ln a$, we have removed the trace part from $\partial_i\partial_j\Phi(\vec{x},\tau)$, which is nothing else than the dark matter overdensity $\delta(\vec{x},\tau)$, and $t_{ij}(\vec{x},\tau)$ is vanishing at first-order in perturbation theory. Notice that these quantities are scalars beyond the linear perturbation theory as the symmetries identified in the previous section are valid at any order in perturbation theory. These symmetries are larger than the Galilean group identified in Ref. [98] for the large-scale dynamics. Furthermore, upon constructing the invariant operators

$$D_\tau^v = \frac{\partial}{\partial\tau} + \vec{v}(\vec{x},\tau)\cdot\vec{\nabla} \tag{3.3.3}$$

and

$$D_\tau^{v_{\rm g}} = \frac{\partial}{\partial\tau} + \vec{v}_{\rm g}(\vec{x},\tau)\cdot\vec{\nabla}, \tag{3.3.4}$$

one can construct two more invariant quantities

$$\vec{\nabla}\Phi(\vec{x},\tau) + D_\tau^v\vec{v}(\vec{x},\tau) + \mathcal{H}\vec{v}(\vec{x},\tau) \tag{3.3.5}$$

and

$$\vec{\nabla}\Phi(\vec{x},\tau) + D_\tau^{v_{\rm g}}\vec{v}_{\rm g}(\vec{x},\tau) + \mathcal{H}\vec{v}_{\rm g}(\vec{x},\tau), \tag{3.3.6}$$

but they are nothing else than the momentum conservation quantities for the dark matter and the galaxy, respectively. They identically vanish on-shell and therefore are trivial.

The set of invariants (3.3.2) are useful in constructing a galaxy bias theory which goes beyond the local bias model [99]. In the latter the galaxy overdensity $\delta_{\rm g}(\vec{x},\tau)$ is written as a completely general function $f[\delta(\vec{x},\tau)]$ of the mass density perturbation $\delta(\vec{x},\tau)$, and then the function is Taylor expanded,

with the unknown coefficients in the series becoming the bias parameters

$$\begin{aligned}\delta_{\rm g}(\vec{x},\tau) &= f[\delta(\vec{x},\tau)] \\ &= b_1\delta(\vec{x},\tau) + \frac{b_2}{2}\delta^2(\vec{x},\tau) + \cdots .\end{aligned} \tag{3.3.7}$$

This local expansion, even though it is consistent with the first invariant of the list (3.3.2), is expected to be valid only on very large scales and small times: as the symmetry dynamics allows the presence of more scalar quantities, there is no reason why they should not be generated along the subsequent evolution. This logic is the same which applies in quantum field theory for operators: even though some of them are not present in the tree-level Lagrangian, they will appear at a certain order in perturbation theory unless they are forbidden by symmetry arguments. Therefore, assuming homogeneity and isotropy, one would expect a more general bias model of the form (where the coefficients should be intended to be the renormalized ones [61])

$$\begin{aligned}\delta_{\rm g}(\vec{x},\tau) = b_1(\tau)\delta(\vec{x},\tau) &+ \frac{b_2(\tau)}{2}\delta^2(\vec{x},\tau) + c_{\nabla^2}(\tau)\nabla^2\delta(\vec{x},\tau) \\ &+ c_{s^2}(\tau)s_{ij}(\vec{x},\tau)s^{ij}(\vec{x},\tau) + c_{s^2\nabla}\partial_k s_{ij}(\vec{x},\tau)\partial^k s^{ij}(\vec{x},\tau) \\ &+ c_{s^2\nabla^2}\nabla^2(s_{ij}(\vec{x},\tau)s^{ij}(\vec{x},\tau)) + c_{s^2\nabla^4}(\tau)\nabla^2 s_{ij}(\vec{x},\tau)\nabla^2 s^{ij}(\vec{x},\tau) \\ &+ \cdots ,\end{aligned} \tag{3.3.8}$$

and the dots stand for the various other terms one can construct out of $s_{ij}(\vec{x},\tau)$ and gradients. We see that an unavoidable consequence of the symmetries of the problem is that the bias model is a non-local bias model [100, 61, 101, 102]; in fact the non-local expansion (3.3.8) has been first proposed in Ref. [61] where the same invariants have been employed based on general arguments on the homogeneous gravitational field and dark matter velocity. Some comments are in order:

- The series does not contain a piece proportional to the gravitational potential $\Phi(\vec{x},\tau)$: it is simply forbidden by the symmetries of the problem as $\Phi(\vec{x},\tau)$ alone is not a scalar quantity.

- The non-local bias expansion (3.3.8) is not dictated solely by rotational invariance. Instead it is the more generic symmetry (1.4.7) together with isotropy which fixes the form of the expansion.

- The fluid equations during the matter-dominated period are also invariant under Lifshitz scalings of the form [103, 56, 77]

$$\tau' = \lambda^z\tau, \quad \vec{x}' = \lambda\vec{x}, \tag{3.3.9}$$

$$\delta'(\vec{x},\tau) = \delta(\vec{x}',\tau'), \tag{3.3.10}$$

$$\delta'_{\rm g}(\vec{x},\tau) = \delta_{\rm g}(\vec{x}',\tau'), \tag{3.3.11}$$

$$\vec{v}'_{\rm g}(\vec{x},\tau) = \lambda^{z-1}\vec{v}(\vec{x}',\tau'), \tag{3.3.12}$$

$$\vec{v}'(\vec{x},\tau) = \lambda^{z-1}\vec{v}_{\rm g}(\vec{x}',\tau'), \tag{3.3.13}$$

$$\Phi'(\vec{x},\tau) = \lambda^{2(z-1)}\Phi(\vec{x}',\tau'), \tag{3.3.14}$$

for a generic Lifshitz weight z and

$$\frac{\partial}{\partial\tau} = \lambda^z\frac{\partial}{\partial\tau'}, \quad \vec{\nabla} = \lambda\vec{\nabla}'. \tag{3.3.15}$$

Therefore, the Lifshitz weights of the bias coefficients should be

$$\begin{aligned}
&[b_1] = [b_2] = 0,\\
&[c_{\nabla^2}] = -2,\\
&[c_{s^2}] = -4z,\\
&[c_{s^2\nabla^2}] = [c_{s^2\nabla}] = -2-4z,\\
&[c_{s^2\nabla^4}] = -4-4z.
\end{aligned} \tag{3.3.16}$$

These Lifshitz weights fix the time-behaviour of the corresponding coefficients for the growing mode. The fact that the Lifshitz weights of b_1 and b_2 are vanishing tell us that their growing mode is constant in time. Indeed, it is well-known that at large times the system experiences the so-called debiasing: b_1 converges to unity and b_2 goes to zero. Furthermore, the Lifshitz weights fix the corresponding time-behaviour of the remaining bias coefficients in their growing modes: c_{∇^2}, c_{s^2}, $c_{s^2\nabla^2}$ and $c_{s^2\nabla^4}$ should scale as $\tau^{2/z}$, τ^4, $\tau^{(4z+2)/z}$ and $\tau^{(4z+4)/z}$, respectively. In particular, if one matches with the linear power spectrum of dark matter with spectral index n, one finds $z = 4/(3+n) \simeq 1$ [98]. This explains why the non-local bias coefficients increase with time during the matter-dominated period. Furthermore, if one expresses the non-local invariant $s_{ij}(\vec{x},\tau)s^{ij}(\vec{x},\tau)$ at second-order in terms of the product of the linear overdensities, one finds that the Lifshitz symmetry imposes that the overall time scaling is τ^{-2} in a matter-dominated universe (once one goes to momentum space). This is precisely the scaling found in Ref. [62] and leads to the so-called debiasing, that is at late times the bias converges to unity and matter and galaxy density fields agree.

- As we already mentioned, galaxies form at a range of redshifts and merge. So it would be interesting to extend our results to the more realistic case when the number density of galaxies changes with redshift due to some arbitrary source including the effects of galaxy formation and

merging. However, if the effective source is a function of the scalar functions described above then our symmetry considerations will apply to this more complete galaxy description too. For instance, in Ref. [102] it was assumed that the effective source was of the form $A(\tau)j(\rho)$, where $A(\tau)$ parametrizes the epoch of galaxy formation and $j(\rho)$ the effects of dark matter on galaxy formation and merging. In such a case the symmetry (1.4.7-1.4.10) holds.

- If the fluid equations are not invariant under the set of transformations (1.4.7-1.4.10), as it happens for example in some modified theories of gravity to be discussed below, one expects other terms to appear in the bias expansion as the bias is scale-dependent. The possibility of testing the Poisson equation with a scale-dependent bias was discussed in [104].

3.3.2 Independence from the smoothing scale

The galaxy consistency relation also holds for smoothed quantities as the smoothing operation commutes with the coordinate transformation (1.4.7). Indeed, suppose we perform a smoothing operation with a window function around a sphere of radius R_L

$$\delta_{R_L}(\vec{x}) = \int \mathrm{d}^3y\, W\left(|\vec{y}-\vec{x}|, R_L\right)\, \delta(\vec{y}), \tag{3.3.17}$$

where W is the appropriate window function. Then we have

$$\begin{aligned}
\delta_{R_L}(\vec{x}') &= \int \mathrm{d}^3y\, W\left(\left|\vec{y}-\vec{x}'\right|, R_L\right)\, \delta(\vec{y}) \\
&= \int \mathrm{d}^3y'\, W\left(\left|\vec{y}'-\vec{x}'\right|, R_L\right)\, \delta(\vec{y}') \\
&= \int \mathrm{d}^3y\, W\left(|\vec{y}-\vec{x}|, R_L\right)\, \delta'(\vec{y}) \\
&= \delta'_{R_L}(\vec{x}),
\end{aligned} \tag{3.3.18}$$

where in the last passage we have made use of the properties $\mathrm{d}^3y' = \mathrm{d}^3y$ and $(\vec{y}'-\vec{x}') = (\vec{y}-\vec{x})$. This has an important consequence. The local abundance of tracers (galaxies), at fixed proper time, is typically a function of the matter density field (and their spatial derivatives) within a finite region of size $R_* \sim$ few Mpc for most tracers. In most models of bias, the overdensities of the tracers and dark matter are understood as smoothed on some large-scale R_L so that they can be interpreted as a counts-in-cells relation. However, no additional smoothing scale R_L should enter in the final value of observables, e.g. the correlation functions on some scale r. This is because the smoothing scale R_L is not physical, it is just a tool for an effective description and an arbitrary ultra-violet cut-off [105].

The symmetries at our disposal provide a simple and straightforward way to show that the galaxy correlation functions do not depend on the smoothing scale R_L. Indeed, suppose we work in Fourier space and that we change the smoothing scale R_L by an infinitesimal amount δR_L. Correspondingly,

the Fourier transformed window function will be

$$W\left[q(R_L+\delta R_L)\right] \simeq W(qR_L) + qW'(qR_L)\delta R_L$$
$$\simeq W(qR_L)\, e^{qW'(qR_L)/W(qR_L)\delta R_L}, \tag{3.3.19}$$

where the prime stands for the differentiation with respect to the variable qR_L. We can perform now an infinitesimal coordinate transformation $\vec{x}' = \vec{x} + \vec{n}(\tau)$. According to the relation (3.3.18), both tracers and dark matter overdensities will transform in momentum space as

$$\delta'_{\vec{q},R_L} = \delta_{\vec{q},R_L}\, e^{i\vec{q}\cdot\vec{n}(\tau)} = \delta_{\vec{q}} W(qR_L)\, e^{i\vec{q}\cdot\vec{n}(\tau)}. \tag{3.3.20}$$

Therefore

$$\delta'_{\vec{q},R_L+\delta R_L} = \delta_{\vec{q}} W\left[q(R_L+\delta R_L)\right]\, e^{i\vec{q}\cdot\vec{n}(\tau)}$$
$$= \delta_{\vec{q},R_L}\, e^{qW'(qR_L)/W(qR_L)\delta R_L}\, e^{i\vec{q}\cdot\vec{n}(\tau)}. \tag{3.3.21}$$

We see that if we choose the infinitesimal vector $\vec{n}(\tau)$ to be

$$\vec{n}(\tau) = i\frac{\vec{q}}{q}\frac{W'(qR_L)}{W(qR_L)}\delta R_L, \tag{3.3.22}$$

we can compensate the infinitesimal change of the smoothing radius R_L and obtain that

$$\delta'_{\vec{q},R_L+\delta R_L} = \delta_{\vec{q},R_L}. \tag{3.3.23}$$

Since the correlators in the old and the new coordinate system have to be the same, we conclude that the dependence on the smoothing radius R_L drops off. Physically, this is due to the fact that changing the large-scale smoothing radius by some amount amounts to include (or exclude) more momentum modes into the smoothed overdensity. This addition (or subtraction) of momentum modes can be compensated by going to a coordinate system where these long wavelength modes have been removed (or added). This argument holds in all epochs, included the Λ-dominated epoch. During the matter-dominated epoch we have another tool to reach the same conclusion: the Lifshitz symmetry. Indeed, The change in the smoothing scale R_L can be compensated by a scaling transformation $\vec{x}' = \lambda\vec{x}$, or $\vec{q}' = \vec{q}/\lambda$. In such a case we have

$$\delta'_{\vec{q},R_L+\delta R_L} = \delta_{\vec{q}/\lambda} W\left[q/\lambda(R_L+\delta R_L)\right]. \tag{3.3.24}$$

If we choose $\lambda = \lambda_{R_L} = (1 + \delta R_L/R_L)$, we obtain

$$\delta'_{\vec{q},R_L+\delta R_L} = \delta_{\vec{q}/\lambda_{R_L},R_L}, \tag{3.3.25}$$

and again we conclude that the smoothing scale dependence drops off when correlators are considered.

3.3.3 Galaxy bispectrum consistency relation at tree-level

Since the bias model (3.3.8) respects the symmetries (1.4.7-1.4.10), the three-point function of galaxies computed in this model should satisfy the consistency relation. In the next two subsections we explicitly verify that this is the case in perturbation theory at the tree and one-loop levels. Let us start with the tree-level case. The equal time DM-galaxy cross-correlation at second order in perturbation theory is

$$\langle \delta_L(\vec{k},\tau)\delta_{\rm g}^L(-\vec{k},\tau)\rangle' = b_1(\tau)P_L(k,\tau), \tag{3.3.26}$$

while the unequal time power spectrum is

$$\langle \delta_{\rm g}^L(\vec{k},\tau_1)\delta_{\rm g}^L(-\vec{k},\tau_2)\rangle' = b_1(\tau_1)b_1(\tau_2)\langle \delta_L(\vec{k},\tau_1)\delta_L(-\vec{k},\tau_2)\rangle'. \tag{3.3.27}$$

The bispectrum of the galaxies at fourth order for unequal times is

$$\begin{aligned}\langle \delta_{\rm g}(\vec{q},\tau)\delta_{\rm g}(\vec{k}_1,\tau_1)\delta_{\rm g}(\vec{k}_2,\tau_2)\rangle'\Big|_{\delta^{(4)}} &= b_1(\tau_1)b_1(\tau_2)\\ &\langle \delta_L(\vec{k}_1,\tau_1)\delta_L(-\vec{k}_1,\tau)\rangle'\langle \delta_L(\vec{k}_2,\tau_2)\delta_L(-\vec{k}_2,\tau)\rangle'\\ &\times\left[2b_1(\tau)F_S^{(2)}(\vec{k}_1,\vec{k}_2)+b_2(\tau)+c_{s^2}(\tau)S(\vec{k}_1,\vec{k}_2)\right]\\ &+\text{cyclic permutations of } (\tau,\vec{q}),(\tau_1,\vec{k}_1) \text{ and } (\tau_2,\vec{k}_2),\end{aligned} \tag{3.3.28}$$

where

$$\begin{aligned}F_S^{(2)}(\vec{k}_1,\vec{k}_2) &= \left[\frac{5}{7}+\frac{1}{2}(\vec{k}_1\cdot\vec{k}_2)\frac{k_1^2+k_2^2}{k_1^2k_2^2}+\frac{2}{7}\frac{(\vec{k}_1\cdot\vec{k}_2)^2}{k_1^2k_2^2}\right],\\ S(\vec{k}_1,\vec{k}_2) &= -\frac{1}{3}+\frac{(\vec{k}_1\cdot\vec{k}_2)^2}{k_1^2k_2^2}.\end{aligned} \tag{3.3.29}$$

In the squeezed limit $q \to 0$, $\vec{k}_1 \simeq -\vec{k}_2$ we find

$$\begin{aligned}
\langle \delta_{\rm g}(\vec{q},\tau)\delta_{\rm g}(\vec{k}_1,\tau_1)\delta_{\rm g}(\vec{k}_2,\tau_2)\rangle'_{q\to 0}\Big|_{\delta^{(4)}} &= b_1(\tau)b_1(\tau_1)b_1(\tau_2)\frac{\vec{q}\cdot\vec{k}_1}{q^2}\langle \delta_L(\vec{k}_1,\tau_1)\delta_L(-\vec{k}_1,\tau_2)\rangle' \\
&\quad \times \left(\langle \delta_L(\vec{q},\tau)\delta_L(-\vec{q},\tau_2)\rangle' - \langle \delta_L(\vec{q},\tau)\delta_L(-\vec{q},\tau_1)\rangle'\right) \\
&= b_1(\tau)b_1(\tau_1)b_1(\tau_2)\frac{\vec{q}\cdot\vec{k}_1}{q^2}\langle \delta_L(\vec{k}_1,\tau_1)\delta_L(-\vec{k}_1,\tau_2)\rangle' \\
&\quad \times P_L(q,\tau)\left(\frac{D(\tau_2)}{D(\tau)} - \frac{D(\tau_1)}{D(\tau)}\right) \\
&= -\left\langle \delta^{(1)}_{\rm g}(\vec{q},\tau)\delta^{(1)}(\vec{q},\tau)\right\rangle'\left(\frac{D(\tau_1)}{D(\tau)} - \frac{D(\tau_2)}{D(\tau)}\right) \\
&\quad \times \frac{\vec{q}\cdot\vec{k}_1}{q^2}\left\langle \delta^{(1)}_{\rm g}(\vec{k}_1,\tau_1)\delta^{(1)}_{\rm g}(\vec{k}_2,\tau_2)\right\rangle'. \qquad (3.3.30)
\end{aligned}$$

We observe that the consistency relation is trivially satisfied at linear order. One should note that non-local terms are sub-leading. We shall therefore ignore them in the one-loop computation and consider only the local-bias model in the following.

3.3.4 Galaxy bispectrum consistency relation at one-loop

To check the consistency relation at one-loop, or more precisely at order 6 in perturbation theory, we have to evaluate the following expression

$$\begin{aligned}
\langle \delta_{\rm g}(\vec{q},\tau)\delta_{\rm g}(\vec{k}_1,\tau_1)\delta_{\rm g}(\vec{k}_2,\tau_2)\rangle'\Big|_{\delta^{(6)}} &= \frac{\vec{q}\cdot\vec{k}_1}{q^2}\left(\frac{D(\tau_2)}{D(\tau)} - \frac{D(\tau_1)}{D(\tau)}\right) \\
&\quad \times \left[\langle \delta^{(1)}(\vec{q},\tau)\delta_{\rm g}(-\vec{q},\tau)\rangle'\langle \delta_{\rm g}(\vec{k}_1,\tau_1)\delta_{\rm g}(\vec{k}_2,\tau_2)\rangle'\right]_{\delta^{(6)}}. \qquad (3.3.31)
\end{aligned}$$

We first consider the right-hand side where one should be careful when expanding the square parenthesis. Indeed, even when δ is in the linear regime, $\delta_{\rm g}$ might be non-linear and higher order corrections to $\delta_{\rm g}$ have to be taken into account. The square parenthesis at order 4 in perturbation theory is therefore

$$\left[\langle \delta^{(1)}(\vec{q},\tau)\delta_{\rm g}(-\vec{q},\tau)\rangle'\langle \delta_{\rm g}(\vec{k}_1,\tau_1)\delta_{\rm g}(\vec{k}_2,\tau_2)\rangle'\right]_{\delta^{(6)}} =$$

$$\langle\delta_L(\vec{q},\tau)\delta_{\rm g}^L(-\vec{q},\tau)\rangle'\ \langle\delta_{\rm g}(\vec{k}_1,\tau_1)\delta_{\rm g}(\vec{k}_2,\tau_2)\rangle'\Big|_{\delta^{(4)}}$$

$$+\ \langle\delta^{(1)}(\vec{q},\tau)\delta_{\rm g}^{(3)}(-\vec{q},\tau)\rangle'\langle\delta_{\rm g}^L(\vec{k}_1,\tau_1)\delta_{\rm g}^L(\vec{k}_2,\tau_2)\rangle', \quad (3.3.32)$$

where $\delta_{\rm g}^{(3)}(\vec{q},\tau)$ is the third order contribution to $\delta_{\rm g}(\vec{q},\tau)$. The first term on the right-hand side can be written using the bias model as

$$\langle\delta_L(\vec{q},\tau)\delta_{\rm g}^L(-\vec{q},\tau)\rangle'\ \langle\delta_{\rm g}(\vec{k}_1,\tau_1)\delta_{\rm g}(\vec{k}_2,\tau_2)\rangle'\Big|_{\delta^{(4)}} =$$

$$b_1(\tau)\langle\delta_L(\vec{q},\tau)\delta_L(-\vec{q},\tau)\rangle'\left(P_{\rm g}^{11}+P_{\rm g}^{12}+P_{\rm g}^{22}+P_{\rm g}^{13}\right), \quad (3.3.33)$$

where

$$P_{\rm g}^{11} = b_1(\tau_1)b_1(\tau_2)\ \langle\delta(\vec{k}_1,\tau_1)\delta(\vec{k}_2,\tau_2)\rangle'\Big|_{\delta^{(4)}}, \quad (3.3.34)$$

$$P_{\rm g}^{12} = \frac{1}{2}b_1(\tau_1)b_2(\tau_2)\int {\rm d}^3p\ \langle\delta(\vec{k}_1,\tau_1)\delta(\vec{p},\tau_2)\delta(\vec{k}_2-\vec{p},\tau_2)\rangle'\Big|_{\delta^{(4)}}$$

$$+\ (\vec{k}_1,\tau_1)\leftrightarrow(\vec{k}_2,\tau_2), \quad (3.3.35)$$

$$P_{\rm g}^{22} = \frac{b_2(\tau_1)b_2(\tau_2)}{2}$$

$$\times\int {\rm d}^3p\,\langle\delta_L(\vec{p},\tau_1)\delta_L(-\vec{p},\tau_2)\rangle'\langle\delta_L(\vec{k}_1-\vec{p},\tau_1)\delta_L(-\vec{k}_1+\vec{p},\tau_2)\rangle', \quad (3.3.36)$$

$$P_{\rm g}^{13} = \frac{b_1(\tau_1)b_3(\tau_2)}{2}\langle\delta_L(\vec{k}_1,\tau_1)\delta_L(\vec{k}_2,\tau_2)\rangle'\sigma_L^2(\tau_2)$$

$$+\ (\vec{k}_1,\tau_1)\leftrightarrow(\vec{k}_2,\tau_2), \quad (3.3.37)$$

while the second term is

$$\langle\delta^{(1)}(\vec{q},\tau)\delta_{\rm g}^{(3)}(-\vec{q},\tau)\rangle'\langle\delta_{\rm g}^L(\vec{k}_1,\tau_1)\delta_{\rm g}^L(\vec{k}_2,\tau_2)\rangle' =$$

$$\frac{1}{2}b_3(\tau)b_1(\tau_1)b_1(\tau_2)\sigma_L^2(\tau)\langle\delta_L(\vec{q},\tau)\delta_L(-\vec{q},\tau)\rangle'\langle\delta_L(\vec{k}_1,\tau_1)\delta_L(\vec{k}_2,\tau_2)\rangle', \quad (3.3.38)$$

where we defined the linear variance

$$\sigma_L^2(\tau) \equiv \int \mathrm{d}^3p \; P_L(p,\tau). \tag{3.3.39}$$

Let us now compute the left-hand side of Eq. (3.3.31) with the help the expressions one can find in Ref. [106] and check that the equality is satisfied. The unequal-time bispectrum $\langle \delta_{\rm g}(\vec{q},\tau)\delta_{\rm g}(\vec{k}_1,\tau_1)\delta_{\rm g}(\vec{k}_2,\tau_2)\rangle'$ is composed by several terms which, for compactness, we shall denote analogously to what done in Ref. [106] by the notation

$$\begin{aligned}\delta^D(\vec{q}+\vec{k}_1+\vec{k}_2)B^{ijk}_{\mathrm{g},q\to 0} \equiv \lim_{q\to 0}\Bigg[&\frac{b_i(\tau)b_j(\tau_1)b_k(\tau_2)}{i!j!k!}\langle \delta^i(\vec{q},\tau)\delta^j(\vec{k}_1,\tau_1)\delta^k(\vec{k}_2,\tau_2)\rangle \\ &+ \text{ permutations } (\tau,\vec{q}),(\tau_1,\vec{k}_1),(\tau_2,\vec{k}_2)\Bigg].\end{aligned} \tag{3.3.40}$$

In the following, we compute each term identifying the ones which behave at least $\mathcal{O}(q^{-1}P_L(q))$ as $q\to 0$.

- The first term is

$$\begin{aligned}B^{111}_{\mathrm{g},q\to 0} &= b_1(\tau)b_1(\tau_1)b_1(\tau_2)\;\langle \delta(\vec{q},\tau)\delta(\vec{k}_1,\tau_1)\delta(\vec{k}_2,\tau_2)\rangle'_{q\to 0}\Big|_{\delta^{(6)}} \\ &= b_1(\tau)b_1(\tau_1)b_1(\tau_2) \\ &\quad\times\left[P_L(q,\tau)\frac{\vec{q}\cdot\vec{k}_1}{q^2}\left(\frac{D(\tau_2)}{D(\tau)}-\frac{D(\tau_1)}{D(\tau)}\right)\langle \delta(\vec{k}_1,\tau_1)\delta(\vec{k}_2,\tau_2)\rangle'\Big|_{\delta^{(4)}}\right],\end{aligned} \tag{3.3.41}$$

where we used the consistency relation for matter. This is exactly the term proportional to $P^{11}_{\rm g}$ in Eq. (3.3.34) in the right-hand side of the consistency relation.

- We express the trispectrum in the integral of the following term using the consistency relation

$$\begin{aligned}B^{112,II}_{\mathrm{g},q\to 0} &= \frac{1}{2}b_1(\tau)b_1(\tau_1)b_2(\tau_2)\int \mathrm{d}^3p\;\langle \delta(\vec{q},\tau)\delta(\vec{k}_1,\tau_1)\delta(\vec{p},\tau_2)\delta(\vec{k}_2-\vec{p},\tau_2)\rangle'_{q\to 0}\Big|_{\delta^{(6)}} \\ &\quad + 2 \text{ perm.} \\ &= \frac{1}{2}b_1(\tau)b_1(\tau_1)b_2(\tau_2)\int \mathrm{d}^3p\;\langle \delta(\vec{q},\tau)\delta(\vec{k}_1,\tau_1)\delta(\vec{p},\tau_2)\delta(\vec{k}_2-\vec{p},\tau_2)\rangle'_{q\to 0}\Big|_{\delta^{(6)}} \\ &\quad + (\tau_1,\vec{k}_1)\leftrightarrow(\tau_2,\vec{k}_2) \\ &= -P_L(q,\tau)\int \mathrm{d}^3p\left[\frac{\vec{q}\cdot\vec{k}_1}{q^2}\frac{D(\tau_1)}{D(\tau)}+\frac{\vec{q}\cdot\vec{p}}{q^2}\frac{D(\tau_2)}{D(\tau)}+\frac{\vec{q}\cdot(\vec{k}_2-\vec{p})}{q^2}\frac{D(\tau_2)}{D(\tau)}\right]\end{aligned}$$

$$\times \langle \delta(\vec{k}_1,\tau_1)\delta(\vec{p},\tau)\delta(\vec{k}_2-\vec{p},\tau_2)\rangle'\Big|_{\delta^{(4)}} + (\tau_1,\vec{k}_1) \leftrightarrow (\tau_2,\vec{k}_2)$$

$$= -P_L(q,\tau)\frac{\vec{q}\cdot\vec{k}_1}{q^2}\left[\frac{D(\tau_1)}{D(\tau)} - \frac{D(\tau_2)}{D(\tau)}\right]\int \mathrm{d}^3p\ \langle \delta(\vec{k}_1,\tau_1)\delta(\vec{p},\tau)\delta(\vec{k}_2-\vec{p},\tau_2)\rangle'\Big|_{\delta^{(4)}}$$

$$+ (\tau_1,\vec{k}_1) \leftrightarrow (\tau_2,\vec{k}_2). \tag{3.3.42}$$

This is equal to the term proportional to $P_{\rm g}^{12}$ in Eq. (3.3.35). In the second line we ignored the permutation containing a bispectrum not in the squeezed limit.

- The following contribution reproduces the term proportional to $P_{\rm g}^{22}$ in Eq. (3.3.36).

$$\begin{aligned}
B^{122,II}_{{\rm g},q\to 0} &= b_1(\tau)b_2(\tau_1)b_2(\tau_2)\int \mathrm{d}^3p\ \langle \delta(\vec{q},\tau)\delta(\vec{p},\tau_1)\delta(-\vec{q}-\vec{p},\tau_2)\rangle'_{q\to 0}\big|_{\delta^{(4)}} \\
&\quad \times \langle \delta_L(\vec{k}_1-\vec{p},\tau_1)\delta_L(-\vec{k}_1+\vec{p},\tau_2)\rangle' + \ 2 \text{ perm.} \\
&= b_1(\tau)b_2(\tau_1)b_2(\tau_2)\int \mathrm{d}^3p\ \langle \delta(\vec{q},\tau)\delta(\vec{p},\tau_1)\delta(\vec{q}+\vec{p},\tau_2)\rangle'_{q\to 0}\big|_{\delta^{(4)}} \\
&\quad \times \langle \delta_L(\vec{k}_1-\vec{p},\tau_1)\delta_L(\vec{k}_1-\vec{p},\tau_2)\rangle' \\
&= -b_1(\tau)b_2(\tau_1)b_2(\tau_2)P_L(q,\tau)\left[\frac{D(\tau_1)}{D(\tau)} - \frac{D(\tau_2)}{D(\tau)}\right] \\
&\quad \times \int \mathrm{d}^3p\,\frac{\vec{q}\cdot(\vec{k}_1-\vec{p})}{q^2}\langle \delta_L(\vec{k}_1-\vec{p},\tau_1)\delta_L(-\vec{k}_1+\vec{p},\tau_2)\rangle' \\
&\quad \times \langle \delta_L(\vec{p},\tau_1)\delta_L(-\vec{p},\tau_2)\rangle' \\
&= -\frac{1}{2}b_1(\tau)b_2(\tau_1)b_2(\tau_2)P_L(q,\tau)\left[\frac{D(\tau_1)}{D(\tau)} - \frac{D(\tau_2)}{D(\tau)}\right]\frac{\vec{q}\cdot\vec{k}_1}{q^2} \\
&\quad \times \int \mathrm{d}^3p\,\langle \delta_L(\vec{k}_1-\vec{p},\tau_1)\delta_L(-\vec{k}_1+\vec{p},\tau_2)\rangle' \\
&\quad \times \langle \delta_L(\vec{p},\tau_1)\delta_L(-\vec{p},\tau_2)\rangle'.
\end{aligned} \tag{3.3.43}$$

In the second equality we kept the only permutation enhanced in the squeezed limit and in the third we used the consistency relation for matter. Finally, we used the fact that

$$\int \mathrm{d}^3p\,\frac{\vec{q}\cdot\vec{p}}{q^2}\langle \delta_L(\vec{k}_1-\vec{p},\tau_1)\delta_L(-\vec{k}_1+\vec{p},\tau_2)\rangle'\langle \delta_L(\vec{p},\tau_1)\delta_L(-\vec{p},\tau_2)\rangle' =$$

$$\frac{1}{2}\int \mathrm{d}^3p\,\frac{\vec{q}\cdot\vec{k}_1}{q^2}\langle\delta_L(\vec{k}_1-\vec{p},\tau_1)\delta_L(-\vec{k}_1+\vec{p},\tau_2)\rangle'\langle\delta_L(\vec{p},\tau_1)\delta_L(-\vec{p},\tau_2)\rangle', \quad (3.3.44)$$

which can be deduced simply by doing the shift $\vec{p}\to\vec{k}_1-\vec{p}$.

• The term below is enhanced in the squeezed limit as it contains a bispectrum at unequal times. It reproduces the term proportional to $P_{\rm g}^{13}$ in Eq. (3.3.37) together with the term in Eq. (3.3.38)

$$\begin{aligned}B^{113,II}_{\mathrm{g},q\to0} &= \left[\frac{1}{2}b_1(\tau)b_1(\tau_1)b_3(\tau_2)\sigma_L^2(\tau_2)+2\text{ perm.}\right]\langle\delta(\vec{q},\tau)\delta(\vec{k}_1,\tau_1)\delta(\vec{k}_2,\tau_2)\rangle'_{q\to0}\Big|_{\delta^{(4)}}\\ &= \left[\frac{1}{2}b_1(\tau)b_1(\tau_1)b_3(\tau_2)\sigma_L^2(\tau_2)+2\text{ perm.}\right]\\ &\quad\times\frac{\vec{q}\cdot\vec{k}_1}{q^2}P_L(q,\tau)\left(\frac{D(\tau_2)}{D(\tau)}-\frac{D(\tau_1)}{D(\tau)}\right)\langle\delta_L(\vec{k}_1,\tau_1)\delta_L(\vec{k}_2,\tau_2)\rangle'. \quad (3.3.45)\end{aligned}$$

• The term

$$\begin{aligned}B^{112,I}_{\mathrm{g},q\to0} &= b_1^2b_2\left[P(q)P(k_1)\right]_{\delta^{(6)}}+\ 2\text{ perm.} \quad (3.3.46)\\ &= \mathcal{O}(P_L(q)) \quad (3.3.47)\end{aligned}$$

is not dominant because the $\mathcal{O}(\delta^{(4)})$ corrections to $P(q)$ are at most $\mathcal{O}(P_L(q))$ when $q\to0$.

• The following terms are not relevant because they involve either terms that are proportional to the non-squeezed bispectrum, which makes them at most $\mathcal{O}(P_L(q))$, or terms containing the bispectrum in the squeezed limit at equal times, which vanish due to the consistency relation. B denotes the bispectrum of matter

$$\begin{aligned}B^{122,I}_{\mathrm{g},q\to0} &= \frac{b_1b_2^2}{2}P_L(k_1)\int\mathrm{d}^3p\ B|_{\delta^{(4)}}(k_2,p,|\vec{k}_2-\vec{p}|)+\ 5\text{ perm.}\\ &= \mathcal{O}(P_L(q)), \quad (3.3.48)\\ B^{113,I}_{\mathrm{g},q\to0} &= \frac{b_1^2b_3}{2}P_L(k_1)\int\mathrm{d}^3p\ B|_{\delta^{(4)}}(k_1,p,|\vec{k}_1-\vec{p}|)+\ 5\text{ perm.}\\ &= \mathcal{O}(P_L(q)). \quad (3.3.49)\end{aligned}$$

• The following terms are not enhanced in the squeezed limit as they are just products of linear

power spectra at this order

$$B^{222}_{\mathrm{g},q\to 0} = \frac{b_2^3}{2}\int \mathrm{d}^3p\, P_L(p)P_L(|\vec{q}+\vec{p}|)P_L(|\vec{k}_1-\vec{p}|)$$
$$= \mathcal{O}(1), \tag{3.3.50}$$
$$B^{123,I}_{\mathrm{g},q\to 0} = \frac{b_1b_2b_3}{2}P_L(q)\int \mathrm{d}^3p\, P_L(|\vec{k}_1-\vec{p}|)P_L(p) + \text{ 5 perm.}$$
$$= \mathcal{O}(P_L(q)), \tag{3.3.51}$$
$$B^{123,II}_{\mathrm{g},q\to 0} = b_1b_2b_3P_L(q)P_L(k_1)\sigma_L^2 + \text{ 2 perm.} = \mathcal{O}(P_L(q)), \tag{3.3.52}$$
$$B^{114,I}_{\mathrm{g},q\to 0} = \frac{b_1^2b_4}{2}P_L(q)P_L(k_1)\sigma_L^2 + \text{ 2 perm.} = \mathcal{O}(P_L(q)). \tag{3.3.53}$$

• Finally, the two- and three-loops corrections ignored in Ref. [106] are at most constant in the squeezed limit such that our result is fully correct at sixth order. Overall, we conclude that the galaxy consistency relation is satisfied at tree- and one-loop level.

3.4 Consistency relation of galaxy correlation functions in redshift space

Let us now discuss how the galaxy consistency relations are modified when going from real space to redshift space where experiments are performed. The mapping from real-space position $\vec{x}$ to redshift space $\vec{s}$ is given by [107]

$$\vec{s} = \vec{x} + \frac{1}{\mathcal{H}}(\vec{v}_{\mathrm{g}}\cdot\hat{x})\hat{x}, \tag{3.4.1}$$

and the density field in redshift space is obtained by imposing mass conservation

$$[1+\delta_{\mathrm{g}}(\vec{s})]\mathrm{d}^3s = [1+\delta_{\mathrm{g}}(\vec{x})]\mathrm{d}^3x. \tag{3.4.2}$$

In Fourier space the condition (3.4.2) reads

$$\delta_{\mathrm{D}}(\vec{k}) + \delta_{\mathrm{g},s}(\vec{k}) = \int \frac{\mathrm{d}^3x}{(2\pi)^3}\, e^{-i\vec{k}\cdot\vec{x}}\, e^{-i\vec{v}_{\mathrm{g}}(\vec{x})\cdot\hat{x}\,(\vec{k}\cdot\hat{x})/\mathcal{H}}[1+\delta_{\mathrm{g}}(\vec{x})]. \tag{3.4.3}$$

By performing a spatial coordinate transformation $\vec{x}\to\vec{x}' = \vec{x}+\vec{n}(\tau)$ we know that, if $\delta_{\mathrm{g}}(\vec{x},\tau)$ and $\vec{v}(\vec{x},\tau)$ satisfy the fluid equations, then $\delta'_{\mathrm{g}}(\vec{x},\tau) = \delta_{\mathrm{g}}(\vec{x}',\tau)$ and $\vec{v}'(\vec{x},\tau) = \vec{v}(\vec{x}',\tau) - \dot{\vec{n}}$ do as well. This

implies that for the new solution we have

$$\begin{aligned}
\delta_{\rm D}(\vec{k}) + \delta'_{{\rm g},s}(\vec{k}) &= \int \frac{{\rm d}^3x}{(2\pi)^3}\, e^{-i\vec{k}\cdot\vec{x}} e^{-i\vec{v}'_{\rm g}(\vec{x})\cdot\hat{x}\,(\vec{k}\cdot\hat{x})/\mathcal{H}}[1+\delta'_{\rm g}(\vec{x})] \\
&= \int \frac{{\rm d}^3x}{(2\pi)^3}\, e^{-i\vec{k}\cdot\vec{x}}\, e^{-i\vec{v}_{\rm g}(\vec{x}')\cdot\hat{x}\,(\vec{k}\cdot\hat{x})/\mathcal{H}}\, e^{i\dot{\vec{n}}\cdot\hat{x}\,(\vec{k}\cdot\hat{x})/\mathcal{H}}[1+\delta_{\rm g}(\vec{x}')] \\
&\simeq \int \frac{{\rm d}^3x}{(2\pi)^3}\, e^{-i\vec{k}\cdot\vec{x}}\, e^{-i\vec{v}_{\rm g}(\vec{x})\cdot\hat{x}\,(\vec{k}\cdot\hat{x})/\mathcal{H}}\, e^{-i[(\vec{n}\cdot\vec{\nabla})\vec{v}_{\rm g}]\cdot\hat{x}\,(\vec{k}\cdot\hat{x})/\mathcal{H}} e^{i\dot{\vec{n}}\cdot\hat{x}\,(\vec{k}\cdot\hat{x})/\mathcal{H}} \\
&\quad \times [1+\delta_{\rm g}(\vec{x}) + (\vec{n}\cdot\vec{\nabla})\delta_{\rm g}(\vec{x})]. \qquad (3.4.4)
\end{aligned}$$

This expression is exact. Expanding for small $\vec{n}(\tau)$, we obtain

$$\begin{aligned}
\delta_{\rm D}(\vec{k}) + \delta'_{{\rm g},s}(\vec{k}) &\simeq \int \frac{{\rm d}^3x}{(2\pi)^3}\, e^{-i\vec{k}\cdot\vec{x}}\, e^{-i\vec{v}_{\rm g}(\vec{x})\cdot\hat{x}\,(\vec{k}\cdot\hat{x})/\mathcal{H}}[1+\delta_{\rm g}(\vec{x})] \\
&\quad + \frac{1}{\mathcal{H}}\int \frac{{\rm d}^3x}{(2\pi)^3}\, e^{-i\vec{k}\cdot\vec{x}}\, e^{-i\vec{v}_{\rm g}(\vec{x})\cdot\hat{x}\,(\vec{k}\cdot\hat{x})/\mathcal{H}}(\vec{k}\cdot\hat{x}) \\
&\qquad \times \left\{-i\left[(\vec{n}\cdot\vec{\nabla})\vec{v}_{\rm g}(\vec{x})\right]\cdot\hat{x} + i(\dot{\vec{n}}\cdot\hat{x})\right\}[1+\delta_{\rm g}(\vec{x})] \\
&\quad + \int \frac{{\rm d}^3x}{(2\pi)^3}\, e^{-i\vec{k}\cdot\vec{x}}\, e^{-i\vec{v}_{\rm g}(\vec{x})\cdot\hat{x}\,(\vec{k}\cdot\hat{x})/\mathcal{H}}\,(\vec{n}\cdot\vec{\nabla})\delta_{\rm g}(\vec{x}) \\
&= \delta_{\rm D}(\vec{k}) + \delta_{{\rm g},s}(\vec{k}) \\
&\quad + \frac{1}{\mathcal{H}}\int \frac{{\rm d}^3x}{(2\pi)^3}\, e^{-i\vec{k}\cdot\vec{x}}\, e^{-i\vec{v}_{\rm g}(\vec{x})\cdot\hat{x}\,(\vec{k}\cdot\hat{x})/\mathcal{H}}(\vec{k}\cdot\hat{x}) \\
&\qquad \times \left\{-i\left[(\vec{n}\cdot\vec{\nabla})\vec{v}_{\rm g}(\vec{x})\right]\cdot\hat{x} + i(\dot{\vec{n}}\cdot\hat{x})\right\}[1+\delta_{\rm g}(\vec{x})] \\
&\quad + \int \frac{{\rm d}^3x}{(2\pi)^3}\, e^{-i\vec{k}\cdot\vec{x}}\, e^{-i\vec{v}_{\rm g}(\vec{x})\cdot\hat{x}\,(\vec{k}\cdot\hat{x})/\mathcal{H}}\,(\vec{n}\cdot\vec{\nabla})\,[1+\delta_{\rm g}(\vec{x})]\,. \qquad (3.4.5)
\end{aligned}$$

If we start from this expression, upon integrating by parts we find

$$\begin{aligned}
\delta_{\rm D}(\vec{k}) + \delta'_{{\rm g},s}(\vec{k}) &= \delta_{\rm D}(\vec{k}) + \delta_{{\rm g},s}(\vec{k}) \\
&\quad + \frac{i}{\mathcal{H}}\int \frac{{\rm d}^3x}{(2\pi)^3}\, e^{-i\vec{k}\cdot\vec{x}}\, e^{-i\vec{v}_{\rm g}(\vec{x})\cdot\hat{x}\,(\vec{k}\cdot\hat{x})/\mathcal{H}}(\vec{k}\cdot\hat{x})
\end{aligned}$$

$$\times \left\{ - \left[(\vec{n}\cdot\vec{\nabla})\vec{v}_{\rm g}(\vec{x}) \right] \cdot \hat{x} + (\dot{\vec{n}}\cdot\hat{x}) \right\} \left[1+\delta_{\rm g}(\vec{x})\right]$$

$$+ \frac{i}{\mathcal{H}} \int \frac{{\rm d}^3x}{(2\pi)^3}\, e^{-i\vec{k}\cdot\vec{x}}\, e^{-i\vec{v}_{\rm g}(\vec{x})\cdot\hat{x}\,(\vec{k}\cdot\hat{x})/\mathcal{H}} (\vec{n}\cdot\vec{\nabla})$$

$$\times \left\{ \vec{v}_{\rm g}(\vec{x})\cdot\hat{x}\,(\vec{k}\cdot\hat{x}) \right\} \left[1+\delta_{\rm g}(\vec{x})\right]$$

$$+ i(\vec{k}\cdot\vec{n})\,\delta_{{\rm g},s}(\vec{k}). \tag{3.4.6}$$

This gives

$$\delta_{\rm D}(\vec{k}) + \delta'_{{\rm g},s}(\vec{k}) = \delta_{\rm D}(\vec{k}) + \delta_{{\rm g},s}(\vec{k}) + i(\vec{k}\cdot\vec{n})\,\delta_{{\rm g},s}(\vec{k})$$

$$+ \frac{i}{\mathcal{H}} \int \frac{{\rm d}^3x}{(2\pi)^3}\, e^{-i\vec{k}\cdot\vec{x}}\, e^{-i\vec{v}_{\rm g}(\vec{x})\cdot\hat{x}\,(\vec{k}\cdot\hat{x})/\mathcal{H}} (\vec{k}\cdot\hat{x})$$

$$\times \left\{ \left[(\vec{n}\cdot\vec{\nabla})\hat{x} \right] \cdot \vec{v}_{\rm g}(\vec{x}) + (\dot{\vec{n}}\cdot\hat{x}) \right\} \left[1+\delta_{\rm g}(\vec{x})\right]$$

$$+ \frac{i}{\mathcal{H}} \int \frac{{\rm d}^3x}{(2\pi)^3}\, e^{-i\vec{k}\cdot\vec{x}}\, e^{-i\vec{v}_{\rm g}(\vec{x})\cdot\hat{x}\,(\vec{k}\cdot\hat{x})/\mathcal{H}} [\vec{v}_{\rm g}(\vec{x})\cdot\hat{x}][1+\delta_{\rm g}(\vec{x})]$$

$$\times (\vec{n}\cdot\vec{\nabla})(\vec{k}\cdot\hat{x}). \tag{3.4.7}$$

At this point we can use the distant observer approximation, that is take the direction of the vector $\vec{x}$ fixed, since it varies little from galaxy to galaxy: galaxies are relatively close to each other on the plane orthogonal to the line-of-sight. This amounts to taking $\vec{\nabla}\hat{x} \simeq \vec{0}$ and we finally obtain

$$\delta_{\rm D}(\vec{k}) + \delta'_{{\rm g},s}(\vec{k}) = \delta_{\rm D}(\vec{k}) + \delta_{{\rm g},s}(\vec{k}) + i(\vec{k}\cdot\vec{n})\,\delta_{{\rm g},s}(\vec{k})$$

$$+ \quad \frac{i}{\mathcal{H}} \int \frac{{\rm d}^3x}{(2\pi)^3}\, e^{-i\vec{k}\cdot\vec{x}}\, e^{-i\vec{v}_{\rm g}(\vec{x})\cdot\hat{x}\,(\vec{k}\cdot\hat{x})/\mathcal{H}} (\vec{k}\cdot\hat{x})(\dot{\vec{n}}\cdot\hat{x})\,[1+\delta_{\rm g}(\vec{x})]. \tag{3.4.8}$$

Note that here the first line corresponds to the field transformation that gives rise to the consistency relation, which in redshift space will contain new terms induced by the second line of this expression. Using the explicit expression for $\dot{\vec{n}}$

$$\dot{\vec{n}}(\tau) = -\vec{v}_L(\tau) = -i\frac{\vec{q}}{q^2}\mathcal{H}f(\tau)\delta_L(\vec{q},\tau), \tag{3.4.9}$$

we obtain,

$$\begin{aligned}\delta_{\rm D}(\vec{k})+\delta'_{{\rm g},s}(\vec{k}) &= \delta_{\rm D}(\vec{k})+\delta_{{\rm g},s}(\vec{k})+\frac{\vec{k}\cdot\vec{q}}{q^2}\,\delta(\vec{q})\delta_{{\rm g},s}(\vec{k}) \\ &\quad + f\frac{k}{q}\delta(\vec{q})\int\frac{{\rm d}^3x}{(2\pi)^3}\,e^{-i\vec{k}\cdot\vec{x}}\,e^{-i\vec{v}_{\rm g}(\vec{x})\cdot\hat{x}\,(\vec{k}\cdot\hat{x})/\mathcal{H}}\mu_{\vec{k}}\mu_{\vec{q}}[1+\delta_{\rm g}(\vec{x})] \\ &= \delta_{\rm D}(\vec{k})+\delta_{{\rm g},s}(\vec{k})+\frac{\vec{k}\cdot\vec{q}}{q^2}\,\delta(\vec{q})\delta_{{\rm g},s}(\vec{k})+f\frac{k}{q}\mu_{\vec{k}}\mu_{\vec{q}}\delta(\vec{q})\delta_{{\rm g},s}(\vec{k})\,, \end{aligned} \tag{3.4.10}$$

where $\mu_{\vec{k}}$ is the cosine between the vector $\hat{k}$ and $\hat{x}$, and we used the distant observer approximation to take the cosines out of the integral in the second equality. We therefore obtain that in redshift space the consistency relations reads

$$\boxed{\begin{aligned}&\frac{\Big\langle\delta_{{\rm g},s}(\vec{q},\tau)\delta_{{\rm g},s}(\vec{k}_1,\tau_1)\cdots\delta_{{\rm g},s}(\vec{k}_n,\tau_n)\Big\rangle'_{q\to0}}{\Big\langle\delta_{{\rm g},s}(\vec{q},\tau_1)\cdots\delta_{{\rm g},s}(\vec{k}_n,\tau_n)\Big\rangle'} = \\ &\qquad -\frac{P_{{\rm g},s}(q,\tau)}{b_1(\tau)+f(\tau)\mu^2_{\vec{q}}}\sum_{a=1}^{n}\frac{D(\tau_a)}{D(\tau)}\left(\frac{\vec{q}\cdot\vec{k}_a}{q^2}+f(\tau_a)\frac{k_a}{q}\mu_{\vec{q}}\mu_{\vec{k}_a}\right)\end{aligned}} \tag{3.4.11}$$

where we have used the linear relation [56]

$$\delta_{{\rm g},s}(\vec{q},\tau)=\left[b_1(\tau)+f(\tau)\mu^2_{\vec{q}}\right]\delta(\vec{q},\tau). \tag{3.4.12}$$

In particular, the consistency relation for the bispectrum in redshift space explicitly reads

$$\begin{aligned}\frac{\Big\langle\delta_{{\rm g},s}(\vec{q},\tau)\delta_{{\rm g},s}(\vec{k}_1,\tau_1)\cdots\delta_{{\rm g},s}(\vec{k}_2,\tau_2)\Big\rangle'_{q\to0}}{\Big\langle\delta_{{\rm g},s}(\vec{k}_1,\tau_1)\delta_{{\rm g},s}(\vec{k}_2,\tau_2)\Big\rangle'} &= -\frac{P_{{\rm g},s}(q,\tau)}{b_1(\tau)+f(\tau)\mu^2_{\vec{q}}} \\ &\quad\times\left[\frac{\vec{q}\cdot\vec{k}_1}{q^2}\left(\frac{D(\tau_1)}{D(\tau)}-\frac{D(\tau_2)}{D(\tau)}\right)+\left(\frac{D(\tau_1)}{D(\tau)}f(\tau_1)-\frac{D(\tau_2)}{D(\tau)}f(\tau_2)\right)\frac{k_1}{q}\mu_{\vec{k}_1}\mu_{\vec{q}}\right].\end{aligned} \tag{3.4.13}$$

3.5 Consequences of the symmetries for the modified theories of gravity

Theories that (attempt to) explain the observed cosmic acceleration by modifying general relativity often introduce a new scalar degree of freedom that is active on large scales, but is screened on small scales to match experiments. All these theories introduce an extra light scalar field to modified gravity in the infrared. Typical examples are represented by the $f(R)$ theories [108], which are equivalent to classic scalar-tensor theories [109] and the screening effect takes place through the so-called chameleon mechanism [110], and by Galileon theories [111] where the extra degree of freedom is appropriately dressed through higher-derivative interactions which decouple it form short-scale physics in accordance with solar system tests.

The chameleon for example, has a potential such that it has long range forces outside of objects while it is massive in their interior. Therefore, the existence of such a field is consistent with solar system and fifth force tests but still can modify gravity at large distances. In the following we shall be interested in two kinds of objects (typically galaxies): those sitting in some high density environment which is itself screened and those residing in an environment where the density is at the cosmic mean or even lower (voids), where the objects can be unscreened. In the first region the chameleon-like field is stuck at the minimum of its potential, while in the second region it is excited. As a result, matter in the first region will follow geodesics, whereas matter in the second region will experience a non-gravitational force, due to scalar gradient, departing from the geodesic motion. The galaxy and dark matter consistency relations are based on a coordinate transformation[1] (in a matter-dominated period) [77, 79]

$$\tau' = \tau, \quad \vec{x}' = \vec{x} + \int^{\tau} \mathrm{d}\eta\, \vec{v}_L(\eta) = \vec{x} + \frac{1}{6}\tau^2 \vec{\nabla}\Phi_L; \tag{3.5.1}$$

we are basically removing the time-dependent, but homogeneous gravitational force via a change of coordinates. This corresponds to an homogeneous acceleration transformation which allows to go to a free-falling observer. Therefore, one expects a violation (or a spatial dependence) of the galaxy consistency relation in modified gravity models where the screening mechanism is in action. Note that the consistency relations do not rely on the Equivalence Principle in a strict sense as pointed out in [81] but only require that large scale overdensities satisfy the same equations of motion. We shall refer to a deviation from this as a violation of the "large-scale EP".

Let us implement the presence of the chameleon-like field in the energy-momentum conservation of the non-relativistic dark matter fluid

$$\nabla_\mu T^{\mu\nu} = f^\nu. \tag{3.5.2}$$

[1] Note that here the gradient of the long-wavelength mode $\vec{\nabla}\Phi_L$ is taken to be a constant vector in space, *i*.e. recall that we are doing an expansion on the space variation of Φ_L and keep only terms linear in its gradients.

One finds

$$\frac{\partial\rho(\vec{x},\tau)}{\partial\tau}+\vec{\nabla}\cdot[\rho(\vec{x},\tau)\vec{v}(\vec{x},\tau)]=0, \tag{3.5.3}$$

$$\frac{\partial\vec{v}(\vec{x},\tau)}{\partial\tau}+\mathcal{H}(\tau)\vec{v}(\vec{x},\tau)+[\vec{v}(\vec{x},\tau)\cdot\vec{\nabla}]\vec{v}(\vec{x},\tau)=-\vec{\nabla}\Phi(\vec{x},\tau)-\frac{q}{\rho}\vec{\nabla}\varphi(\vec{x},\tau), \tag{3.5.4}$$

where we assumed that

$$f^i=-q\partial^i\varphi(\vec{x},\tau), \tag{3.5.5}$$

with $\varphi(\vec{x},\tau)$ the scalar field that has environmental couplings that causes a violation of the "large-scale EP" and q is the scalar charge density of the fluid. We follow the parametrization used in Ref. [112] and we assume $q=\epsilon\alpha\rho$, where α is a constant and ϵ is a parameter that describes the degree of screening (ϵ =0 for screened objects and $\epsilon=1$ for unscreened ones). We should supplement the above equations with the Poisson equation for the gravitational potential $\Phi(\vec{x},\tau)$ and a corresponding equation for $\varphi(\vec{x},\tau)$ which we write as

$$\nabla^2\Phi(\vec{x},\tau)=4\pi Ga^2\rho(\vec{x},\tau), \tag{3.5.6}$$

$$\nabla^2\varphi(\vec{x},\tau)=\left(\frac{\partial V}{\partial\varphi}+8\pi G\alpha\rho(\vec{x},\tau)\right)a^2, \tag{3.5.7}$$

where $V(\varphi)$ is the scalar potential of the chameleon-like field. We may now consider perturbations $\rho(\vec{x},\tau)=\overline{\rho}(1+\delta(\vec{x},\tau))$ and $\varphi(\vec{x},\tau)=(\overline{\varphi}+\delta\varphi(\vec{x},\tau))$ around the corresponding background values $\overline{\rho}$ and $\overline{\varphi}$ and we find that these perturbations satisfy the equations

$$\frac{\partial\delta(\vec{x},\tau)}{\partial\tau}+\vec{\nabla}\cdot[(1+\delta(\vec{x},\tau))\vec{v}(\vec{x},\tau)]=0, \tag{3.5.8}$$

$$\frac{\partial\vec{v}(\vec{x},\tau)}{\partial\tau}+\mathcal{H}(\tau)\vec{v}(\vec{x},\tau)+[\vec{v}(\vec{x},\tau)\cdot\vec{\nabla}]\vec{v}(\vec{x},\tau)=-\vec{\nabla}\Phi(\vec{x},\tau)-\epsilon\alpha\vec{\nabla}\delta\varphi(\vec{x},\tau), \tag{3.5.9}$$

$$\nabla^2\Phi(\vec{x},\tau)=4\pi Ga^2\overline{\rho}\delta(\vec{x},\tau), \tag{3.5.10}$$

$$\nabla^2\delta\varphi(\vec{x},\tau)=\left(m^2\delta\varphi(\vec{x},\tau)+8\pi G\alpha\overline{\rho}\delta(\vec{x},\tau)\right)a^2, \tag{3.5.11}$$

where

$$m^2(\vec{x},\tau)=\left.\frac{\partial^2V}{\partial\varphi^2}\right|_{\overline{\varphi}} \tag{3.5.12}$$

is the mass of the scalar field. Restricting ourselves to the matter-dominated case, it can be checked

that Eqs. (3.5.8-3.5.11) are invariant under the transformations

$$\tau' = \tau, \quad \vec{x}' = \vec{x} + \vec{n}(\tau), \tag{3.5.13}$$

$$\delta'(\vec{x}, \tau) = \delta(\vec{x}', \tau'), \tag{3.5.14}$$

$$\vec{v}'(\vec{x}, \tau) = \vec{v}(\vec{x}', \tau') - \dot{\vec{n}}(\tau), \tag{3.5.15}$$

$$\delta\varphi'(\vec{x}, \tau) = \delta\varphi(\vec{x}', \tau'), \tag{3.5.16}$$

$$\Phi'(\vec{x}, \tau) = \Phi(\vec{x}', \tau') - \Big(\ddot{\vec{n}}(\tau) + \mathcal{H}(\tau)\dot{\vec{n}}(\tau)\Big) \cdot \vec{x}. \tag{3.5.17}$$

As a result, it is still possible to remove a long wavelength mode for the velocity perturbation $\vec{v}_L(\tau, \vec{0})$ by properly choosing the vector $\vec{n}(\tau)$ in order.

Indeed, in the linear regime in momentum space the dynamical equations are given by

$$\frac{\partial \delta_L(\vec{q}, \tau)}{\partial \tau} + i\vec{q} \cdot \vec{v}_L(\vec{q}, \tau) = 0, \tag{3.5.18}$$

$$\frac{\partial \vec{v}_L(\vec{q}, \tau)}{\partial \tau} + \mathcal{H}(\tau)\vec{v}_L(\vec{q}, \tau) = -i\vec{q}\Big(\Phi_L(\vec{q}, \tau) + \alpha\epsilon\delta\varphi(\vec{q}, \tau)\Big), \tag{3.5.19}$$

$$q^2\Phi_L(\vec{q}, \tau) = -\frac{3}{2}\mathcal{H}^2\Omega_{\rm m}\delta_L(\vec{q}, \tau), \tag{3.5.20}$$

$$q^2\delta\varphi(\vec{q}, \tau) = -(m^2\delta\varphi)(\vec{q}, \tau)a^2 - 3\alpha\mathcal{H}^2\Omega_{\rm m}\delta_L(\vec{q}, \tau), \tag{3.5.21}$$

where $(m^2\delta\varphi)(\vec{q}, \tau)$ is the Fourier mode of $m^2(\vec{x}, \tau)\delta\varphi(\vec{x}, \tau)$. In particular consider the configurations shown in figure 3.1, in a region outside the spherical over-density of radius R_0 where the chameleon-like field is not screened and its mass may be neglected, one has

$$\delta\varphi(\vec{q}, \tau) \simeq -\frac{3}{q^2}\mathcal{H}^2\Omega_{\rm m}\delta_L(\vec{q}, \tau), \tag{3.5.22}$$

where the equation for the linear matter overdensity satisfies the equation[2]

$$\ddot{\delta}_L + \mathcal{H}(\tau)\dot{\delta}_L - 4\pi G a^2(1 + 2\alpha^2\epsilon)\overline{\rho}\delta_L = 0, \quad r \gtrsim R_0, \tag{3.5.23}$$

with solution $\delta_L^>(\tau) = D^>(\tau)/D^>(\tau_{\rm in})\delta(\tau_{\rm in})$ where $D^>(\tau)$ is the growth function for (3.5.23).

On the contrary, in a screened region, where the field $\delta\varphi$ is massive enough so that φ is not excited, but fixed to some constant background value within a sphere of radius R_0. In such a case the equation

[2]We use dots to denote derivatives with respect to conformal time.

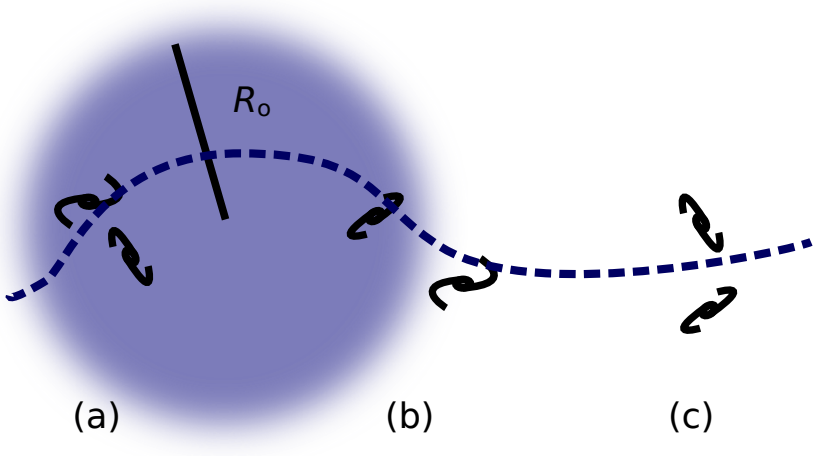

Figure 3.1: *Schematic representation of a large-scale spherical over-density of radius R_0 where the chameleon field is screened, and in the presence of a long-wavelength perturbation of the gravitational field (here represented by the dark blue dashed line). The consistency relation will be given by the correlation of the modulation of the power spectrum with the long-wavelength gravitational field. The case (a) corresponds to the case in which the galaxies are all in the screened region, Eq. (3.5.29), case (c) corresponds to the case in which all the galaxies are in the unscreened region, Eq. (3.5.30), and case (b) corresponds to the case in which there are both screened and unscreened galaxies, Eq. (3.5.31).*

for the overdensity is given by

$$\ddot{\delta}_L + \mathcal{H}(\tau)\dot{\delta}_L - 4\pi G a^2 \bar{\rho}\delta_L = 0, \quad r \lesssim R_0 \tag{3.5.24}$$

and it is solved by $\delta_L^<(\tau) = D^<(\tau)/D^<(\tau_{\rm in})\delta_L(\tau_{\rm in})$.

Therefore $\vec{v}_L$ will be different in the two regions $r \lesssim R_0$ and $r \gtrsim R_0$. As a result, two different vectors $\vec{n}$'s will be needed to generate (or remove) the long wave velocity perturbation, one for $r \lesssim R_0$ and the other $r \gtrsim R_0$: in the presence of modified gravity exploiting the screening effect, it is not possible to find a spatially independent vector $\vec{n}(\tau)$ and the consistency relations must be violated for objects which are unscreened. This violation of the consistency relation should be attributed to the fact that the effect of the long mode of the velocity cannot be reabsorbed completely by a change of coordinates. As indicated in figure 1, galaxies residing in the same region (a) or (b) for example, fall differently even if they are of the same mass, due to the difference in their scalar charge.

The vector $\vec{n}(\tau)$ is chosen such as to have a free-falling frame, defined by

$$\ddot{\vec{n}} + \mathcal{H}\dot{\vec{n}} + \vec{\nabla}\Phi = 0. \tag{3.5.25}$$

The solution to this equation is

$$\dot{\vec{n}}(\tau) = -i\frac{\vec{q}}{a(\tau)}\int^\tau {\rm d}\eta\, a(\eta)\Phi(\vec{q},\eta) = i\frac{\vec{q}}{q^2}\frac{1}{a(\tau)}\int^\tau {\rm d}\eta\, a^3(\eta)4\pi G\bar{\rho}\delta_L(\vec{q},\eta). \tag{3.5.26}$$

Then, by using Eqs. (3.5.23) and (3.5.24), we find that the free-falling frame is specified by

$$\vec{n}(\tau) = i\frac{\vec{q}}{q^2}\delta_L^<(\vec{q},\tau)\,, \quad r \lesssim R_0, \tag{3.5.27}$$

$$\vec{n}(\tau) = i\frac{\vec{q}}{q^2}\frac{\delta_L^>(\vec{q},\tau)}{1+2\alpha^2\epsilon}\,, \quad r \gtrsim R_0, \tag{3.5.28}$$

where $<$ and $>$ denote quantities respectively in the two regions $r \lesssim R_0$ and $r \gtrsim R_0$. This notation may look odd at first sight but we use it to indicate that linear modes grow differently in screened and unscreened regions as they may or may not feel the presence of the chameleon field. Thus, although the wavelenth q^{-1} is larger than the two regions, the linear overdensity amplitude is different in these regions and for local observers, this linear mode is like a background average density field with different amplitudes in the two regions. This is also connected to the fact that there is no universal free falling frame according to (3.5.27,3.5.28). Consider for example n-galaxies within a sphere of radius $R \gtrsim R_0$ much smaller than the long wavelength mode of size $\sim 1/q$ and centered at the origin of the coordinates. Then, if all points are at distances $r \lesssim R_0$, then the consistency relation for the n-point correlator is the one we already described

$$\left\langle \delta_{\rm g}^<(\vec{q},\tau)\delta_{\rm g}^<(\vec{k}_1,\tau_1)\cdots\delta_{\rm g}^<(\vec{k}_n,\tau_n)\right\rangle'_{q\to 0} = \\ -\sum_{a=1}^{n}\frac{\vec{q}\cdot\vec{k}_a}{q^2}\left\langle \delta_{{\rm g},L}^<(\vec{q},\tau)\delta_L^<(\vec{q},\tau_a)\right\rangle\left\langle \delta_{\rm g}^<(\vec{k}_1,\tau_1)\cdots\delta_{\rm g}^<(\vec{k}_n,\tau_n)\right\rangle'. \tag{3.5.29}$$

If instead all points are at $r \gtrsim R_0$, we shall have in this case

$$\left\langle \delta_{\rm g}^>(\vec{q},\tau)\delta_{\rm g}^>(\vec{k}_1,\tau_1)\cdots\delta_{\rm g}^>(\vec{k}_n,\tau_n)\right\rangle'_{q\to 0} = \\ -\sum_{a=1}^{n}\frac{\vec{q}\cdot\vec{k}_a}{q^2}\frac{\left\langle \delta_{{\rm g},L}^>(\vec{q},\tau)\delta_L^>(\vec{q},\tau_a)\right\rangle}{1+2\alpha^2\epsilon}\left\langle \delta_{\rm g}^>(\vec{k}_1,\tau_1)\cdots\delta_{\rm g}^>(\vec{k}_n,\tau_n)\right\rangle'. \tag{3.5.30}$$

The case in which galaxies are both screened and unscreened is more complex[3], however we expect a violation of the consistency relation due to the difference in the growth factor. Indeed, consider those configurations in which m galaxies are at $r \gtrsim R_0$ and $(n-m)$ are at $r \lesssim R_0$, the consistency relation

[3] At the boundary between the over-dense region and the exterior waves of the scalar field will be generated and might propagate both to the interior and exterior. We shall ignore these effects since we expect the scalar field to have small oscillations around the static solution deep inside the screened region, and in the unscreened region we expect the scalar field to go to a constant far from the boundary. Close to the boundary our results might not apply, but one can expect even larger violations to the consistency relation due to the gradient of the scalar field being large.

will be written as

$$\frac{\left\langle \delta_{\rm g}(\vec{q},\tau)\delta_{\rm g}^{>}(\vec{k}_1,\tau_1)\cdots\delta_{\rm g}^{>}(\vec{k}_m,\tau_m)\delta_{\rm g}^{<}(\vec{k}_{m+1},\tau_{m+1})\cdots\delta_{\rm g}^{<}(\vec{k}_n,\tau_n)\right\rangle'_{q\to 0}}{\left\langle \delta_{\rm g}^{>}(\vec{k}_1,\tau_1)\cdots\delta_{\rm g}^{>}(\vec{k}_m,\tau_m)\delta_{\rm g}^{<}(\vec{k}_{m+1},\tau_{m+1})\cdots\delta_{\rm g}^{<}(\vec{k}_n,\tau_n)\right\rangle'} =$$

$$-\left(\sum_{a=1}^{m}\frac{\vec{q}\cdot\vec{k}_a}{q^2}\frac{\left\langle \delta_{{\rm g},L}(\vec{q},\tau)\delta_L^{>}(\vec{q},\tau_a)\right\rangle}{1+2\alpha^2\epsilon}+\sum_{a=m+1}^{n}\frac{\vec{q}\cdot\vec{k}_a}{q^2}\left\langle \delta_{{\rm g},L}(\vec{q},\tau)\delta_L^{<}(\vec{q},\tau_a)\right\rangle\right).$$

Notice that the right-hand side for the configuration (3.5.31) is not vanishing even for correlators at equal time for the n-points. This is due to the fact that the long wavelength chameleon-like field correlates only with the overdensity located in the unscreened region, the one in the screened region being completely independent of the chameleon-like perturbation. For instance, for $n=2$ and $m=1$, the corresponding bispectrum reads

$$\boxed{\begin{aligned}&\frac{\left\langle \delta_{\rm g}(\vec{q},\tau)\delta_{\rm g}^{>}(\vec{k}_1,\tau)\delta_{\rm g}^{<}(\vec{k}_2,\tau)\right\rangle'_{q\to 0}}{\left\langle \delta_{\rm g}^{>}(\vec{k}_1,\tau)\delta_{\rm g}^{<}(\vec{k}_2,\tau)\right\rangle'}=\\&\left[\frac{2\alpha^2\epsilon}{1+2\alpha^2\epsilon}\left\langle \delta_{{\rm g},L}(\vec{q},\tau)\overline{\delta}_L(\vec{q},\tau)\right\rangle-\left\langle \delta_{{\rm g},L}(\vec{q},\tau)\Delta\delta_L(\vec{q},\tau)\right\rangle\right]\frac{\vec{q}\cdot\vec{k}_1}{q^2},\end{aligned}} \tag{3.5.31}$$

where $\overline{\delta}_L$, $\Delta\delta_L$ are the formal quantities $\overline{\delta}_L=(\delta_L^{<}+\delta_L^{>})/2$ and $\Delta\delta_L=(\delta_L^{<}-\delta_L^{>})$. The latter is also suppressed by $\alpha^2\epsilon$ which therefore gives an estimate of the violation of EP.

Consider now, for instance, a cluster of galaxies of mass $M\sim 10^{14.5\div 15}\,M_\odot$ and radius $R_0\sim(2\div 10)$ Mpc. Inside it $\Phi_{\rm cl}=-GM/R_0\sim -10^{-5}$ and one has [112]

$$\frac{\overline{\varphi}}{2\alpha}\ll 10^{-6}\lesssim\frac{GM}{R_0}, \tag{3.5.32}$$

where $\overline{\varphi}$ is the asymptotic background value of the scalar φ and the upper bound comes from the solar system [113]. In such a dense object the scalar field is screened, $\epsilon\simeq-\overline{\varphi}/(2\alpha\Phi_{\rm cl})\lesssim 10^{-1}$, and we may take $(n-m)$ galaxies residing there. Away from the cluster there might be small m galaxies with $\Phi_{\rm g}\sim -10^{-8}$ which are unscreened (therefore preferably residing in voids) and $\epsilon\simeq 1$. For this configuration, one expects to see a violation of the consistency relation as predicted by Eq. (3.5).

Notice also that our considerations hold as long as the Compton wavelength m^{-1} associated to

the chameleon-like field is larger than the scale where perturbations may be considered in the linear regime. At redshift $z = 0$, there is a strong upper bound of about 1 Mpc on such Compton wavelength $m^{-1}(a_0)$ coming from the solar system tests [114, 115], implying that the desired effects on the large-scale structure are restricted to non-linear scales. However, at higher redshifts a Compton wavelength of the form $m^{-1}(a) = m^{-1}(a_0)(a/a_0)^p$ with $p < -3$ satisfies the experimental constraints and can lead to a modified gravity regime on large linear scales [114]. This scaling of m is faster than the one deduced from the Lifshitz scaling of the scale $k_{\rm NL}(a) \sim a^{-2/(n+4)}$ (during matter domination) at which cosmological perturbations become non-linear [103, 77] and the condition $m(a) < k_{\rm NL}(a)$ is easily attained going back in time.

An interesting question is how well one can constrain these theories through the galaxy consistency relation. Though an accurate estimate is beyond the scope of this chapter, let us try to make a simple back-of-the-envelope computation by noting that the form of the bispectrum (3.5) is almost the same one as obtained in the galaxy local bias model in the presence of a primordial local non-Gaussianity [116] (see also Ref. [78]). Supposing that the combination $\alpha^2\epsilon$ is smaller than unity, one needs basically to identify (barring coefficient of order unity and assuming redshift $z = 0$) $\alpha^2\epsilon(\vec{q}\cdot\vec{k}_1)$ with $f_{\rm NL}H_0^2$, where $f_{\rm NL}$ is the non-linear coefficient parametrizing the level of non-Gaussianity and H_0 is the present Hubble rate. The Fisher matrix analysis applied to the galaxy (reduced) bispectrum performed in Ref. [116] has shown that one can measure $f_{\rm NL}$ up to $\mathcal{O}(10)$ for $k_1 \sim k_{\rm max} \sim 0.1\,h$ Mpc^{-1}, being $k_{\rm max}$ the smallest scale included in the analysis. Therefore, again very roughly, we expect to be able to measure the modification of gravity of the type we consider at redshifts $z \gtrsim 1$ of the order of $\mathcal{O}(10)(H_0/\,k_{\rm max}) \sim 10^{-3}(0.1\,h\,{\rm Mpc}^{-1}/k_{\rm max})$, where we have taken $q \sim 10^2\,H_0$.

Similar considerations apply also to more conventional modifications of gravity induced by scalars, like Brans-Dicke theory, or dilaton gravity. In these theories, in spite of the fact that there is a universal coupling of the scalar to matter, there is a violation of the *strong* EP because a gravitational experiment can yield different results in different points in spacetime. However, this violation is subleading in the post-Newtonian approximation for non-relativistic matter and it can only give order one effects in strongly bound systems as binary systems and black holes [117]. To be more precise here, let us consider an action of the general form

$$S = \int {\rm d}^4x\sqrt{-g}\Big(f(R,\phi,X) + \mathcal{L}_{\rm m}\Big), \tag{3.5.33}$$

where $f(R,\phi,X)$ is a function of the Ricci scale R, a scalar ϕ and its kinetic term and $X = -\frac{1}{2}\partial_\mu\phi\partial^\mu\phi$. This form of the action describes many models of modified gravity like Brans-Dicke theory, dilaton gravity, $f(R)$ and many others. In this general class of models, the non-relativistic matter still satisfies Eqs.(1.3.2-1.3.4), where now $\Omega_{\rm m} = 8\pi G_{\rm eff}\bar{\rho}a^2/3\mathcal{H}^2$ and $G_{\rm eff}$ is an effective Newton constant which encodes the modification of gravity given by [118]

$$G_{\rm eff}(\tau) = \frac{1}{8\pi F}\frac{f_{,X} + 4\left(f_{,X}\frac{k^2}{a^2}\frac{F_{,R}}{F} + \frac{F_{,\phi}^2}{F}\right)}{f_{,X} + 3\left(f_{,X}\frac{k^2}{a^2}\frac{F_{,R}}{F} + \frac{F_{,\phi}^2}{F}\right)}, \tag{3.5.34}$$

where $F = \frac{\partial f}{\partial R}$. Therefore, when

$$f_{,X}\frac{k^2}{a^2}\frac{F_{,R}}{F} \ll 1, \tag{3.5.35}$$

the effective Newton constant is only time dependent and it just modifies the temporal dependence of the local growth function of the overdensity evolution. In this case, still, one may generate a long wavelength velocity mode by a vector $\vec{n}(\tau)$ as in Eq. (1.4.13). In the opposite case, Eq. (3.5.35) is not satisfied and $G_{\rm eff}$ turns out to be space-dependent. The overdensity δ turns out to be also space-dependent as well and there may be no $\vec{n}(\tau)$ to generate a long wavelength velocity mode within the sphere of radius R_0. To see when this is possible, let us mention that there is a crossover scale when the k-dependence of $G_{\rm eff}$ starts become strong and which is defined by

$$R_0 = \frac{a}{k} \approx \left(\frac{F_{,R}}{F} f_{,X}\right)^{1/2}. \tag{3.5.36}$$

If $R \lesssim R_0$, one may still define $\vec{n}(\tau)$ and so long wavelength modes may be generated. On the other side if $R \gtrsim R_0$, *i.e.* modification of gravity appears within the sphere, then there is no globally defined $\vec{n}(\tau)$ inside the sphere of radius R, which will cause a modification of the consistency relation. So the lesson here is that violation of the consistency relations is a signal of the spatial dependence of the effective Newton constant $G_{\rm eff}$ and of a modification of gravity at large scales.

We should also note that we have not considered here intrinsic violation of the EP, *i.e.* at the microscopic level [119, 120, 121, 122]. One for example may consider the case of extra scalar, vector or tensor couplings to only one component, say baryonic matter or dark matter. Such a model has been studied in Ref [84]. It has been recently realized that in the modified gravity models where there is an efficient screening phenomenon to make the set-up experimentally consistent there might also be order unity violation of the EP [112]. Such possibilities has been considered recently in Ref. [123] where it has been pointed out the interesting feature that if a large scale velocity bias exists between the different components new terms appear in the consistency relations with respect to the single species case.

3.6 Summary

In this chapter, we have discussed the implications of the symmetry enjoyed by the Newtonian equations of motion describing the dark matter and galaxy fluids coupled through gravity. The fact that such symmetry applies to both galaxies and dark matter is particularly welcome because one can reach conclusions which are independent from the galaxy bias. On the contrary, one can use the power of the symmetry to deduce relevant informations on the theory of galaxy bias. In particular, we have shown that an unavoidable consequence of the symmetries at our disposal is that the bias is expected to be non-local. Furthermore, we have studied the modification (or violation) of the consistency relation in the case in which gravity is modified because of the presence of extra degrees of freedom propagating unscreened at large cosmological distances. Let us reiterate that our results

are based on the assumption that the galaxy number is conserved. Eventually, one would like to extend our considerations by accounting for phenomena like halo formation and merging, nevertheless if the modification in the proper equations are such that the symmetries studied in this chapter are preserved, e.g. if the new terms are a local function of the dark matter density, then our considerations remain valid. Also, apart from applying to non-linear scales and directly to galaxies, our results have the virtue of not being sensitive to the single stream approximation and to be valid also in the presence of velocity bias and/or vorticity (which is generated at higher-order in perturbation theory). Assuming that primordial perturbations satisfy the consistency relations of [14], the observation of a deviation from the consistency relation for the bispectrum of galaxies, Eq. (3.2.12), could signal either the inapplicability of the Eulerian bias model even including "non-local" terms as in Eq. (3.3.8) or of a modification of theory of gravity.

Chapter 4

Consistency relation for the observed galaxy bispectrum

4.1 Observed quantities and LSS surveys

The enhanced precision of upcoming LSS surveys requires high accuracy theoretical predictions for the observed quantities rather than theoretically convenient quantities. Moreover, on the very large-scales probed by these surveys, the Newtonian description of galaxy clustering is not valid.

The relativistic description of the observed galaxy number density, in terms of the observed redshift and angle of galaxies, have been developed up to first order in perturbation theory [65, 20, 64, 66, 124], which has allowed them to compute the impact of relativistic effects on the galaxy power spectrum.

The galaxy bispectrum contains much additional information not present in the power spectrum as there are many more modes and it suffers from different systematics. The computation of this bispectrum in principle needs the use of second order perturbation theory which is very involved and non-trivial. Unlike the CMB, where the non-linearities are small and therefore (for Gaussian initial conditions) the fluctuations are nearly Gaussian, the large-scale structure statistics is intrinsically non-Gaussian due to the gravitational collapse. One needs therefore to go beyond the two-point statistics and hence beyond the linear level in perturbation theory. Recently, several groups have performed the second-order calculation [68, 67, 125, 19].

The expression for the observed galaxy three-point correlator (bispectrum) obtained from the second-order calculation is rather complicated and has contributions from various terms. Moreover the region of validity of this calculation is only in the weakly non-linear regime.

In this chapter we derive a consistency relation for the observed galaxy bispectrum that can be obtained in a non-perturbative manner in the squeezed limit. This consistency relation allows to express the observed bispectrum in terms of the observed galaxy power spectrum. This is exactly computable since the effect of a long mode on the short-scale dynamics is simply a change of frame (or a residual gauge transformation).

The advantage of using the consistency relations in the large-scale structure is that they are directly valid for the observed (and therefore gauge-invariant) quantities, in the same way they are for the CMB bispectrum [71, 70, 11, 74], and this is what we are going to exploit in this chapter. Our results are useful as a consistency check for the analytical second-order computations of the bispectrum of

the observed galaxy overdensity and provide a simple and easy way to produce the squeezed limit.

Furthermore, since some of these relativistic effects in galaxy number counts give rise to the three point function that mimics that of a local primordial non-Gaussianity (for a review, see Ref. [126]), removing their contribution is important for obtaining constraint on primordial non-Gaussianity from galaxy surveys. We shall estimate the effective local non-Gaussianity parameter from the non-linear General Relativity (GR) corrections that we derive. The exact value depends on the redshift, the magnification bias, see figure 4.2. At redshift of $z = 1.5$ and in the absence of the magnification bias we obtain $f_{\rm NL}^{\rm GR} \simeq -0.7$.

We should however point out that for practical purposes, on sub-horizon scales, other terms dominate the squeezed limit. It is only when the long mode is super-Hubble that this relation gives the exact amount of local NG from relativistic effects. We shall see in chapter 5 that these terms can also give a large contamination to the estimated local NG. However, our expression is still valid in the sense that we capture the scaling of the galaxy bispectrum as one takes the squeezed limit $1/\lambda_L \to 0$ up to terms $H^2\lambda_L^2$ and H/λ_L with respect to the tree level PT bispectrum.

This chapter is organized as follows. In section 4.2, we review the coordinate transformation that induces the long wavelength mode and continue in section 4.3 to describe the effect of the long wavelength perturbation mode on the observed galaxy overdensity. We use this result to calculate the bispectrum in the squeezed limit by correlating two short-mode overdensities with a long wavelength mode. We then decompose the bispectrum in terms of spherical harmonics in section 4.4 and in section 4.4.1 we discuss our findings in the distant observer approximation. In section 4.5 we estimate the value of the effective $f_{\rm NL}^{\rm GR}$ induced by these relativistic corrections. Finally, we conclude in section 4.6.

4.2 Adiabatic modes and residual gauge symmetry

In this section, we compute the squeezed limit of the galaxy number counts overdensity $\Delta_{\rm g}$. As seen before, the squeezed limit of an $(n+1)$-point correlation function in which one of the scales is much larger than the other n can be written as the correlation of a long-wavelength mode with the n-point function in the presence of that long mode, *e.g.*

$$\Big\langle \Phi(\lambda_L)\Delta_{\rm g}(\lambda_1)\dots\Delta_{\rm g}(\lambda_n)\Big\rangle_{\lambda_L\gg\lambda_i} = \Big\langle \Phi(\lambda_L)\Big\langle \Delta_{\rm g}(\lambda_1)\dots\Delta_{\rm g}(\lambda_n)\Big\rangle_L\Big\rangle\,, \tag{4.2.1}$$

where Φ is Bardeen's potential, λ is the characteristic scale of each variable, and $\langle\cdots\rangle_L$ is to be interpreted in the conditional probability sense: it is an average given the condition that when smoothed at large-scales Bardeen's potential takes the value $\Phi(\lambda_L)$.

It thus suffices to compute the effect of the long-wavelength potential on the short scale dynamics. This task is greatly simplified by the fact that on large enough scales, one can approximate Bardeen's potential as a Taylor expansion

$$\Phi_L(\tau,\vec{x}) = \Phi_L(\tau,\vec{x}_{\mathcal{E}}) + (\vec{x}-\vec{x}_{\mathcal{E}})\cdot\vec{\nabla}\Phi_L(\tau,\vec{x}_{\mathcal{E}})\,, \tag{4.2.2}$$

where we have centered the Taylor expansion around an arbitrary point close to where we evaluate the short-scale n-point function. We shall now show that in a ΛCDM universe this large-scale potential is a gauge mode: an appropriate coordinate transformation can set these first two terms of the Taylor expansion to zero. We shall summarize the derivation given in Refs. [14, 79].

We shall work to first order in the gradient of the long mode, which means we shall ignore its curvature $\nabla^2\Phi_L$ and tidal forces $\partial_i\partial_j\Phi_L$. Though these effects are in general large at sub-horizon scales, their effect would not be confused in observations with a violation of the consistency relation connecting the squeezed limit of the 3-point function with the power spectrum. For simplicity, we also choose to be perturbative in the short-mode potential $\Phi_\mathcal{E}$ and velocities $\sim \partial_i\Phi_\mathcal{E}$ which are expected to be small even at very small scales. Note that we never assume the short-mode density $\sim \nabla^2\Phi_\mathcal{E}$ to be small and in this sense we are non-perturbative.

Let us use the perturbed metric in the Poisson gauge (1.2.2) (with scalar perturbations only for simplicity) and consider the following coordinate transformation

$$\tau \mapsto \widetilde{\tau} = \tau + \epsilon(\tau) + \vec{x}\cdot\vec{\xi}'(\tau) + \alpha(\tau,\vec{x})\,, \tag{4.2.3}$$

$$x^i \mapsto \widetilde{x}^i = x^i(1+\lambda+2\vec{x}\cdot\vec{b}) - b^i\vec{x}^2 + \xi^i(\tau) \tag{4.2.4}$$

where α satisfies $\vec{\nabla}^2\alpha = -2\partial_i(\Phi+\Psi)\xi'^i$, λ and $\vec{b}$ are constants, and ϵ and $\vec{\xi}$ are functions of time.

The key point is that, after performing this transformation, the metric is still of the form given by Eq. (1.2.2). The potentials are now

$$\widetilde{\Phi} = \Phi + \left[\epsilon' + \vec{x}\cdot\vec{\xi}'' + \mathcal{H}(\epsilon + \vec{x}\cdot\vec{\xi}')\right], \tag{4.2.5}$$

$$\widetilde{\Psi} = \Psi - \left[\lambda + 2\vec{x}\cdot\vec{b} + \mathcal{H}(\epsilon + \vec{x}\cdot\vec{\xi}')\right]. \tag{4.2.6}$$

Note that the transformation leaves the dynamics unchanged, while it changes perturbation quantities. Therefore, since these perturbations are still described by the same gauge condition, the symmetry at issue is a non-linearly realized symmetry. The transformation we have performed is a residual gauge symmetry of the Poisson gauge[1]. This means that even when one completely fixes the gauge to be the Poisson gauge in which the quantities appearing in the metric are Bardeen's potentials, there is a residual gauge freedom under some coordinate transformations that do not leave the background invariant, such as Eqs. (4.2.3, 4.2.4). From now on we shall ignore α in Eq. (4.2.3) since its effect is of higher order under our approximations.

An arbitrary coordinate transformation that does not leave the background FLRW metric invariant can be interpreted as inducing perturbations of the metric which would have no physical meaning whatsoever. However, in a context where the curvature perturbation ζ is conserved, such as for ΛCDM even deep inside the horizon, the transformations (4.2.3, 4.2.4) can be chosen to solve the large wavelength limit of Einstein's equations. In order to satisfy this, the transformation parameters

[1] A residual gauge symmetry is of course there for any other gauge different from the Poisson one, which we have chosen because it is usually adopted as a starting point in the computation for the large-scale structure.

obey the following conditions [14, 79],

$$v_L = -(\epsilon + \vec{x}\cdot\vec{\xi}')\,, \tag{4.2.7}$$

where v is the velocity potential $v^i = \partial_i v$. We see that $\vec{\xi}'$ corresponds to a long-wavelength velocity mode. Additionally we require,

$$\epsilon' + 2\mathcal{H}\epsilon = -\lambda\,, \qquad \vec{\xi}'' + 2\mathcal{H}\vec{\xi}' = -2\vec{b}\,. \tag{4.2.8}$$

In order to see when these conditions are consistent, we note that from the definition of the comoving curvature perturbation $\zeta \equiv -\Psi + \mathcal{H}v$ and from equation (4.2.6) we have

$$\zeta_L = \lambda + 2\vec{x}\cdot\vec{b}\,. \tag{4.2.9}$$

Thus, *a long-wavelength solution is a gauge mode if on those large-scales the comoving curvature perturbation is constant in time.* This means that the long-wavelength limit of a physical solution of Bardeen's potentials is equivalent to a coordinate transformation and it is what Weinberg calls adiabatic modes [127]. Indeed, since ζ is conserved outside the sound horizon which is nearly zero in a ΛCDM universe, this would hold up to scales where baryonic physics start being important. Note that this constancy of ζ must be satisfied only by the long-wavelength mode for our arguments to be valid; the short-wavelength modes can be at any scale.

4.3 Observed galaxy overdensity in the presence of long mode

In this section we compute the effect of a large-scale mode approximated by a constant plus a gradient as in Eq. (4.2.2). We start by defining the galaxy number density, we then include the effect of the long mode and we show that if the long mode has a characteristic scale that is much larger than all other scales in the problem (including the distance between the observer and the galaxies), its effect is zero as expected.

4.3.1 Galaxy number density

In galaxy surveys, the observed galaxy number density at a given redshift and angle on the sky $n_{\rm g}^{\rm obs}$, is obtained by counting the number of galaxies, $\mathrm{d}N_{\rm g}$ within the observed volume, $\mathrm{d}V = \mathrm{d}\Omega\mathrm{d}z$

$$n_{\rm g}^{\rm obs}(z,\hat{n}) = \frac{\mathrm{d}N_{\rm g}(z,\hat{n})}{\mathrm{d}V}. \tag{4.3.1}$$

From here, one defines the galaxy number overdensity $\Delta_{\rm g}$ as

$$n_{\rm g}^{\rm obs}(z,\hat{n}) \equiv \bar{n}_{\rm g}(z)(1+\Delta_{\rm g}(z,\hat{n}))\,. \tag{4.3.2}$$

where $\bar{n}_{\rm g}(z) \equiv \langle n_{\rm g}^{\rm obs}(z)\rangle$ is the observed number density of galaxies averaged over the angle at a fixed redshift.

In order to study the effect of a long-wavelength mode on the galaxy number density, we must first relate it to the physical density. In the inhomogenous universe, the observed redshift and the propagation direction of the photons differ from the true redshift and angle. Therefore the observed volume defined in terms of the observed redshift and solid angle differs from the physical volume occupied by the source

$$dV_{\rm phys} = {\rm d}V_{\rm obs}(1+\delta V) \tag{4.3.3}$$

Thus the observed number density of galaxies which is obtained by counting the number of galaxies within the observed volume differs from the physical number density by a factor due to the volume distortions

$$n_{\rm g}^{\rm obs}(z,\hat{n}) = n_{\rm g}^{\rm phys}(z,\hat{n})(1+\delta V)\,. \tag{4.3.4}$$

Moreover, galaxy surveys are flux limited, *i.e.*, only galaxies above some threshold luminosity are observed. This threshold luminosity is inferred from the observed flux

$$\hat{L} = 4\pi\bar{\mathcal{D}}_l^2(z) f_{\rm obs}, \tag{4.3.5}$$

where the luminosity distance $\bar{\mathcal{D}}_l(z)$ is that in a homogenous universe and $\hat{L}$ is the inferred luminosity. However the physical luminosity of the galaxy is different than the inferred luminosity since the luminosity distance to the galaxy is not that of the homogenous universe and the photon propagation is affected by the fluctuations along the path

$$L^{\rm phys} = 4\pi\mathcal{D}_l(z)^2 f_{\rm obs} = 4\pi\bar{\mathcal{D}}_l(z)^2 f_{\rm obs}(1+\delta\mathcal{D}_l)^2 = \hat{L}(1+\delta\mathcal{D}_l)^2 \tag{4.3.6}$$

Therefore the observed number of galaxies at observed redshift z, angle $\hat{n}$ and above a threshold L is related to the physical number count as

$$\begin{aligned} n_{\rm g}^{\rm obs}(z,\hat{n},\hat{L}) &= n_{\rm g}^{\rm phys}(z,\hat{n},\hat{L}(1+\delta\mathcal{D}_l)^2)(1+\delta V) \\ &= n_{\rm g}^{\rm phys}(z,\hat{n})(1+\delta V)(1+t\delta\mathcal{D}_l) \end{aligned} \tag{4.3.7}$$

where $t = 2\frac{d\ln\bar{n}_{\rm g}^{\rm phys}(z)}{d\ln L}$. In writing the second line in Eq. (4.3.7), as explained in the beginning of this section, we made two assumptions: first we only kept the linear contributions to the luminosity distance and volume perturbations. This is because if we neglect the strong lensing, the perturbations in the luminosity distance and volume are proportional to the gravitational potential and its gradient and thus their higher order contributions are subdominant with respect to the higher order contribution of the matter density. Thus we neglect these terms. Second in writing the contribution

from the magnification bias, we assumed that the perturbations and the background have the same dependence on the luminosity.

4.3.2 Long-short couplings

We now wish to compute the galaxy over-density measured in a small patch of the sky and in a small range of redshifts, in the presence of a mode of Bardeen's potential which is much larger than the size of this patch. Following the arguments of section 4.2, this mode should have no effect on the local physics of that small region since it is equivalent to a coordinate transformation. However, we take here this large-scale mode to have a characteristic size which is smaller than the distance between the observer and the small patch, which means that it will indeed have an effect on the correlations measured by the observer. This effect is purely due to the fact that we measure the galaxy correlation functions in terms of the redshift and angular position of the galaxies rather than the physical separation between galaxies and their proper time. For this reason this non-zero correlation is a "projection effect".

In the presence of the long mode, the observed redshift and angle of the galaxies are modified with respect to those in the absence of long mode. First let us compute the effect of the large-scale mode on the observed angular position of the galaxy

$$\hat{n}^i_{\mathcal{O}} \equiv \frac{-T^i_\mu P^\mu(\tau_{\mathcal{O}})}{\sqrt{\delta_{jk} T^j_\nu P^\nu T^k_\eta P^\eta}}\,, \tag{4.3.8}$$

where $T^i_\mu P^\mu = (\delta^i_\mu + u^{\mathcal{O}\,i} u^{\mathcal{O}}{}_\mu) P^\mu$ is the projection of the photon 4-momentum P^μ, orthogonal to the observer's 4-velocity $u^{\mathcal{O}}$. At linear order the solution to the photon geodesic gives

$$\hat{n}_{\mathcal{O}} = \hat{n}_{\mathcal{E}} + \vec{v}^{\perp}_{\mathcal{O}} - \int_{\tau_{\mathcal{O}}}^{\tau_{\mathcal{E}}} \mathrm{d}\tau'\, \vec{\nabla}^{\perp} \left(\Phi(\tau') + \Psi(\tau')\right)\,, \tag{4.3.9}$$

where the direction of emission is defined as $\hat{n}_{\mathcal{E}} \equiv -P^i(\tau_{\mathcal{E}})/\sqrt{\delta_{jk} P^j(\tau_{\mathcal{E}}) P^k(\tau_{\mathcal{E}})}$ and the superscript $^\perp$ denotes a projection orthogonal to $\hat{n}_{\mathcal{E}}$, e.g. $v^{i\,\perp} = (\delta^{ij} + \hat{n}^i_{\mathcal{E}} \hat{n}^j_{\mathcal{E}}) v^j$. The second term on the right hand side corresponds to an aberration due to the motion of the observer and the last term is the lensing of the photon trajectory.

The presence of the large-scale mode will contribute to the lensing integral in Eq. (4.3.9), and it will also cause the photon to be emitted in a different direction (in the coordinate system with the long mode). This change in the direction of emission can be computed simply by remembering that at the point of emission the large-scale mode is equivalent to a coordinate transformation which will transform the vector $P^i(\tau_{\mathcal{E}})$ giving

$$\hat{n}_{\mathcal{E}} \mapsto \hat{\tilde{n}}_{\mathcal{E}} = \hat{n}_{\mathcal{E}} - \vec{\xi}^{\perp}(\tau_{\mathcal{E}}) + 2\vec{b}^{\perp}(\tau_{\mathcal{E}} - \tau_{\mathcal{O}})\,, \tag{4.3.10}$$

where we used the fact that at zeroth order $\vec{x}_{\mathcal{E}} = -\hat{n}_{\mathcal{E}}(\tau_{\mathcal{E}} - \tau_{\mathcal{O}})$. Writing $\vec{\xi}$ and $\vec{b}$ in terms of the potentials as in Eqs. (4.2.7) and (4.2.9) and isolating the contribution of the long mode to the lensing

integral in Eq. (4.3.9) we obtain

$$\hat{\tilde{n}}_{\mathcal{O}} = \hat{n}_{\mathcal{O}} - \vec{v}^{\perp}_{\mathcal{O}} + (1 + \mathcal{H}(\tau_{\mathcal{E}} - \tau_{\mathcal{O}}))\vec{v}^{\perp}_{L}(x_{\mathcal{E}}) \\ - (\tau_{\mathcal{E}} - \tau_{\mathcal{O}})\nabla^{\perp}\Psi_L(x_{\mathcal{E}}) + \int_{\tau_{\mathcal{O}}}^{\tau_{\mathcal{E}}} \mathrm{d}\tau' \, \nabla^{\perp}\left(\Phi_L(\tau') + \Psi_L(\tau')\right) . \tag{4.3.11}$$

The redshift is defined as the ratio of the energies of a photon at emission and observation

$$(1 + z) \equiv \frac{P^{\mu}(\tau_{\mathcal{E}})u_{\mathcal{E}\,\mu}}{P^{\nu}(\tau_{\mathcal{O}})u_{\mathcal{O}\,\nu}} ,$$

and a calculation analogous to the one performed for the direction gives

$$\tilde{z} = z + (1 + z)\Big[\mathcal{H}v_L(x_{\mathcal{E}}) - \mathcal{H}_{\mathcal{O}}v_{\mathcal{O}} + \Phi_L(x_{\mathcal{E}}) - \Phi_{\mathcal{O}} - \hat{n}\cdot(\vec{v}_L(x_{\mathcal{E}}) - \vec{v}_{\mathcal{O}}) \\ - \int_{\tau_{\mathcal{O}}}^{\tau_{\mathcal{E}}} \mathrm{d}\tau' \, (\Phi'_L + \Psi'_L)(\tau')\Big] . \tag{4.3.12}$$

The observed number density of galaxies in the presence of the long mode is therefore given by

$$\begin{aligned} n_{\mathrm{g}}^{\mathrm{obs}}(z, \hat{n}, \hat{L})\Big|_L &= n_{\mathrm{g}}^{\mathrm{phys}}(z + \Delta z, \hat{n} + \Delta\hat{n})(1 + \delta V^{(L)})(1 + \delta V^{(S)}) \\ &\quad \times (1 + t\delta\mathcal{D}_l^{(S)})(1 + t\delta\mathcal{D}_l^{(L)}) \\ &= \bar{n}_{\mathrm{g}}(z)\left[1 + \Delta_{\mathrm{g}}(z + \Delta z, \hat{n} + \Delta\hat{n})\right] \\ &\quad \times \left(1 + e\Delta z + \delta V^{(L)} + t\delta\mathcal{D}_l^{(L)}\right) , \end{aligned} \tag{4.3.13}$$

where[2] $e \equiv \frac{\mathrm{d}\ln\bar{n}_{\mathrm{g}}^{\mathrm{phys}}}{\mathrm{d}z}$, and Δ_{g} has contributions from the luminosity distance and volume perturbations due to the short modes as well as the density perturbations due to the short modes. Note that $\Delta z = \tilde{z} - z$ and $\Delta\hat{n} = \hat{\tilde{n}} - \hat{n}$ are the corrections to the observed angle and redshift due to the long

[2] In the literature the evolution bias is often defined as $f_{\mathrm{evo}} \equiv \frac{\mathrm{d}\ln(a^3\bar{n}_{\mathrm{g}}^{\mathrm{phys}})}{\mathcal{H}\mathrm{d}\tau_{\mathcal{E}}}$, therefore $f_{\mathrm{evo}} = 3 - e/a$.

mode. Expanding Eq. (4.3.13) linearly the galaxy number overdensity is finally given by

$$\boxed{\begin{aligned}\Delta_{\rm g}(z,\hat{n})|_L = \Delta_{\rm g}(z,\hat{n}) + (1+\Delta_{\rm g}(z,\hat{n}))\left(e\Delta z + t\delta\mathcal{D}_l^{(L)} + \delta V^{(L)}\right)\\ + \Delta z\frac{\partial}{\partial z}\Delta_{\rm g}(z,\hat{n}) + \Delta\hat{n}\cdot\frac{\partial}{\partial\hat{n}}\Delta_{\rm g}(z,\hat{n}) + \mathcal{O}\left(\frac{\Phi_L}{\lambda_L^2\mathcal{H}^2}\Delta_{\rm g}\right)\end{aligned}} \tag{4.3.14}$$

For our purposes it suffices to use the perturbative expressions for the quantities $\delta V^{(L)}$ and $\delta\mathcal{D}_l^{(L)}$ at first order [128, 20, 65]

$$\begin{aligned}\delta V^{(L)} =& -2(\Phi_L+\Psi_L) + \frac{1}{\mathcal{H}}\Psi_L' + \left(\frac{\mathcal{H}'}{\mathcal{H}^2}+\frac{2}{r\mathcal{H}}\right)\Phi_L\\ &+\left(-3+\frac{\mathcal{H}'}{\mathcal{H}^2}+\frac{2}{r\mathcal{H}}\right)\left(-\vec{v}_L\cdot\hat{n}+\int_\tau^{\tau_\mathcal{O}}\mathrm{d}\tau'(\Phi_L'+\Psi_L')(\tau')\right)\\ &+\int_\tau^{\tau_\mathcal{O}}\mathrm{d}\tau'\left(\frac{2}{r}-\frac{r-r(\tau')}{rr(\tau')}\Delta_\Omega\right)(\Phi_L+\Psi_L)(\tau')\,,\end{aligned} \tag{4.3.15}$$

and

$$\begin{aligned}\delta\mathcal{D}_l^{(L)} =& \left(\frac{1}{r\mathcal{H}}-1\right)\left(-\vec{v}_L\cdot\hat{n}+\Phi_L+\int_\tau^{\tau_\mathcal{O}}\mathrm{d}\tau'\,(\Psi_L'+\Phi_L')(\tau')\right)\\ &+\frac{1}{2}\int_\tau^{\tau_\mathcal{O}}\mathrm{d}\tau'\left[\frac{2}{r}-\frac{r-r(\tau')}{rr(\tau')}\Delta_\Omega\right](\Psi_L+\Phi_L)(\tau')-\Psi_L\,,\end{aligned} \tag{4.3.16}$$

where all the quantities without an argument are evaluated at the point of emission. Note that we have kept the term containing the angular Laplacian Δ_Ω as it actually is non zero when applied to a constant gradient of the gravitational potential.

The last step we need to take is to correlate the expression (4.3.14) with another short-scale $\Delta_{\rm g}$ and a long-scale one, and go to harmonic space to obtain the consistency relation of the galaxy three-point function in the squeezed limit

$$\left\langle\Delta_{\rm g}^L(z_1,\hat{n}_1)\Delta_{\rm g}(z_2,\hat{n}_2)\Delta_{\rm g}(z_3,\hat{n}_3)\right\rangle = \left[\left\langle\Delta_{\rm g}^L(z_1,\hat{n}_1)d(z_2,\hat{n}_2)\right\rangle\right.$$

$$+\left\langle \Delta_{\rm g}^{L}(z_1,\hat{n}_1)\Delta z(z_2,\hat{n}_2)\right\rangle \frac{\partial}{\partial z_2}+\left\langle \Delta_{\rm g}^{L}(z_1,\hat{n}_1)\Delta\hat{n}(z_2,\hat{n}_2)\right\rangle \cdot\frac{\partial}{\partial\hat{n}_2}\Bigg]$$

$$\times\left\langle \Delta_{\rm g}(z_2,\hat{n}_2)\Delta_{\rm g}(z_3,\hat{n}_3)\right\rangle +(2\leftrightarrow 3)\,, \quad (4.3.17)$$

where we have introduced

$$d\equiv(e\Delta z+t\delta\mathcal{D}_l^{(L)}+\delta V^{(L)}). \quad (4.3.18)$$

Let us close this section by commenting on the corrections to Eq. (4.3.14). In general, we also expect corrections going like the curvature induced by the long-wavelength mode, that is $(\Phi_L\Delta_{\rm g}/\lambda_L^2\mathcal{H}^2)$. Parametrically, these are subdominant with respect to the lensing and redshift space distortions which behave as $(\Phi_L\Delta_{\rm g}/\lambda_L\lambda_S\mathcal{H}^2)$, but they are larger than the other relativistic corrections like the one we are computing. However as we shall discuss in section 4.4.2, there are additional suppressions for the lensing and the redshift space distortions.

In spite of this, our result is a consistency relation in the following sense : If the evolution of the Universe is adiabatic (single-field inflation and a subsequent evolution that conserves ζ on the scales of interest) our relation captures the terms that scale as $H^2\lambda_L^2$ and $H\lambda_L$ as one takes the squeezed limit of the galaxy bispectrum. The terms we computed could be mistaken for a non-zero local non-Gaussianity, which corresponds to a physical coupling between Φ_L and Δ_g, or for a signal of violation of the Equivalence Principle if they are not taken into account. Furthermore, there are several approaches to compute these curvature terms in the literature, which correspond to computing the evolution of the short modes in a curved universe [88, 129, 130] (see also [10, 83]) but they can only be approximate since it is in general impossible to analytically compute the effect of curvature on the evolution of these non-perturbative short modes.

Note that in real observations, one counts the number of galaxies within a finite redshift bin which has two effects. First, the characteristic scale of the short mode is determined both by its angular scale and the assumed width of the redshift slices. Therefore it makes sense to study the scaling of the bispectrum as function of the long mode only if $\lambda_L \gg \delta z/\mathcal{H}$. Second as we shall explain in more details in section 4.4, in order to relate the theoretically calculated bispectrum to the one measured in a survey, one needs to integrate over the window functions describing the redshift bins. Note that the consistency relation *does not break down* when performing this integration as long as the characteristic spatial scale of the redshift bin is smaller than the characteristic scale of the long-wavelength mode. This is easily achieved especially for large redshifts $z \gtrsim 1$.

4.3.3 Validity checks

Let us now perform various validity checks on our results.

- We expect a large mode to have no observable effect when its scale is larger than all the scales in the problem, *i.e.* the distance between the source galaxies and the distance between them and the observer. This is similar to what happens for CMB [70, 74]. One way to check that our calculation is consistent with this fact is to perform a coordinate transformation that induces

such a large-scale mode and check that the galaxy number over-density remains invariant. Let us begin by checking that this is indeed the case for $\hat{n}_{\mathcal{O}}$, setting the observer's position to zero $\vec{x}_{\mathcal{O}} = \vec{0}$, we obtain

$$\hat{\tilde{n}}_{\mathcal{O}} = \hat{n}_{\mathcal{O}} + \vec{\xi}'^{\perp}(\tau_{\mathcal{O}}) - \vec{\xi}'^{\perp}(\tau_{\mathcal{E}}) + 2(\tau_{\mathcal{E}} - \tau_{\mathcal{O}})\vec{b}^{\perp} + \int_{\tau_{\mathcal{O}}}^{\tau_{\mathcal{E}}} \mathrm{d}\tau' \left(\vec{\xi}''(\tau') - 2\vec{b}\right)^{\perp} , \tag{4.3.19}$$

where all the terms of the transformation cancel. An analogous argument holds for the redshift z, and we obtain

$$\tilde{z} = z + (1+z)\Bigg[\epsilon'(\tau_{\mathcal{E}}) + \vec{x}_{\mathcal{E}} \cdot \vec{\xi}''(\tau_{\mathcal{E}}) + \hat{n} \cdot \vec{\xi}'(\tau_{\mathcal{E}}) - \epsilon'(\tau_{\mathcal{O}}) - \hat{n} \cdot \vec{\xi}'(\tau_{\mathcal{O}}) \\ - \int_{\tau_{\mathcal{O}}}^{\tau_{\mathcal{E}}} \mathrm{d}\tau' \left(\epsilon'(\tau') + \vec{x} \cdot \vec{\xi}''(\tau')\right)' \Bigg] , \tag{4.3.20}$$

where all the terms in the parenthesis cancel after writing the partial time derivative in terms of a total derivative in the integral $\partial_\tau = \mathrm{d}/\mathrm{d}\tau + \hat{n} \cdot \vec{\nabla}$. For these cancellations to happen it is important to replace the Bardeen's potentials Φ and Ψ inside the integral by an exact constant plus a gradient, Eq. (4.2.2), which does not hold if the long mode oscillates between the observer and the source, *i.e.* if the characteristic scale of the long mode is smaller than the distance between the observer and the source. We thus obtain

$$n_{\mathrm{g}}^{\mathrm{obs}}(z,\hat{n})|_L = \bar{n}_{\mathrm{g}}(z)\left(1 + \Delta_{\mathrm{g}}(z,\hat{n})\right)\left(1 + \delta V^{(L)} + 2t\delta\mathcal{D}_l^{(L)}\right) . \tag{4.3.21}$$

Finally, the average in this equation $\bar{n}_{\mathrm{g}}$ assumes that the observer has access to the large-scale mode, such that the terms in the second parenthesis give zero when averaged over angles. However, when the mode is much larger than all the scales in the problem, the angular averages of these terms do not vanish,

$$\langle n_{\mathrm{g}}^{\mathrm{obs}}(z,\hat{n})\rangle|_L = \langle \bar{n}_{\mathrm{g}}(z)\rangle \left(1 + \langle \delta V^{(L)}\rangle + \langle 2t\delta\mathcal{D}_l^{(L)}\rangle\right) , \tag{4.3.22}$$

but they are zero-modes on the observed patch and they can be reabsorbed in the average of the galaxy number density

$$n_{\mathrm{g}}^{\mathrm{obs}}(z,\hat{n})|_L = \langle n_{\mathrm{g}}^{\mathrm{obs}}(z,\hat{n})\rangle|_L \left(1 + \Delta_{\mathrm{g}}(z,\hat{n})\right) . \tag{4.3.23}$$

We thus conclude that a mode with a characteristic scale much larger than all the scales in the problem has no effect on the Δ_{g}. We remark once more that *when the large-scale mode is smaller than the distance between the source and the observer, these contributions will all be*

non-zero.

- As a further check of the validity of our calculation we take the super-horizon limit in equation (4.3.14) and work to first order in the long modes and zeroth order in the short modes. We expect to obtain the same results as the linear calculation of Ref. [65, 20, 64, 66], which in a pressureless medium is given by

$$\Delta_{\rm g}^{(1)} = b\delta_{\rm m,sync} + (-e\delta z_{\rm sync} + t\delta\mathcal{D}_L + \delta V) \ ,$$

where $\delta_{\rm m,sync}$ and $\delta z_{\rm sync}$ are the matter over density and redshift perturbations in the synchronous gauge. Indeed, $\Delta z = -\delta z_{\rm sync}$ and at super-horizon scales $\delta_{\rm m,sync}$ is suppressed by $1/\lambda_L^2\mathcal{H}^2$, and we recover our result.

4.4 Spherical harmonic decomposition

In both N-body simulations and data from galaxy surveys, the three-point function is often measured and analysed in Fourier-space. This is a convenient decomposition if the galaxies have similar redshifts. However here we are interested in large-scales for the long mode where the relativistic effects can be important. Hence a single Fourier mode of large wavelength may include galaxies with significantly different redshifts. Due to the evolution of the Universe, there is no translation invariance in the radial direction of the redshift space, *i.e.* z. Therefore the Fourier space bispectrum is not proportional to the Dirac delta: triangles do not close. We thus choose to decompose the three-point function in spherical harmonics[3], which could prove advantageous or even necessary for this type of analysis,

$$\left\langle a_{\ell_1 m_1}(z_1)a_{\ell_2 m_2}(z_2)a_{\ell_3 m_3}(z_3)\right\rangle_{\ell_1\ll\ell_2,\ell_3} = \int {\rm d}\Omega_1{\rm d}\Omega_2{\rm d}\Omega_3$$
$$\times\, Y^*_{\ell_1 m_1}(\hat{n}_1)Y^*_{\ell_2 m_2}(\hat{n}_2)Y^*_{\ell_3 m_3}(\hat{n}_3)\left\langle \Delta_{\rm g}^L(z_1,\hat{n}_1)\Delta_{\rm g}(z_2,\hat{n}_2)\Delta_{\rm g}(z_3,\hat{n}_3)\right\rangle . \quad (4.4.1)$$

This basis naturally fits the sphere and does not have the problem of triangles not closing. We now compute each of the terms contributing to the above equation in turn[4]. The contribution of the terms in the first line of Eq. (4.3.17) are easy to compute and give

$$\left\langle a_{\ell_1 m_1}(z_1)a_{\ell_2 m_2}(z_2)a_{\ell_3 m_3}(z_3)\right\rangle_{\ell_1\ll\ell_2,\ell_3} \supset \mathcal{G}^{m_1m_2m_3}_{\ell_1\ell_2\ell_3}$$
$$\times\left[C_{\ell_1}^{\Delta_{\rm g}d}(z_1,z_2) + C_{\ell_1}^{\Delta_{\rm g}\Delta z}(z_1,z_2)\frac{\partial}{\partial z_2}\right]C_{\ell_3}^{\Delta_{\rm g}\Delta_{\rm g}}(z_2,z_3) + (2\leftrightarrow 3) \ , \quad (4.4.2)$$

[3] Useful relations involving the spherical harmonics are summarized in appendix A.

[4] From now on, we do not make any approximation. The subscript $_{\ell_1\ll\ell_2,\ell_3}$ is present only to remind the reader that the bispectrum computed is valid only in the squeezed limit.

where the Gaunt integral is defined as

$$\mathcal{G}^{m_1m_2m_3}_{\ell_1\ell_2\ell_3} = \int \mathrm{d}\Omega\; Y_{\ell_1m_1}(\hat{n})\; Y_{\ell_2m_2}(\hat{n})\; Y_{\ell_3m_3}(\hat{n})$$
$$= \begin{pmatrix} \ell_1 & \ell_2 & \ell_3 \\ m_1 & m_2 & m_3 \end{pmatrix} \begin{pmatrix} \ell_1 & \ell_2 & \ell_3 \\ 0 & 0 & 0 \end{pmatrix} \sqrt{\frac{(2\ell_1+1)(2\ell_2+1)(2\ell_3+1)}{4\pi}}. \tag{4.4.3}$$

The third term of Eq. (4.3.17) is slightly more complex

$$\Big\langle a_{\ell_1m_1}(z_1)a_{\ell_2m_2}(z_2)a_{\ell_3m_3}(z_3)\Big\rangle_{\ell_1\ll\ell_2,\ell_3} \supset \int \mathrm{d}\Omega_1\mathrm{d}\Omega_2\mathrm{d}\Omega_3\, Y^*_{\ell_1m_1}(\hat{n}_1)Y^*_{\ell_2m_2}(\hat{n}_2)Y^*_{\ell_3m_3}(\hat{n}_3)$$
$$\times \frac{\partial}{\partial\hat{n}_2}\Big\langle \Delta_{\mathrm{g}}(z_1,\hat{n}_1)I(z_2,\hat{n}_2)\Big\rangle \cdot \frac{\partial}{\partial\hat{n}_2}\Big\langle \Delta_{\mathrm{g}}(z_2,\hat{n}_2)\Delta_{\mathrm{g}}(z_3,\hat{n}_3)\Big\rangle + (2\leftrightarrow 3) \tag{4.4.4}$$

where

$$I(z_2,\hat{n}_2) \equiv \Psi_L + \left(\frac{1}{r(\tau_2)} - \mathcal{H}(\tau_2)\right) v_L + \int_{\tau_{\mathcal{O}}}^{\tau_2} \frac{\mathrm{d}\tau'}{r(\tau')}(\Phi_L+\Psi_L)(\tau', \hat{n}_2 r(\tau')). \tag{4.4.5}$$

This can be further simplified by decomposing the two-point functions in spherical harmonics, giving

$$\Big\langle a_{\ell_1m_1}(z_1)a_{\ell_2m_2}(z_2)a_{\ell_3m_3}(z_3)\Big\rangle_{\ell_1\ll\ell_2,\ell_3} \supset \int \mathrm{d}\Omega \left(\frac{\partial}{\partial\hat{n}^i}Y^*_{\ell_1m_1}(\hat{n})\right) Y^*_{\ell_2m_2}(\hat{n})$$
$$\times \left(\frac{\partial}{\partial\hat{n}^i}Y^*_{\ell_3m_3}(\hat{n})\right) C^{\Delta_{\mathrm{g}}I}_{\ell_1}(z_1,z_2)C^{\Delta_{\mathrm{g}}\Delta_{\mathrm{g}}}_{\ell_3}(z_2,z_3) + (2\leftrightarrow 3)\,. \tag{4.4.6}$$

The integral in the first line can be rewritten as

$$\frac{1}{2}\int \mathrm{d}\Omega\Big[\Delta_\Omega\big(Y^*_{\ell_1m_1}(\hat{n})Y^*_{\ell_3m_3}(\hat{n})\big) - \big(\Delta_\Omega Y^*_{\ell_1m_1}(\hat{n})\big)Y^*_{\ell_3m_3}(\hat{n})$$
$$- Y^*_{\ell_1m_1}(\hat{n})\big(\Delta_\Omega Y^*_{\ell_3m_3}(\hat{n})\big)\Big] Y^*_{\ell_2m_2}(\hat{n})\,. \tag{4.4.7}$$

The second and third terms in the parenthesis give simply

$$\frac{1}{2}\mathcal{G}^{m_1m_2m_3}_{\ell_1\ell_2\ell_3}(\ell_1(\ell_1+1)+\ell_3(\ell_3+1)). \tag{4.4.8}$$

We write the product of spherical harmonics of the first term as a Clebsch-Gordan decomposition

$$\frac{1}{2}\int \mathrm{d}\Omega\Bigg[\Delta_\Omega \sum_{LM}\sqrt{\frac{(2\ell_1+1)(2\ell_3+1)(2L+1)}{4\pi}} \times \begin{pmatrix}\ell_1 & \ell_3 & L\\ m_1 & m_3 & M\end{pmatrix}\begin{pmatrix}\ell_1 & \ell_3 & L\\ 0 & 0 & 0\end{pmatrix} Y_{LM}(\hat{n})\Bigg] Y^*_{\ell_2 m_2}(\hat{n}) = -\frac{1}{2}\ell_2(\ell_2+1)\mathcal{G}^{m_1m_2m_3}_{\ell_1\ell_2\ell_3}\,. \quad (4.4.9)$$

Putting everything together for $b_{\ell_1,\ell_2,\ell_3}(z_1,z_2,z_3)$, the observed reduced bispectrum of galaxies defined as

$$\Big\langle a_{\ell_1 m_1}(z_1)a_{\ell_2 m_2}(z_2)a_{\ell_3 m_3}(z_3)\Big\rangle = \mathcal{G}^{m_1m_2m_3}_{\ell_1\ell_2\ell_3}\; b_{\ell_1,\ell_2,\ell_3}(z_1,z_2,z_3), \quad (4.4.10)$$

we obtain the main result of this chapter, namely the consistency relation in the squeezed limit in multipole space

$$\lim_{\ell_1\ll\ell_2,\ell_3} b_{\ell_1,\ell_2,\ell_3}(z_1,z_2,z_3) = \Bigg[C_{\ell_1}^{\Delta_{\rm g}d}(z_1,z_2) + C_{\ell_1}^{\Delta_{\rm g}\Delta z}(z_1,z_2)\frac{\partial}{\partial z_2} + \frac{1}{2}\left(\ell_1(\ell_1+1)-\ell_2(\ell_2+1)+\ell_3(\ell_3+1)\right)C_{\ell_1}^{\Delta_{\rm g}I}(z_1,z_2)\Bigg] \times C_{\ell_3}^{\Delta_{\rm g}\Delta_{\rm g}}(z_2,z_3) + (2\leftrightarrow 3). \quad (4.4.11)$$

As pointed out before, since in real observation, one counts the number of galaxies within a finite redshift bin, in order to compare with observed galaxy bispectrum, one needs to integrate our theoretically calculated bispectrum in (4.4.11) over the three window functions describing the redshift bins

$$b^W_{\ell_1,\ell_2,\ell_3}(z_1,z_2,z_3) = \int \mathrm{d}z_1'\;\mathrm{d}z_2'\;\mathrm{d}z_3'\; W(z_1,z_1')W(z_2,z_2')W(z_3,z_3') \times b_{\ell_1,\ell_2,\ell_3}(z_1',z_2',z_3')\,. \quad (4.4.12)$$

Given our expression in (4.4.11), it is straightforward to compute $b^W_{\ell_1,\ell_2,\ell_3}(z_1,z_2,z_3)$.

4.4.1 The distant observer approximation

In order to build some intuition, let us rewrite our expression (4.4.11) in the distant observer approximation where we choose to decompose in Fourier modes only the direction perpendicular to the line of sight,

$$\left\langle \Delta_{\rm g}(z_1,\vec{\ell}_1)\Delta_{\rm g}(z_2,\vec{\ell}_2)\Delta_{\rm g}(z_3,\vec{\ell}_3)\right\rangle_{\ell_1\ll\ell_2,\ell_3} = (2\pi)^2\delta_{\rm D}(\vec{\ell}_1+\vec{\ell}_2+\vec{\ell}_3)$$
$$\times\left[C_{\ell_1}^{\Delta_{\rm g}d}(z_1,z_2)+C_{\ell_1}^{\Delta_{\rm g}\Delta z}(z_1,z_2)\frac{\partial}{\partial z_2}+\vec{\ell}_1\cdot\vec{\ell}_3 C_{\ell_1}^{\Delta_{\rm g}I}(z_1,z_2)\right]$$
$$\times C_{\ell_3}^{\Delta_{\rm g}\Delta_{\rm g}}(z_2,z_3)+(2\leftrightarrow 3). \quad (4.4.13)$$

Note that the third term in the square brackets, when added to the corresponding one coming from $(2\leftrightarrow 3)$, is $\mathcal{O}(\ell_1^2)$ in the equal time limit as expected due to momentum conservation, while the other terms are different from zero in that limit. Note also that the Newtonian consistency relations take into account only the redshift space distortions induced by the long-wavelength velocity, which are included here in Δz. This Newtonian contribution is not zero in the equal-time limit. The same would hold if one also decomposes the direction parallel to the line of sight in Fourier modes. This is due to the fact that one performs measurements on the light-cone, and since there is no translation invariance in the radial direction in redshift space, the two momenta connected to this radial direction would not cancel. However, this non-cancellation will be governed by how much the power spectrum changes with redshift; when it is a good approximation to ignore the evolution of the power spectrum this Newtonian consistency relation is expected to be zero as was previously found. Indeed, in the above expression it is proportional to a derivative of the power spectrum with respect to redshift. Let us mention, however, that the contribution from this term is very small due to the fact that velocity and density are not correlated in harmonic space.

In the rest of this chapter, we use the general expression given in Eq. (4.4.11) without resorting to the flat sky approximation.

4.4.2 Second-order limit

As an illustration, we plot in figure 4.1 different terms contributing to the reduced bispectrum appearing in the relation (4.4.11) in the case where the short modes are linear. The second-order computation of the three-point correlator of the observed galaxies should reproduce this result in the squeezed limit. We do this using a modified version of the code CLASSgal[5] [22]. The result is presented in the simple case of no galaxy bias $b=1$, no magnification bias $t=0$ and no galaxy evolution $f_{\rm evo}=0$ for equal redshifts of $z=0.55$ and up to scales of $\ell=200$ which are still linear.

[5] We present explicit expressions implemented in the code in appendix D.1.

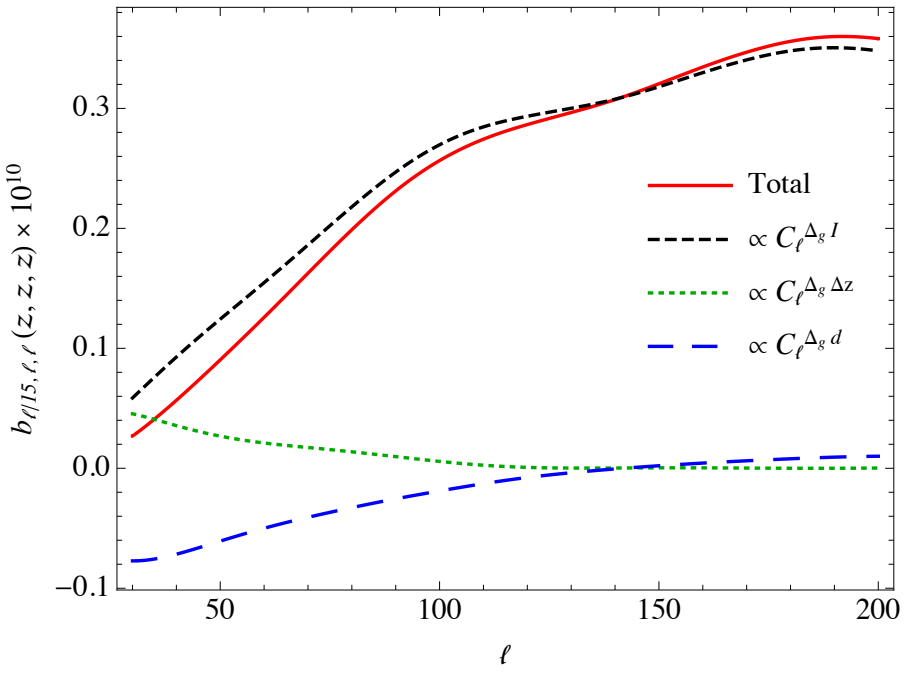

Figure 4.1: *Reduced observed bispectrum in the squeezed limit at equal-time (z=0.55) on linear scales. Note that the consistency relation is also valid when the short modes ℓ_2, ℓ_3 are in the non-linear regime. The vertical line indicates the linear scale up to which the numerical code is valid.*

One could be surprised by the small size of the cross correlation between $\Delta_{\rm g}$ and Δz. In the Newtonian approximation and working at a fixed time slice, the terms proportional to Δz are indeed believed to be the dominant effect. However, the term is suppressed in harmonic space due to the fact that the Bessel functions corresponding to the $\Delta_{\rm g}$ term and the $\hat{n}\cdot\vec{v}_L$ term are j_ℓ and j'_ℓ which oscillate at a similar frequency but out of phase and therefore cancel. In Fourier space, this can be intuitively understood from the fact that the regions where the velocities are at the maximum correspond to the minima (in absolute value) of the density and vice versa. Moreover the lensing contribution is smaller than one would expect parametrically. This is due to the fact that the integration along the line of sight tends to average out the perturbations.

4.5 Effective local non-Gaussianities from non-linear Relativistic Corrections from the consistency relation

As mentioned in previous sections, the terms proportional to $\Phi\Delta_{\rm g}$ would induce a signal in the observations that might be misinterpreted as primordial non-Gaussianity with a local shape. In order to see this, let us estimate the squeezed limit of the galaxy bispectrum induced by the primordial

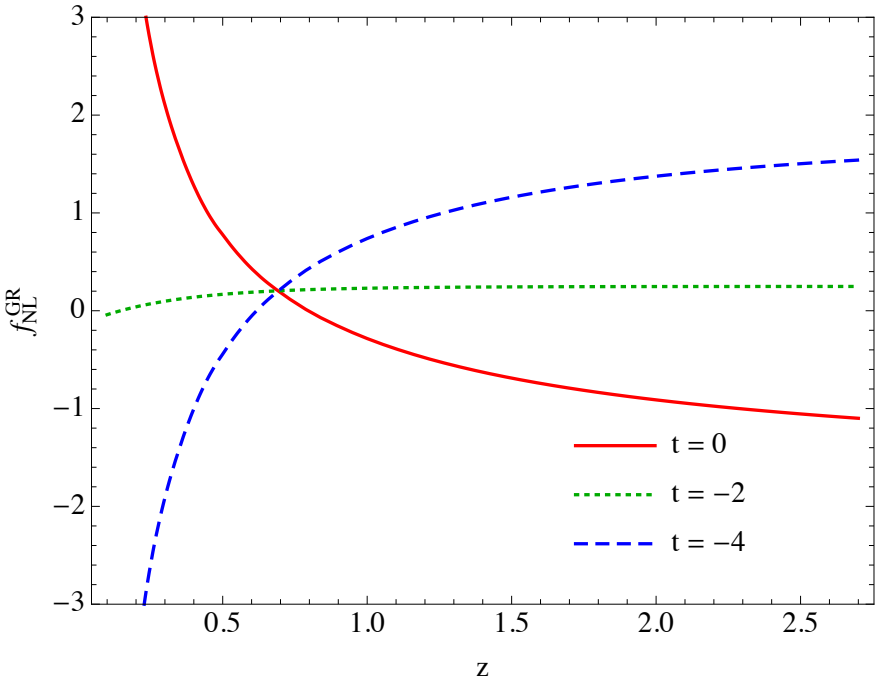

Figure 4.2: *Effective* $f_{\rm NL}^{\rm GR}$ *induced by the relativistic effects computed in this chapter. The three different lines correspond to different magnification bias parameters. We have assumed* $e = 3/a$ *for all cases and evaluated equation* (4.5.5) *at* $\ell_1 = 50$*. This estimate is valid for* $z \gtrsim 1$*. At lower redshifts, integration over the redshift bins can change this result.*

local non-Gaussianity. From a Newtonian calculation and assuming linear biasing we have[6]

$$\left\langle a_{\ell_1 m_1}(z_1) a_{\ell_2 m_2}(z_2) a_{\ell_3 m_3}(z_3) \right\rangle_{\ell_1 \ll \ell_2, \ell_3} = \mathcal{G}^{m_1 m_2 m_3}_{\ell_1 \ell_2 \ell_3} \times 4 f_{\rm NL} C_{\ell_1}^{\Delta_{\rm g}\Phi}(z_1, z_2) C_{\ell_3}^{\Delta_{\rm g}\Delta_{\rm g}}(z_2, z_3)\,, \quad (4.5.1)$$

where $f_{\rm NL} \sim 1$ is the non-linear non-Gaussianity parameter parametrizing the strength of the primordial non-Gaussianity with a local shape.

To see the impact of the non-linear relativistic contributions, we compute the ratio of Eq. (4.4.11) to $C_{\ell_1}^{\Delta_{\rm g}\Phi} C_{\ell_2}^{\Delta_{\rm g}\Delta_{\rm g}}$ where we have isolated the terms with the same ℓ-dependence as Eq. (4.5.1). Rewriting the partial derivatives with respect to τ as total ones as gradients have a different scale dependence,

[6] A similar expression is obtained in Ref. [78] for the dark matter over-density bispectrum and it is expected to hold at the non-perturbative level. However, it is not clear whether this is also true for galaxies. In Appendix D.2, we present an explicit derivation of this template for the matter overdensity.

we obtain

$$f_{NL}^{GR} = \frac{\left[C_{\ell_1}^{\Delta_g \tilde{d}}(z) + C_{\ell_1}^{\Delta_g \widetilde{\Delta z}}(z)\frac{\partial}{\partial z}\right] C_{\ell_2}^{\Delta_g \Delta_g}(z)}{C_{\ell_1}^{\Delta_g(\Phi+\Psi)}(z) C_{\ell_2}^{\Delta_g \Delta_g}(z)}, \tag{4.5.2}$$

where

$$\widetilde{\Delta z} = (1+z)\left[\Psi + aHv + \int_\tau^{\tau_0} \mathrm{d}\tilde{\tau}(\Phi' + \Psi')\right] \tag{4.5.3}$$

$$\begin{aligned}\tilde{d} = {} & (3 - f_{evo})aHv + (5s-2)\Phi + \frac{1}{aH}\Psi' + \int_\tau^{\tau_0} \mathrm{d}\tilde{\tau}\left(\frac{2-5s}{\tau_0 - \tilde{\tau}}\right)(\Phi + \Psi) \\ & + \left(2 - f_{evo} + \frac{H'}{aH^2} + \frac{2-5s}{(\tau_0 - \tau)aH} + 5s\right)\Psi. \\ & + \left(1 - f_{evo} + \frac{H'}{aH^2} + \frac{2-5s}{(\tau_0 - \tau)aH} + 5s\right)\int_\tau^{\tau_0} \mathrm{d}\tilde{\tau}(\Phi' + \Psi').\end{aligned} \tag{4.5.4}$$

In the above expression, we have accounted for the terms (2) $\leftrightarrow$ (3), set the two potentials to be equal and defined $s = -t/5$.

We notice that we can neglect the term proportional to $C_{\ell_1}^{\Delta_g \Delta z}\partial_z C_{\ell_2}^{\Delta_g \Delta_g}$. As one can easily check at second-order, this term has a different ℓ-dependence than Eq. (4.5.1). This is because the derivative with respect to redshift acting on the short mode power spectrum, acts on the Bessel function and will induce a different ℓ-dependence. A similar ℓ-dependence will also arise at higher orders.

We therefore obtain a fully non-perturbative estimate for $f_{\rm NL}$ as the short non-linear modes cancel

$$f_{NL}^{GR} \simeq \frac{C_{\ell_1}^{\Delta_g \tilde{d}}(z)}{C_{\ell_1}^{\Delta_g(\Phi+\Psi)}(z)}. \tag{4.5.5}$$

We illustrate this estimate in figure 4.2 for different magnification bias and as a function of redshift.

In order to compare with the observed bispectrum in a galaxy survey, one needs to integrate over the window functions defining the redshift bins before taking this ratio. Unless the window functions are delta functions, which for a realistic survey they are not, this integration will change both the amplitude and the ℓ-dependence of the bispectrum. However, due to the nearly constant behaviour of the transfer functions at $z \gtrsim 1$, the non-linear power spectrum of the short modes still cancels in the ratio. Therefore this integration does not modify our estimate of $f_{\rm NL}^{\rm GR}$ for those redshifts. For lower redshifts, one can explicitly carry out the integration, though the results would be only perturbative in the short modes. It should be noted that since the signal for the primordial non-Gaussianity is strongest at higher redshifts, removing the GR effects that mimic this signal is of crucial importance at those redshifts.

The exact value of $f_{\rm NL}^{\rm GR}$ will depend on redshift and the magnification bias. We plot its value as a

function of redshift in figure 4.2 for three different values of the magnification bias. From these results we deduce that at redshift $z = 1.5$ and for a vanishing magnification bias, the value of the effective $f_{\rm NL}^{\rm GR}$ is about -0.7. A qualitatively similar result was obtained in [65] for the power spectrum. They found a very similar dependence on redshift and magnification bias as well as a value for $f_{\rm NL}^{\rm GR}$ of the same order of magnitude. Since they considered a different observable, the exact values are different though their behaviour is qualitatively the same.

Also, these relativistic effects could also induce terms that would be mistaken for a violation of the Equivalence Principle in a naive analysis [84, 9].

4.6 Summary

In this chapter we have exploited the fact that a long-wavelength mode of Bardeen's potential is an adiabatic mode to write a non-perturbative relativistic relation for the squeezed limit of the galaxy number overdensity three-point function. Adiabatic modes are physical large-scale solutions to the dynamics that can be cancelled by a residual gauge transformation. The latter is realized non-linearly by Bardeen's potential. Thus, computing their effect on short-scale physics reduces trivially to a change of frame.

The effect of these transformations on the observed galaxy number density $n_{\rm g}^{\rm obs}$ corresponds to a change in the redshift and the direction of the photons at observation which in turn changes the relation between the observed volume and the physical volume, and a magnification bias. When computing the galaxy number overdensity $\Delta_{\rm g}$, one should also include the change of the average $\bar{n}_{\rm g}$ as a result of distortions to the redshift, the so-called evolution bias.

Curvature and tidal contributions, proportional to second derivatives of the gravitational potential, are not captured by our argument and are expected to be larger inside the horizon than some of the relativistic corrections which we keep, even though they would naively be expected to be parametrically subdominant with respect to the redshift space distortions and lensing induced by the long mode. However, redshift space distortions, which were also obtained in a Newtonian computation, are small due to the requirement that the small-scale modes be on similar redshifts (though they will be non-zero even at equal redshift), and the lensing is suppressed since it averages in the trajectory of the photon from emission to observation. We argue that the relativistic corrections we compute can however be distinguished by their dependence on the large scale as one takes the squeezed limit, and they serve as a consistency check for our cosmological model. Indeed, the violation of the Equivalence Principle at large scales or the presence of primordial local non-Gaussianity would induce a squeezed limit with the shape of these contributions. They need to be kept in order not to confuse them with these deviations from the vanilla cosmological scenario. The exact value of the effective local non-Gaussianity parameter from these non-linear GR corrections depends on the redshift and the magnification bias. At redshift of $z = 1.5$ and in the absence of magnification bias we estimate $f_{\rm NL}^{\rm GR} = -0.7$.

Finally, since the Universe evolves and there is no translation invariance in the radial direction of redshift space, Fourier-space triangles do not close and we thus present our expressions after decomposing them in spherical harmonics. Notably, we find that the Newtonian redshift space distortions induce a term that does not go to zero at equal redshifts, but is however very small.

Chapter 5

Non-Gaussianities from relativistic corrections

5.1 The bispectrum of galaxy number counts

Given the large scales that will be probed by upcoming LSS surveys, the Newtonian description of galaxy clustering is insufficient and a full general relativistic (GR) treatment is necessary. In the previous chapter, we have been able to compute the squeezed limit of the galaxy number count bispectrum using the idea of the consistency condition. While this approach, compared to a perturbative expansion, allows to include non-linear modes, the trade-off is that it is valid only for squeezed configurations, which make up a small percentage of all observable configurations. In order to fully exploit upcoming bispectrum data, it is therefore necessary to compute the bispectrum at tree-level (at least) for generic configurations, which makes it necessary compute the number counts overdensity contrast at second order in the perturbations $\Delta_{\rm g}^{(2)}(\hat{n}, z)$. This has been achieved recently by several groups [67, 68, 125, 19]. In this case, the down side is of course that this perturbative expansion is valid only on weakly non-linear scales.

Analogously to what is been done for the CMB, one needs to subtract any contribution to the bispectrum which can look like primordial non-Gaussianity (PNG) if one desires to measure the actual level of primordial NG. In the case of the CMB, the main contamination to $f_{\rm NL}^{\rm loc}$ is found to be the ISW-lensing effect [72, 75]. In the following[1], we shall evaluate the level of NG induced by the bispectrum associated from several terms present in the second order number counts computation of [19]. Let us emphasize that the aim of this work is not to make an exhaustive analysis of all (hundreds) of terms appearing in the second order expression, but only to give examples of the level of NG that some of them can generate. Because cancellations between terms can happen, a full analysis will very likely be required in the end and we leave it for future work. To this end, we compute numerically the local and equilateral templates in $z\ell m$-space. The level of NG is then given by projecting the different bispectra on the templates. We shall also evaluate the local NG induced from the terms appearing in the consistency relation (4.4.11) using the exact templates. This will allow us to confirm the "naive" estimate done in section 4.5.

[1] This chapter is based on the draft of an upcoming paper [131]

Note that the contributions that we are computing should not be confused with the NG coming from the dynamics beyond the Newtonian approximation as in [132]. The effects that we are computing here come from the fact that compute observed number counts. These are therefore usually called *projection effects*. The dynamics are still assumed to be given by SPT, that is, Newtonian dynamics.

Let us define what mean by "relativistic corrections" and how we classify them. The main contribution to the number counts at second order are the density terms $\Delta_{\rm g}^{(2)} \supset (\delta^{(1)})^2$ giving rise to a bispectrum which we represent symbolically as $b \sim \langle(\delta\delta)\delta\delta\rangle$. This Newtonian contribution corresponds to the one from standard perturbation theory and is also what is measured in simulations (on applicable scales). Here δ has to be understood as the matter overdensity contrast in the synchronous gauge. Indeed, it is the overdensity satisfying the Poisson equation which is used in SPT and solved in simulations. With respect to the gravitational potential in the Poisson gauge Φ, we therefore have $\delta \sim \partial^2\Phi$. These Newtonian terms have already been computed and are known to give a very large contribution to local NG of order $10^3 - 10^4$ [133].

In this work we shall consider subleading corrections due to relativistic effects. We shall classify the various "corrections" coming from the difference between number counts and density by the number of derivatives and integrals they contain. The contributions appearing in the terms "three derivatives" and "Newtonian $\times$ Lensing" are of the type $b \sim \langle(\Phi\partial^3\Phi)\delta\delta\rangle$ and $b \sim \langle(\int\Phi\delta)\delta\delta\rangle$ respectively while the ones from the consistency relation considered in section 4.5 have various contributions of order $b \sim \langle(\Phi\delta)\delta\delta\rangle$, $b \sim \langle(\partial\Phi\delta)\delta\delta\rangle$ and $b \sim \langle(\partial^2\Phi\delta)\delta\delta\rangle$.

This chapter is organized as follows: In section 5.2, we begin by defining non-Gaussian templates in Fourier space. Next we calculate their counter part in $z\ell m$-space and point out to some subtleties in numerical evaluations of the integrals. We close this section by defining the shape correlation in $z\ell m$-space between local and equilateral templates and define the effective $f_{\rm NL}$ as the normalized amplitude of the projected bispectrum of the relatistic contributions onto a particular PNG template. In section 5.3, we summarize the relativistic contributions to the tree-level bispectrum that we consider. In section 5.4 we present the estimates for $f_{\rm NL}$ from various terms that we have considered for local and equilateral shapes and discuss their significance. Finally we draw our conclusions in section 5.5.

5.2 Non-Gaussianities from the observed bispecturm

To quantify the contamination from the relativistic effects to the measured primordial $f_{\rm NL}$ of a given shape, we need to project the bispectrum from relativistic corrections onto the corresponding primordial bispectrum template for that shape. For the rest of our discussion, we focus on local and equilateral shapes. Below we first set the basic notation and define the two bispectrum templates in Fourier space. Next we derive the corresponding templates in $z\ell m$-space and discuss in details some subtleties in evaluating the numerical integrals.

5.2.1 NG shapes in Fourier space

While the statistics of Gaussian fluctuations is fully determined by the lowest order correlation function, one needs to consider higher order correlation functions to describe a non-Gaussian field. We focus on the lowest order non-Gaussian statistics of primordial fluctuations, the 3-point function and

its counterpart in Fourier space, the bispectrum defined by equation (1.2.8). For the rest of our discussion, we consider two of the commonly used separable shapes, the local and equilateral. For a scale-invariant primordial power spectrum $P_\zeta(k) = Ak^{-3}$, the local template is given by [134, 135, 133, 136]

$$\begin{aligned} F_{\rm local}(k_1,k_2,k_3) &= \frac{6}{5} f_{\rm NL}^{\rm loc} \left(P_\zeta(k_1)P_\zeta(k_2) + P_\zeta(k_2)P_\zeta(k_3) + P_\zeta(k_3)P_\zeta(k_1)\right) \\ &= \frac{6}{5} f_{\rm NL}^{\rm loc} A^2 \left(\frac{1}{k_2^3 k_3^3} + \frac{1}{k_3^3 k_1^3} + \frac{1}{k_1^3 k_2^3}\right), \end{aligned} \tag{5.2.1}$$

while the equilateral template is defined as [137]

$$\begin{aligned} F_{\rm equil}(k_1,k_2,k_3) = \frac{18}{5} f_{\rm NL}^{\rm eq} A^2 \\ \times \left(-\frac{1}{k_1^3 k_2^3} - \frac{1}{k_1^3 k_3^3} - \frac{1}{k_2^3 k_3^3} - \frac{2}{k_1^2 k_2^2 k_3^2} + \left(\frac{1}{k_1 k_2^2 k_3^3} + 5\, perm.\right)\right). \end{aligned} \tag{5.2.2}$$

The amplitude of the shape is $f_{\rm NL}^{\rm shape}$ while $F_{\rm shape}(k_1,k_2,k_3)$ encodes the functional dependence of the primordial bispectrum on the momenta. Constraints on PNG are reported as constraints on the amplitude parameter for a particular shape.

5.2.2 Computing the NG shapes in $z\ell m$-space

We now compute the angular bispectrum for the number counts resulting from the two primordial shapes above. The number counts of galaxies are expanded in spherical harmonics (see appendix D.1.1 for more details). The harmonic coefficients are given by [20]

$$a_{\ell m}^{\Delta_g} = (-i)^l \frac{4\pi}{(2\pi)^3} \int d^3k Y_{\ell m}^*(\hat{k}) \Delta_\ell(k) \zeta(\vec{k}), \tag{5.2.3}$$

where we have defined

$$\Delta_\ell(k) = \sum_i \Delta_\ell^i(k), \tag{5.2.4}$$

with i running on the different angular transfer functions defined in Appendix A.4 of [22]. We have omitted the redshift dependence for sake of simplicity. The bispectrum is then given by correlating three coefficients and taking the expectation value

$$B_{\ell_1\ell_2\ell_3}^{m_1m_2m_3}(z_1,z_2,z_3) = \left\langle a_{\ell_1,m_1}^{\Delta_g}(z_1) a_{\ell_2 m_2}^{\Delta_g}(z_2) a_{\ell_3 m_3}^{\Delta_g}(z_3) \right\rangle$$

$$= (-i)^{\ell_1+\ell_2+\ell_3} \int \prod_{p=1}^{3} \left\{ d^3k_p \frac{4\pi}{(2\pi)^3} Y^*_{\ell_p m_p}(\hat{k}_p) \Delta_{\ell_p}(k_p) \right\} \langle \zeta(\vec{k}_1)\zeta(\vec{k}_2)\zeta(\vec{k}_3) \rangle$$

$$= (-i)^{\ell_1+\ell_2+\ell_3} \int \prod_{p=1}^{3} \left\{ d^3k_p \frac{4\pi}{(2\pi)^3} Y^*_{\ell_p m_p}(\hat{k}_p) \Delta_{\ell_p}(k_p) \right\}$$

$$\times (2\pi)^3 \delta^{(3)}(\vec{k}_1 + \vec{k}_2 + \vec{k}_3) F(k_1, k_2, k_3) \tag{5.2.5}$$

One then expands the delta-Dirac function

$$\begin{aligned} \delta^{(3)}(\vec{k}_1 + \vec{k}_2 + \vec{k}_3) &= \int d^3x \, \frac{1}{(2\pi)^3} \, e^{i(\vec{k}_1+\vec{k}_2+\vec{k}_3)\cdot\vec{x}} \\ &= \frac{1}{(2\pi)^3} \int dr r^2 d\Omega_{\hat{n}} \, e^{i(\vec{k}_1+\vec{k}_2+\vec{k}_3)\cdot r\hat{n}} \\ &= \frac{1}{(2\pi)^3} \int dr r^2 d\Omega_{\hat{n}} \\ &\quad \times \prod_{q=1}^{3} \left\{ 4\pi \sum_{l'_q=0}^{\infty} \sum_{m'_q=-l'_q}^{l'_q} i^{l'_q} j_{l'_q}(rk_q) Y_{l'_q m'_q}(\hat{k}_q) Y^*_{l'_q m'_q}(\hat{n}) \right\} , \end{aligned} \tag{5.2.6}$$

where $\hat{n}$ is the unit vector representing the direction of the galaxy. By performing the angular integral over $d\Omega_{\hat{n}}$ we obtain

$$B^{m_1 m_2 m_3}_{\ell_1 \ell_2 \ell_3} = \mathcal{G}^{m_1 m_2 m_3}_{\ell_1 \ell_2 \ell_3}$$

$$\times \left(\frac{2}{\pi}\right)^3 \int dk_1 dk_2 dk_3 \int dr r^2 \prod_{p=1}^{3} \left\{ k_p^2 \Delta_{\ell_p}(k_p) j_{\ell_p}(rk_p) \right\} F(k_1, k_2, k_3) \, . \tag{5.2.7}$$

We can define the reduced bispectrum

$$b_{\ell_1 \ell_2 \ell_3} = (-i)^{\ell_1+\ell_2+\ell_3} \left(\frac{2}{\pi}\right)^3 \int dk_1 dk_2 dk_3 \int dr r^2 \prod_{p=1}^{3} \left\{ k_p^2 \Delta_{\ell_p}(k_p) j_{\ell_p}(rk_p) \right\} F(k_1, k_2, k_3) \, . \tag{5.2.8}$$

where $F(k_1, k_2, k_3)$ is the primordial NG shape. Even if the shape is separable, as it is the case for the templates (5.2.1), (5.2.2), the individual k_i integrals do not generally converge, contrarily to what happens for the CMB [138]. It is however possible to simplify this result by performing the r integral analytically, reducing the dimension of the integral from four to three and getting rid of three spherical

Bessel functions. We use the results of [139] :

$$\int dr\, r^2\, j_{\ell_1}(rk_1) j_{\ell_2}(rk_2) j_{\ell_3}(rk_3) = \frac{\pi\Delta}{4k_1k_2k_3} \frac{i^{-(\ell_1+\ell_2+\ell_3)}}{\begin{pmatrix} \ell_1 & \ell_2 & \ell_3 \\ 0 & 0 & 0 \end{pmatrix}}$$

$$\times \sum_m (-1)^m \left[\frac{(\ell_1-m)!(\ell_2+m)!}{(\ell_1+m)!(\ell_2-m)!}\right]^{1/2} \begin{pmatrix} \ell_1 & \ell_2 & \ell_3 \\ m & -m & 0 \end{pmatrix} P_{\ell_1}^m(\cos\theta_{13}) P_{\ell_2}^{-m}(\cos\theta_{23}),$$

where $|m| \leq \ell_1, \ell_2$. Therefore, taking ℓ_3 to be the largest one, the sum contains $2\min_i(\ell_i)+1$ terms, $\Delta = 1$ if $\vec{k}_i$ form a non degenerate triangles and $1/2$ for degenerate ones, zero if they do not form a triangle. The θ_{ij} are the angles between the sides i and j of the triangle.

We implement these expressions in Mathematica and compute the integrals using the Suave[2] Monte Carlo integrator for Mathematica. The different transfer functions are computed with the CLASSgal code [22]. However, we have omitted integrated terms such as lensing, ISW and time-delay in $\Delta_\ell(k)$ for numerical reasons as they would require to output functions of both k and ℓ. We limit ourselves to "local" terms that can be expressed as a product of Bessel function times a k-dependent transfer function. At equal-times, integrated terms terms are also expected be sub-dominant. Moreover, as these integrals are computationally very demanding, we compute only some configurations with ℓ values spaced by $\Delta\ell = 4$ and interpolate to obtain the values of the template for any configuration.

In addition to the exact numerical templates computed numerically, we shall also consider the simple template for local NG used in the previous chapter (4.5.1) which corresponds to the reduced bispectrum

$$b_{\ell_1 \ll \ell_2, \ell_3} = 4 f_{\rm NL} C_{\ell_1}^{\Delta_{\rm g}\Phi}(z_1, z_2) C_{\ell_3}^{\Delta_{\rm g}\Delta_{\rm g}}(z_2, z_3)\,, \tag{5.2.9}$$

which is valid only in the squeezed limit $\ell_1 \ll \ell_2 = \ell_3$.

5.2.3 NG shapes in $z\ell m$ space

It is useful to define the scalar product between two bispectra b^{S1} and b^{S2} in $z\ell m$-space :

$$(S_1, S_2) = \sum_{\ell_1 \leq \ell_2 \leq \ell_3} I_{\ell_1\ell_2\ell_3} \frac{b^{S_1}_{\ell_1\ell_2\ell_3}\, b^{S_2}_{\ell_1\ell_2\ell_3}}{f_{\ell_1\ell_2\ell_3} C_{\ell_1} C_{\ell_2} C_{\ell_3}} \tag{5.2.10}$$

with

$$I_{\ell_1\ell_2\ell_3} = \frac{(2\ell_1+1)\,(2\ell_2+1)\,(2\ell_3+1)}{4\pi} \begin{pmatrix} \ell_1 & \ell_2 & \ell_3 \\ 0 & 0 & 0 \end{pmatrix}^2 \tag{5.2.11}$$

[2] http://www.feynarts.de/cuba/

and

$$f_{\ell_1\ell_2\ell_3} = \begin{cases} 6 & \ell_1 = \ell_2 = \ell_3 \\ 2 & \ell_1 = \ell_2 \neq \ell_3 \text{ or perm.} \\ 1 & \text{else} \end{cases} \tag{5.2.12}$$

The angular power spectra include the full number counts $C_\ell = C_\ell^{\Delta_{\rm g}\Delta_{\rm g}}$ and the sum is taken between $\ell = 2$ and $\ell_{\rm max}$. We can determine how orthogonal are two bispectra b^{S1} and b^{S2} by computing the cosine

$$\cos(S_1, S_2) = \frac{\sum_{\ell_1\leq\ell_2\leq\ell_3} I_{\ell_1\ell_2\ell_3} \frac{b^{S_1}_{\ell_1\ell_2\ell_3} b^{S_2}_{\ell_1\ell_2\ell_3}}{f_{\ell_1\ell_2\ell_3} C_{\ell_1} C_{\ell_2} C_{\ell_3}}}{\sqrt{\sum_{\ell_1\leq\ell_2\leq\ell_3} I_{\ell_1\ell_2\ell_3} \frac{\left(b^{S_1}_{\ell_1\ell_2\ell_3}\right)^2}{f_{\ell_1\ell_2\ell_3} C_{\ell_1} C_{\ell_2} C_{\ell_3}}} \sqrt{\sum_{\ell_1\leq\ell_2\leq\ell_3} I_{\ell_1\ell_2\ell_3} \frac{\left(b^{S_2}_{\ell_1\ell_2\ell_3}\right)^2}{f_{\ell_1\ell_2\ell_3} C_{\ell_1} C_{\ell_2} C_{\ell_3}}}}. \tag{5.2.13}$$

As we see in figure 5.1 the two templates are not orthogonal with a cosine of about 0.94 at $\ell_{\rm max} = 100$. This means for example that terms which have a large local component will 'leak' in the equilateral shape and give a substantial contribution to $f_{\rm NL}^{\rm eq}$. We also observe that the cosine between the two shapes diminishes considering smaller scales as adding more information helps discriminate the two shapes better.

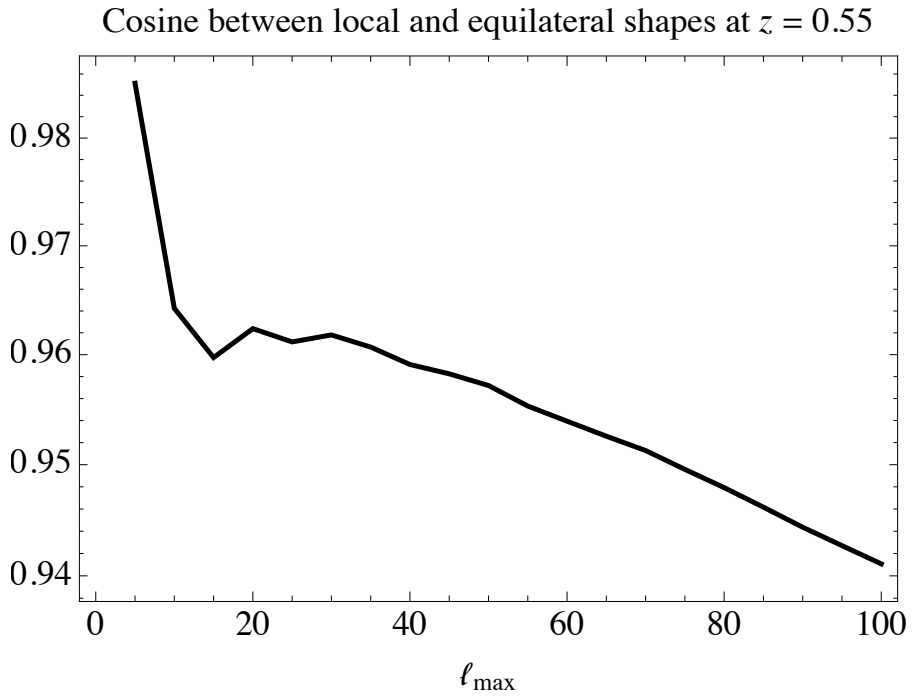

Figure 5.1: Cosine defined through Eq. (5.2.13) between local and equilateral shapes for galaxy bispectra at $z = 0.55$ in $z\ell m$ space as a function the maximum $\ell_{\rm max}$ included in the sum.

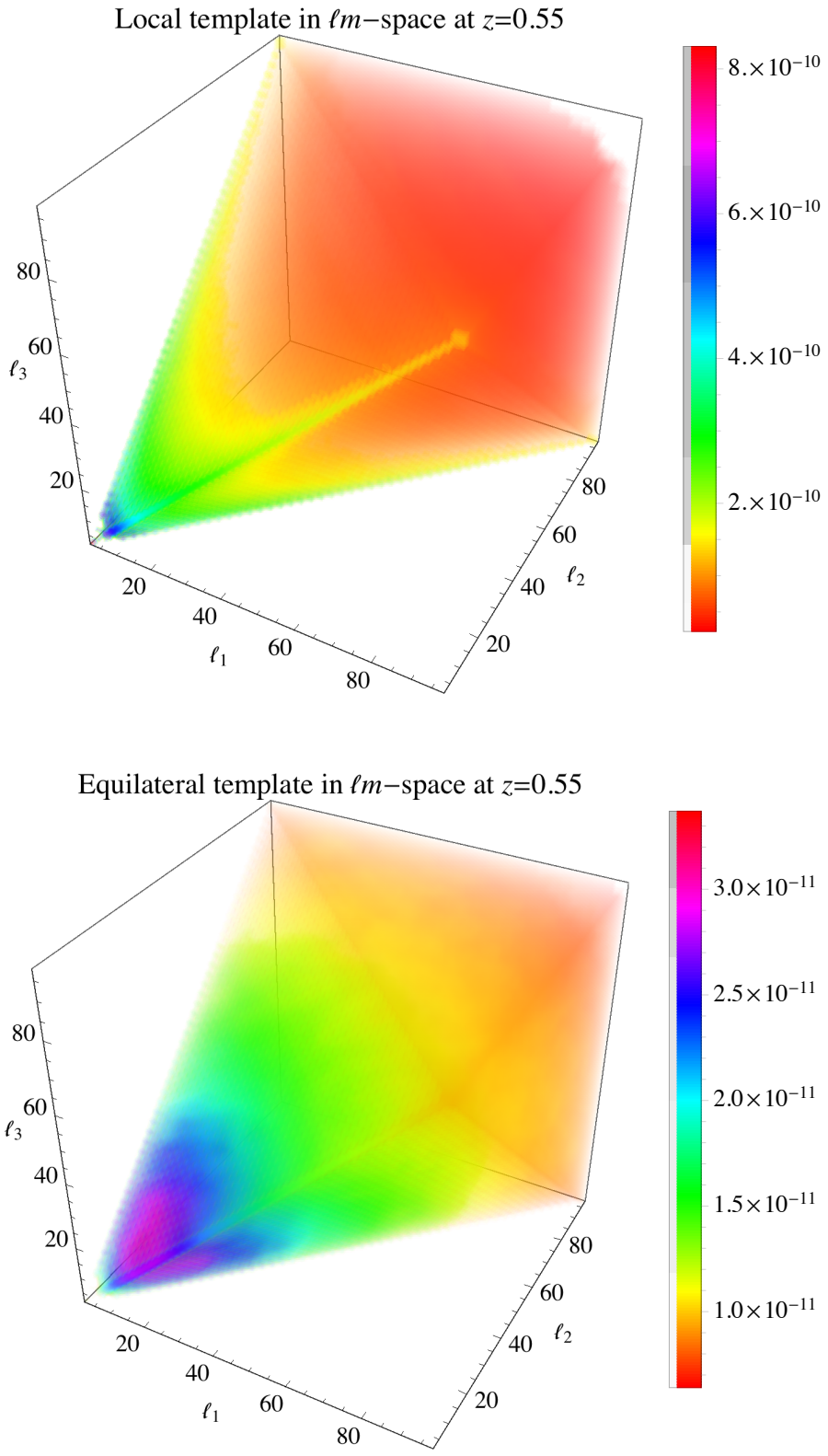

Figure 5.2: Absolute value of the reduced bispectrum for the non-Gaussianity template: local (top) and equilateral (bottom). We have considered three galaxies at the same redshift $z = 0.55$

In figure 5.2 we present the reduced bispectra corresponding to the local and equilateral templates for three galaxies at the same redshift $z = 0.55$. We see that the local non-Gaussianity template peaks in the squeezed limit ($\ell_1 \ll \ell_2 \sim \ell_3$) while the equilateral template is largest when ℓ_1, ℓ_2 and ℓ_3 are roughly equal. The peaking is however less pronounced than in Fourier space because of the harmonic decomposition.

Let us finish this section by comparing the full template (5.2.8) with the simple template (5.2.9) used for the estimation of section 4.5. To this aim, we compute the ratio of the simple template to the full template. As the simple template should be valid only in squeezed configurations, we evaluate the ratio for configurations with $\ell_1 = 2$ and $\ell_2 = \ell_3$ as function of ℓ_2. The result is presented in figure 5.3. We find that the templates coincide at a factor 0.5 for $\ell_2/\ell_1 \sim 10$ and up to 0.7 in the most squeezed configurations $\ell_2/\ell_1 \sim 50$. The naive estimation of $f_{\rm NL}^{\rm loc}$ from the terms of the consistency relation presented in section 4.5 is therefore expected to hold at order of magnitude level. We shall confirm this in section 5.4.1 where we perform the full projection of the bispectrum from the consistency relation on the local template.

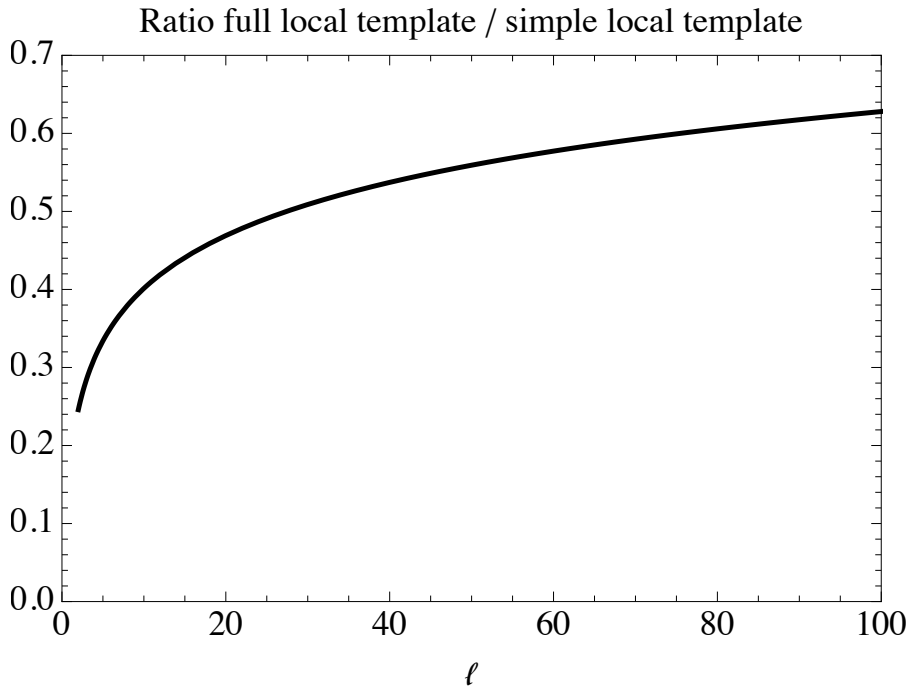

Figure 5.3: Ratio of the simple local template (5.2.9) to the full local template (5.2.8) as function of $\ell = \ell_2 = \ell_3$ at $\ell_1 = 2$.

5.2.4 Effective non-Gaussianity

Having the non-Gaussianity templates in $z\ell m$-space at our disposal, we can now estimate the amount of non-Gaussianity imprinted from the different contributions to the galaxy bispectrum by projecting

them on the relevant shape. The effective $f_{\rm NL}$ is given by

$$f_{\rm NL}^{\rm shape} = \frac{\sum_{\ell_1\leq\ell_2\leq\ell_3} I_{\ell_1\ell_2\ell_3} \frac{b_{\ell_1\ell_2\ell_3} b^{\rm shape}_{\ell_1\ell_2\ell_3}}{f_{\ell_1\ell_2\ell_3} C_{\ell_1} C_{\ell_2} C_{\ell_3}}}{\sum_{\ell_1\leq\ell_2\leq\ell_3} I_{\ell_1\ell_2\ell_3} \frac{\left(b^{\rm shape}_{\ell_1\ell_2\ell_3}\right)^2}{f_{\ell_1\ell_2\ell_3} C_{\ell_1} C_{\ell_2} C_{\ell_3}}}\,, \tag{5.2.14}$$

where $b_{\ell_1\ell_2\ell_3}$ is the reduced bispectrum associated to the contribution of interest. When summing over all configurations, we sum over configurations involving ℓ's from 2 to ℓ_{max}. When considering only squeezed configurations, we sum over the subset of configurations for which $\ell_1 \leq \min(\ell_2, \ell_3)/10$.

5.3 Contributions to the bispectrum from relativistic corrections

In this section, we present the different relativistic contributions to the bispectrum that we shall study.

5.3.1 Consistency condition bispectrum

The terms derived from the consistency relation (4.4.11) are the following

$$\begin{aligned}\lim_{\ell_1\ll\ell_2,\ell_3} b_{\ell_1,\ell_2,\ell_3}(z_1,z_2,z_3) = \Bigg[& C_{\ell_1}^{\Delta_{\rm g} d}(z_1,z_2) + C_{\ell_1}^{\Delta_{\rm g}\Delta z}(z_1,z_2)\frac{\partial}{\partial z_2} \\ & + \frac{1}{2}\left(\ell_1(\ell_1+1) - \ell_2(\ell_2+1) + \ell_3(\ell_3+1)\right) C_{\ell_1}^{\Delta_{\rm g} I}(z_1,z_2)\Bigg] \\ & \times C_{\ell_3}^{\Delta_{\rm g}\Delta_{\rm g}}(z_2,z_3) + (2\leftrightarrow 3)\end{aligned} \tag{5.3.1}$$

which we shall denote it by "CR" in the figures. We shall also consider the terms from this relation that have the same scale dependence ($b \sim \langle(\Phi\delta)\delta\delta\rangle$) as the local template in the squeezed limit (5.2.9). These terms are the same that we have kept in the numerator of (4.5.2). For a general squeezed configuration ($\ell_2 \neq \ell_3$) they read

$$\begin{aligned}\lim_{\ell_1\ll\ell_2,\ell_3} b_{\ell_1,\ell_2,\ell_3}(z_1,z_2,z_3) = & \left[C_{\ell_1}^{\Delta_{\rm g}\tilde{d}}(z_1,z_2) + C_{\ell_1}^{\Delta_{\rm g}\widetilde{\Delta z}}(z_1,z_2)\frac{\partial}{\partial z_2}\right] \\ & \times C_{\ell_3}^{\Delta_{\rm g}\Delta_{\rm g}}(z_2,z_3) + (2\leftrightarrow 3).\end{aligned} \tag{5.3.2}$$

where

$$\widetilde{\Delta z} = (1+z)\left[\Psi + aHv + \int_\tau^{\tau_0} {\rm d}\tilde{\tau}(\Phi'+\Psi')\right] \tag{5.3.3}$$

$$\tilde{d} = (3 - f_{evo})aHv + (5s-2)\Phi + \frac{1}{aH}\Psi' + \int_\tau^{\tau_0} \mathrm{d}\tilde{\tau}\left(\frac{2-5s}{\tau_0 - \tilde{\tau}}\right)(\Phi + \Psi)$$
$$+ \left(2 - f_{evo} + \frac{H'}{aH^2} + \frac{2-5s}{(\tau_0 - \tau)aH} + 5s\right)\Psi.$$
$$+ \left(1 - f_{evo} + \frac{H'}{aH^2} + \frac{2-5s}{(\tau_0 - \tau)aH} + 5s\right)\int_\tau^{\tau_0} \mathrm{d}\tilde{\tau}(\Phi' + \Psi'). \tag{5.3.4}$$

This contribution will be denoted by "CR simple" as it is the dominant term in the perfect squeezed limit when ℓ_1 is almost constant and therefore all gradients are negligible. We stress again that these contributions are only valid in the squeezed limit $\ell_1 \ll \ell_2 \simeq \ell_3$.

5.3.2 "Newtonian × Lensing" terms

Next, we consider the contribution "Newtonian × Lensing" to the second order number counts, computed in [18]. They correspond to the reduced bispectrum denoted by

$$b_{\ell_1\ell_2\ell_3} = b^{\kappa\delta}_{\ell_1\ell_2\ell_3} + b^{\nabla\delta\nabla\psi}_{\ell_1\ell_2\ell_3} + b^{v'\kappa}_{\ell_1\ell_2\ell_3} + b^{\nabla v'\nabla\psi}_{\ell_1\ell_2\ell_3}\,. \tag{5.3.5}$$

We now generalize it to include first order redshift-space distortions. This leads to the reduced bispectrum

$$\langle \Delta_{\text{Newt}\,\times\,\text{Lens}}(\hat{n}_1, z_1)\left(\delta - \mathcal{H}^{-1}\partial_r^2 v\right)(\hat{n}_2, z_2)\left(\delta - \mathcal{H}^{-1}\partial_r^2 v\right)(\hat{n}_3, z_3)\rangle + \text{perms.} \tag{5.3.6}$$

It is schematically given by

$$\begin{aligned}
b^{\text{N}\times\text{L}}_{\ell_1\ell_2\ell_3} \;\sim\; & \Big[C^{A\delta}_{\ell_2}(z_1,z_2)\,C^{B\delta}_{\ell_3}(z_1,z_3) + C^{B\delta}_{\ell_2}(z_1,z_2)\,C^{A\delta}_{\ell_3}(z_1,z_3) \\
& + C^{A\delta}_{\ell_3}(z_2,z_3)\,C^{B\delta}_{\ell_1}(z_2,z_1) + C^{B\delta}_{\ell_3}(z_2,z_3)\,C^{A\delta}_{\ell_1}(z_2,z_1) \\
& + C^{A\delta}_{\ell_1}(z_3,z_1)\,C^{B\delta}_{\ell_2}(z_3,z_2) + C^{B\delta}_{\ell_1}(z_3,z_1)\,C^{A\delta}_{\ell_2}(z_3,z_2)\Big] \\
& + \Big[C^{Av'}_{\ell_2}(z_1,z_2)\,C^{Bv'}_{\ell_3}(z_1,z_3) + C^{Bv'}_{\ell_2}(z_1,z_2)\,C^{Av'}_{\ell_3}(z_1,z_3) \\
& + C^{Av'}_{\ell_3}(z_2,z_3)\,C^{Bv'}_{\ell_1}(z_2,z_1) + C^{Bv'}_{\ell_3}(z_2,z_3)\,C^{Av'}_{\ell_1}(z_2,z_1) \\
& + C^{Av'}_{\ell_1}(z_3,z_1)\,C^{Bv'}_{\ell_2}(z_3,z_2) + C^{Bv'}_{\ell_1}(z_3,z_1)\,C^{Av'}_{\ell_2}(z_3,z_2)\Big]
\end{aligned}$$

$$
\begin{aligned}
&+ \quad \Big[C^{A\delta}_{\ell_2}(z_1,z_2)\, C^{Bv'}_{\ell_3}(z_1,z_3) + C^{B\delta}_{\ell_2}(z_1,z_2)\, C^{Av'}_{\ell_3}(z_1,z_3) \\
&+ \quad C^{A\delta}_{\ell_3}(z_2,z_3)\, C^{Bv'}_{\ell_1}(z_2,z_1) + C^{B\delta}_{\ell_3}(z_2,z_3)\, C^{Av'}_{\ell_1}(z_2,z_1) \\
&+ \quad C^{A\delta}_{\ell_1}(z_3,z_1)\, C^{Bv'}_{\ell_2}(z_3,z_2) + C^{B\delta}_{\ell_1}(z_3,z_1)\, C^{Av'}_{\ell_2}(z_3,z_2) \Big] \\
&+ \quad \Big[C^{A\delta}_{\ell_3}(z_1,z_3)\, C^{Bv'}_{\ell_2}(z_1,z_2) + C^{B\delta}_{\ell_3}(z_1,z_3)\, C^{Av'}_{\ell_2}(z_1,z_2) \\
&+ \quad C^{A\delta}_{\ell_1}(z_2,z_1)\, C^{Bv'}_{\ell_3}(z_2,z_3) + C^{B\delta}_{\ell_1}(z_2,z_1)\, C^{Av'}_{\ell_3}(z_2,z_3) \\
&+ \quad C^{A\delta}_{\ell_2}(z_3,z_2)\, C^{Bv'}_{\ell_1}(z_3,z_1) + C^{B\delta}_{\ell_2}(z_3,z_2)\, C^{Av'}_{\ell_1}(z_3,z_1) \Big]
\end{aligned}
\tag{5.3.7}
$$

where A and B denote the first order perturbations leading to $\Delta_{\mathrm{N\times L}}$ (or Δ_{Newt}). This term will be denoted by "N×L" in the figures and scales as $b \sim \langle (\int \Phi\delta)\delta\delta \rangle$.

5.3.3 Three derivatives terms

Finally, we shall consider the bispectrum for some terms computed in the full second order number counts [19] which contain three derivatives of the metric perturbations: $b \sim \langle (\partial^3\Phi\Phi)\delta\delta \rangle$. These are namely

$$
\Delta_{3d}(\hat{n},z) = \frac{1}{\mathcal{H}_s^2}\left(\partial_r^2\Phi_W\partial_r v - \Phi_W\partial_r^3 v\right) + \frac{1}{\mathcal{H}_s}\frac{\Psi+\Phi}{2}\partial_r\delta. \tag{5.3.8}
$$

5.4 Results

5.4.1 Local NG

Let us start by computing the contamination of the "Newtonian × Lensing" and the "three derivatives" terms to local non-Gaussianity. As the expressions (5.3.8) and (5.3.5) are valid for any configurations, we include all configurations in the sums of (5.2.14). Figure 5.4 shows the resulting $f_{\mathrm{NL}}^{\mathrm{loc}}$ and the cosine between the terms and the local shape as a function of the maximum value of ℓ included. We find that both the "Newtonian × Lensing" terms and the "three derivatives" induce a small contamination of order

$$
f_{\mathrm{NL}}^{\mathrm{loc,\,N\times L}} \simeq 0.2, \tag{5.4.1}
$$

$$
f_{\mathrm{NL}}^{\mathrm{loc,\,3\,d}} \simeq -0.4\,. \tag{5.4.2}
$$

The cosine with the local shape is very close to one for both terms although we would naively not expect this as they have a different scale dependence than the local terms.

The terms computed from the consistency relation are correct only in the squeezed limit. We therefore present on figure 5.5 the effective local NG computed from (5.2.14) summing only over squeezed configurations with a squeezing factor of $\ell_2/\ell_1 \geq 10$. We detail different contributions : the full consistency relation (5.3.1) and the terms scaling like $b \sim \langle(\Phi\delta)\delta\delta\rangle$ (5.3.2). For comparison, we also present the effective NG from the second-order terms "Newtonian × Lensing" and "three derivatives".

We find that the estimate of the NG induced by the terms "Newtonian × Lensing" and "three derivative" are very similar to what we have found by taking into account all configurations: $f_{\rm NL}^{\rm loc,\,N\times L} \simeq 0.13$ and $f_{\rm NL}^{\rm loc,\,3\,d} \simeq -0.5$. This is reassure us in the belief that a large proportion of the information in the local shape is contained in the squeezed limit. We therefore expect that the local NG associated to the terms related to the consistency condition, which we know only in the squeezed limit, should be reliable.

The terms derived from the consistency relation are found to give a relevant contribution to $f_{\rm NL}^{\rm loc}$:

$$f_{\rm NL}^{\rm loc,\,CR} \simeq -3.0, \tag{5.4.3}$$

$$f_{\rm NL}^{\rm loc,\,CR\,simple} \simeq 0.4\,. \tag{5.4.4}$$

Comparing the effective NG from the term "CR" to the "CR simple" one, we see that the difference is non negligible. This is due to the fact that terms which *do not* scale like $b \sim (\Phi)\delta\delta\delta$ also give large contributions to the local shape because the cosines are relatively high. This was also seen in figure 5.1 when computing the cosine between the local and equilateral shapes.

We conclude that to attain a precision of $\sigma_{f_{\rm NL}^{\rm loc}} = 1$, it is necessary to take at least the terms from the consistency condition into account. Although the contamination associated to the "Newtonian × Lensing" and 'three derivatives" are smaller than one, they are not totally negligible. Indeed, there are many more terms appearing in the second order number counts expression. If they all give a similar contribution, the total contamination might easily be above $f_{\rm NL}^{\rm loc} \sim 1$.

5.4.2 Equilateral NG

The results for equilateral NG are presented on figures 5.6. We find that for $\ell_{max} = 100$ the "Newtonian × Lensing" and the "three derivatives" terms lead to a similar contamination of

$$f_{\rm NL}^{\rm eq,\,N\times L} \simeq 1.1, \tag{5.4.5}$$

$$f_{\rm NL}^{\rm eq,\,3\,d} \simeq -1.8\,. \tag{5.4.6}$$

For lower ℓ_{max} the contamination is bigger, up to $f_{\rm NL}^{\rm eq} \sim \mathcal{O}(5)$ as the overlap with the equilateral shape is greater. We interpret this as the fact that by including less configurations the peculiarity of the shape is weaker and the overlap with the terms above is therefore greater.

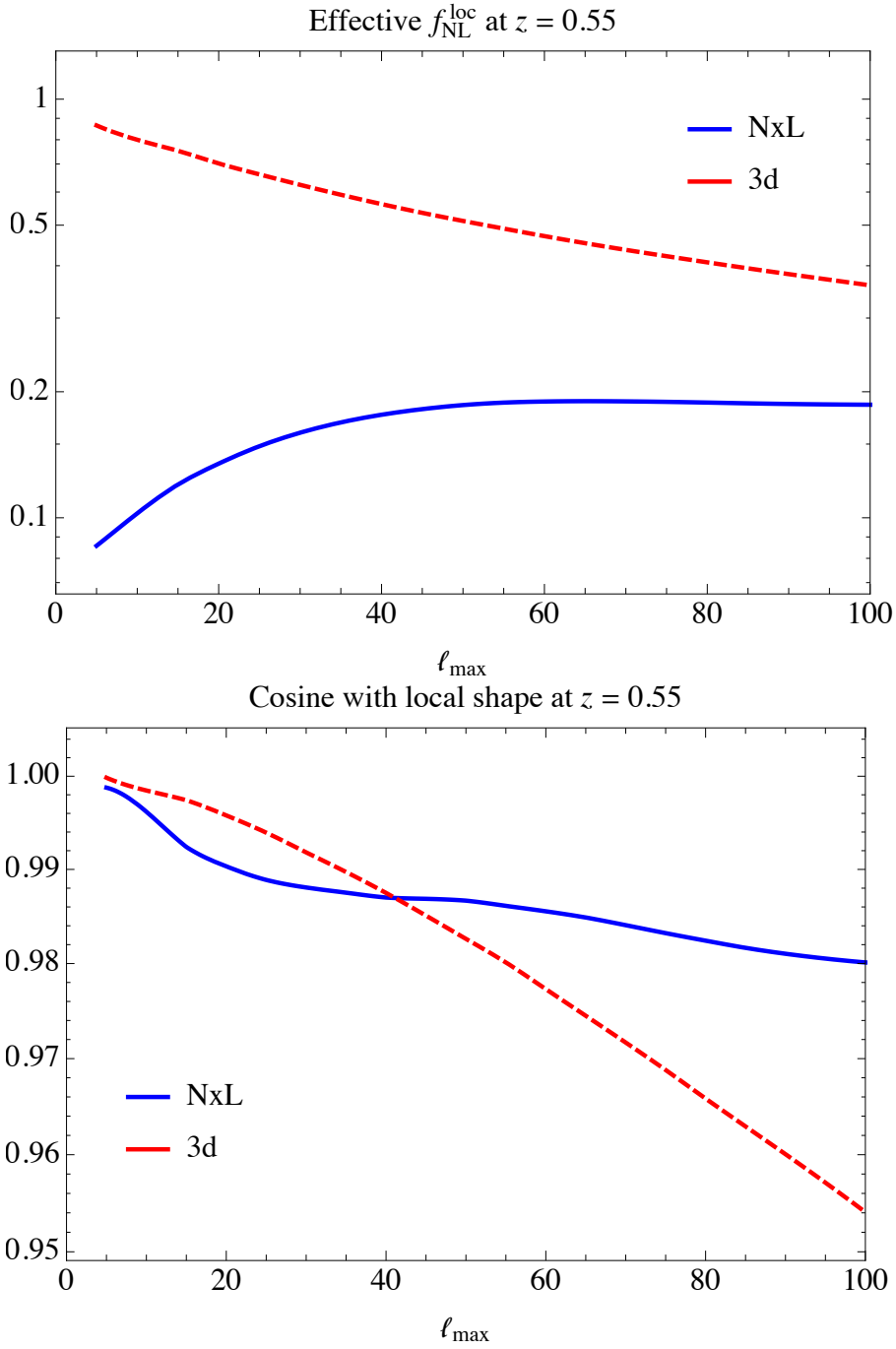

Figure 5.4: Effective local non-Gaussianity (top) and cosine with local shape (bottom) from "Newtonian × Lensing" and the "three derivatives" terms summing over all configurations up to ℓ_{max} at equal time $z = 0.55$. Dashed lines indicate negative values.

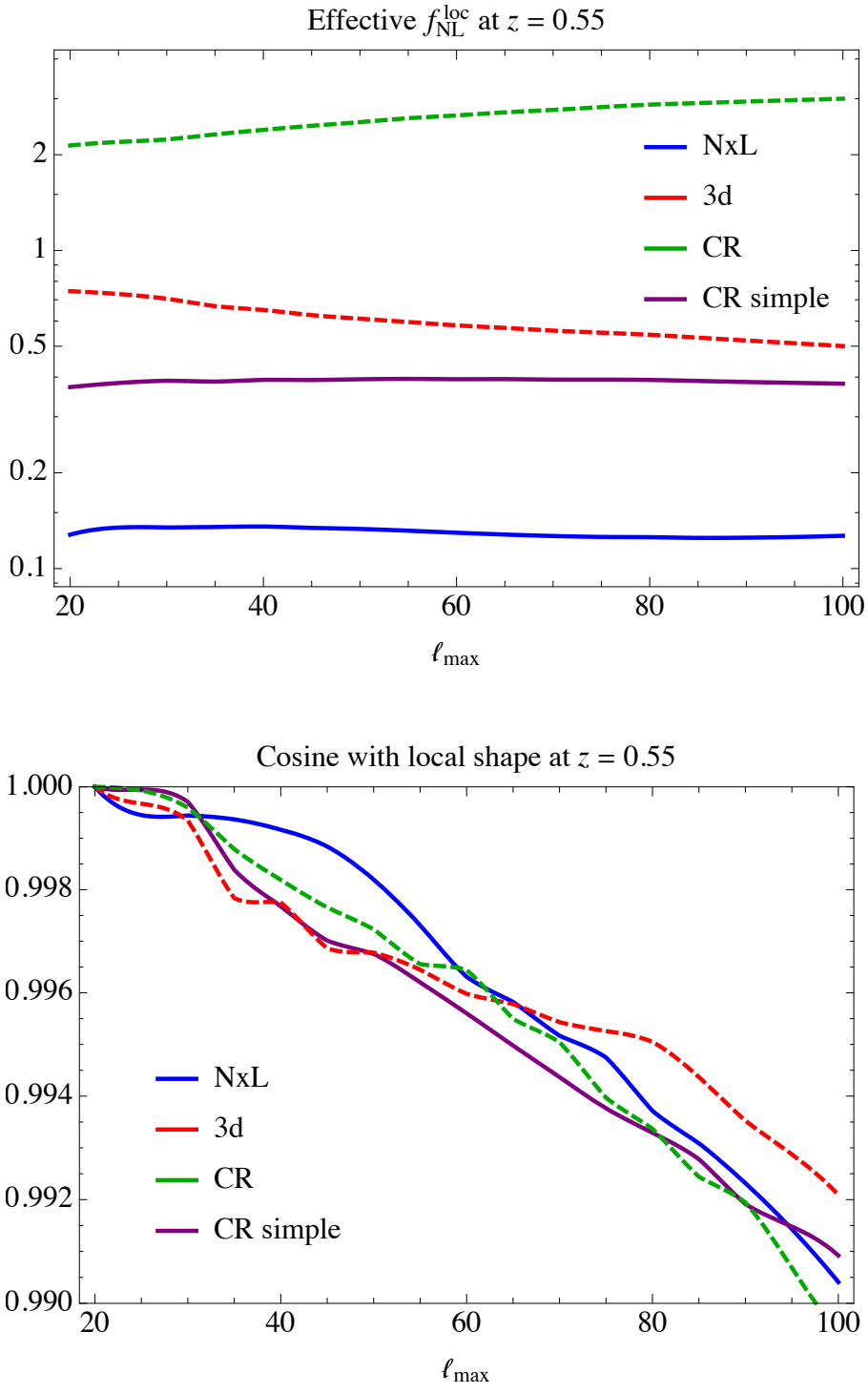

Figure 5.5: Effective local non-Gaussianity (top) and cosine with local shape (bottom) from various contributions summing over squeezed configurations only up to ℓ_{max} at equal time $z = 0.55$. Dashed lines indicate negative values.

Considering the cosine between these two contributions and the equilateral shape, it can be surprising that the cosine is larger for the "Newtonian × Lensing" terms which are the ones which produce the smallest contamination to $f_{\rm NL}^{\rm eq}$. We explain this by the fact that the amplitude of the "three derivatives" terms is probably greater than the one of the "Newtonian × Lensing" terms.

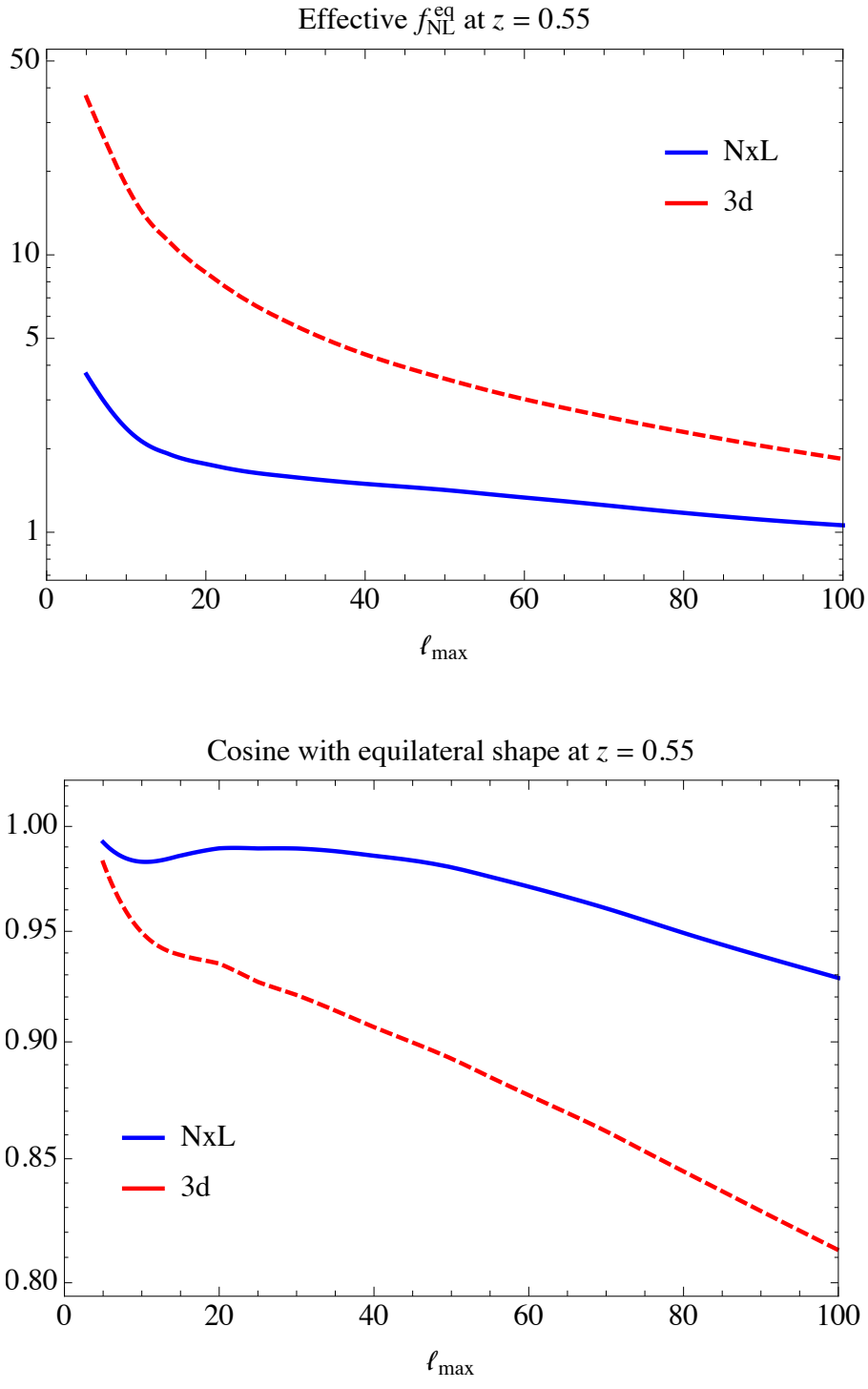

Figure 5.6: Effective equilateral NG $f_{\rm NL}^{\rm eq}$ (top) and cosine with equilateral shape (bottom) as a function of the maximum ℓ included in the configurations at equal time $z = 0.55$. Dashed lines indicate negative values.

5.5 Summary

We have computed the effective non-Gaussianity imprinted from some relativistic corrections to the bispectrum of galaxy number counts.

Because the transformation from Fourier space to $z\ell m$-space mixes scales, even terms which have a different k-dependence than a given non-Gaussian shape in Fourier space, can give rise to a large contamination in observables. This is particularly true for the pure Newtonian terms contributions $b \sim \langle(\delta\delta)\delta\delta\rangle$. In this work, we have assumed that these contaminations have been taken care of and we have estimated other relativistic contributions.

Among the terms studied, we have found that the terms derived from the consistency condition (4.4.11) give the largest contamination for local NG with $f_{\rm NL}^{\rm loc} \simeq -3$.

The terms from second-order perturbation theory that we have called "Newtonian $\times$ Lensing" produce a contamination $f_{\rm NL}^{\rm loc} \sim 0.2$ for the local shape, while it is $f_{\rm NL}^{\rm eq} \simeq 1$ for equilateral shape. The terms "three derivatives" produce a similar value of $f_{\rm NL}^{\rm loc} \sim -0.4$ and $f_{\rm NL}^{\rm eq} \sim -1.8$. These are relevant contaminations as they are only a small subset of all the second-order terms. If each term gives rise to a comparable contamination, one will easily reach $f_{\rm NL} \sim 1$ which is the goal to be attained with LSS data.

In an estimation of NG from real data, one would of course need to include *all* terms from second order galaxy number counts as there could be combinations leading to higher or lower level of contamination. We leave this for future work.

Chapter 6

Consistency relation for the CMB B-mode polarization in the squeezed limit

6.1 The CMB B-modes

The recent detection of B-mode polarization pattern in the Cosmic Microwave Background (CMB) on degree-angular scales by the BICEP2 collaboration [140], has generated a great deal of excitement in the field, although it has since been shown that this observation is coming from the polarized radiation emitted by interstellar dust [141, 142, 143].

Nevertheless, these results open the possibility that a detailed observational study of B-mode polarization is not too far from our technological reach. One may wonder whether measuring the three-point function in future experiments can help extract information contained in the B-mode signal. In particular, a large-scale temperature perturbation has a non-zero correlation with the power spectrum of B-modes of cosmological origin on short scales while the corresponding correlation is expected to be zero for B-modes sourced by galactic foregrounds.

In this chapter, we compute the squeezed limit of a three-point function in which one correlates the temperature fluctuations at large scales with two (E-mode or B-mode) polarization fluctuations at small scales using a method similar to the one used for deriving the consistency relations (in particular, we extend the approach of [70] to include polarization). To simplify the calculation, we do the computation in the flat-sky approximation and ignore late-time effects such as those induced by the late integrated Sachs-Wolfe (ISW) effect. The main contribution to the squeezed limit of such a correlation function comes from the lensing induced by the long-wavelength mode, and we estimate this signal to be observable for a futuristic experiment. This is similar to what happens for the CMB temperature bispectrum [144, 72]. An interesting feature of this result is that for the case of B-mode polarization we obtain a relation that connects the squeezed limit of the TBB three-point function with the primordial tensor power spectrum, which could in principle be used as a consistency relation for the tensor perturbations. Since the B-mode pattern sourced by inter-stellar dust is not expected to correlate with the temperature signal sourced at the CMB, this could help in distinguishing between

dust and a primordial signal. It turns out, however, that the observation of this relation is difficult even for a very futuristic experiment.

It is noteworthy that the full calculation of the temperature bispectrum in the absence of primordial non-Gaussianity can now be carried out numerically (see e.g. [145]). While this work was being prepared, an analytical and numerical study of the correlation function involving E-mode polarization appeared [146]. Considering that the main contribution to the intrinsic bispectrum, as pointed out in this reference, comes from the E-polarisation and from squeezed configurations, and given that one would expect EEE and TEE to give similar contributions to the signal to noise, our signal to noise estimate for TEE bispectrum in squeezed limit for various experiments should be roughly compatible with their results given the differences in our calculations. Table [6.1] confirms this expectation.

We begin in Section 6.2 by computing the effect of a long-wavelength metric perturbation on the polarization power spectrum; we do this by closely following the approach of [70]. This two-point function can then be correlated with a long-wavelength temperature fluctuation to compute the squeezed limit of the temperature-polarization-polarization (TBB or TEE) bispectrum, which we perform in Section 6.3. Finally, in Section 6.4 we analyze whether such a bispectrum can be observable in an experiment similar to COrE, PRISM or an ideal noiseless experiment that probes very small scales. We draw conclusions in Section 6.5.

6.2 The effect of the long scalar mode on the polarization power spectrum

In this section, we start by reviewing the effect of a long-wavelength background mode on the CMB temperature anisotropies as described in [70] (see also [71]) and then extend this treatment to the polarization field.

The long-wavelength mode acts as a background for the short modes. We take the long mode to be constant at the scale of the short modes at recombination such that its effect is equivalent to a coordinate transformation (*i.e.* it is what Weinberg [127] calls an adiabatic mode)

$$\begin{aligned} \tilde{\tau} &= \tau + \epsilon(\tau)\,, \\ \tilde{x}^i &= x^i(1-\lambda)\,, \end{aligned} \tag{6.2.1}$$

where ϵ is an arbitrary function of time and λ is an arbitrary constant. In the limit of instantaneous recombination and considering matter dominance, the observed CMB temperature anisotropies ignoring the ISW effect[1] are given to first order by

$$\Theta_{\rm obs}(\hat{n}) \equiv \left[\Theta + \Phi + \hat{n}\cdot\vec{v}\right](\tau_{\rm rec}, \vec{x}_{\rm rec})\,, \tag{6.2.2}$$

[1]The early ISW effect due to the evolution of Bardeen's potentials during the transition from radiation to matter domination has been taken into account since the standard calculation of the Sachs-Wolfe effect does not depend on this transition (see the discussion in Ref. [70]). So this approximation only ignores the late ISW effect due to the evolutions of the potentials in the presence of dark energy.

In this expression, Θ is the intrinsic temperature anisotropy defined as

$$T(\tau, x^i) = \bar{T}(\tau)(1 + \Theta(\tau, x^i))\,, \tag{6.2.3}$$

Φ is the gravitational potential and $\vec{v}$ is the velocity of the photon-baryon fluid. One can compute the effect of a long mode on the short scale temperature anisotropy by applying the coordinate transformation given in Eq. (6.2.1) to each term in Eq. (6.2.2). During matter-domination ($a \propto \tau^2$), we have $\epsilon = \tau\ \Phi_L/3$ and $\lambda = 5\Phi_L/3$. Doing the coordinate transformation explicitly therefore gives

$$\begin{aligned}\Theta_{\rm obs}(\hat{n}) = \Theta_{{\rm obs},S}(\hat{n}) + \Theta_{{\rm obs},L}(\hat{n}) \\ + \Theta_{{\rm obs},L}(\hat{n}) \left(\frac{\partial}{\partial\ \ln\ \tau_{\rm rec}} + 1 - 5\ \hat{n}\cdot\nabla_{\hat{n}} \right) \Theta_{{\rm obs},S}(\hat{n})\,.\end{aligned} \tag{6.2.4}$$

Note that this expression is valid when the long mode is taken to be larger than the sound horizon at recombination but the short modes can be taken to be at arbitrarily small scales, as it relies only on the fact that a constant gravitational potential has no physical effect and is therefore equivalent to a coordinate transformation. Also note that this expression is indeed compatible with the explicit second order calculation performed e.g. in references [147, 148]. The time derivative in equation (6.2.4) will be suppressed by $\tau_{\rm rec}/\tau_{\rm obs}$ and will thus be subdominant with respect to the rescaling.

The presence of the long-wavelength mode will also change the relation between the direction of the observation $\hat{n}$ and the physical position at recombination $\vec{x}_{\rm rec}$. In the absence of the long-wavelength mode they are related through the zeroth order geodesic equation, $\vec{x}_{\rm rec} = \hat{n}(\tau_{\rm obs} - \tau_{\rm rec})$. In writing Eq. (6.2.4) this relation is used to rewrite $\vec{x}_{\rm rec}\cdot\nabla_{\vec{x}_{\rm rec}} = \hat{n}\cdot\nabla_{\hat{n}}$. In the presence of the long-wavelength mode the relation between $\vec{x}$ and $\hat{n}$ is modified as

$$\begin{aligned}\vec{x} = \hat{n}\left[\left(1 - \frac{1}{3}\Phi_L(x_{\rm obs})\right)\tau_{\rm obs} - \left(1 - \frac{1}{3}\Phi_L(x_{\rm rec})\right)\tau_{\rm rec}\right] \\ + 2\hat{n}\int_{\tau_{\rm rec}}^{\tau_{\rm obs}} \Phi_L(\vec{x})d\tau - 2\int_{\tau_{\rm rec}}^{\tau_{\rm obs}} {\rm d}\tau(\tau - \tau_{\rm rec})\vec{\nabla}_\perp\Phi_L(\vec{x})\,.\end{aligned} \tag{6.2.5}$$

This relation is obtained by solving the photon geodesic equation at first order. As described in [70], only the last term of the above expression, which is the lensing term, will contribute to the bispectrum. The first term in the square brackets does not contribute since it only depends on the gravitational potential at observation. The second term in the square bracket changes the distance to the last scattering surface and is suppressed by a factor of $\tau_{\rm rec}/\tau_{\rm obs}$. The second term is also suppressed since the integral of Φ along the line of sight, the so called Shapiro effect, tends to average out along the line of sight for high enough multipoles.

Therefore the effect of the long-wavelength mode on the short modes reduces to the lensing induced by the long mode (the last term in Eq. (6.2.5)) and a stretching perpendicular to the line of sight

(the last term in Eq. (6.2.4)). From now on for simplicity, we drop the subscript *observed* in the temperature anisotropy. The short-wavelength mode, Θ_S, in the presence of long-wavelength mode, Θ_L, is modified as

$$\Theta(\hat{n}) = \Theta_S\left(\hat{n} + \vec{\alpha}(\hat{n})\right) + \Theta_L(\hat{n})\left(1 - 5\ \hat{n}\cdot\nabla_{\hat{n}}\right)\Theta_S(\hat{n}), \tag{6.2.6}$$

where $\vec{\alpha}$ is the deviation due to the lensing term and we dropped the subscript S for the short modes.

We can similarly find the effect of a long-wavelength temperature mode on the short-scale polarization mode. In the presence of the long mode, the short-wavelength polarization field Θ_P will be

$$\Theta_P(\hat{n}) = \Theta_{P,S}(\hat{n} + \vec{\alpha}(\hat{n})) - 5\Theta_L\hat{n}\cdot\nabla_{\hat{n}}\Theta_{P,S}(\hat{n}), \tag{6.2.7}$$

Notice that the constant term in Eq. (6.2.6), which corresponds to change in the average temperature of CMB, does not affect the polarization field. This is because it corresponds to the monopole of the temperature field and the polarization is only sensitive to the quadruple moment. Using the flat-sky approximation $\hat{n} \sim (1, \vec{m})$ we obtain the power spectrum of the two short polarization modes in the presence of a long-wavelength temperature mode

$$\begin{aligned}\langle\Theta_P(\vec{m}_1)\Theta_P(\vec{m}_2)\rangle_L =& \langle\Theta_P(\vec{m}_1)\Theta_P(\vec{m}_2)\rangle \\ &+ (\alpha^i(\vec{m}_1) - \alpha^i(\vec{m}_2))\nabla_i\langle\Theta_P(\vec{m}_1)\Theta_P(\vec{m}_2)\rangle \\ &- 5\Theta_L\vec{m}\cdot\nabla_{\vec{m}}\langle\Theta_P(\vec{m}_1)\Theta_P(\vec{m}_2)\rangle.\end{aligned} \tag{6.2.8}$$

where we have used the fact that the power spectrum depends only on the distance $\vec{m} = \vec{m}_1 - \vec{m}_2$, which is small due to the fact that we are in the flat-sky or distant observer approximation. From now on we shall ignore the first term which does not contribute to the bispectrum.

Next, by decomposing the polarization field into E and B modes we calculate how the presence of the long-wavelength temperature mode modifies the polarization power spectrum. This will then lead us to the calculation of the TBB and TEE bispectra in the next section. The polarization matrix for linearly polarized radiation is a real spin-2 object parametrized in terms of Stokes parameters Q and U

$$P = \begin{pmatrix} Q & U \\ U & -Q \end{pmatrix}. \tag{6.2.9}$$

Under a counterclockwise rotation through an angle ϕ, the stokes parameters transform as

$$\begin{aligned} Q' &= Q\cos 2\phi + U\sin 2\phi, \\ U' &= U\cos 2\phi - Q\sin 2\phi, \end{aligned} \tag{6.2.10}$$

or in a more compact form

$$(Q \pm iU)' = e^{\mp 2i\phi}(Q \pm iU), \tag{6.2.11}$$

which indicates that the polarization field $\Theta_P = Q \pm iU$ is a spin-2 quantity. Note that Q is parity even while U is parity odd. Putting together quantities of the same parity, we can construct spin-0 quantities E and B by applying the spin raising and lowering operators on Q and U. In the flat-sky approximation, where one neglects the curvature of the sphere and considers it as a plane normal to $\mathbf{e}_z$ the spin raising and lowering operators reduce to

$$L_\pm = L_x \pm iL_y = \partial_x \pm i\partial_y. \tag{6.2.12}$$

Therefore the spin-0 quantities $\tilde{E}$ and $\tilde{B}$ can be defined as [149]

$$\tilde{E} = -\frac{1}{2}\left(L_+^2(Q - iU) + L_-^2(Q + iU)\right), \tag{6.2.13}$$

$$\tilde{B} = \frac{1}{2i}\left(L_+^2(Q - iU) - L_-^2(Q + iU)\right), \tag{6.2.14}$$

and under a Fourier transform

$$a_{\tilde{E}}(\vec{\ell}) = \int \mathrm{d}\vec{m}\, \ell^2 (Q\cos 2\phi_\ell + U \sin 2\phi_\ell) e^{-i\vec{\ell}\cdot\vec{m}}, \tag{6.2.15}$$

$$a_{\tilde{B}}(\vec{\ell}) = \int \mathrm{d}\vec{m}\, \ell^2 (-Q\sin 2\phi_\ell + U \cos 2\phi_\ell) e^{-i\vec{\ell}\cdot\vec{m}}\,. \tag{6.2.16}$$

We shall write our final results in terms of a rescaled coefficients $a_{(E,B)} = a_{(\tilde{E},\tilde{B})}/\ell^2$.

Next we use Eqs. (6.2.12) and (6.2.14) to compute the effect of a rescaling on the B modes. First we consider the last term in Eq. (6.2.8), putting aside the lensing term for now. Note that

$$L_\pm^2 \vec{m}\cdot\nabla_{\vec{m}} = (2 + \vec{m}\cdot\nabla_{\vec{m}})L_\pm^2\,, \tag{6.2.17}$$

where we used the fact that $L_\pm^2$ is given simply by a combination of second derivatives. Therefore the contribution from the last term to the polarization is given by

$$\begin{aligned}\tilde{B}(\vec{m}) \mapsto &\tilde{B}(\vec{m}) - 5\Theta_L\big[-iL_+^2\vec{m}\cdot\nabla_{\vec{m}}(Q - iU) + iL_-^2\vec{m}\cdot\nabla_{\vec{m}}(Q + iU)\big] \\ = &\tilde{B}(\vec{m}) - 5\Theta_L(2 + \vec{m}\cdot\nabla_{\vec{m}})\tilde{B}(\vec{m})\end{aligned} \tag{6.2.18}$$

and analogously for the E modes

$$\tilde{E}(\vec{m}) \mapsto \tilde{E}(\vec{m}) - 5\Theta_L(2 + \vec{m}\cdot\nabla_{\vec{m}})\tilde{E}(\vec{m})\,. \tag{6.2.19}$$

Hence its contribution to the polarization power spectrum is given by

$$\begin{aligned}\langle a_{\tilde{X}}(\vec{\ell}_1)a_{\tilde{X}}(\vec{\ell}_2)\rangle_L \supset -\int \mathrm{d}\vec{m}_1\mathrm{d}\vec{m}_2\, e^{-i(\vec{\ell}_1\cdot\vec{m}_1+\vec{\ell}_2\cdot\vec{m}_2)} \\ \times 5\Theta_L(\vec{M})\left(4+\sum_i \vec{m}_i\cdot\nabla_{\vec{m}_i}\right)\langle\tilde{X}(\vec{m}_1)\tilde{X}(\vec{m}_2)\rangle,\end{aligned} \tag{6.2.20}$$

where $\vec{M} \equiv (\vec{m}_1 + \vec{m}_2)/2$ and X stands for either E or B.

Next, we consider the contribution from the lensing piece, which is given by

$$\begin{aligned}\Theta_P(\vec{m}+\vec{\alpha}(\vec{m})) &= (Q \pm iU)(\vec{m}+\vec{\alpha}(\vec{m})) \\ &\simeq (Q\pm iU)(\vec{m}) + \alpha^i(\vec{M})\nabla^i_m(Q\pm iU)(\vec{m}) \\ &\quad + (m^j - M^j)\nabla^j_M\alpha^i(\vec{M})\nabla^i_m(Q\pm iU)(\vec{m})\,,\end{aligned} \tag{6.2.21}$$

where in the last line we have assumed that α varies slowly since it is given by the long-wavelength mode and we have Taylor expanded it around $\vec{M}$. Since the polarization modes are combinations of $L^2_\pm$ acting on these objects, let us act on the above equations with the raising and lowering operators. Also let us focus only on the piece in the last line proportional to $\vec{m}$, since it is the only non-trivial one

$$\begin{aligned}L^2_\pm m^j\nabla^j_M\alpha^i(\vec{M})\nabla^i_m(Q\pm iU)(\vec{m}) &= m^j\nabla^j_M\alpha^i(\vec{M})\nabla^i_m L^2_\pm(Q\pm iU)(\vec{m}) \\ &\quad + (L^2_\pm\nabla^2_M + L^{(M)\,2}_\pm\nabla^2_m)\psi(M)(Q\pm iU)(\vec{m})\,,\end{aligned} \tag{6.2.22}$$

where we write the derivatives with respect to M in terms of raising and lowering operators written in terms of the capital coordinates $L^{(M)}_\pm = \pm(\partial_{M_1} \pm i\partial_{M_2})$ with $\vec{M} = (M_1, M_2)$. We also write the deflection angle $\vec{\alpha} = \vec{\nabla}\psi$ By putting together Eqs. (6.2.14, 6.2.21, 6.2.22) we obtain

$$\begin{aligned}\tilde{B}(\vec{m}) \mapsto \Big(1 + \nabla^i_M\psi(\vec{M})\nabla^i_m - M^j\nabla^j_M\nabla^i_M\psi(\vec{M})\nabla^i_m \\ + m^j\nabla^j_M\nabla^i_M\psi(\vec{M})\nabla^i_m + \nabla^2_M\psi(\vec{M})\Big)\tilde{B}(\vec{m})\end{aligned}$$

$$
\begin{aligned}
&- \frac{i}{2} L_+^{(M)\,2} \psi(\vec{M}) \nabla_m^2 (Q - iU)(\vec{m}) \\
&+ \frac{i}{2} L_-^{(M)\,2} \psi(\vec{M}) \nabla_m^2 (Q + iU)(\vec{m}),
\end{aligned} \tag{6.2.23}
$$

where only the second and third line will contribute to the final answer. Using the definitions of Eqs. (6.2.13) and (6.2.14), it's easy to rewrite the third line as

$$
\frac{i}{2} L_+^{(M)\,2} \psi(\vec{M}) \frac{L_-^2}{\nabla_m^2} (\tilde{E} - i\tilde{B})(\vec{m}) - \frac{i}{2} L_-^{(M)\,2} \psi(\vec{M}) \frac{L_+^2}{\nabla_m^2} (\tilde{E} + i\tilde{B})(\vec{m})\,. \tag{6.2.24}
$$

Analogously for the E-modes,

$$
\begin{aligned}
\tilde{E}(\vec{m}) \mapsto &\Big(1 + \nabla_M^i \psi(\vec{M}) \nabla_m^i - M^j \nabla_M^j \nabla_M^i \psi(\vec{M}) \nabla_m^i \\
&+ m^j \nabla_M^j \nabla_M^i \psi(\vec{M}) \nabla_m^i + \nabla_M^2 \psi(\vec{M}) \Big) \tilde{E}(\vec{m}) \\
&+ \frac{1}{2} L_+^{(M)\,2} \psi(\vec{M}) \nabla_m^2 (\tilde{E} - i\tilde{B})(\vec{m}) \\
&+ \frac{1}{2} L_-^{(M)\,2} \psi(\vec{M}) \nabla_m^2 (\tilde{E} + i\tilde{B})(\vec{m}).
\end{aligned} \tag{6.2.25}
$$

Therefore the contribution of the lensing term to the polarization power spectrum in the presence of long-wavelength temperature mode is given by

$$
\begin{aligned}
\langle a_{\tilde{X}}(\vec{\ell}_1) a_{\tilde{X}}(\vec{\ell}_2) \rangle_L \supset &\int \mathrm{d}\vec{m}_1 \mathrm{d}\vec{m}_2\, e^{-i(\vec{\ell}_1 \cdot \vec{m}_1 + \vec{\ell}_2 \cdot \vec{m}_2)} \\
&\times \Big[2\nabla_M^2 + \nabla_M^i \nabla_M^j m^i \nabla_m^j + L_+^{(M)\,2} L_-^2 \nabla_m^{-2} + L_-^{(M)\,2} L_+^2 \nabla_m^{-2} \Big] \\
&\times \psi(\vec{M}) \langle \tilde{X}(\vec{m}_1) \tilde{X}(\vec{m}_2) \rangle.
\end{aligned} \tag{6.2.26}
$$

6.3 The bispectrum in the squeezed limit

Having calculated the polarization power spectrum in the presence of long-wavelength temperature mode given by Eqs. (6.2.20, 6.2.26), we can finally calculate the TBB and TEE bispectra in the squeezed limit by correlating this power spectrum with the long-wavelength temperature mode. Again let's first consider only the contribution from the rescaling part. Using the fact that the two-point

function depends only on $\vec{m} \equiv \vec{m}_1 - \vec{m}_2$ we obtain

$$\begin{aligned}\langle a_{\tilde{X}}(\vec{\ell}_1) a_{\tilde{X}}(\vec{\ell}_2) a(\vec{\ell}_3)\rangle \overset{\vec{\ell}_3\to 0}{\supset} & - \int \mathrm{d}\vec{m}\mathrm{d}\vec{M}\mathrm{d}\vec{M}_L\, e^{-i((\vec{\ell}_1+\vec{\ell}_2)\cdot\vec{M}+\vec{\ell}_3\cdot\vec{M}_L+(\vec{\ell}_1-\vec{\ell}_2)\cdot\vec{m}/2)} \\ & \times 5\langle\Theta(\vec{M}_L)\Theta_L(\vec{M})\rangle(4+\vec{m}\cdot\nabla_{\vec{m}})\langle\tilde{X}(\vec{m}_1)\tilde{X}(\vec{m}_2)\rangle \\ & = (2\pi)^2\delta(\vec{\ell}_1+\vec{\ell}_2+\vec{\ell}_3)5\big(-2+\vec{\ell}_1\cdot\nabla_{\ell_1}\big) \\ & \times C_{\ell_1}^{\tilde{X}\tilde{X}} C_{\ell_3}\,. \end{aligned} \tag{6.3.1}$$

Now we want to write the corresponding relation for a_X (without the tilda), remembering that $a_X = a_{\tilde{X}}/\ell^2$, that is

$$\begin{aligned}\langle a_X(\vec{\ell}_1) a_X(\vec{\ell}_2) a(\vec{\ell}_3)\rangle \overset{\vec{\ell}_3\to 0}{\supset} & (2\pi)^2\delta(\vec{\ell}_1+\vec{\ell}_2+\vec{\ell}_3)\frac{5}{\ell_1^4}\big(-2+\vec{\ell}_1\cdot\nabla_{\ell_1}\big)(\ell_1^4 C_{\ell_1}^{XX})C_{\ell_3} \\ & = (2\pi)^2\delta(\vec{\ell}_1+\vec{\ell}_2+\vec{\ell}_3) \\ & \times 5 C_{\ell_1}^{XX} C_{\ell_3}\frac{\mathrm{d}\ln\left(\ell_1^2 C_{\ell_1}^{XX}\right)}{\mathrm{d}\ln\ell_1}. \end{aligned} \tag{6.3.2}$$

Next we consider the contribution of lensing term to the bispectrum by correlating Eq.(6.2.26) with the long temperature mode. Let's consider each term in the square parenthesis separately: the first term in the square parenthesis of Eq. (6.2.26) is just trivially computed to be

$$\langle a_{\tilde{X}}(\vec{\ell}_1) a_{\tilde{X}}(\vec{\ell}_2) a(\vec{\ell}_3)\rangle \overset{\vec{\ell}_3\to 0}{\supset} -(2\pi)^2\delta(\vec{\ell}_1+\vec{\ell}_2+\vec{\ell}_3)2\ell_3^2 C_{\ell_1}^{\tilde{X}\tilde{X}} C_{\ell_3}^{T\psi}\,. \tag{6.3.3}$$

The second term, which has a similar structure to the lensing of the temperature power spectrum, is

$$\begin{aligned}\langle a_{\tilde{X}}(\vec{\ell}_1) a_{\tilde{X}}(\vec{\ell}_2) a(\vec{\ell}_3)\rangle \overset{\vec{\ell}_3\to 0}{\supset} & \int \mathrm{d}\vec{m}\mathrm{d}\vec{s}\mathrm{d}\vec{S}\, e^{-i((\vec{\ell}_1+\vec{\ell}_2+\vec{\ell}_3)\cdot\vec{S}-(\vec{\ell}_1+\vec{\ell}_2-\vec{\ell}_3)\cdot\vec{s}/2+(\vec{\ell}_1-\vec{\ell}_2)\cdot\vec{m}/2)} \\ & \times m^i\nabla_{\vec{s}}^i\nabla_{\vec{s}}^j\langle\Theta(\vec{M}_L)\psi(\vec{M})\rangle\nabla_{\vec{m}}^j\langle\tilde{X}(\vec{m}_1)\tilde{X}(\vec{m}_2)\rangle \\ & = -(2\pi)^2\delta(\vec{\ell}_1+\vec{\ell}_2+\vec{\ell}_3)\ell_3^2 C_{\ell_1}^{\tilde{X}\tilde{X}} C_{\ell_3}^{T\psi} \\ & \times\left[\cos(2\varphi)-\cos^2\varphi\frac{\mathrm{d}\ln\left(\ell_1^2 C_{\ell_1}^{\tilde{X}\tilde{X}}\right)}{\mathrm{d}\ln\ell_1}\right], \end{aligned} \tag{6.3.4}$$

where φ is the angle between the vectors $\vec{\ell}_1$ and $\vec{\ell}_3$. Finally, the third and fourth terms in the square parenthesis of Eq. (6.2.26) have a more complicated structure but their computation is straightforward

$$\begin{aligned}\langle a_{\tilde{X}}(\vec{\ell}_1)a_{\tilde{X}}(\vec{\ell}_2)a(\vec{\ell}_3)\rangle &\overset{\vec{\ell}_3\to 0}{\supset} -(2\pi)^2\delta(\vec{\ell}_1+\vec{\ell}_2+\vec{\ell}_3)C_{\ell_1}^{\tilde{X}\tilde{X}}C_{\ell_3}^{T\psi}\\ &\quad\times\frac{2}{\ell_1^2}\Big[\big((\ell_3^x)^2-(\ell_3^y)^2\big)\big((\ell_1^x)^2-(\ell_1^y)^2\big)+4\ell_1^x\ell_1^y\ell_3^x\ell_3^y\Big]\\ &= -(2\pi)^2\delta(\vec{\ell}_1+\vec{\ell}_2+\vec{\ell}_3)\\ &\quad\times 2\ell_3^2\cos(2\varphi)C_{\ell_1}^{\tilde{X}\tilde{X}}C_{\ell_3}^{T\psi}\,. \end{aligned}\tag{6.3.5}$$

Putting everything together we obtain the lensing contribution to the bispectrum

$$\begin{aligned}\langle a_{\tilde{X}}(\vec{\ell}_1)a_{\tilde{X}}(\vec{\ell}_2)a(\vec{\ell}_3)\rangle \supset &-(2\pi)^2\delta(\vec{\ell}_1+\vec{\ell}_2+\vec{\ell}_3)\ell_3^2C_{\ell_1}^{\tilde{X}\tilde{X}}C_{\ell_3}^{T\psi}\\ &\times\left[2+3\cos(2\varphi)-\cos^2\varphi\frac{\mathrm{d}\ln\left(\ell_1^2C_{\ell_1}^{\tilde{X}\tilde{X}}\right)}{\mathrm{d}\ln\ell_1}\right]\,.\end{aligned}\tag{6.3.6}$$

Finally, after changing from $\tilde{X}$ to X, we obtain

$$\begin{aligned}\langle a_X(\vec{\ell}_1)a_X(\vec{\ell}_2)a(\vec{\ell}_3)\rangle &\overset{\ell_3\to 0}{\supset} -(2\pi)^2\delta(\vec{\ell}_1+\vec{\ell}_2+\vec{\ell}_3)\ell_3^2C_{\ell_1}^{XX}C_{\ell_3}^{T\psi}\\ &\quad\times\left[\cos(2\varphi)-\cos^2\varphi\frac{\mathrm{d}\ln\left(\ell_1^2C_{\ell_1}^{XX}\right)}{\mathrm{d}\ln\ell_1}\right]\,.\end{aligned}\tag{6.3.7}$$

Adding the rescaling and lensing contributions to the bispectrum given in Eqs. (6.2.20, 6.2.26), we obtain the TBB and TEE bispectrum in the squeezed limit where the temperature mode has a much

longer wavelength than the two polarization modes.

$$\langle a_X(\vec{\ell}_1)a_X(\vec{\ell}_2)a(\vec{\ell}_3)\rangle \overset{\ell_3\to 0}{=} (2\pi)^2\delta(\vec{\ell}_1+\vec{\ell}_2+\vec{\ell}_3)C_{\ell_1}^{XX}\Bigg[\ell_3^2 C_{\ell_3}^{T\psi} \times\left(-\cos(2\varphi)+\cos^2\varphi\frac{\mathrm{d}\ln\left(\ell_1^2 C_{\ell_1}^{XX}\right)}{\mathrm{d}\ln\ell_1}\right) + 5C_{\ell_3}^{TT}\frac{\mathrm{d}\ln\left(\ell_1^2 C_{\ell_1}^{XX}\right)}{\mathrm{d}\ln\ell_1}\Bigg], \tag{6.3.8}$$

where X denotes either E or B. In [6.1] we plot this result where we have fixed the small mode $\ell_3 = 20$ and set $\ell_1 = \ell_2 = \ell$. In order to normalise the result, we divided by 100 $C_{\ell_3}^{TT}C_{\ell}^{XX}$.

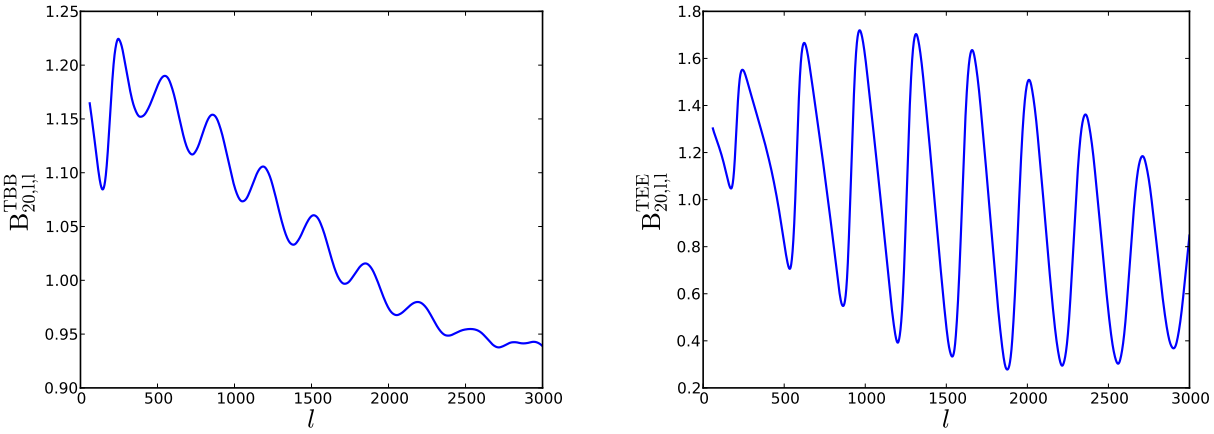

Figure 6.1: *TBB and TEE bispectra as computed in equation (6.3.8). We have fixed the small mode* $\ell_3 = 20$ *and set* $\ell_1 = \ell_2 = \ell$ *and normalised the two bispectra by a factor of* 100 $C_{\ell_3}^{TT}C_{\ell}^{XX}$. *The fiducial model used to calculate the bispectra is the same as that in section [6.4] in which* $r = 0.1$, $n_s = 0.962$ *and* n_T *is set by the consistency relation.*

Note that in Eq. (6.3.8), the logarithmic derivative will be sensitive to the tilt of the primordial power spectra. In particular, when computing the TBB bispectrum, it will receive a contribution proportional to the tilt of the tensor power spectrum n_T. However, as we shall see in the next section it is difficult, to say the least, to observe this contribution.

6.4 Signal-to-noise estimation

Similar to the temperature bispectrum [150], for the TBB and TEE bispectra given in Eq. (6.3.8), the signal-to-noise is given by

$$\left(\frac{S}{N}\right)^2 = \frac{f_{\rm sky}}{\pi}\frac{1}{(2\pi)^2}\iint \mathrm{d}^2\ell_1\ \mathrm{d}^2\ell_3\ \frac{\left(B^{\rm TXX}_{\ell_1\ell_2\ell_3}\right)^2}{\rm Var}, \tag{6.4.1}$$

where again X can be either E or B. Assuming $\ell_3 < \ell_2 < \ell_1$, the variance is given by

$$\mathrm{Var} = \langle \tilde{a}^*_T(\ell_3)\tilde{a}^*_X(\ell_1)\tilde{a}^*_X(\ell_2)\tilde{a}_T(\ell_3)\tilde{a}_X(\ell_1)\tilde{a}_X(\ell_2)\rangle \approx \tilde{C}^{TT}_{\ell_3}\tilde{C}^{XX}_{\ell_1}\tilde{C}^{XX}_{\ell_2}. \tag{6.4.2}$$

The spectra with a tilde are the theoretical power spectra plus the instrumental noise

$$\tilde{C}^{YY}_\ell = C^{YY}_\ell + N^{YY}_\ell, \tag{6.4.3}$$

where Y can be T, E or B mode. The noise power spectrum for a multi-frequency experiment like Planck is given by [151]

$$N^{YY}_\ell = \left(\sum_c \frac{1}{N^{YY}_{\ell,c}}\right)^{-1}. \tag{6.4.4}$$

The noise in each channel is given by

$$N^{YY}_{\ell,c} = \theta^2_{\rm fwhm}\sigma^2_Y\ \exp\left[\ell(\ell+1)\frac{\theta^2_{\rm fwhm}}{8\ln 2}\right], \tag{6.4.5}$$

where $\theta_{\rm fwhm}$ is the full width at half maximum of the Gaussian beam and σ_Y is the root mean square of the instrumental noise. Non-diagonal noise terms are supposed to vanish since the noise contribution from different maps are uncorrelated. In our signal-to-noise estimation we use the values of $\theta_{\rm fwhm}$ and σ_Y for three frequency channels of the Planck 14-month mission [152], seven frequency channels of the COrE 4-year mission [153], five frequency channels of the PRISM 4-year mission [154] as given in Tables [2-4] of the Appendix and an ideal noiseless experiment with $\ell_{\rm max} = 3000$. For all four cases we take the sky fraction to be $f_{\rm sky} = 0.65$. For the fiducial model, we consider a 6 parameter cosmology with $\{A_s = 2.215\times10^{-9},\ \Omega_m = 0.1199,\ \Omega_b = 0.02205,\ \tau = 0.0925,\ n_s = 0.962,\ r = 0.1\}$ and $n_T = -(r/8)(2-r/8-n_s)$ satisfying the single-field inflationary consistency relation. We evaluate the integrals in the squeezed limit, we choose the long-wavelength mode to be in the range $20 \le \ell_3 \le 300$ and the two short-wavelength modes to be equal and in the range $10\ \ell_3 \le \ell_1 \le \ell_{\rm max}$. The power spectra are computed by the numerical code CLASS [155].

The signal-to-noise of the TBB and TEE bispectra in the squeezed limit for these three experiments and a zero noise experiment are given in table [6.1]. We quote two cases: considering only the rescaling

Modes	long-mode lensing	Planck	COrE	PRISM	Ideal
TBB	no	6.7×10^{-5}	2.4×10^{-2}	5.0×10^{-2}	1.1
TBB	yes	9.8×10^{-4}	0.40	0.72	8.7
TEE	no	0.16	1.7	2.3	3.1
TEE	yes	1.8	14	18	23

Table 6.1: *Bispectrum signal-to-noise.*

part of Eq. (6.3.8), and using the full formula. We also present the signal to noise ratios for the full TBB and TEE bispectra as a function of the maximum ℓ in figure [6.2]. The signal is dominated by the lensing induced by the long mode. In principle this can be subtracted from observations; for the TEE correlation the resulting signal would still be observable in the admittedly far-fetched noiseless experiment, while for the TBB correlation the signal-to-noise would barely be greater than one even for such a futuristic experiment. In particular, the contribution to TBB coming from the tilt of the primordial tensor power spectrum is inaccessible to a direct measurement. The E-modes signal-to-noise is larger as it is also sourced by temperature anisotropies. Comparing with [146], we obtain compatible values taking into account that we have differences in our computations: on the one hand we only include triangles in the squeezed limit whereas they include all triangles which tends to lower our signal-to-noise although most of their signal comes form squeezed configurations.

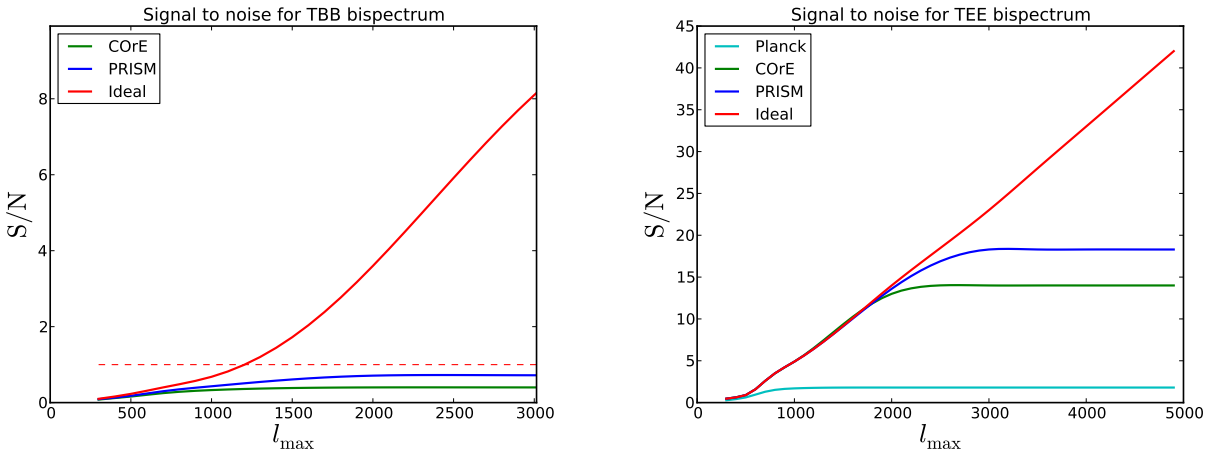

Figure 6.2: *Signal to noise ratios for the full TBB and TEE bispectra including both the lensing and rescaling contributions for various experiments. The calculation is done using the fiducial model described in the main text. In the case of the TBB bispectrum the signal to noise ratio for Planck is too small to be shown and the dashed line corresponds to a signal to noise ratio of one.*

6.5 Summary

We have computed the squeezed limit of the correlation function involving one temperature and two polarization fluctuations. This has been done by appealing to the fact that a constant gravitational potential (or metric fluctuation in the Poisson gauge) can have no physical effect on the local observables. It is worth noting that we do not expect interstellar dust to give any contribution to Eq. (6.3.8), since, being within our galaxy, it should not correlate with a long-wavelength fluctuation at the CMB.

Our results indicate that a direct observation of this squeezed limit for the B-mode polarization is possible only for very futuristic experiments, while its observation for E-mode polarization is more plausible. As pointed out in [146], this effect has to be correctly taken into account if one is to use the E-mode bispectrum in order to constrain primordial non-Gaussianity.

One could have hoped to use the B-mode bispectrum to learn something about the nature of the primordial universe. An example of this is the dependence of the bispectrum on the tilt of the primordial tensor power spectrum, which would then be expected to be compatible with the tilt measured in the B-mode two-point function. However, most of the signal comes from the lensing induced by the long-wavelength mode, an effect that contains little information about the shape of the primordial bispectrum. Even if one were to subtract this lensing effect, the contribution of the lensing to the variance would still hamper observations. An adventurous alternative would be to measure the variation of the B-mode power spectrum among different small patches in the sky and correlate this with the average temperature of each patch, similar to what was proposed for the large-scale structure in ref. [156]. One could then attempt to subtract the lensing in each patch using lensing potential maps in order to reduce the lensing variance. We leave a detailed analysis of such a technique as future work if it proves interesting.

Chapter 7

Conclusions and outlook

In this thesis, we have developed theoretical tools called *consistency conditions* enabling a better understanding of cosmological observables, in particular, of the large-scale structure. All the projects were ultimately geared towards enabling to improve constraints on primordial non-Gaussianity from the large-scale structure which is believed to the be the next big source of data for cosmology. Better constraints on NG are key to discriminate between different models of inflation and any detection would eliminate a large class of models.

We have further developed the consistency relations in the context of cosmological observables like the dark matter overdensity, the CMB polarization and the observed galaxy number counts. We have also shown how these can be used to constrain and check various models of both perturbative and non-perturbative approaches describing the LSS, among which the halo model and bias models.

Considering the effect of a long wavelength mode of the gravitational potential up to second derivatives on the short density modes, we derived a consistency relation involving the soft limit of the $(n+1)$-correlator functions of dark matter at equal times, extending the existing relations which considered the effect of a gravitational potential up to a gradient. This produces a non-vanishing relation for the squeezed bispectrum. This enabled a test of the halo model, a successful phenomenological model which describes the matter distribution on short scales. We have shown that this model satisfies the consistency condition to good accuracy up to scales of $\mathcal{O}(1)$ h/Mpc which is remarkable.

We have also explored the consequences of the fluid derivation of the consistency conditions. We have shown that the local Eulerian bias expansion satisfies the consistency conditions but that the symmetries of the fluid equations imply that the bias expansion should be non-local. As a first step towards predictions for quantities, we have derived a consistency condition including redshift space distortions. Finally, we have studied how the consistency conditions could be violated and provided an example in the form of a toy model of Modified Gravity.

Finally, we have computed the squeezed bispectrum of the observed quantity which future LSS survey will measure: the galaxy numbers counts. This is of great importance in the precision cosmology era which we are entering. Indeed, the size and precision of forthcoming surveys will enable cosmologists to measure correlations and estimate parameters of models down to the percent accuracy. At this level, it is important to go beyond the quantities which are convenient from a model perspective and make predictions for actual observables. In this derivation, we found that so-called projection

effects produce a non-zero correlation between the two-point function and a constant gradient of the gravitational potential. This simple approach, which is based on symmetries of the underlying physics, is able to estimate the contamination to local NG which would in theory only be accessible from a complicated second-order computation. The terms we have derived can indeed be misinterpreted as a local NG in a naive analysis. This demonstrates once again, how using the symmetries in physics can dramatically simplify the description of a system.

In a more in-depth analysis, we have computed different shapes of primordial NG in terms of galaxy number counts, a numerically challenging computation. This enabled to confirm that the terms obtained form the consistency condition have to be taken into account if one hopes to reach a precision of $f_{\rm NL}^{\rm loc} \sim 1$ from LSS data. Comparing with the effective NG generated by selected terms derived from the full second-order number counts, we have shown that this might even be the dominant contribution. Concerning equilateral NG, the second-order terms which we have considered, so-called "Newtonian $\times$ Lensing" and "three derivatives", are found to produce an $f_{\rm NL}^{\rm eq} \sim 1$ which again has to be taken into account.

Finally, a long mode of the temperature anisotropy affect the two point function of polarization. After the direct observation of gravitational waves which have been made by the LIGO interferometers, the hopes for the existence of a primordial gravitational wave background have never been higher. Any detection would be a big step in the confirmation of the existence inflation. However, as the failed discovery of the primordial B-modes by the BICEP2 experiment have shown, many other astrophysical sources and systematic effects need to be put under control before it is possible to confirm a primordial sign of GW. We have shown that the consistency relation which has been derived can be used to distinguish the galactic dust polarization from polarization generated by primordial gravitational waves. This is because it is not expected that dust emission correlates with a long temperature mode.

Ultimately, if one were to analyse real data, one will have to include all second-order terms (at least), as cancellation between different terms might occur. Moreover, this treatment has ignored issues such as bias or astrophysical effects. From our arguments based on the symmetries of the fluid equations, we expect the various terms in the non-local bias to be present. The way to include these in the general relativistic treatment is still to be determined.

We have also seen that the effective value of $f_{\rm NL}$ is affected by the magnification bias, among other factors. A realistic modelling of this effect will be essential in the future. The galaxy bias will also have to be included in the relativistic treatment. There is also a risk that the uncertainty on astrophysical phenomena will dominate over the relativistic effect, in particular due to the fact that a lot of them are poorly understood. The failed discovery of primordial B-modes is an example of this problematic. The usefulness of our results will probably depend on the understanding of astrophysical processes.

It would also be interesting to see how well one could measure or constrain the consistency conditions from real surveys. The prospect is promising since one can use arbitrarily small scales for the short modes given that the consistency relations are non-perturbative. However, if one hopes to fully exploit all the non-linear data which will be provided by future surveys, one will probably need to resort to numerical simulations. While some simulations including redshift space distortions and ray-tracing will probably be available in the coming years, there is still a long way to go until we have fully relativistic cosmological simulations over a large range of scales. It would be interesting to use

consistency conditions as a check on such simulations as they are valid also for non-linear scales.

Of course cosmological observables are not limited to the CMB and the galaxy distribution. Future knowledge about the Universe will also come from other sources such as the *cosmic infrared background*, *gravitational waves* and *21 cm emission*, and a lot remain to be understood. Even with better constraints on the characteristics of inflation, dark matter and dark energy, many models are still possible. The question is then: *Will the Universe make enough information available to enable its understanding?*

Appendices

Appendix A

Useful mathematical relations

A.1 Spherical harmonics

Useful identities are the Rayleigh expansion

$$e^{i\vec{k}\cdot\vec{r}} = 4\pi \sum_{\ell m} i^\ell j_\ell(kx) Y^*_{\ell m}(\hat{k}) Y_{\ell m}(\hat{x}) \tag{A.1.1}$$

and the orthogonality relations

$$\int dr r^2 k k' \frac{2}{\pi} j_\ell(kr) j_\ell(k'r) = \delta(k-k'), \tag{A.1.2}$$

$$\int d\hat{x} Y_{\ell m}(\hat{x}) Y^*_{\ell' m'}(\hat{x}) = \delta_{\ell\ell'}\delta_{mm'}, \tag{A.1.3}$$

as well as the parity

$$Y_{\ell m}(-\hat{k}) = (-1)^\ell Y_{\ell m}(\hat{k}), \tag{A.1.4}$$

$$j_\ell(-x) = (-1)^\ell j_\ell(x) \tag{A.1.5}$$

and the conjugation

$$Y^*_{\ell m}(x) = (-1)^m Y_{\ell -m}(x). \tag{A.1.6}$$

The Gaunt integral is

$$\int d\hat{n} Y^*_{\ell_1 m_1}(\hat{n}) Y^*_{\ell_2 m_2}(\hat{n}) Y^*_{\ell_3 m_3}(\hat{n}) = (-1)^{m_1+m_2+m_3} \mathcal{G}^{-m_1-m_2-m_3}_{\ell_1\ell_2\ell_3} \tag{A.1.7}$$

$$= (-1)^{m_1+m_2+m_3}(-1)^{\ell_1+\ell_2+\ell_3}\mathcal{G}^{m_1m_2m_3}_{\ell_1\ell_2\ell_3} \tag{A.1.8}$$

The Gaunt integral is

$$\mathcal{G}^{m_1m_2m_3}_{\ell_1\ell_2\ell_3} = \int d\hat{n} Y_{\ell_1 m_1}(\hat{n}) Y_{\ell_2 m_2}(\hat{n}) Y_{\ell_3 m_3}(\hat{n}) \tag{A.1.9}$$

$$= \sqrt{\frac{(2\ell_1+1)(2\ell_2+1)(2\ell_3+1)}{4\pi}} \begin{pmatrix} \ell_1 & \ell_2 & \ell_3 \\ 0 & 0 & 0 \end{pmatrix} \begin{pmatrix} \ell_1 & \ell_2 & \ell_3 \\ m_1 & m_2 & m_3 \end{pmatrix}$$

and $b_{\ell_1\ell_2\ell_3}$ is called the *reduced bispectrum* and contains all information of the bispectrum for a statistically isotropic and homogeneous field.

Appendix B

Primordial NG shapes

We consider several primordial NG shapes following [157, 158] that we write in terms of the curvature perturbation ζ by first defining the "shape function" F as

$$\langle \zeta_{\vec{k}_1} \zeta_{\vec{k}_2} \zeta_{\vec{k}_3} \rangle = (2\pi)^3 \delta^{(3)}(\vec{k}_1 + \vec{k}_2 + \vec{k}_3) F(k_1, k_2, k_3). \tag{B.0.1}$$

We parametrize the curvature power spectrum as $P_\zeta(k) = \frac{A}{k^3} \left(\frac{k}{k_p}\right)^{n_s - 1}$ and define A_* to be its amplitude as some fiducial momentum k_*. The equilateral shape is defined to be

$$\begin{aligned} F_{equil.}(k_1, k_2, k_3) = \frac{18}{5} f_{NL}^{equil.} A_*^2 \Bigg(& -\frac{1}{k_1^{4-n_s} k_2^{4-n_s}} - \frac{1}{k_1^{4-n_s} k_3^{4-n_s}} - \frac{1}{k_2^{4-n_s} k_3^{4-n_s}} \\ & - \frac{2}{k_1^{2(4-n_s)/3} k_2^{2(4-n_s)/3} k_3^{2(4-n_s)/3}} \\ & + \left(\frac{1}{k_1^{(4-n_s)/3} k_2^{2(4-n_s)/3} k_3^{4-n_s}} + 5\, perm. \right) \Bigg). \end{aligned} \tag{B.0.2}$$

The orthogonal shape is

$$\begin{aligned} F_{orthog.}(k_1, k_2, k_3) = \frac{18}{5} f_{NL}^{orth.} A_*^2 \Bigg(& -\frac{3}{k_1^{4-n_s} k_2^{4-n_s}} - \frac{3}{k_1^{4-n_s} k_3^{4-n_s}} - \frac{3}{k_2^{4-n_s} k_3^{4-n_s}} \\ & - \frac{8}{k_1^{2(4-n_s)/3} k_2^{2(4-n_s)/3} k_3^{2(4-n_s)/3}} \\ & + \left(\frac{3}{k_1^{(4-n_s)/3} k_2^{2(4-n_s)/3} k_3^{4-n_s}} + 5\, perm. \right) \Bigg). \end{aligned} \tag{B.0.3}$$

The local shape is

$$F_{loc.}(k_1,k_2,k_3) = \frac{6}{5} f_{NL}^{loc.} \left(P_\zeta(k_1)P_\zeta(k_2) + P_\zeta(k_2)P_\zeta(k_3) + P_\zeta(k_3)P_\zeta(k_1)\right)$$
$$= \frac{6}{5} f_{NL}^{loc.} A_*^2 \left(\frac{1}{k_2^{4-n_s}k_3^{4-n_s}} + \frac{1}{k_3^{4-n_s}k_1^{4-n_s}} + \frac{1}{k_1^{4-n_s}k_2^{4-n_s}}\right). \tag{B.0.4}$$

The orthogonal and equilateral are normalized such that they have the same amplitude as the local shape for equilateral triangles for a scale invariant power spectrum.

The matter bispectrum at time z is given by

$$B_L(k_1,k_2,k_3) = T_\delta(k_1,z)T_\delta(k_2,z)T_\delta(k_3,z)F(k_1,k_2,k_3), \tag{B.0.5}$$

where T_δ is the transfer function between the curvature perturbation ζ and the matter perturbation $\delta(k,z)$.

Appendix C

B-modes

C.1 Applying the coordinate transformations directly to BB power spectrum

In this appendix we derive the rescaling contribution to the B-mode power spectrum given in Eq. (6.2.20), by applying the rescaling directly to the B-mode power spectrum in Fourier space. We shall confirm that that it is given by

$$C_\ell \longmapsto C_\ell \left(1 + 5\, a(\ell_3) \frac{\mathrm{d}\ln \ell^2 C_\ell}{\mathrm{d}\ln \ell}\right) , \tag{C.1.1}$$

where $a(l_3)$ is the multipole moment of the long mode temperature perturbation, which is related to the gravitational potential by $\Theta = (T - \bar{T})/\bar{T} = \Phi/3$. During matter-domination, the effect of the long-wavelength mode corresponds to a rescaling of the wave vector $\vec{k}$ and the time coordinate τ given by

$$\vec{k} \longmapsto \vec{k}\, e^{5\Phi_L/3}, \qquad \tau \longmapsto \tau\, e^{\Phi_L/3}. \tag{C.1.2}$$

The BB power spectrum is given by [159]

$$C_\ell^{BB} = \frac{4\pi}{25}\Delta\tau_{\rm rec}^2 \int_0^\infty \mathrm{d}\ln k\; P_T(k)\mathfrak{h}'^2(k,\tau_{\rm rec}) \times \left[\frac{\ell+2}{2\ell+1} j_{\ell-1}(k\tau_{\rm obs}) - \frac{\ell-1}{2\ell+1} j_{\ell+1}(k\tau_{\rm obs})\right]^2 \tag{C.1.3}$$

with primordial tensor power spectrum given by

$$P_T(k) = A_T \left(\frac{k}{k_*}\right)^{n_T} , \tag{C.1.4}$$

and transfer function is

$$\mathfrak{h}'(k,\tau_{\rm rec}) = -3\frac{j_2(k\tau_{\rm rec})}{\tau_{\rm rec}}. \tag{C.1.5}$$

The term in the square brackets can be rewritten in terms of the Bessel function and its derivative. At $\ell \gg 1$ the asymptotic behaviour of spherical Bessel function is given by a cosine function. Therefore since the phase of the Bessel function and its derivative differs by $\pi/2$ the cross term that is proportional to $j_\ell \cdot j'_\ell$ can be neglected. Averaging the oscillating function of j_ℓ and j'_ℓ one obtains

$$C_\ell^{BB} \simeq \frac{36\pi}{25}\Delta\tau_{\rm rec}^2 \int_{(\ell+1/2)/\tau_{\rm obs}}^{\infty} d\ln k\ P_T(k) \times \frac{j_2^2(k\tau_{\rm rec})}{\tau_{\rm rec}^2}\left[\frac{\sqrt{(k\tau_{\rm obs})^2-(\ell+1/2)^2}}{2(k\tau_{\rm obs})^3}\right]. \tag{C.1.6}$$

There are some subtleties in applying the above rescaling to the B-mode power spectrum as the rescaling should be applied on the power spectrum at recombination (primordial power spectrum times the transfer function) but not on the geometrical projection effect, in this case given the square brackets in Eq. (C.1.3). One can also ignore any rescaling of the time at the observer because it is not observable. Finally, and most importantly, the addition of a long mode to the gravitational potential locally changes the average temperature as

$$\bar{T} \to \bar{T} e^{2\Phi_L/3}. \tag{C.1.7}$$

Recombination happens however at a fixed physical temperature. In the patch at recombination where the long mode is present, recombination is therefore delayed to time

$$\tau_{\rm rec} \to \tau_{\rm rec}\, e^{\Phi_L/3}, \tag{C.1.8}$$

which exactly compensates the effect of the time transformation. This amounts to the fact that we effectively only need to rescale $\vec{k}$ to account for a long-wavelength mode.

We restrict ourselves to the case $n_T = 0$ for now and derive the results in two limits:

- $10 \lesssim \ell \lesssim 50$: for $\ell < \tau_{\rm obs}/\tau_{\rm rec}$ one can extend the lower integral bound to zero and obtain

$$C_\ell^{BB} \simeq \frac{18\pi}{25}\left(\frac{\Delta\tau_{\rm rec}}{\tau_{\rm obs}}\right)^2 A_T \int_0^\infty \frac{dy}{y^3}\, j_2^2(y), \tag{C.1.9}$$

  where we have made the change of variable $y = k\tau_{\rm rec}$. The integral above equals $1/72$. From

Eq. (C.1.1) we deduce that the effect on C_ℓ^{BB} is

$$C_\ell^{BB} \to C_\ell^{BB}(1 + (5 \times 2)a(\ell_3)). \tag{C.1.10}$$

On the other hand, by rescaling the power spectrum we obtain

$$\begin{aligned} C_\ell^{BB} &\simeq \frac{18\pi}{25}\Delta\tau_{\rm rec}^2 \int_{(\ell+1/2)/\tau_{\rm obs}}^{\infty} d\ln k\ A_T \frac{j_2^2(e^{5\Phi_L/3}k\tau_{\rm rec})}{\tau_{\rm rec}^2}\left[\frac{1}{(k\tau_{\rm obs})^2}\right] \\ &= \frac{18\pi}{25}\left(\frac{\Delta\tau_{\rm rec}}{\tau_{\rm obs}}\right)^2 A_T \int_0^{\infty}\frac{dy}{y^3}\, j_2^2(y) e^{10\Phi_L/3} \end{aligned} \tag{C.1.11}$$

where we defined $y = k\, e^{5\Phi_L/3}/\tau_{\rm rec}$. This produces the same effect at first order as expected.

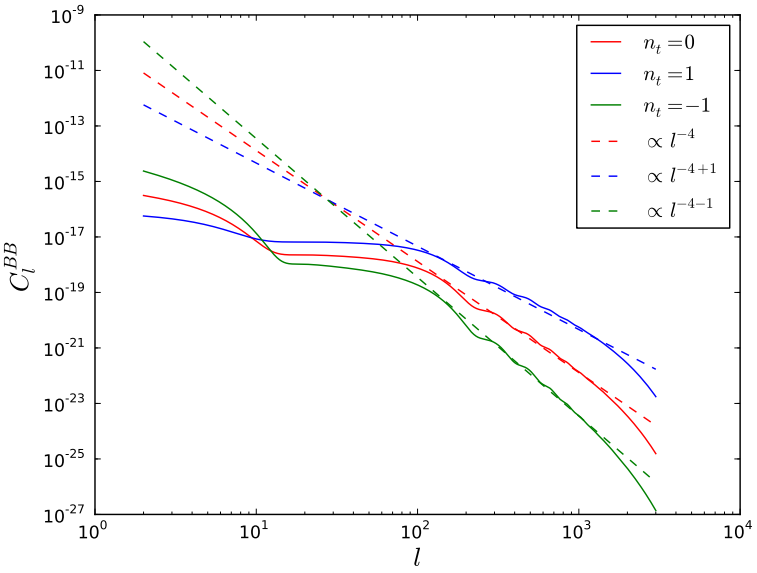

Figure C.1: *Comparison of the slope of the power spectrum with the analytical approximation for the derivative as function of n_T.*

- $50 \lesssim \ell \lesssim 10^3$: in this regime, one cannot extend the lower integral bound to zero. The main contribution to the integral comes from modes $k \sim \ell/\tau_{\rm obs}$ so $k\tau_{\rm rec} \gg 1$ and we can use the large argument limit of the transfer function

$$\frac{j_2^2(k\tau_{\rm rec})}{\tau_{\rm rec}^2} \simeq \frac{\sin^2((k\tau_{\rm rec})^2)}{\tau_{\rm rec}^2(k\tau_{\rm rec})^2} \tag{C.1.12}$$

leading to

$$C_\ell^{BB} \simeq \frac{36\pi}{25}\left(\frac{\Delta\tau_{\rm rec}}{\tau_{\rm rec}}\right)^2 A_T \int_{(\ell+1/2)/\tau_{\rm obs}}^{\infty} d\ln k \times \frac{\sin^2((k\tau_{\rm rec})^2)}{(k\tau_{\rm rec})^2}\left[\frac{\sqrt{(k\tau_{\rm obs})^2-(\ell+1/2)^2}}{2(k\tau_{\rm obs})^3}\right]. \quad \text{(C.1.13)}$$

The sine can be averaged and upon defining $u = k\tau_{\rm obs}/(\ell+1/2)$ one obtains

$$C_\ell^{BB} \simeq \frac{9\pi}{25} A_T \left(\frac{\Delta\tau_{\rm rec}}{\tau_{\rm rec}}\right)^2 \left(\frac{\tau_{\rm obs}}{\tau_{\rm rec}}\right)^2 \frac{1}{(\ell+1/2)^4}\int_1^\infty \frac{du}{u^6}\sqrt{u^2-1}. \quad \text{(C.1.14)}$$

The integral equals 2/15. From Eq. (C.1.1), we deduce that the effect on C_ℓ^{BB} is

$$C_\ell^{BB} \to C_\ell^{BB}(1+(5\times(-2))a(\ell_3)), \quad \text{(C.1.15)}$$

while the rescaling acts only on the transfer function $j_2 \propto k^{-2}$ which produces

$$C_\ell^{BB} \to C_\ell^{BB} e^{-10\Phi_L/3} \simeq C_\ell^{BB}(1-10a(\ell_3)). \quad \text{(C.1.16)}$$

Finally, one can compute the effect for $n_T \neq 0$ from the rescaling easily. Following the same procedure we obtain

$$C_\ell^{BB} \to C_\ell^{BB}(1+10a(\ell_3)) \qquad 10 \lesssim \ell \lesssim 50, \quad \text{(C.1.17)}$$

$$C_\ell^{BB} \to C_\ell^{BB}(1+5(n_T-2)a(\ell_3)) \qquad 50 \lesssim \ell \lesssim 10^3, \quad \text{(C.1.18)}$$

which also coincides with the result computed using Eq. (C.1.1). The above expressions can be confirmed by numerical evaluations of the logarithmic derivative $d\ln(\ell^2 C_\ell)/d\ln\ell$. Figure [C.1] shows a qualitative agreement between the numerical and analytical behavior in the two regimes, namely $d\ln(\ell^2 C_\ell)/d\ln\ell = 2$ and $d\ln(\ell^2 C_\ell)/d\ln\ell = (n_T-2)$ for low and high ℓ respectively.

C.2 Planck, COrE and PRISM instrumental characteristics

Frequency (Hz)	$\theta_{\rm fwhm}$ (arcmin)	σ_T ($\mu K/K$)	σ_P ($\mu K/K$)
100	10	2.5	4.0
143	7.1	2.2	4.2
217	5.0	4.8	9.8

Table C.1: *Planck (14-month mission)*

Frequency (Hz)	$\theta_{\rm fwhm}$ (arcmin)	σ_T (μK)	σ_P (μK)
105	10	0.268	0.463
135	7.8	0.338	0.583
165	6.4	0.417	0.72
195	5.4	0.487	0.841
225	4.7	0.562	0.972
255	4.1	1.48	2.56
285	3.7	2.73	4.7

Table C.2: *COrE (4-year mission)*

Frequency (Hz)	$\theta_{\rm fwhm}$ (arcmin)	σ_T (μK)	σ_P (μK)
105	4.8	0.601	0.849
135	3.8	0.682	0.963
160	3.2	0.760	1.074
185	2.8	0.899	1.27
200	2.5	1.03	1.47

Table C.3: *PRISM (4-year mission)*

Appendix D

Observed consistency relation

D.1 Implementation in CLASSgal

In this appendix, we present a detailed computation of the different spectra appearing in the consistency relation for observed galaxy number counts of chapter 4 that we have implemented by modifying the CLASSgal code. In the code, one can output the transfer function "_tk.dat" at any desired time. They are normalized w.r.t $\zeta(k)$ such that e.g., for the quantity $Q(k,z)$ the transfer function is

$$T_Q(k,z) \equiv \frac{Q(\vec{k},z)}{\zeta(\tau_{in},\vec{k})}. \tag{D.1.1}$$

The power spectrum output "_pk.dat" from CLASSgal is dimensionfull power spectrum $P_\delta(k)$

D.1.1 Spectra with CLASSgal

We first compute the *transfer function* (in the CLASSgal sense) for a contribution $\Delta(z,\hat{n}) \supset \Psi(\tau(z),\hat{n}r(\tau(z)))$. Here $\hat{n}$ it the direction of galaxy and we decompose $\hat{n}$ in spherical harmonics. Note that this is the opposite convention from the CLASSgal code [22] and Bonvin & Durrer's paper [20] where $\hat{n}$ is the direction of the photon. This has consequences only for the Doppler terms. In addition, in our convention for the metric, Ψ and Φ are swapped with respect to [20, 21] but in this appendix, we adopt the CLASS convention for the potentials. The harmonic coefficients are given by

$$a^{\Psi}_{\ell m}(z) = \int d\Omega_{\hat{n}} Y^*_{\ell m}(\hat{n})\Psi(z,\hat{n}r(z)), \tag{D.1.2}$$

where $\hat{n}r(z)$ is the position of the source which has redshift z and $r(z) = \tau_o - \tau(z)$ is the comoving distance to it with τ_o the conformal time at the observer. We then write Ψ in terms of its Fourier transform

$$\Psi(\tau,\vec{x}) = \int \frac{d^3k}{(2\pi)^3}\Psi(\tau,\vec{k})e^{-i\vec{k}\cdot\vec{x}}. \tag{D.1.3}$$

and obtain

$$a^{\Psi}_{\ell m}(z) = \int d\Omega_{\hat{n}} (-1)^{\ell} Y^*_{\ell m}(\hat{n}) \int \frac{d^3k}{(2\pi)^3} \Psi(\tau, \vec{k}) e^{i\vec{k}\cdot\hat{n}r(z)}, \tag{D.1.4}$$

where we flipped the integration over $\hat{n}$. We expand the exponential in spherical Bessel and Legendre polynomials, then expand the Legendre polynomials in spherical harmonics

$$\begin{aligned} a^{\Psi}_{\ell m}(z) &= \int d\Omega_{\hat{n}} (-1)^{\ell} Y^*_{\ell m}(\hat{n}) \int \frac{d^3k}{(2\pi)^3} \Psi(\tau(z), \vec{k}) \sum_{\ell'=0}^{\infty} (2\ell'+1) i^{\ell'} j_{\ell'}(kr(z)) P_{\ell'}(\hat{k}\cdot\hat{n}) \\ &= \int d\Omega_{\hat{n}} (-1)^{\ell} Y^*_{\ell m}(\hat{n}) \int \frac{d^3k}{(2\pi)^3} \Psi(\tau(z), \vec{k}) \\ &\quad \times \sum_{\ell'=0}^{\infty} \sum_{m'=-\ell'}^{\ell'} 4\pi i^{\ell'} j_{\ell'}(kr(z)) Y^*_{\ell' m'}(\hat{k}) Y_{\ell' m'}(\hat{n}) \\ &= \frac{(-i)^{\ell}}{2\pi^2} \int d^3k \Psi(\tau(z), \vec{k}) j_{\ell}(kr(z)) Y^*_{\ell m}(\hat{k}). \end{aligned} \tag{D.1.5}$$

All terms computed this way will have the $(-i)^{\ell}$ factors and the spherical harmonic. Correlating with itself (or analogously with other terms) gives

$$\begin{aligned} \left\langle a^{\Psi}_{\ell m}(z_1) a^{\Psi *}_{\ell' m'}(z_2) \right\rangle &= \frac{(-i)^{\ell} i^{\ell'}}{(2\pi^2)^2} \int d^3k \int d^3k' \left\langle \Psi(\tau(z_1), \vec{k}) \Psi(\tau(z_2), \vec{k}) \right\rangle \\ &\quad \times j_{\ell}(kr(z_1)) j_{\ell'}(k'r(z_2)) Y^*_{\ell m}(\hat{k}) Y_{\ell' m'}(\hat{k}') \\ &= \frac{(-i)^{\ell} i^{\ell'}}{(2\pi^2)^2} \int d^3k \int d^3k' S_{\Psi}(\tau(z_1), k) S_{\Psi}(\tau(z_2), k') \left\langle \zeta(\vec{k}) \zeta(\vec{k'}) \right\rangle \\ &\quad \times j_{\ell}(kr(z_1)) j_{\ell'}(k'r(z_2)) Y^*_{\ell m}(\hat{k}) Y_{\ell' m'}(\hat{k}'), \end{aligned} \tag{D.1.6}$$

where S_{Ψ} is the normalized transfer function for the field Ψ. This is referred as a *source function* in CLASSgal and is computed in the *source* module. It is related to the primordial curvature perturbation by

$$\left\langle \Psi(\tau(z_1), \vec{k}) \Psi(\tau(z_2), \vec{k}) \right\rangle = S_{\Psi}(\tau(z_1), k) S_{\Psi}(\tau(z_2), k') \left\langle \zeta(\vec{k}) \zeta(\vec{k'}) \right\rangle. \tag{D.1.7}$$

and

$$\left\langle \zeta(\vec{k}) \zeta(\vec{k'}) \right\rangle = (2\pi)^3 \delta^{(3)}(\vec{k} - \vec{k}') P_{\zeta}(k) = (2\pi)^3 \delta^{(3)}(\vec{k} - \vec{k}') \frac{A}{k^3} \left(\frac{k}{k_p} \right)^{n_s - 1}. \tag{D.1.8}$$

We obtain

$$\left\langle a^{\Psi}_{\ell m}(z_1) a^{\Psi}_{\ell' m'}(z_2)\right\rangle = \frac{4\pi}{2\pi^2}\int d^3k S_\Psi(\tau(z_1),k) S_\Psi(\tau(z_2),k') P_\zeta(k)$$

$$\times\, j_\ell(kr(z_1)) j_\ell(kr(z_2)) Y^*_{\ell m}(\hat{k}) Y_{\ell' m'}(\hat{k})$$

$$= C_\ell(z_1,z_2)\delta_{\ell,\ell'}\delta_{m,m'}, \tag{D.1.9}$$

with

$$C_\ell(z_1,z_2) = \frac{4\pi}{2\pi^2}\int dk\, k^2 S_\Psi(\tau(z_1),k) S_\Psi(\tau(z_2),k')$$

$$\times\, P_\zeta(k) j_\ell(kr(z_1)) j_\ell(kr(z_2)). \tag{D.1.10}$$

We finally obtain

$$C_\ell(z_1,z_2) = 4\pi\int \frac{dk}{k}\,\Delta^\Psi_\ell(\tau(z_1),k)\Delta^\Psi_\ell(\tau(z_2),k)\mathcal{P}_\zeta(k). \tag{D.1.11}$$

where $\Delta^\Psi_\ell(\tau(z_1),k) = j_\ell(\tau(z_1),k)S_\Psi(\tau(z_1),k)$ To be more realistic, we should add a window function W_i in redshift, defining the redshift bin i with mean redshift z_i. This window function serves two roles: for a spectroscopic survey, it can be taken to be a Dirac function as the precision is very high (or tophat for a fixed uncertainty), about $\sigma_z = 0.001(1+z)$. However, a photometric survey has a larger error of about $\sigma_z = 0.05(1+z)$ which is Gaussian. Taking it into account is necessary. Secondly, one can use the window function to reduce the shot noise by optimal binning of the survey. The condition on the choice of windows functions is that they cannot be sharper than the intrinsic error measurements [160]. With the window function the transfer functions are simply modified to

$$\Delta^{i,\Psi}_\ell(k) = \int_0^{\tau_0} W_i(\tau)\Delta^\Psi_\ell(\tau,k)d\tau. \tag{D.1.12}$$

where the window function in τ is related to the one in z by $W_i(\tau) \equiv -\frac{dz}{d\tau}W_z(z) = H(\tau)W_z(\tau)$ (note a typo in the CLASSgal paper). One obtains

$$\Delta^{i,\Psi}_\ell(k) = \int_0^{\infty} W_z(z)\Delta^\Psi_\ell(z,k)dz. \tag{D.1.13}$$

D.1.2 The spectrum $C_\ell^{\Delta_g \Delta z}$

In this section and rest of this appendix, all expressions are written in terms of the CLASSgal convention for the fields Φ and Ψ. We consider the term

$$\begin{aligned}\Delta z(\tau,\hat{n}) = (1+z(\tau,\hat{n})\,[&\mathcal{H}v(\tau,\hat{n}r(\tau)) - \mathcal{H}_{\mathcal{O}}v_{\mathcal{O}} + \Psi(\tau,\hat{n}r(\tau))\\ &- \Psi_{\mathcal{O}} - \hat{n}\cdot(\vec{v}(\tau,\hat{n}r(\tau)) - \vec{v}_{\mathcal{O}})\\ &- \int_{\tau_{\mathcal{O}}}^{\tau_{\mathcal{E}}} \mathrm{d}\tau'\,(\Phi'(\tau') + \Psi'(\tau))\Big]. \end{aligned} \tag{D.1.14}$$

Ignoring perturbations at the observer we obtain

$$\begin{aligned}\Delta z(\tau,\hat{n}) = (1+z(\tau,\hat{n})\,[&\Psi(\tau,\hat{n}r(\tau)) + aHv(\tau,\hat{n}r(\tau))\\ &- \hat{n}\cdot\vec{v}(\tau,\hat{n}r(\tau)) + \int_{\tau}^{\tau_o} \mathrm{d}\tau'\,(\Phi'(\tau') + \Psi'(\tau))\Big]. \end{aligned} \tag{D.1.15}$$

We define separate transfer functions corresponding to the terms above

$$\Delta_\ell^{\Delta z} = \Delta_\ell^{(1+z)\Psi} + \Delta_\ell^{Hv} + \Delta_\ell^{-(1+z)\vec{v}\cdot\hat{n}} + \Delta_\ell^{(1+z)\int \Phi'+\Psi'}. \tag{D.1.16}$$

Transfer function for $(1+z)\Psi$ The factor simply goes through

$$\Delta_\ell^{(1+z)\Psi}(\tau,k) = \frac{1}{a(\tau)} S_\Psi(\tau,k) j_\ell(kr(\tau)), \tag{D.1.17}$$

and

$$\Delta_\ell^{i,(1+z)\Psi}(k) = \int_0^{\tau_o} W_i(\tau)\frac{1}{a(\tau)} S_\Psi(\tau,k) j_\ell(kr(\tau))d\tau. \tag{D.1.18}$$

Transfer function for Hv We consider the the term

$$Hv(\tau, -\hat{n}(\tau_0 - \tau)), \tag{D.1.19}$$

where v is the velocity potential. The transfer function is then

$$\Delta_\ell^{Hv}(\tau,k) = -H\frac{S_\Theta(\tau,k)}{k^2} j_\ell(kr(\tau)). \tag{D.1.20}$$

Adding a window function W_i in τ leads to

$$\Delta_\ell^{i,Hv}(k) = -\int_0^{\tau_o} d\tau\, W_i(\tau)\frac{H(\tau)}{k^2}S_\Theta(\tau,k)j_\ell(kr(\tau)). \tag{D.1.21}$$

Transfer function for $-(1+z)(\hat{n}\cdot\vec{v})$ We consider the contribution

$$-(1+z(\tau))\hat{n}\cdot\vec{v}(\tau,\hat{n}(\tau_o-\tau)). \tag{D.1.22}$$

One has

$$a_{\ell m}^{\hat{n}\cdot\vec{v}}(z) = \int d\Omega_{\hat{n}}(-1)^\ell Y^*_{\ell m}(\hat{n})\int\frac{d^3k}{(2\pi)^3}(-k)v(\tau,\vec{k})\partial_{kr}\left(e^{i\vec{k}\cdot\hat{n}r(z)}\right) \tag{D.1.23}$$

$$= \frac{(-i)^\ell}{2\pi^2}\int d^3k(-k)v(\tau(z),\vec{k})j'_\ell(kr(z))Y^*_{\ell m}(k), \tag{D.1.24}$$

which gives the transfer function

$$\Delta_\ell^{-(1+z)\hat{n}\cdot\vec{v}}(\tau,k) = -\frac{S_\Theta(\tau,k)}{a(\tau)k}j'_\ell(k(\tau_o-\tau)), \tag{D.1.25}$$

and the smoothed one is

$$\Delta_\ell^{i,\,-(1+z)\hat{n}\cdot\vec{v}}(k) = -\int_0^{\tau_o} W_i(\tau)\frac{S_\Theta(\tau,k)}{a(\tau)k}j'_\ell(k(\tau_0-\tau))d\tau. \tag{D.1.26}$$

Transfer function for $(1+z)\int\Phi'+\Psi'$ We compute the transfer function for the term

$$\frac{1}{a(\tau)}\int_\tau^{\tau_o} d\tilde{\tau}\,(\Phi'+\Psi')(\tilde{\tau},\hat{n}(\tau_o-\tilde{\tau})). \tag{D.1.27}$$

The integral simply goes through and we obtain

$$\Delta_\ell^{(1+z)\int\Phi'+\Psi'}(\tau,k) = \frac{1}{a(\tau)}\int_\tau^{\tau_0} d\tilde{\tau}\,S_{(\Phi+\Psi)'}(\tilde{\tau},k)j_\ell(kr(\tilde{\tau})). \tag{D.1.28}$$

Adding a window function W_i in τ gives

$$\Delta_\ell^{i,(1+z)\int\Phi+\Psi'}(k) = \int_0^{\tau_o} d\tau\,\frac{W_i(\tau)}{a(\tau)}\int_\tau^{\tau_o} d\tilde{\tau}\,S_{\Phi'+\Psi'}(\tilde{\tau},k)j_\ell(kr(\tilde{\tau})). \tag{D.1.29}$$

To write it in the same way as in CLASSgal, one flips the order of the integrals ($\int_a^b dx \int_a^x dy = \int_a^b dy \int_y^b dx$) and rename the variables to obtain

$$\Delta_\ell^{i,(1+z)\int \Phi'+\Psi'}(k) = \int_0^{\tau_0} d\tau\, S_{\Phi'+\Psi'}(\tau,k) j_\ell(kr(\tau)) \int_0^{\tau} d\tilde{\tau}\, \frac{W_i(\tilde{\tau})}{a(\tilde{\tau})}. \tag{D.1.30}$$

As a check, changing variables to r gives the expressions of [20].

D.1.3 The spectrum $C_\ell^{\Delta_g I}$

We look at the lensing term (ignoring terms at the observer's location).

$$I(\tau,\hat{n}) = \Phi(\tau,\hat{n}r(\tau)) + \left(\frac{1}{r(\tau)} - aH\right) v(\tau,\hat{n}r(\tau)) \\ - \int_\tau^{\tau_o} \frac{d\tilde{\tau}}{r(\tilde{\tau})} (\Phi+\Psi)(\tilde{\tau},\hat{n}(r(\tilde{\tau})). \tag{D.1.31}$$

We write it as

$$\Delta^I = \Delta^\Phi + \Delta^{(1/r-aH)v} + \Delta^{-\int(\Phi+\Psi)/r}. \tag{D.1.32}$$

Transfer function for Φ The first term is just the transfer function for the source S_Φ

$$\Delta^\Phi(\tau,k) = S_\Phi(\tau,k))j_\ell(k(\tau_o-\tau)). \tag{D.1.33}$$

Adding a window functions gives

$$\Delta_\ell^{\Phi,i}(k) = \int_0^{\tau_o} W_i(\tau) S_\Phi(\tau,k))j_\ell(k(\tau_o-\tau))\mathrm{d}\tau. \tag{D.1.34}$$

Transfer function for $(1/r - aH)v$ The second term gives

$$\Delta_\ell^{(1/r-aH)v}(\tau,k) = -\left(\frac{1}{\tau_o-\tau} - a(\tau)H(\tau)\right)\frac{S_\Theta(\tau,k)}{k^2} j_\ell(k(\tau_o-\tau)). \tag{D.1.35}$$

Adding a window function gives

$$\Delta_\ell^{(1/r-aH)v,i}(k) = -\int_0^{\tau_o} W_i(\tau)\left(\frac{1}{\tau_o-\tau} - a(\tau)H(\tau)\right)$$

$$\times \frac{S_\Theta(\tau,k)}{k^2} j_\ell(k(\tau_o-\tau))\mathrm{d}\tau. \quad \text{(D.1.36)}$$

Transfer function for $-\int(\Phi+\Psi)/r$ Finally the third term proceeds as $\int \Phi'+\Psi'$ and we obtain

$$\Delta_\ell^{-\int(\Phi+\Psi)/r}(\tau,k) = -\int_\tau^{\tau_0} \frac{d\tilde{\tau}}{\tau_0-\tilde{\tau}} S_{\Phi+\Psi}(\tilde{\tau},k) j_\ell(kr(\tilde{\tau})). \quad \text{(D.1.37)}$$

Adding a window function gives

$$\Delta_\ell^{i,-\int(\Phi+\Psi)/r}(k) = -\int_0^{\tau_o} \mathrm{d}\tau S_{\Phi+\Psi}(\tau,k) j_\ell(kr(\tau)) \int_0^{\tau} \frac{\mathrm{d}\tilde{\tau}}{\tau_o-\tilde{\tau}} W_i(\tilde{\tau}). \quad \text{(D.1.38)}$$

D.1.4 The spectrum $C_\ell^{\Delta_g d}$

We compute the transfer function for the term

$$d(\tau,\hat{n}) = e(\tau)\Delta z(\tau,\hat{n}) + t(\tau)\delta\mathcal{D}_L(\tau,\hat{n}) + \delta v(\tau,\hat{n}). \quad \text{(D.1.39)}$$

Transfer function for $e\Delta z$ In our work, we define the "evolution bias" by

$$e \equiv \frac{\mathrm{d}\ln\bar{n}_g}{\mathrm{d}z}, \quad \text{(D.1.40)}$$

where $\bar{n}_g$ is the number density of sources per physical volume. In CLASSgal, one works with the quantity

$$f_{evo}(z) \equiv \frac{\mathrm{d}\ln(a^3\bar{n}_g)}{\mathcal{H}\mathrm{d}\tau} = \left(3-\frac{e}{a}\right). \quad \text{(D.1.41)}$$

Conservation of the number of galaxies corresponds to $a^3\bar{n}_g =$ constant or $f_{evo}=0$ which gives the default value of $e=3a$. We consider the term

$$e\Delta z = (3-f_{evo})\left(\Psi + aHv - \hat{n}\cdot\vec{v} + \int_\tau^{\tau_0} d\tilde{\tau}\,(\Phi'+\Psi')\right). \quad \text{(D.1.42)}$$

We obtain the transfer function

$$\Delta_\ell^{i,e\Delta z}(k) = \Delta_\ell^{i,(3-f)\Psi}(k) + \Delta_\ell^{i,(3-f)aHv}(k) + \Delta_\ell^{i,-(3-f)\vec{v}\cdot\hat{n}}(k) + \Delta_\ell^{i,(3-f)\int\Phi'+\Psi'}(k), \quad \text{(D.1.43)}$$

with

$$\Delta_\ell^{i,(3-f)\Psi}(k) = \int_0^{\tau_o} W_i(\tau)(3-f)(\tau) S_\Psi(\tau,k) j_\ell(kr(\tau)) d\tau, \tag{D.1.44}$$

$$\Delta_\ell^{i,(3-f)aHv}(k) = -\int_0^{\tau_o} d\tau\, W_i(\tau) a(\tau)(3-f)(\tau) \frac{H(\tau)}{k^2} S_\Theta(\tau,k) j_\ell(kr(\tau)), \tag{D.1.45}$$

$$\Delta_\ell^{i,-(3-f)\vec{v}\cdot\hat{n}}(k) = -\int_0^{\tau_o} W_i(\tau)(3-f)(\tau) \frac{S_\Theta(\tau,k)}{k} j'_\ell(k(\tau_0-\tau)) d\tau, \tag{D.1.46}$$

$$\Delta_\ell^{i,(3-f)\int \Phi'+\Psi'}(k) = \int_0^{\tau_o} d\tau\, S_{\Phi'+\Psi'}(\tau,k) j_\ell(kr(\tau)) \int_0^{\tau} d\tilde{\tau}\, W_i(\tilde{\tau})(3-f)(\tilde{\tau}). \tag{D.1.47}$$

Luminosity perturbation $t\delta D$ We now turn to the term $t\delta D$. The quantity δD corresponds to the fractional fluctuation in the luminosity at fixed flux induced by the long mode. Its explicit expression at linear order can be found in the CLASSgal paper [22] which, using our convention for $\hat{n}$ and the CLASSgal convention for the potentials, reads

$$\begin{aligned}
\delta D = &-\left(\frac{1}{raH}-1\right)\vec{v}\cdot\hat{n} \\
&+\left(\frac{1}{raH}-1\right)\Psi \\
&+\left(\frac{1}{raH}-1\right)\int_\tau^{\tau_o}(\Psi'+\Phi')dr \\
&+\frac{1}{2}\int_\tau^{\tau_o}\left[\frac{2}{\tau_o-\tau}-\frac{(\tau_o-\tau)-(\tau_o-\tilde{\tau})}{(\tau_o-\tilde{\tau})(\tau_o-\tau)}\Delta_\Omega\right](\Psi+\Phi)\,d\tilde{\tau} \\
&-\Phi
\end{aligned} \tag{D.1.48}$$

and

$$t = 2\left.\frac{d\ln\hat{n}_g(s,\ln L_S)}{d\ln L_S}\right|_{\bar{L}_*} = -5s(z,m_*) \tag{D.1.49}$$

where s is the *magnification bias*.

Transfer function for $\delta V + t\delta D$ The volume perturbation is given by

$$\delta V = -2(\Phi+\Psi)$$

$$
\begin{aligned}
&+\frac{1}{aH}\Phi' \\
&+\left(1+\frac{H'}{aH^2}+\frac{2}{(\tau_0-\tau)aH}\right)\Psi \\
&+\left(-2+\frac{H'}{aH^2}+\frac{2}{(\tau_0-\tau)aH}\right)(-\hat{n}\cdot\vec{v}) \\
&+\left(-2+\frac{H'}{aH^2}+\frac{2}{(\tau_0-\tau)aH}\right)\int_\tau^{\tau_0}\mathrm{d}\tilde{\tau}(\Psi'+\Phi') \\
&+\int_\tau^{\tau_0}\mathrm{d}\tilde{\tau}\left(\frac{2}{\tau_0-\tau}-\frac{(\tau_0-\tau)-(\tau_0-\tilde{\tau})}{(\tau_0-\tau)(\tau_0-\tilde{\tau})}\Delta_\Omega\right)(\Phi+\Psi)
\end{aligned}
\tag{D.1.50}
$$

where we have used $\mathcal{H}'/\mathcal{H}^2 = 1 + H'/(aH^2)$. We now combine $\delta V + t\delta D$ and write it in terms of new and existing transfer functions

$$
\begin{aligned}
\delta V + t\delta D = \quad & -2(\Phi+\Psi) && \leftrightarrow -2\Delta_\ell^{i,\Phi+\Psi} \\
& +\tfrac{1}{aH}\Phi' && \leftrightarrow \Delta_\ell^{i,G3} \\
& +\left(1+\tfrac{H'}{aH^2}+\tfrac{2-5s}{(\tau_0-\tau)aH}+5s\right)\Psi && \leftrightarrow \Delta_\ell^{i,G1}+\Delta_\ell^{i,-\Psi} \\
& +\left(-2+\tfrac{H'}{aH^2}+\tfrac{2-5s}{(\tau_0-\tau)aH}+5s\right)(-\hat{n}\cdot\vec{v}) && \leftrightarrow \Delta_\ell^{i,D1}+\Delta_\ell^{i,3\vec{v}\cdot\hat{n}} \\
& +\left(-2+\tfrac{H'}{aH^2}+\tfrac{2-5s}{(\tau_0-\tau)aH}+5s\right)\int_\tau^{\tau_0}\mathrm{d}\tilde{\tau}(\Psi'+\Phi') && \leftrightarrow \Delta_\ell^{i,G5}+\Delta_\ell^{i,-3\int\Phi'+\Psi'} \\
& +\left(1-\tfrac{5s}{2}\right)\int_\tau^{\tau_0}\mathrm{d}\tilde{\tau}\left(\tfrac{2}{\tau_0-\tilde{\tau}}-\tfrac{(\tau_0-\tau)-(\tau_0-\tilde{\tau})}{(\tau_0-\tau)(\tau_0-\tilde{\tau})}\Delta_\Omega\right)(\Phi+\Psi) && \leftrightarrow \Delta_\ell^{i,G4}+\Delta_\ell^{i,Len} \\
& +5s\Phi, && \leftrightarrow \Delta_\ell^{i,5s\Phi}
\end{aligned}
$$

where the functions $G1$ to $G5$, $D1$ and $D2$ are defined as in the CLASSgal code and we have defined new transfer functions

$$
\Delta_\ell^{i,-\Psi}(k) = -\int_0^{\tau_0} W_i(\tau) S_\Psi(\tau,k) d\tau,
$$

$$
\Delta_\ell^{i,-3\vec{v}\cdot\hat{n}}(k) = 3\int_0^{\tau_0}\frac{W_i(\tau)}{k} j_\ell'(kr(\tau)) S_\Theta(k,\tau) d\tau,
$$

$$
\Delta_\ell^{i,-3\int\Phi'+\Psi'}(k) = -3\int_0^{\tau_0} d\tau\, S_{\Phi'+\Psi'}(\tau,k) j_\ell(kr(\tau)) \int_0^{\tau} d\tilde{\tau}\, W_i(\tilde{\tau}),
$$

$$\Delta_\ell^{i,5s\Phi}(k) = 5s \int_0^{\tau_0} W_i(\tau) j_\ell(kr(\tau)) S_\Phi(k,\tau) d\tau. \tag{D.1.51}$$

This is valid when neglecting evolution $f_{evo} = 0$. Note that we removed the terms proportional to $\partial_r(\vec{v}\cdot\hat{n})$ from the linear expression as it is zero for a constant gradient of the gravitational potential.

D.2 Harmonic decomposition of the squeezed matter bispectrum

As seen in chapter 5, it seems not possible to compute analytically the local template in general. However, considering only the squeezed limit in Fourier space, it is possible if one includes only terms for which the transfer function can be expressed as a product of a spherical Bessel function and k dependent function $\Delta_\ell(k) = j_\ell(kr)S(\tau,k)$. In this appendix, we compute the squeezed limit in harmonic space the matter overdensity only.

The squeezed limit ($k_1 \ll k_2 \simeq k_3$) of the local-shape-type contribution to the galaxy bispectrum is given by

$$\begin{aligned}
\langle \delta(z_1,k_1)\delta(z_2,k_2)\delta(z_3,k_3)\rangle' &\supset (6/5) f_{NL} \left(P_\zeta(k_1)P_\zeta(k_2) + 2 \text{ perm.}\right) T_\delta(z_1,k_1) \\
&\quad \times T_\delta(z_2,k_2) T_\delta(z_3,k_3) \\
&\simeq (12/5) f_{NL} P_\zeta(k_1) P_\zeta(k_2) T_\delta(z_1,k_1) T_\delta(z_2,k_2) T_\delta(z_3,k_2) \\
&= (12/5) f_{NL} P_{\zeta\delta}(z_1,k_1) P_\delta(z_2,z_3,k_2).
\end{aligned} \tag{D.2.1}$$

where $T_\delta(z_3,k_3)$ is the transfer function between ζ and δ. The key to the following computations is that we in the squeezed limit $k_2 = k_3$, such that the bispectrum is only a function of two of the momenta k_1 and k_2.

$$\begin{aligned}
B^{m_1,m_2,m_3}_{\ell_1,\ell_2,\ell_3} &= \langle a_{\ell_1,m_1} a_{\ell_2,m_2} a_{\ell_3,m_3}\rangle \\
&= \int d\Omega_{\hat{n}_1} d\Omega_{\hat{n}_2} d\Omega_{\hat{n}_3} Y^*_{\ell_1,m_1}(\hat{n}_1) Y^*_{\ell_2,m_2}(\hat{n}_2) Y^*_{\ell_3,m_3}(\hat{n}_3) \\
&\quad \times (-1)^{\ell_1+\ell_2+\ell_3} \int \frac{d^3k_1 d^3k_2 d^3k_3}{(2\pi)^9} e^{i(\vec{k}_1\cdot\hat{n}_1 r_1 + \vec{k}_2\cdot\hat{n}_2 r_2 + \vec{k}_3\cdot\hat{n}_3 r_3)} \\
&\quad \times \langle \delta(z_1,k_1)\delta(z_2,k_2)\delta(z_3,k_3)\rangle \\
&= (-1)^{\ell_1+\ell_2+\ell_3} \int d\Omega_{\hat{n}_1} d\Omega_{\hat{n}_2} d\Omega_{\hat{n}_3} Y^*_{\ell_1,m_1}(\hat{n}_1) Y^*_{\ell_2,m_2}(\hat{n}_2) Y^*_{\ell_3,m_3}(\hat{n}_3) \\
&\quad \times \int \frac{d^3k_1 d^3k_2}{(2\pi)^6} e^{i(\vec{k}_1\cdot\hat{n}_1 r_1 + \vec{k}_2\cdot\hat{n}_2 r_2)} e^{-i\vec{k}_1\cdot\hat{n}_3 r_3 - i\vec{k}_2\cdot\hat{n}_3 r_3}
\end{aligned}$$

$$\times ((12/5) f_{NL} P_{\zeta\delta}(z_1, k_1) P_\delta(z_2, z_3, k_2))$$

$$= (-1)^{\ell_1+\ell_2+\ell_3} (4\pi)^2 i^{\ell_1+\ell_2} \int d\Omega_{\hat{n}_3} Y^*_{\ell_3,m_3}(\hat{n}_3) \int \frac{d^3k_1 d^3k_2}{(2\pi)^6} e^{-i\vec{k}_1\cdot\hat{n}_3 r_3 - i\vec{k}_2\cdot\hat{n}_3 r_3}$$

$$\times j_{\ell_1}(k_1 r_1) j_{\ell_2}(k_2 r_2) Y^*_{\ell_1,m_1}(\hat{k}_1) Y^*_{\ell_2,m_2}(\hat{k}_2)$$

$$\times ((12/5) f_{NL} P_{\zeta\delta}(z_1, k_1) P_\delta(z_2, z_3, k_2)) \,. \tag{D.2.2}$$

Using the completeness relation

$$\delta(\hat{n} - \hat{n}') = \sum_{l,m} Y^*_{l,m}(\hat{n}) Y_{l,m}(\hat{n}'), \tag{D.2.3}$$

we obtain

$$B^{m_1,m_2,m_3}_{\ell_1,\ell_2,\ell_3} = (-1)^{\ell_1+\ell_2+\ell_3} (4\pi)^2 i^{\ell_1+\ell_2} \int d\Omega_{\hat{n}_3} Y^*_{\ell_3,m_3}(\hat{n}_3)$$

$$\times \int d\Omega_{\hat{n}'_1} \sum_{\ell'_1,m'_1} Y_{\ell'_1,m'_1}(\hat{n}'_1) Y^*_{\ell'_1,m'_1}(\hat{n}_3)$$

$$\times \int d\Omega_{\hat{n}'_2} \sum_{\ell'_2,m'_2} Y_{\ell'_2,m'_2}(\hat{n}'_2) Y^*_{\ell'_2,m'_2}(\hat{n}_3) \int \frac{d^3k_1 d^3k_2}{(2\pi)^6} e^{-i\vec{k}_1\cdot\hat{n}'_1 r_3 - i\vec{k}_2\cdot\hat{n}'_2 r_3}$$

$$\times j_{\ell_1}(k_1 r_1) j_{\ell_2}(k_2 r_2) Y^*_{\ell_1,m_1}(\hat{k}_1) Y^*_{\ell_2,m_2}(\hat{k}_2)$$

$$\times ((12/5) f_{NL} P_{\zeta\delta}(z_1, k_1) P_\delta(z_2, z_3, k_2)) \,. \tag{D.2.4}$$

Expanding the exponentials

$$B^{m_1,m_2,m_3}_{\ell_1,\ell_2,\ell_3} = (-1)^{\ell_1+\ell_2+\ell_3} (4\pi)^4 i^{\ell_1+\ell_2} \int d\Omega_{\hat{n}_3} Y^*_{\ell_3,m_3}(\hat{n}_3)$$

$$\times \int d\Omega_{\hat{n}'_1} \sum_{\ell'_1,m'_1} Y_{\ell'_1,m'_1}(\hat{n}'_1) Y^*_{\ell'_1,m'_1}(\hat{n}_3)$$

$$\times \int d\Omega_{\hat{n}'_2} \sum_{\ell'_2,m'_2} Y_{\ell'_2,m'_2}(\hat{n}'_2) Y^*_{\ell'_2,m'_2}(\hat{n}_3)$$

$$\times \int \frac{d^3k_1 d^3k_2}{(2\pi)^6} \sum_{l''_1,m''_1} \sum_{l''_2,m''_2} (-i)^{l''_1+l''_2} j_{l''_1}(k_1 r_3) j_{l''_2}(k_2 r_3)$$

$$\times Y^*_{l_1'',m_1''}(\hat{n}_1')Y^*_{l_2'',m_2''}(\hat{n}_2')Y_{l_1'',m_1''}(\hat{k}_1)Y_{l_2'',m_2''}(\hat{k}_2)$$

$$\times j_{\ell_1}(k_1r_1)j_{\ell_2}(k_2r_2)Y^*_{\ell_1,m_1}(\hat{k}_1)Y^*_{\ell_2,m_2}(\hat{k}_2)$$

$$\times ((12/5)f_{NL}P_{\zeta\delta}(z_1,k_1)P_\delta(z_2,z_3,k_2))\,. \tag{D.2.5}$$

Performing the angular integrals over $\hat{n}_1'$ and $\hat{n}_2'$

$$\begin{aligned}
B^{m_1,m_2,m_3}_{\ell_1,\ell_2,\ell_3} &= (-1)^{\ell_1+\ell_2+\ell_3}(4\pi)^4 i^{\ell_1+\ell_2}\int d\Omega_{\hat{n}_3}Y^*_{\ell_3,m_3}(\hat{n}_3)\sum_{\ell_1',m_1'}Y_{\ell_1',m_1'}(\hat{n}_3)\\
&\times\sum_{\ell_2',m_2'}Y_{\ell_2',m_2'}(\hat{n}_3)\int\frac{d^3k_1d^3k_2}{(2\pi)^6}\sum_{l_1'',m_1''}\sum_{l_2'',m_2''}\delta_{\ell_1'l_1'',m_1'm_1''}\delta_{\ell_2'l_2'',m_2'm_2''}\\
&\times(-i)^{l_1''+l_2''}j_{l_1''}(k_1r_3)j_{l_2''}(k_2r_3)Y_{l_1'',m_1''}(\hat{k}_1)Y_{l_2'',m_2''}(\hat{k}_2)\\
&\times j_{\ell_1}(k_1r_1)j_{\ell_2}(k_2r_2)Y^*_{\ell_1,m_1}(\hat{k}_1)Y^*_{\ell_2,m_2}(\hat{k}_2)\\
&\times((12/5)f_{NL}P_{\zeta\delta}(z_1,k_1)P_\delta(z_2,z_3,k_2))\\
&= (-1)^{\ell_1+\ell_2+\ell_3}(4\pi)^4 i^{\ell_1+\ell_2}\sum_{\ell_1',m_1'}\sum_{\ell_2',m_2'}\int d\Omega_{\hat{n}_3}Y^*_{\ell_3,m_3}(\hat{n}_3)Y^*_{\ell_1',m_1'}(\hat{n}_3)Y^*_{\ell_2',m_2'}(\hat{n}_3)\\
&\times\int\frac{d^3k_1d^3k_2}{(2\pi)^6}(-i)^{\ell_1'+\ell_2'}j_{\ell_1'}(k_1r_3)j_{\ell_2'}(k_2r_3)j_{\ell_1}(k_1r_1)j_{\ell_2}(k_2r_2)\\
&\times Y_{\ell_1',m_1'}(\hat{k}_1)Y_{\ell_2',m_2'}(\hat{k}_2)Y^*_{\ell_1,m_1}(\hat{k}_1)Y^*_{\ell_2,m_2}(\hat{k}_2)\\
&\times((12/5)f_{NL}P_{\zeta\delta}(z_1,k_1)P_\delta(z_2,z_3,k_2))\\
&= (-1)^{\ell_1+\ell_2+\ell_3}(4\pi)^4 i^{\ell_1+\ell_2}\sum_{\ell_1',m_1'}\sum_{\ell_2',m_2'}\int d\Omega_{\hat{n}_3}Y^*_{\ell_3,m_3}(\hat{n}_3)Y^*_{\ell_1',m_1'}(\hat{n}_3)Y^*_{\ell_2',m_2'}(\hat{n}_3)\\
&\times\int\frac{d\Omega_{\hat{k}_1}dk_1k_1^2d\Omega_{\hat{k}_2}dk_2k_2^2}{(2\pi)^6}(-i)^{\ell_1'+\ell_2'}j_{\ell_1'}(k_1r_3)j_{\ell_2'}(k_2r_3)j_{\ell_1}(k_1r_1)j_{\ell_2}(k_2r_2)\\
&\times Y_{\ell_1',m_1'}(\hat{k}_1)Y_{\ell_2',m_2'}(\hat{k}_2)Y^*_{\ell_1,m_1}(\hat{k}_1)Y^*_{\ell_2,m_2}(\hat{k}_2)\\
&\times((12/5)f_{NL}P_{\zeta\delta}(z_1,k_1)P_\delta(z_2,z_3,k_2))\\
&= (-1)^{\ell_1+\ell_2+\ell_3}(4\pi)^4\int d\Omega_{\hat{n}_3}Y^*_{\ell_3,m_3}(\hat{n}_3)Y^*_{\ell_1,m_1}(\hat{n}_3)Y^*_{\ell_2,m_2}(\hat{n}_3)
\end{aligned}$$

$$
\begin{aligned}
&\times \int \frac{dk_1 k_1^2 dk_2 k_2^2}{(2\pi)^6} j_{\ell_1}(k_1 r_3) j_{\ell_2}(k_2 r_3) j_{\ell_1}(k_1 r_1) j_{\ell_2}(k_2 r_2) \\
&\times ((12/5) f_{NL} P_{\zeta\delta}(z_1, k_1) P_\delta(z_2, z_3, k_2)) \\
&= (-1)^{\ell_1+\ell_2+\ell_3} (-1)^{m_1+m_2+m_3} \mathcal{G}^{-m_1,-m_2,-m_3}_{\ell_1,\ell_2,\ell_3} (4\pi)^4 \\
&\times \int \frac{dk_1 k_1^2 dk_2 k_2^2}{(2\pi)^6} j_{\ell_1}(k_1 r_3) j_{\ell_2}(k_2 r_3) j_{\ell_1}(k_1 r_1) j_{\ell_2}(k_2 r_2) \\
&\times ((12/5) f_{NL} P_{\zeta\delta}(z_1, k_1) P_\delta(z_2, z_3, k_2)) \\
&= \mathcal{G}^{m_1,m_2,m_3}_{\ell_1,\ell_2,\ell_3} \frac{12}{5} f_{NL} \tilde{C}^{\zeta\delta}_{\ell_1}(z_1, z_3) C^{\delta\delta}_{\ell_2}(z_2, z_3),
\end{aligned}
\tag{D.2.6}
$$

where $C^{\delta\delta}_\ell(z, z')$ is the usual one and

$$
\tilde{C}^{\zeta\delta}_l(z, z') \equiv \frac{(4\pi)^2}{(2\pi)^3} \int dk\, k^2 P_\zeta(k) T_\delta(z, k) j_l(kr(z)) j_l(kr(z')). \tag{D.2.7}
$$

Note that there is only one transfer function here and we have used that $m_1 + m_2 + m_3 = 0$ is needed for the Gaunt to be non zero.

Now, assuming that z_3 is during matter domination and that the transfer function for Φ is roughly 3/5 (although it exact only on super-horizon scales), we can express the bispectrum (D.2.6) in terms of regular C_ℓ's as

$$
B^{m_1,m_2,m_3}_{\ell_1,\ell_2,\ell_3}(z_1, z_2, z_3) = \mathcal{G}^{m_1,m_2,m_3}_{\ell_1,\ell_2,\ell_3} 4 f_{NL} C^{\Phi\delta}_{\ell_1}(z_1, z_3) C^{\delta\delta}_{\ell_2}(z_2, z_3). \tag{D.2.8}
$$

Bibliography

[1] A. Einstein, *Feldgleichungen der Gravitation*, *Preussische Akademie der Wissenschaften, Sitzungsberichte* (1915) 844–847.

[2] A. H. Guth, *The Inflationary Universe: A Possible Solution to the Horizon and Flatness Problems*, *Phys. Rev.* **D23** (1981) 347–356.

[3] A. Albrecht and P. J. Steinhardt, *Cosmology for Grand Unified Theories with Radiatively Induced Symmetry Breaking*, *Phys. Rev. Lett.* **48** (1982) 1220–1223.

[4] A. D. Linde, *A New Inflationary Universe Scenario: A Possible Solution of the Horizon, Flatness, Homogeneity, Isotropy and Primordial Monopole Problems*, *Phys. Lett.* **B108** (1982) 389–393.

[5] A. A. Starobinsky, *A New Type of Isotropic Cosmological Models Without Singularity*, *Phys. Lett.* **B91** (1980) 99–102.

[6] V. Acquaviva, N. Bartolo, S. Matarrese and A. Riotto, *Second order cosmological perturbations from inflation*, *Nucl. Phys.* **B667** (2003) 119–148, [astro-ph/0209156].

[7] J. M. Maldacena, *Non-Gaussian features of primordial fluctuations in single field inflationary models*, *JHEP* **0305** (2003) 013, [astro-ph/0210603].

[8] A. Kehagias, A. M. Dizgah, J. Noreña, H. Perrier and A. Riotto, *A Consistency Relation for the Observed Galaxy Bispectrum and the Local non-Gaussianity from Relativistic Corrections*, *JCAP* **1508** (2015) 018, [1503.04467].

[9] A. Kehagias, J. Noreña, H. Perrier and A. Riotto, *Consequences of Symmetries and Consistency Relations in the Large-Scale Structure of the Universe for Non-local bias and Modified Gravity*, *Nucl.Phys.* **B883** (2014) 83–106, [1311.0786].

[10] A. Kehagias, H. Perrier and A. Riotto, *Equal-time Consistency Relations in the Large-Scale Structure of the Universe*, *Mod.Phys.Lett.* **A29** (2014) 1450152, [1311.5524].

[11] A. Kehagias, A. Moradinezhad Dizgah, J. Noreña, H. Perrier and A. Riotto, *A Consistency Relation for the CMB B-mode Polarization in the Squeezed Limit*, *JCAP* **1410** (2014) 011, [1407.6223].

[12] P. Creminelli and M. Zaldarriaga, *Single field consistency relation for the 3-point function*, *JCAP* **0410** (2004) 006, [astro-ph/0407059].

[13] P. Creminelli, G. D'Amico, M. Musso and J. Noreña, *The (not so) squeezed limit of the primordial 3-point function*, *JCAP* **1111** (2011) 038, [1106.1462].

[14] P. Creminelli, J. Noreña and M. Simonović, *Conformal consistency relations for single-field inflation*, *JCAP* **1207** (2012) 052, [1203.4595].

[15] A. Kehagias and A. Riotto, *Operator Product Expansion of Inflationary Correlators and Conformal Symmetry of de Sitter*, *Nucl.Phys.* **B864** (2012) 492–529, [1205.1523].

[16] V. Assassi, D. Baumann and D. Green, *On Soft Limits of Inflationary Correlation Functions*, *JCAP* **1211** (2012) 047, [1204.4207].

[17] K. Hinterbichler, L. Hui and J. Khoury, *An Infinite Set of Ward Identities for Adiabatic Modes in Cosmology*, *JCAP* **1401** (2014) 039, [1304.5527].

[18] E. Di Dio, R. Durrer, G. Marozzi and F. Montanari, *The bispectrum of relativistic galaxy number counts*, *JCAP* **1601** (2016) 016, [1510.04202].

[19] E. Di Dio, R. Durrer, G. Marozzi and F. Montanari, *Galaxy number counts to second order and their bispectrum*, *JCAP* **1412** (2014) 017, [1407.0376].

[20] C. Bonvin and R. Durrer, *What galaxy surveys really measure*, *Phys.Rev.* **D84** (2011) 063505, [1105.5280].

[21] C.-P. Ma and E. Bertschinger, *Cosmological perturbation theory in the synchronous and conformal Newtonian gauges*, *Astrophys. J.* **455** (1995) 7–25, [astro-ph/9506072].

[22] E. Di Dio, F. Montanari, J. Lesgourgues and R. Durrer, *The CLASSgal code for Relativistic Cosmological Large Scale Structure*, *JCAP* **1311** (2013) 044, [1307.1459].

[23] A. Friedman, *Über die krümmung des raumes*, *Zeitschrift für Physik* **10** (1922) 377–386.

[24] G. Lemaître, *Un Univers homogène de masse constante et de rayon croissant rendant compte de la vitesse radiale des nébuleuses extra-galactiques*, *Annales de la Société Scientifique de Bruxelles* **47** (1927) 49–59.

[25] H. P. Robertson, *Kinematics and World-Structure*, *ApJ* **82** (Nov., 1935) 284.

[26] A. G. Walker, *On Milne's Theory of World-Structure*, *Proc. London Math. Soc.* **s2-42 (1)** (1937) 90–127.

[27] E. Hubble, *A Relation between Distance and Radial Velocity among Extra-Galactic Nebulae*, *Proceedings of the National Academy of Science* **15** (Mar., 1929) 168–173.

[28] A. G. Riess, A. V. Filippenko, P. Challis, A. Clocchiatti, A. Diercks, P. M. Garnavich et al., *Observational evidence from supernovae for an accelerating universe and a cosmological constant*, *The Astronomical Journal* **116** (1998) 1009.

[29] V. C. Rubin, N. Thonnard and W. K. Ford, Jr., *Rotational properties of 21 SC galaxies with a large range of luminosities and radii, from NGC 4605 /R = 4kpc/ to UGC 2885 /R = 122 kpc/*, *Astrophys. J.* **238** (1980) 471.

[30] M. B. Einhorn and K. Sato, *Monopole Production in the Very Early Universe in a First Order Phase Transition*, *Nucl. Phys.* **B180** (1981) 385–404.

[31] K. Sato, *Cosmological Baryon Number Domain Structure and the First Order Phase Transition of a Vacuum*, *Phys. Lett.* **B99** (1981) 66–70.

[32] D. Kazanas, *Dynamics of the Universe and Spontaneous Symmetry Breaking*, *Astrophys. J.* **241** (1980) L59–L63.

[33] D. H. Lyth and A. Riotto, *Particle physics models of inflation and the cosmological density perturbation*, *Phys. Rept.* **314** (1999) 1–146, [hep-ph/9807278].

[34] Planck collaboration, P. A. R. Ade et al., *Planck 2015 results. XX. Constraints on inflation*, 1502.02114.

[35] Virgo, LIGO Scientific collaboration, B. P. Abbott et al., *Observation of Gravitational Waves from a Binary Black Hole Merger*, *Phys. Rev. Lett.* **116** (2016) 061102, [1602.03837].

[36] A. D. Linde and V. F. Mukhanov, *Nongaussian isocurvature perturbations from inflation*, *Phys. Rev.* **D56** (1997) 535–539, [astro-ph/9610219].

[37] S. Mollerach, *Isocurvature Baryon Perturbations and Inflation*, *Phys. Rev.* **D42** (1990) 313–325.

[38] D. H. Lyth, *Generating the primordial curvature perturbation from inflation*, in *Proceedings, 37th Rencontres de Moriond, The cosmological Model*, pp. 221–227, 2003. hep-ph/0205266.

[39] Planck collaboration, P. A. R. Ade et al., *Planck 2015 results. XVII. Constraints on primordial non-Gaussianity*, 1502.01592.

[40] N. Dalal, O. Dore, D. Huterer and A. Shirokov, *The imprints of primordial non-gaussianities on large-scale structure: scale dependent bias and abundance of virialized objects*, *Phys. Rev.* **D77** (2008) 123514, [0710.4560].

[41] V. Desjacques and U. Seljak, *Primordial non-Gaussianity in the large scale structure of the Universe*, *Adv. Astron.* **2010** (2010) 908640, [1006.4763].

[42] S. Furlanetto, S. P. Oh and F. Briggs, *Cosmology at Low Frequencies: The 21 cm Transition and the High-Redshift Universe*, *Phys. Rept.* **433** (2006) 181–301, [astro-ph/0608032].

[43] J. R. Pritchard and A. Loeb, *21-cm cosmology*, *Rept. Prog. Phys.* **75** (2012) 086901, [1109.6012].

[44] A. Kogut et al., *The Primordial Inflation Explorer (PIXIE): A Nulling Polarimeter for Cosmic Microwave Background Observations*, *JCAP* **1107** (2011) 025, [1105.2044].

[45] E. Pajer and M. Zaldarriaga, *A New Window on Primordial non-Gaussianity*, *Phys. Rev. Lett.* **109** (2012) 021302, [1201.5375].

[46] M. Biagetti, H. Perrier, A. Riotto and V. Desjacques, *Testing the running of non-Gaussianity through the CMB μ-distortion and the halo bias*, *Phys. Rev.* **D87** (2013) 063521, [1301.2771].

[47] A. A. Penzias and R. W. Wilson, *A Measurement of excess antenna temperature at 4080-Mc/s*, *Astrophys. J.* **142** (1965) 419–421.

[48] WITH INPUT FROM THE SDSS-III collaboration, D. Schlegel, M. White and D. Eisenstein, *The Baryon Oscillation Spectroscopic Survey: Precision measurements of the absolute cosmic distance scale*, 0902.4680.

[49] DARK ENERGY SURVEY collaboration, T. Abbott et al., *The dark energy survey*, astro-ph/0510346.

[50] LSST SCIENCE COLLABORATIONS, LSST PROJECT collaboration, P. A. Abell et al., *LSST Science Book, Version 2.0*, 0912.0201.

[51] LSST DARK ENERGY SCIENCE collaboration, A. Abate et al., *Large Synoptic Survey Telescope: Dark Energy Science Collaboration*, 1211.0310.

[52] DESI COLLABORATION collaboration, M. Levi et al., *The DESI Experiment, a whitepaper for Snowmass 2013*, 1308.0847.

[53] D. Spergel, N. Gehrels, J. Breckinridge, M. Donahue, A. Dressler et al., *Wide-Field InfraRed Survey Telescope-Astrophysics Focused Telescope Assets WFIRST-AFTA Final Report*, 1305.5422.

[54] EUCLID collaboration, J. Amiaux et al., *Euclid Mission: building of a Reference Survey*, *Proc. SPIE Int. Soc. Opt. Eng.* **8442** (2012) 84420Z, [1209.2228].

[55] EUCLID THEORY WORKING GROUP collaboration, L. Amendola et al., *Cosmology and fundamental physics with the Euclid satellite*, *Living Rev.Rel.* **16** (2013) 6, [1206.1225].

[56] F. Bernardeau, S. Colombi, E. Gaztanaga and R. Scoccimarro, *Large scale structure of the universe and cosmological perturbation theory*, *Phys. Rept.* **367** (2002) 1–248, [astro-ph/0112551].

[57] M. Crocce and R. Scoccimarro, *Renormalized cosmological perturbation theory*, *Phys. Rev.* **D73** (2006) 063519, [astro-ph/0509418].

[58] J. J. M. Carrasco, M. P. Hertzberg and L. Senatore, *The Effective Field Theory of Cosmological Large Scale Structures*, *JHEP* **09** (2012) 082, [1206.2926].

[59] T. Matsubara, *Integrated Perturbation Theory and One-loop Power Spectra of Biased Tracers*, *Phys. Rev.* **D90** (2014) 043537, [1304.4226].

[60] A. Cooray and R. K. Sheth, *Halo models of large scale structure*, *Phys. Rept.* **372** (2002) 1–129, [astro-ph/0206508].

[61] P. McDonald and A. Roy, *Clustering of dark matter tracers: generalizing bias for the coming era of precision LSS*, *JCAP* **0908** (2009) 020, [0902.0991].

[62] T. Baldauf, U. Seljak, V. Desjacques and P. McDonald, *Evidence for Quadratic Tidal Tensor Bias from the Halo Bispectrum*, *Phys. Rev.* **D86** (2012) 083540, [1201.4827].

[63] N. Kaiser, *Clustering in real space and in redshift space*, *Mon. Not. Roy. Astron. Soc.* **227** (1987) 1–27.

[64] A. Challinor and A. Lewis, *The linear power spectrum of observed source number counts*, *Phys.Rev.* **D84** (2011) 043516, [1105.5292].

[65] D. Jeong, F. Schmidt and C. M. Hirata, *Large-scale clustering of galaxies in general relativity*, *Phys.Rev.* **D85** (2012) 023504, [1107.5427].

[66] J. Yoo, *General Relativistic Description of the Observed Galaxy Power Spectrum: Do We Understand What We Measure?*, *Phys.Rev.* **D82** (2010) 083508, [1009.3021].

[67] D. Bertacca, R. Maartens and C. Clarkson, *Observed galaxy number counts on the lightcone up to second order: I. Main result*, *JCAP* **1409** (2014) 037, [1405.4403].

[68] J. Yoo and M. Zaldarriaga, *Beyond the Linear-Order Relativistic Effect in Galaxy Clustering: Second-Order Gauge-Invariant Formalism*, *Phys. Rev.* **D90** (2014) 023513, [1406.4140].

[69] P. Creminelli, A. Nicolis and E. Trincherini, *Galilean Genesis: An Alternative to inflation*, *JCAP* **1011** (2010) 021, [1007.0027].

[70] P. Creminelli, C. Pitrou and F. Vernizzi, *The CMB bispectrum in the squeezed limit*, *JCAP* **1111** (2011) 025, [1109.1822].

[71] N. Bartolo, S. Matarrese and A. Riotto, *Non-Gaussianity in the Cosmic Microwave Background Anisotropies at Recombination in the Squeezed limit*, *JCAP* **1202** (2012) 017, [1109.2043].

[72] A. Lewis, *The full squeezed CMB bispectrum from inflation*, *JCAP* **1206** (2012) 023, [1204.5018].

[73] E. Pajer, F. Schmidt and M. Zaldarriaga, *The Observed Squeezed Limit of Cosmological Three-Point Functions*, *Phys. Rev.* **D88** (2013) 083502, [1305.0824].

[74] M. Mirbabayi and M. Zaldarriaga, *CMB Anisotropies from a Gradient Mode*, *JCAP* **1503** (2015) 056, [1409.4777].

[75] J. Kim, A. Rotti and E. Komatsu, *Removing the ISW-lensing bias from the local-form primordial non-Gaussianity estimation*, *JCAP* **1304** (2013) 021, [1302.5799].

[76] D. Hanson, K. M. Smith, A. Challinor and M. Liguori, *CMB lensing and primordial non-Gaussianity*, *Phys. Rev.* **D80** (2009) 083004, [0905.4732].

[77] A. Kehagias and A. Riotto, *Symmetries and Consistency Relations in the Large Scale Structure of the Universe*, *Nucl.Phys.* **B873** (2013) 514–529, [1302.0130].

[78] M. Peloso and M. Pietroni, *Galilean invariance and the consistency relation for the nonlinear squeezed bispectrum of large scale structure*, *JCAP* **1305** (2013) 031, [1302.0223].

[79] P. Creminelli, J. Noreña, M. Simonović and F. Vernizzi, *Single-Field Consistency Relations of Large Scale Structure*, *JCAP* **1312** (2013) 025, [1309.3557].

[80] A. Kehagias and A. Riotto, *Conformal Symmetries of FRW Accelerating Cosmologies*, *Nucl. Phys.* **B884** (2014) 547–565, [1309.3671].

[81] P. Valageas, *Kinematic consistency relations of large-scale structures*, *Phys. Rev.* **D89** (2014) 083534, [1311.1236].

[82] P. Creminelli, J. Gleyzes, M. Simonović and F. Vernizzi, *Single-Field Consistency Relations of Large Scale Structure. Part II: Resummation and Redshift Space*, *JCAP* **1402** (2014) 051, [1311.0290].

[83] P. Valageas, *Angular averaged consistency relations of large-scale structures*, *Phys.Rev.* **D89** (2014) 123522, [1311.4286].

[84] P. Creminelli, J. Gleyzes, L. Hui, M. Simonović and F. Vernizzi, *Single-Field Consistency Relations of Large Scale Structure. Part III: Test of the Equivalence Principle*, *JCAP* **1406** (2014) 009, [1312.6074].

[85] T. Nishimichi and P. Valageas, *Testing the equal-time angular-averaged consistency relation of the gravitational dynamics in N-body simulations*, *Phys. Rev.* **D90** (2014) 023546, [1402.3293].

[86] B. Horn, L. Hui and X. Xiao, *Soft-Pion Theorems for Large Scale Structure*, *JCAP* **1409** (2014) 044, [1406.0842].

[87] P. Berger, A. Kehagias and A. Riotto, *Testing the Origin of Cosmological Magnetic Fields through the Large-Scale Structure Consistency Relations*, *JCAP* **1405** (2014) 025, [1402.1044].

[88] T. Baldauf, U. Seljak, L. Senatore and M. Zaldarriaga, *Galaxy Bias and non-Linear Structure Formation in General Relativity*, *JCAP* **1110** (2011) 031, [1106.5507].

[89] B. D. Sherwin and M. Zaldarriaga, *The Shift of the Baryon Acoustic Oscillation Scale: A Simple Physical Picture*, *Phys. Rev.* **D85** (2012) 103523, [1202.3998].

[90] M. Pietroni, *Flowing with Time: a New Approach to Nonlinear Cosmological Perturbations*, *JCAP* **0810** (2008) 036, [0806.0971].

[91] U. Seljak, *Analytic model for galaxy and dark matter clustering*, *Mon. Not. Roy. Astron. Soc.* **318** (2000) 203, [astro-ph/0001493].

[92] C.-P. Ma and J. N. Fry, *Deriving the nonlinear cosmological power spectrum and bispectrum from analytic dark matter halo profiles and mass functions*, *Astrophys. J.* **543** (2000) 503–513, [astro-ph/0003343].

[93] J. F. Navarro, C. S. Frenk and S. D. M. White, *A Universal density profile from hierarchical clustering*, *Astrophys. J.* **490** (1997) 493–508, [astro-ph/9611107].

[94] A. R. Zentner, *The Excursion Set Theory of Halo Mass Functions, Halo Clustering, and Halo Growth*, *Int. J. Mod. Phys.* **D16** (2007) 763–816, [astro-ph/0611454].

[95] R. K. Sheth and G. Tormen, *Large scale bias and the peak background split*, *Mon. Not. Roy. Astron. Soc.* **308** (1999) 119, [astro-ph/9901122].

[96] D. G. Figueroa, E. Sefusatti, A. Riotto and F. Vernizzi, *The Effect of Local non-Gaussianity on the Matter Bispectrum at Small Scales*, *JCAP* **1208** (2012) 036, [1205.2015].

[97] J. N. Fry, *The Evolution of Bias*, *Astrophys. J.* **461** (1996) L65.

[98] R. Scoccimarro and J. Frieman, *Loop corrections in nonlinear cosmological perturbation theory*, *Astrophys. J. Suppl.* **105** (1996) 37, [astro-ph/9509047].

[99] J. N. Fry and E. Gaztanaga, *Biasing and hierarchical statistics in large scale structure*, *Astrophys. J.* **413** (1993) 447–452, [astro-ph/9302009].

[100] V. Desjacques, *Baryon acoustic signature in the clustering of density maxima*, *Phys. Rev.* **D78** (2008) 103503, [0806.0007].

[101] T. Matsubara, *Nonlinear Perturbation Theory Integrated with Nonlocal Bias, Redshift-space Distortions, and Primordial Non-Gaussianity*, *Phys. Rev.* **D83** (2011) 083518, [1102.4619].

[102] K. C. Chan, R. Scoccimarro and R. K. Sheth, *Gravity and Large-Scale Non-local Bias*, *Phys. Rev.* **D85** (2012) 083509, [1201.3614].

[103] M. Davis and P. J. E. Peebles, *On the integration of the BBGKY equations for the development of strongly nonlinear clustering in an expanding universe*, *Astrophys. J., Suppl. Ser.* **34** (Aug., 1977) 425–450.

[104] L. Hui and K. P. Parfrey, *The Evolution of Bias: Generalized*, *Phys. Rev.* **D77** (2008) 043527, [0712.1162].

[105] F. Schmidt, D. Jeong and V. Desjacques, *Peak-Background Split, Renormalization, and Galaxy Clustering*, *Phys. Rev.* **D88** (2013) 023515, [1212.0868].

[106] E. Sefusatti, *1-loop Perturbative Corrections to the Matter and Galaxy Bispectrum with non-Gaussian Initial Conditions*, *Phys. Rev.* **D80** (2009) 123002, [0905.0717].

[107] S. Dodelson, *Modern Cosmology*. Academic Press, Amsterdam, 2003.

[108] T. P. Sotiriou and V. Faraoni, *f(R) Theories Of Gravity*, *Rev. Mod. Phys.* **82** (2010) 451–497, [0805.1726].

[109] T. Chiba, *Generalized gravity and ghost*, *JCAP* **0503** (2005) 008, [gr-qc/0502070].

[110] J. Khoury and A. Weltman, *Chameleon fields: Awaiting surprises for tests of gravity in space*, *Phys. Rev. Lett.* **93** (2004) 171104, [astro-ph/0309300].

[111] A. Nicolis, R. Rattazzi and E. Trincherini, *The Galileon as a local modification of gravity*, *Phys. Rev.* **D79** (2009) 064036, [0811.2197].

[112] L. Hui, A. Nicolis and C. Stubbs, *Equivalence Principle Implications of Modified Gravity Models*, *Phys. Rev.* **D80** (2009) 104002, [0905.2966].

[113] W. Hu and I. Sawicki, *Models of f(R) Cosmic Acceleration that Evade Solar-System Tests*, *Phys. Rev.* **D76** (2007) 064004, [0705.1158].

[114] P. Brax, A.-C. Davis and B. Li, *Modified Gravity Tomography*, *Phys. Lett.* **B715** (2012) 38–43, [1111.6613].

[115] J. Wang, L. Hui and J. Khoury, *No-Go Theorems for Generalized Chameleon Field Theories*, *Phys. Rev. Lett.* **109** (2012) 241301, [1208.4612].

[116] E. Sefusatti and E. Komatsu, *The bispectrum of galaxies from high-redshift galaxy surveys: Primordial non-Gaussianity and non-linear galaxy bias*, *Phys. Rev.* **D76** (2007) 083004, [0705.0343].

[117] C. M. Will, *The Confrontation between General Relativity and Experiment*, *Living Rev. Rel.* **17** (2014) 4, [1403.7377].

[118] S. Tsujikawa, *Matter density perturbations and effective gravitational constant in modified gravity models of dark energy*, *Phys. Rev.* **D76** (2007) 023514, [0705.1032].

[119] J. A. Frieman and B. A. Gradwohl, *Dark matter and the equivalence principle*, *Science* **260** (1993) 1441–1442.

[120] C. W. Stubbs, *Experimental limits on any long range nongravitational interaction between dark matter and ordinary matter*, *Phys. Rev. Lett.* **70** (1993) 119–122.

[121] P. Fayet, *Equivalence principle tests, equivalence theorems and new long range forces*, *C. R. Acad. Sci. IV Phys. Astrophys.* **2** (2001) 1257, [hep-ph/0111282].

[122] F. Saracco, M. Pietroni, N. Tetradis, V. Pettorino and G. Robbers, *Non-linear Matter Spectra in Coupled Quintessence*, *Phys. Rev.* **D82** (2010) 023528, [0911.5396].

[123] M. Peloso and M. Pietroni, *Ward identities and consistency relations for the large scale structure with multiple species*, *JCAP* **1404** (2014) 011, [1310.7915].

[124] M. Bruni, R. Crittenden, K. Koyama, R. Maartens, C. Pitrou and D. Wands, *Disentangling non-Gaussianity, bias and GR effects in the galaxy distribution*, *Phys. Rev.* **D85** (2012) 041301, [1106.3999].

[125] D. Bertacca, R. Maartens and C. Clarkson, *Observed galaxy number counts on the lightcone up to second order: II. Derivation*, *JCAP* **11** (2014) 013, [1406.0319].

[126] N. Bartolo, E. Komatsu, S. Matarrese and A. Riotto, *Non-Gaussianity from inflation: Theory and observations*, *Phys.Rept.* **402** (2004) 103–266, [astro-ph/0406398].

[127] S. Weinberg, *Adiabatic modes in cosmology*, *Phys.Rev.* **D67** (2003) 123504, [astro-ph/0302326].

[128] J. Yoo, A. L. Fitzpatrick and M. Zaldarriaga, *A New Perspective on Galaxy Clustering as a Cosmological Probe: General Relativistic Effects*, *Phys.Rev.* **D80** (2009) 083514, [0907.0707].

[129] P. Creminelli, A. Perko, L. Senatore, M. Simonovi¿ and G. Trevisan, *The Physical Squeezed Limit: Consistency Relations at Order q^2*, *JCAP* **1311** (2013) 015, [1307.0503].

[130] L. Dai, E. Pajer and F. Schmidt, *Conformal Fermi Coordinates*, *JCAP* **1511** (2015) 043, [1502.02011].

[131] E. Di Dio, H. Perrier, R. Durrer, G. Marozzi, A. Moradinezhad Dizgah, J. Noreña et al., *Non-Gaussianities due to Relativistic Corrections to the Observed Galaxy Bispectrum*, *prepared for submission to JCAP* (2016) .

[132] E. Villa, L. Verde and S. Matarrese, *General relativistic corrections and non-Gaussianity in large scale structure*, *Class. Quant. Grav.* **31** (2014) 234005, [1409.4738].

[133] L. Verde, L.-M. Wang, A. Heavens and M. Kamionkowski, *Large scale structure, the cosmic microwave background, and primordial non-gaussianity*, *Mon. Not. Roy. Astron. Soc.* **313** (2000) L141–L147, [astro-ph/9906301].

[134] A. Gangui, F. Lucchin, S. Matarrese and S. Mollerach, *The Three point correlation function of the cosmic microwave background in inflationary models*, *Astrophys. J.* **430** (1994) 447–457, [astro-ph/9312033].

[135] L.-M. Wang and M. Kamionkowski, *The Cosmic microwave background bispectrum and inflation*, *Phys. Rev.* **D61** (2000) 063504, [astro-ph/9907431].

[136] E. Komatsu and D. N. Spergel, *Acoustic signatures in the primary microwave background bispectrum*, *Phys. Rev.* **D63** (2001) 063002, [astro-ph/0005036].

[137] D. Babich, P. Creminelli and M. Zaldarriaga, *The Shape of non-Gaussianities*, *JCAP* **0408** (2004) 009, [astro-ph/0405356].

[138] J. R. Fergusson, M. Liguori and E. P. S. Shellard, *The CMB Bispectrum*, *JCAP* **1212** (2012) 032, [1006.1642].

[139] A. D. Jackson and L. C. Maximon, *Integrals of products of bessel functions*, *SIAM Journal on Mathematical Analysis* **3** (1972) 446–460, [http://dx.doi.org/10.1137/0503043].

[140] BICEP2 Collaboration collaboration, P. Ade et al., *Detection of B-Mode Polarization at Degree Angular Scales by BICEP2*, *Phys.Rev.Lett.* **112** (2014) 241101, [1403.3985].

[141] R. Flauger, J. C. Hill and D. N. Spergel, *Toward an Understanding of Foreground Emission in the BICEP2 Region*, *JCAP* **1408** (2014) 039, [1405.7351].

[142] M. J. Mortonson and U. Seljak, *A joint analysis of Planck and BICEP2 B modes including dust polarization uncertainty*, *JCAP* **1410** (2014) 035, [1405.5857].

[143] BICEP2, Planck collaboration, P. Ade et al., *Joint Analysis of BICEP2/Keck Array and Planck Data*, *Phys. Rev. Lett.* **114** (2015) 101301, [1502.00612].

[144] L. Boubekeur, P. Creminelli, G. D'Amico, J. Noreña and F. Vernizzi, *Sachs-Wolfe at second order: the CMB bispectrum on large angular scales*, *JCAP* **0908** (2009) 029, [0906.0980].

[145] Z. Huang and F. Vernizzi, *The full CMB temperature bispectrum from single-field inflation*, *Phys.Rev.* **D89** (2014) 021302, [1311.6105].

[146] G. W. Pettinari, C. Fidler, R. Crittenden, K. Koyama, A. Lewis and D. Wands, *Impact of polarization on the intrinsic cosmic microwave background bispectrum*, *Phys. Rev.* **D90** (2014) 103010, [1406.2981].

[147] N. Bartolo, S. Matarrese and A. Riotto, *CMB Anisotropies at Second Order I*, *JCAP* **0606** (2006) 024, [astro-ph/0604416].

[148] N. Bartolo, S. Matarrese and A. Riotto, *CMB Anisotropies at Second-Order. 2. Analytical Approach*, *JCAP* **0701** (2007) 019, [astro-ph/0610110].

[149] M. Zaldarriaga and U. Seljak, *An all sky analysis of polarization in the microwave background*, *Phys.Rev.* **D55** (1997) 1830–1840, [astro-ph/9609170].

[150] W. Hu, *Weak lensing of the CMB: A harmonic approach*, *Phys.Rev.* **D62** (2000) 043007, [astro-ph/0001303].

[151] M. Bowden, A. Taylor, K. Ganga, P. Ade, J. Bock et al., *Scientific optimization of a ground - based CMB polarization experiment*, *Mon.Not.Roy.Astron.Soc.* **349** (2004) 321, [astro-ph/0309610].

[152] Planck Collaboration collaboration, J. Tauber et al., *The Scientific programme of Planck*, astro-ph/0604069.

[153] COrE Collaboration collaboration, F. Bouchet et al., *COrE (Cosmic Origins Explorer) A White Paper*, 1102.2181.

[154] PRISM Collaboration collaboration, P. Andre et al., *PRISM (Polarized Radiation Imaging and Spectroscopy Mission): A White Paper on the Ultimate Polarimetric Spectro-Imaging of the Microwave and Far-Infrared Sky*, 1306.2259.

[155] J. Lesgourgues, *The Cosmic Linear Anisotropy Solving System (CLASS) I: Overview*, 1104.2932.

[156] C.-T. Chiang, C. Wagner, F. Schmidt and E. Komatsu, *Position-dependent power spectrum of the large-scale structure: a novel method to measure the squeezed-limit bispectrum*, *JCAP* **1405** (2014) 048, [1403.3411].

[157] D. Baumann, *Inflation*, in *Physics of the large and the small, TASI 09, proceedings of the Theoretical Advanced Study Institute in Elementary Particle Physics, Boulder, Colorado, USA, 1-26 June 2009*, pp. 523–686, 2011. 0907.5424. DOI.

[158] L. Senatore, K. M. Smith and M. Zaldarriaga, *Non-Gaussianities in Single Field Inflation and their Optimal Limits from the WMAP 5-year Data*, *JCAP* **1001** (2010) 028, [0905.3746].

[159] D. S. Gorbunov and V. A. Rubakov, *Introduction to the theory of the early universe: Cosmological perturbations and inflationary theory*. 2011, 10.1142/7874.

[160] E. Di Dio, F. Montanari, R. Durrer and J. Lesgourgues, *Cosmological Parameter Estimation with Large Scale Structure Observations*, *JCAP* **1401** (2014) 042, [1308.6186].